FOR THE FUTURE OF ALKALIPHILES: 50TH ANNIVERSARY YEAR SINCE THE REDISCOVERY OF ALKALIPHILES BY DR. KOKI HORIKOSHI

EDITED BY: Masahiro Ito and Terry Ann Krulwich
PUBLISHED IN: Frontiers in Microbiology

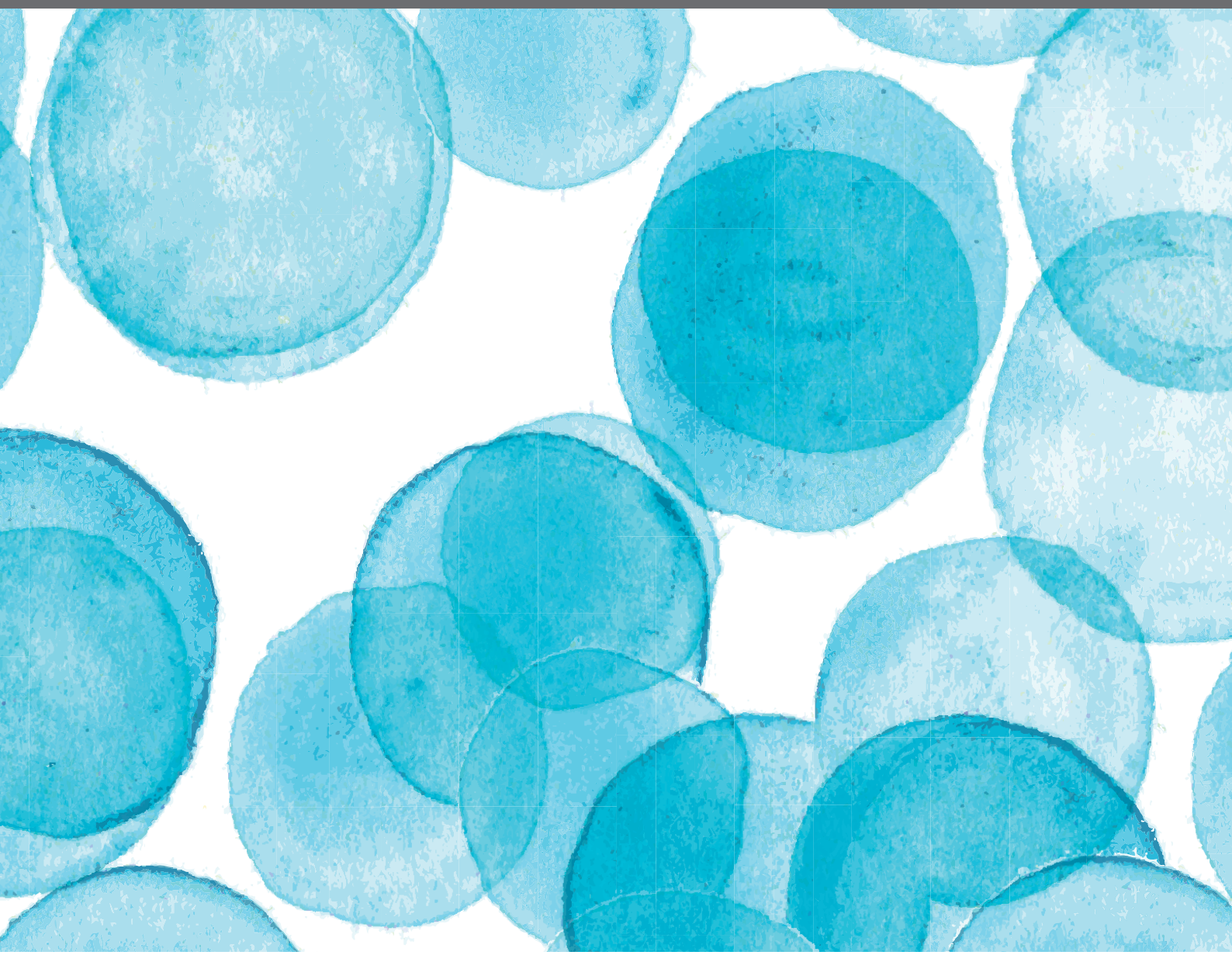

frontiers Research Topics

frontiers

ISSN 1664-8714
ISBN 978-2-88963-187-2
DOI 10.3389/978-2-88963-187-2

About Frontiers

Frontiers is more than just an open-access publisher of scholarly articles: it is a pioneering approach to the world of academia, radically improving the way scholarly research is managed. The grand vision of Frontiers is a world where all people have an equal opportunity to seek, share and generate knowledge. Frontiers provides immediate and permanent online open access to all its publications, but this alone is not enough to realize our grand goals.

Frontiers Journal Series

The Frontiers Journal Series is a multi-tier and interdisciplinary set of open-access, online journals, promising a paradigm shift from the current review, selection and dissemination processes in academic publishing. All Frontiers journals are driven by researchers for researchers; therefore, they constitute a service to the scholarly community. At the same time, the Frontiers Journal Series operates on a revolutionary invention, the tiered publishing system, initially addressing specific communities of scholars, and gradually climbing up to broader public understanding, thus serving the interests of the lay society, too.

Dedication to Quality

Each Frontiers article is a landmark of the highest quality, thanks to genuinely collaborative interactions between authors and review editors, who include some of the world's best academicians. Research must be certified by peers before entering a stream of knowledge that may eventually reach the public - and shape society; therefore, Frontiers only applies the most rigorous and unbiased reviews.
Frontiers revolutionizes research publishing by freely delivering the most outstanding research, evaluated with no bias from both the academic and social point of view. By applying the most advanced information technologies, Frontiers is catapulting scholarly publishing into a new generation.

What are Frontiers Research Topics?

Frontiers Research Topics are very popular trademarks of the Frontiers Journals Series: they are collections of at least ten articles, all centered on a particular subject. With their unique mix of varied contributions from Original Research to Review Articles, Frontiers Research Topics unify the most influential researchers, the latest key findings and historical advances in a hot research area! Find out more on how to host your own Frontiers Research Topic or contribute to one as an author by contacting the Frontiers Editorial Office: researchtopics@frontiersin.org

FOR THE FUTURE OF ALKALIPHILES: 50TH ANNIVERSARY YEAR SINCE THE REDISCOVERY OF ALKALIPHILES BY DR. KOKI HORIKOSHI

Topic Editors:
Masahiro Ito, Toyo University, Japan
Terry Ann Krulwich, Icahn School of Medicine at Mount Sinai, United States

Citation: Ito, M., Krulwich, T. A., eds. (2019). For the Future of Alkaliphiles: 50th Anniversary Year Since the Rediscovery of Alkaliphiles by Dr. Koki Horikoshi. Lausanne: Frontiers Media. doi: 10.3389/978-2-88963-187-2

Table of Contents

frontiers in Microbiology

EDITORIAL
published: 03 September 2019
doi: 10.3389/fmicb.2019.02017

Editorial: For The Future of Alkaliphiles: 50th Anniversary Year Since the Rediscovery of Alkaliphiles by Dr. Koki Horikoshi

Masahiro Ito[1]* *and Terry Ann Krulwich*[2]*

[1] Graduate School of Life Sciences, Toyo University, Gunma, Japan, [2] Icahn School of Medicine at Mount Sinai, New York, NY, United States

Keywords: alkaliphiles, Na^+/H^+ antiporter, alkaliphilicity, ESKAPE pathogens, alkaliphilic streptomyces, indigo-reduced microorganisms, the candidate phylum NPL-UPA2, the cedars

Editorial on the Research Topic

For The Future of Alkaliphiles: 50th Anniversary Year Since the Rediscovery of Alkaliphiles by Dr. Koki Horikoshi

OPEN ACCESS

Edited by:
Thulani Peter Makhalanyane, University of Pretoria, South Africa

Reviewed by:
Brian E. Jones, Retired, Leidschendam, Netherlands

***Correspondence:**
Masahiro Ito
masairo.ito@toyo.jp
Terry Ann Krulwich
terry.krulwich@gmail.com

Specialty section:
This article was submitted to Extreme Microbiology, a section of the journal Frontiers in Microbiology

Received: *26 June 2019*
Accepted: *19 August 2019*
Published: *03 September 2019*

Citation:
Ito M and Krulwich TA (2019) Editorial: For The Future of Alkaliphiles: 50th Anniversary Year Since the Rediscovery of Alkaliphiles by Dr. Koki Horikoshi. Front. Microbiol. 10:2017. doi: 10.3389/fmicb.2019.02017

Dr. Koki Horikoshi, one of the founders of the International Society for Extremophiles (ISE), its first president and founding editor of the journal Extremophiles, passed away on the 16th of March 2016. Dr. Horikoshi devoted his time as a researcher to understanding the molecular basis for microbial survival under extreme conditions and leaves behind an enduring legacy as a pioneer of extremophile research. He is particularly famous for rediscovering alkaliphiles (alkaline-loving microorganisms), for leading multiple studies on their physiology and adaptive mechanisms, and for successfully industrializing a number of alkaliphilic enzymes. Dr. Horikoshi was a consummate academic and leader, deeply devoted to the development of research institutions such as the renowned Japanese Agency for Marine-Earth Science and Technology (JAMSTEC). He was also a highly personable man, dedicated to his family, country and the mentoring of young academics. Thanks to his immense contributions, Japan is a global leader in several areas of extremophile research, including alkaliphile and hyperthermophile microbiology.

Dr. Horikoshi received several awards for his scientific contributions, including the prestigious Medal of Honor with Purple Ribbon from the Japanese Government (1987), the Gold Medal from the International Institute of Biotechnology by Prince Michael of Kent at the Royal Society, London (1991), the Honda Prize (1993), and the Japan Academy Prize (2006).

The first encounter between Dr. Horikoshi and alkaliphiles dates back 50 years (Horikoshi and Akiba, 1982; Horikoshi, 2016). At the end of October 1968, he visited Florence in Italy and the sight of the Renaissance architecture, so different from that of Japan, helped to develop and crystallize his ideas regarding unknown microorganisms living in different extreme environments.

When he returned to Japan, he initiated a new program of research on alkaliphilic organisms. There followed nearly 50 years of research of alkaliphilic microbiology during which time over two thousand relevant research papers have been published. Dr. Horikoshi and his coworkers have made substantial contributions in this field and their pioneering work has established a solid baseline for exploring the molecular basis of alkaliphilic adaptation.

It is because of this vast legacy of research that we decided to honor Dr. Horikoshi by assembling a Research Topic on alkaliphilic microbiology. These articles cover a wide range of topics and provide new insights into alkaliphilicity.

Aino et al. review structural changes in bacterial communities during indigo fermentations, which occur under alkaline anaerobic conditions, and discuss the stability of the microflora. The authors consider the role of the microflora and how diversity plays an important role in maintaining the reduced state of long-term indigo fermentation. The second review by Matsuno et al. focuses on Mitchell's chemiosmotic theory and the inconsistencies of ATP production of alkaliphiles in highly alkaline environments. Several variations on efficient ATP production and adaptation of bacteria to alkaline environments are noted. Finally, the authors discuss the cytochrome c-related "H^+ capacitor mechanism" is as an alkaline adaptation strategy. The third review by the Ito et al. evaluates our understanding of bacterial and archaeal Mrp-type Na^+/H^+ antiporters. The authors consider the ion transport pathway of Mrp, which is known to play an important role in pathogens. The primary article by Suzuki et al. presents interesting results from the first metagenome assembled genome (MAG) and *in-situ* gene expression data of the candidate phylum NPL-UPA2 in a serpentinization site called The Cedars. Terra et al. investigated the ethnopharmacological healing of alkaline/radon in soils from the Boho region of Northern Ireland and isolated a new *Streptomyces* sp. which grew at high alkaline pH and was resistant to gamma radiation. *In vitro* testing of isolates also yielded important results in inhibiting ESKAPE pathogens. The research article by Takahashi et al. showed that BpOF4_01690, a monocistronic small hydrophobic protein of the alkaliphilic microorganism *Bacillus pseudofirmus*, plays an essential role in oxidative phosphorylation under highly alkaline conditions. Yang et al. generated chimeras of the NhaD-type Na^+/H^+ antiporters NhaD1 and NhaD2 of halotolerant and alkaliphilic *Halomonas* sp. Y2 and demonstrated functional changes and responses to pH. The studies by Fujinami and Ito both dealt with CsaB-deficient mutants involved in the anchoring of S-layer homology (SLH) domain-containing proteins of alkaliphilic *Bacillus pseudofirmus* to the cell surface and investigated cell surface proteins and the mechanism of "alkaliphilicity."

AUTHOR CONTRIBUTIONS

MI and TK are co-editors of the Research Topic and discussed the writing.

ACKNOWLEDGMENTS

We thank our authors for their outstanding contributions and are delighted to present this Research Topic in Frontiers in Microbiology. It is our wish that the ideas shared in the review articles and the primary data reported in this e-book will contribute to advancing our understanding of alkaliphilic microorganisms. We hope that the field of alkaliphilic microorganisms, that Dr. Horikoshi established, will continue to develop over the next 50 years.

REFERENCES

Horikoshi, K. (2016). Chapter 4 "Alkaliphilesm," in *Extremophiles, Where it All Began* (Tokyo: Springer), 53–55. doi: 10.1007/978-4-4321-55408-0

Horikoshi, K., and Akiba, T. (1982). "Preface", in *Alkalophilic Microorganisms, a New Microbial World* (Berlin, Heidelberg, NY: Springer-Verlag).

Conflict of Interest Statement: The authors declare that the research was conducted in the absence of any commercial or financial relationships that could be construed as a potential conflict of interest.

frontiers in Microbiology

REVIEW
published: 23 November 2017
doi: 10.3389/fmicb.2017.02325

Mrp Antiporters Have Important Roles in Diverse Bacteria and Archaea

Masahiro Ito[1,2], Masato Morino[1,3] and Terry A. Krulwich[3]*

[1] Graduate School of Life Sciences, Toyo University, Gunma, Japan, [2] Bio-Nano Electronics Research Center, Toyo University, Kawagoe, Japan, [3] Department of Pharmacological Sciences, Icahn School of Medicine at Mount Sinai, New York, NY, United States

Mrp (Multiple resistance and pH) antiporter was identified as a gene complementing an alkaline-sensitive mutant strain of alkaliphilic *Bacillus halodurans* C-125 in 1990. At that time, there was no example of a multi-subunit type Na^+/H^+ antiporter comprising six or seven hydrophobic proteins, and it was newly designated as the monovalent cation: proton antiporter-3 (CPA3) family in the classification of transporters. The Mrp antiporter is broadly distributed among bacteria and archaea, not only in alkaliphiles. Generally, all Mrp subunits, *mrpA–G*, are required for enzymatic activity. Two exceptions are Mrp from the archaea *Methanosarcina acetivorans* and the eubacteria *Natranaerobius thermophilus*, which are reported to sustain Na^+/H^+ antiport activity with the MrpA subunit alone. Two large subunits of the Mrp antiporter, MrpA and MrpD, are homologous to membrane-embedded subunits of the respiratory chain complex I, NuoL, NuoM, and NuoN, and the small subunit MrpC has homology with NuoK. The functions of the Mrp antiporter include sodium tolerance and pH homeostasis in an alkaline environment, nitrogen fixation in *Schizolobium meliloti*, bile salt tolerance in *Bacillus subtilis* and *Vibrio cholerae*, arsenic oxidation in *Agrobacterium tumefaciens*, pathogenesis in *Pseudomonas aeruginosa* and *Staphylococcus aureus*, and the conversion of energy involved in metabolism and hydrogen production in archaea. In addition, some Mrp antiporters transport K^+ and Ca^{2+} instead of Na^+, depending on the environmental conditions. Recently, the molecular structure of the respiratory chain complex I has been elucidated by others, and details of the mechanism by which it transports protons are being clarified. Based on this, several hypotheses concerning the substrate transport mechanism in the Mrp antiporter have been proposed. The MrpA and MrpD subunits, which are homologous to the proton transport subunit of complex I, are involved in the transport of protons and their coupling cations. Herein, we outline other recent findings on the Mrp antiporter.

Keywords: alkaliphile, cation/proton antiporter, Mrp, complex I, multi-subunit antiporter, *Bacillus*, *Thermomicrobium*

OPEN ACCESS

Edited by:
Baolei Jia,
Chung-Ang University, South Korea

Reviewed by:
Saori Kosono,
The University of Tokyo, Japan
Sung Gyun Kang,
Korea Institute of Ocean Science and Technology, South Korea

****Correspondence:***
Masahiro Ito
masahiro.ito@toyo.jp

Specialty section:
This article was submitted to Extreme Microbiology, a section of the journal Frontiers in Microbiology

Received: *27 August 2017*
Accepted: *10 November 2017*
Published: *23 November 2017*

Citation:
Ito M, Morino M and Krulwich TA (2017) Mrp Antiporters Have Important Roles in Diverse Bacteria and Archaea. Front. Microbiol. 8:2325. doi: 10.3389/fmicb.2017.02325

DIVERSITY OF Na^+/H^+ ANTIPORTERS

The Na^+/H^+ antiporter is a secondary active transporter that utilizes the proton motive force to efflux intracellular sodium ions (Padan et al., 2005; Krulwich et al., 2011; Fuster and Alexander, 2014; Padan and Landau, 2016). It is a widely distributed membrane protein, and studies of it are being conducted in eukaryotic-derived NHE families as well as bacterial-derived NhaA families

(Wakabayashi et al., 1997; Orlowski and Grinstein, 2004; Padan, 2014; Padan and Landau, 2016). The main physiological roles of the Na^+/H^+ antiporter are intracellular pH homeostasis and Na^+ efflux. Na^+ efflux by the Na^+/H^+ antiporter plays a critical role for sodium circulation inside and outside the cell because many bacteria, including marine bacteria, utilize both the proton motive force and sodium motive force (Zilberstein et al., 1982; Padan and Schuldiner, 1994; Vimont and Berche, 2000; Dibrov, 2005; Krulwich et al., 2011).

NHE, a mammalian Na^+/H^+ exchanger, is a group of 12-transmembrane membranes protein with multiple isoforms (Wakabayashi et al., 1997; Orlowski and Grinstein, 2011; Padan and Landau, 2016). The antiporters designated as NHE1–NHE5 are localized in the cell plasma membrane, while NHE6–NHE9 are present in the membranes of intracellular organelles (Ohgaki et al., 2011; Fuster and Alexander, 2014). Furthermore, NHE has a hydrophilic domain on the carboxyl-terminal side exposed to the cytoplasm. The interaction between this hydrophilic domain and calcineurin, which is a Ca^{2+}-dependent serine/threonine protein phosphatase, is reportedly involved in intracellular pH homeostasis and is crucial for NHE ion transport activity (Wakabayashi et al., 1997; Pang et al., 2001; Hisamitsu et al., 2012). In NHE 1, it has been reported that enzymatic activity is activated in response to various stimuli including hormones, growth factors, and mechanical stress (Wakabayashi et al., 1997; Hisamitsu et al., 2012). Mammalian NHE has high homology with the bacterial NhaP family, while it has low homology with the bacterial NhaA family, a member of the bacterial Na^+/H^+ antiporter family (Waditee et al., 2001; Resch et al., 2011; Padan and Landau, 2016). In addition, the NhaP antiporter family has been shown to have a large hydrophilic domain at its carboxy-terminal side like NHE (Waditee et al., 2001; Mourin et al., 2017).

In general, bacteria have multiple Na^+/H^+ antiporters that are thought to exert appropriate responses to the ambient conditions of the growth environment and its associated stresses (Padan et al., 2005; Krulwich et al., 2011; Padan, 2014; Preiss et al., 2015). For example, *Escherichia coli* has three major Na^+/H^+ antiporters designated as NhaA, NhaB, and ChaA. It has been shown that NhaA is expressed as a response to the stress associated with alkaline pH and sodium ions in *E. coli* (Padan et al., 2001, 2005; Padan, 2014; Padan and Landau, 2016). Furthermore, NhaA is activated in alkaline pH while NhaB retains activity only in neutral pH; therefore, NhaA is thought to play a central role in the adaptation of *E. coli* to an alkaline environment. In addition to these findings, it has been shown that ChaA is a Ca^{2+}/H^+ antiporter and MdfA is a multidrug/proton antiporter that retains Na^+/H^+ antiport activity (Ivey et al., 1993; Shijuku et al., 2002; Lewinson et al., 2003).

DISCOVERY OF THE Mrp GENE CLUSTER

Mrp was first discovered in work on an alkaline-sensitive strain of alkaliphilic *Bacillus halodurans* C-125 in Kudo et al. (1990). It was found that the gene cluster encoded a Na^+/H^+ antiporter (Hamamoto et al., 1994). The *mrp* gene cluster of *B. halodurans* C-125 comprises seven *mrp* genes (*mrpABCDEFG*), and the expressed proteins are predicted, from the amino acid sequence, to all be membrane proteins (**Figure 1** and **Table 1**). The Mrp antiporter has been suggested to function as a complex of multiple membrane proteins (Kajiyama et al., 2007; Morino et al., 2008). Apart from the maintenance of cytoplasmic pH, the Mrp complex has various other physiological roles in different species, such as bile acid resistance in *Bacillus subtilis* and *Vibrio cholera* (Ito et al., 1999; Dzioba-Winogrodzki et al., 2009), Na^+ homeostasis/tolerance in *B. subtilis* (Ito et al., 1999; Kosono et al., 1999; Ito et al., 2000), sporulation in *B. subtilis* (Kosono et al., 2000), plant infection in *Sinorhizobium meliloti* (Putnoky et al., 1998), pathogenesis in *Pseudomonas aeruginosa* (Kosono et al., 2005) and arsenic resistance in *Agrobacterium tumefaciens* (Kashyap et al., 2006).

PHYLOGENETIC ANALYSIS OF THE Mrp GENE CLUSTER

The Mrp antiporter has been found in alkaliphilic bacteria as well as in many other bacteria and archaea. Genome analyses in a wide range of microorganisms clarified that the structure of the *mrp* gene cluster is diverse (**Figure 2**) (Swartz et al., 2005; Krulwich et al., 2009). Because of its distinctive properties, Mrp antiporter systems have been classified in their own category, cation: proton antiporter-3 (CPA3), in the transporter classification system (Saier et al., 2009, 2016). So far, the *mrp* gene cluster has been classified into three groups. Group 1 antiporters are composed of seven *mrp* genes, and it is found in many *Bacillus* spp. and in *Staphylococcus aureus*. Group 2 has a *mrp* gene cluster *(mrpA'CDEFG*) of six genes. This group belongs to bacteria such as *Pseudomonas aeruginosa* and *Vibrio cholerae*, in which it appears that the *mrpA* gene is fused with the *mrpB* gene encoding a fusion protein (Kosono et al., 2005; Swartz et al., 2005; Dzioba-Winogrodzki et al., 2009). *Sinorhizobium meliloti* has two sets of *mrp* (alias *pha*) gene clusters, one belongs to Group 1 (Pha2) and the other belongs to Group 2 (Pha1) (Putnoky et al., 1998; Yamaguchi et al., 2009). The *mrp* gene cluster belonging to Group 3 has each subunit, but the gene order is irregular. For example, the *mrp* of cyanobacteria has two *mrpB* genes, and the gene sequence in the gene cluster is as follows: *mrpCDCDEFGBB* (Waditee et al., 2001).

Staphylococcus aureus has been shown to have two sets of group 1 type *mrp* (alias *mnh*) gene clusters, *mnh1* and *mnh2*. *mnh1* has been found to encode the Na^+/H^+ antiporter; however, the function of the product encoded by *mnh2* remains unknown (Swartz et al., 2007). Similarly, genomic analyses have revealed that alkaliphilic *Bacillus clausii* and the marine bacterium *Oceanobacillus iheyensis* have two sets of *mrp* gene clusters (Krulwich and Ito, 2013). However, there are no reported examples of the physiological and functional differences between them. In addition, analysis of many microbial genomes has revealed three *mrp* gene clusters. For example, *Microbacterium*

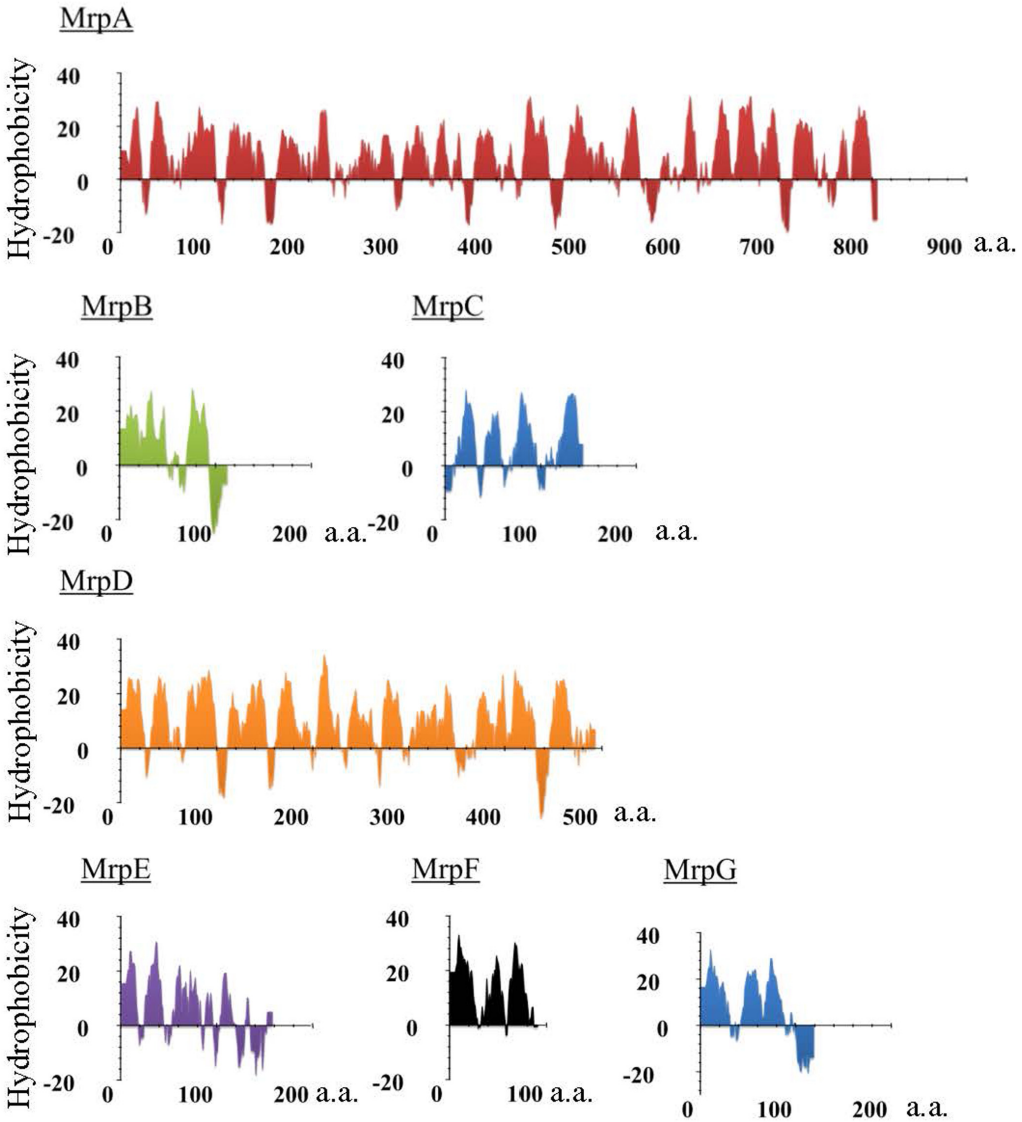

FIGURE 1 | Hydropathy profile of the Mrp subunits derived from alkaliphilic *B. pseudofirmus* OF4. The hydropathy profile of the Mrp subunits derived from *B. pseudofirmus* OF4 was predicted using Kyte and Doolittle method. The vertical axis represents the degree of hydrophobicity, and the horizontal axis represents the number of amino acids (a.a.).

sp. TS-1 has three sets of Mrp gene clusters, two of them (locus tags, MTS1_01879-01874 and MTS1_02182-02187) belong to Group 2 and the third one (locus tags, MTS1_02374-02382; *mrpFGBCDDAE*) belongs to Group 3 (Fujinami et al., 2013) and hyperthermophilic archaeon, *Thermococcus onnurineus* NA1 has three sets of Mrp gene clusters, all of which (locus tags; TON_0272-0266, TON_1574-1580, TON_1025-1031) belong to Group 1 (Lim et al., 2010).

The *mrp* gene cluster of anaerobic bacteria has a gene structure that is markedly different from that of aerobic bacterial-derived *mrp* gene clusters. For example, the *mrp* gene cluster of *Natranaerobius thermophilus* retains three overlapping *mrpB* genes (Mesbah et al., 2009). In addition, in the *mrp* gene cluster derived from *Synechocystis* sp. PCC 6803, duplication of the *mrpD* and *mrpC* genes as well as the *mrpB* gene is observed (Krulwich et al., 2009). Similar gene arrangements have been reported in other cyanobacteria (Fukaya et al., 2009).

RELATIONSHIP BETWEEN Mrp ANTIPORTER AND RESPIRATORY CHAIN COMPLEX I

MrpA and MrpD subunits have homology with the respiratory chain complex I subunit (**Figures 3**, **4**) (Mathiesen and Hägerhäll, 2003; Moparthi and Hägerhäll, 2011; Moparthi et al., 2014). The respiratory chain complex I is a protein complex belonging to the electron transport system, which oxidizes NADH supplied

TABLE 1 | Molecular weight of each Mrp subunit derived from the *B. pseudofirmus* OF4 strain and the estimated number of transmembrane regions.

Protein	Estimated molecular weight (kDa)	Estimated transmembrane segment number[a]
MrpA	89.4	19–21
MrpB	15.8	4
MrpC	12.2	3
MrpD	54.4	14
MrpE	18.4	2–3
MrpF	10.0	3
MrpG	13.1	3
Total	213.4	48–51

[a]*The estimated transmembrane segment number was estimated by using the TMHMM (http://www.cbs.dtu.dk/services/TMHMM/) and HMMTOP (http://www.enzim.hu/hmmtop/) programs, which are transmembrane segment prediction software, for the amino acid sequence of each subunit. MrpA was predicted as a 21-transmembrane proten by TMMTOP and TMHMM, but as a 19-transmembrane proteins by ConPred II. MrpE was predicted as a two-transmembrane protein by TMMTOP and TMHMM, but as a three-transmembrane one by ConPred II.*

from the TCA cycle, among other sources. It reduces quinone and effluxes protons from the cell. The NuoL, NuoM, and NuoN subunits, which are subunits of the respiratory chain complex I in *E. coli*, have been analyzed because of homology with the Mrp antiporter subunit (Nakamaru-Ogiso et al., 2003a,b, 2010; Torres-Bacete et al., 2007; Ohnishi et al., 2010; Torres-Bacete et al., 2011; Sperling et al., 2016; Morino et al., 2017). These three Nuo subunits have highly conserved glutamic acid residues and lysine residues (**Figure 4**), which have been suggested to be the core of the proton transport pathway, based on the crystal structure of *E. coli* (Baranova et al., 2007; Efremov and Sazanov, 2011; Sazanov, 2014). In MrpA and MrpD subunits, these charged residues are highly conserved, and it has been reported that glutamate residues are also conserved at the same position in *B. subtilis* and *B. pseudofirmus* OF4. Mrp antiporters have been shown to be essential for antiport activity in various settings (Kosono et al., 2005; Kajiyama et al., 2009; Morino et al., 2010).

The crystal structure of the *E. coli* respiratory chain complex I revealed that the NuoL subunit had a long helical chain at its carboxy terminus (Efremov and Sazanov, 2011; Sazanov, 2014). Analysis of a long-chain, helix-deficient strain of the NuoL subunit in *E. coli* respiratory chain complex I indicated that this helix is indispensable for proton transport, complex formation, and NADH oxidation (Ohnishi et al., 2010; Efremov and Sazanov, 2011; Torres-Bacete et al., 2011; Sazanov, 2014). This suggested that it functions as a "piston" that couples oxidation and quinone reduction to proton transport. The MrpA subunit has an additional transmembrane region at the carboxy terminus similar to the NuoL subunit. In addition, part of the MrpA carboxy terminus has high sequence homology with MrpB, as shown by PSI-Blast analysis; it is speculated that it is a characteristic region only of the Mrp antiporter (Krulwich et al., 2009). Recently, it was reported that the MrpA carboxy-terminal region of *B. pseudofirmus* OF4 has indispensable roles in antiport function (Morino et al., 2017).

FEATURES OF THE Mrp ANTIPORTER FROM ALKALIPHILIC *Bacillus pseudofirmus* OF4

Within the Mrp antiporter family, the *B. pseudofirmus* OF4-derived Mrp antiporter (Bp–Mrp) has undergone advanced functional and structural analyses that has revealed: (1) formation of the complex and role of each subunit; (2) identification of amino acid residues with important structural and functional roles, as determined by site-specific functional analysis; (3) analysis of the specific C-terminal region of MrpA; and (4) purification and reconstitution of the Bp–Mrp antiporter.

Formation of Bp–Mrp Complex and the Role of Each Mrp Subunit

Bp–Mrp was estimated to form a membrane protein complex expressed from seven *mrp* genes. Bp–Mrp expressed in *E. coli* was separated by Blue native PAGE (BN-PAGE); subsequently, each Mrp subunit was detected by Western blotting to investigate whether the Mrp antiporter successfully formed a complex (Morino et al., 2008). The results confirmed formation of a Mrp complex (220 kDa), estimated to be a monomer consisting of all subunits, as well as a MrpABCDEFG complex (400 kDa), estimated to be a dimer. A MrpABCD subcomplex comprising MrpA, B, C, and D subunits was also detected; this subcomplex was shown not to be catalytically active (Morino et al., 2008).

Mutants were also constructed, each with the deletion of a single *mrp*, to enable investigation of the role of each Mrp subunit in complex formation (Morino et al., 2008). The results showed that, in the membrane fraction of the *mrpD* deletion mutant, no other Mrp subunits were detected. On the other hand, Mrp subunits other than MrpE could be detected in the membrane of the *mrpE*-deficient mutant. From BN-PAGE analysis, it was confirmed that the Mrp subunits other than MrpE form a complex in the *mrpE* deletion mutant. These results suggested that the MrpD subunit is important in the formation of the Bp–Mrp complex. It may have a role as a scaffold when other Mrp subunits are expressed in the cell membrane. By contrast, the MrpE subunit appears to be incorporated in the final step of complex formation and possibly plays an important role in ensuring that the Mrp complex can exert its full activity. However, in *B. subtilis*, it was reported that MrpE is dispensable for ion transport activity (Yoshinaka et al., 2003; Morino et al., 2008).

Site-Directed Amino Acid Substitution Mutagenesis and Identification of Residues in the Bp–Mrp Antiporter Important for Ion Transport

The Bp–Mrp antiporter was studied to identify amino acid residues within it that are important for ion transport and Mrp complex formation. Site-specific mutations were introduced at amino acid residues conserved between Mrp homologs. In MrpA and MrpD subunits, mutations were also introduced

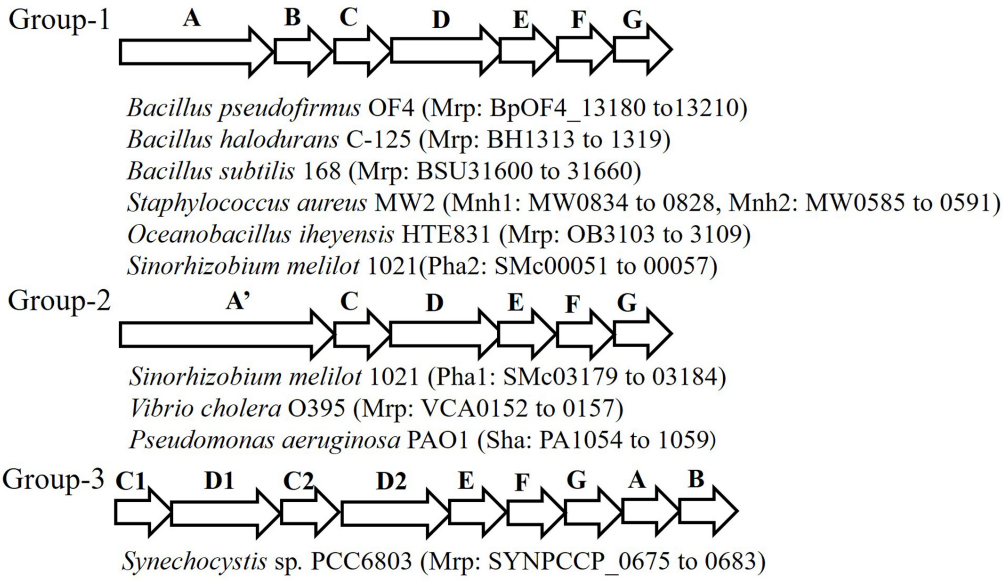

FIGURE 2 | Schematic of the diversity of the *mrp* gene cluster in several bacteria. This figure depicts the genetic structure of the *mrp* gene cluster of each bacterium. The locus tag numbers of each Mrp subunit gene are listed after the bacterial name. *mrpA'* is a gene involving the fusion of *mrpA* and *mrpB*.

at amino acid residues conserved among the NuoL, NuoM, and NuoN subunits of the homologous *E. coli* respiratory chain complex I (Morino et al., 2010). The mutants were expressed in the *E. coli* KNabc strain, in which three major Na^+/H^+ antiporter genes (*nhaA*, *nhaB*, and *chaA*) are deleted; subsequently, the mutants were tested for sodium sensitivity, antiport activity, and their complex formation ability. Each amino acid substitution mutant could be classified into one of eight categories from each phenotype. **Figure 5** shows a summary of the phenotype at each mutation site (Morino et al., 2010, 2017). Mutants classified into categories 1 and 2 have been shown to affect Mrp complex formation. Mutants classified into categories 3–7 were confirmed to undergo complex formation but resulted in a decrease in Na^+/H^+ antiport activity and a decrease in the sodium-sensitive complementary activity of *E. coli* KNabc.

In category 1, MrpD-D75A, MrpD-R258A, MrpE-T113Y, and MrpF-D32A were studied, and their Na^+/H^+ antiport activity was found to be completely lost, with no Mrp complex detected.

In category 2, MrpA-P677G, MrpB-P37G, and MrpC-Q70A mutations were associated with the retention of Na^+/H^+ antiport activity but failure to show formation of the Mrp complex monomer in BN-PAGE analysis. These mutations were assumed to destabilize the interaction between the MrpABCD subcomplex and each of the MrpE, MrpF, and MrpG subunits.

MrpA-E140A, MrpA-K223A, MrpA-K299A, MrpA-G392R, MrpA-R773A, MrpA-E780A, MrpD-E137A, MrpD-K219A, and MrpE-T113A, which are classified into category 3, retained the Mrp complex but Na^+/H^+ antiport activity was completely lost.

MrpC-G82I and MrpF-R33A, classified into category 4, exhibited Na^+/H^+ antiport activity that was decreased by approximately 70% compared with wild-type activity.

In category 5, the apparent K_m for Na^+ of Na^+/H^+ antiport activity increased in MrpA-H230K, MrpA-H700A, MrpA-H700K, MrpA-H700W, MrpA-P702G, MrpD-F136G, MrpD-E137D, MrpD-F341A, and MrpE-P114G. Because MrpA-H230, MrpA-H700, MrpA-P702, and MrpD-F136 are adjacent to charged residues essential for activity (MrpA-K223, MrpA-E687, MrpD-E137), along with these charged residues, it is assumed that they are involved in ion transport along with these chargeable residues. Although the functional roles of MrpD-F341 and MrpE-P114 are unknown, it is inferred that the low-molecular-weight subunit MrpE may also be involved in ion transport.

MrpB-F41A and MrpC-T75A, classified into category 6, retained normal Na^+/H^+ antiport activity but could not completely complement the sodium sensitivity in *E. coli* KNabc.

Na^+/H^+ antiport activity was completely inactivated in MrpG-P81A, classified into category 7. Surprisingly, however, the sodium sensitivity of *E. coli* KNabc could be complemented similarly to that of the wild type (see below).

The amino acid substitution mutants that showed the same phenotype as the wild type were designated into category 8.

In MrpA-E140, MrpA-K223, MrpD-E137A, and MrpD-K219A, there was conservation of not only the MrpA and MrpD subunits but also the respiratory chain complex I subunit. They are extremely important for Na^+/H^+ antiport activity, and it was speculated from the complex I crystal structure that the respiratory chain complex I also participates in ion transport. In addition, MrpG-P81A in category 7 did not retain Na^+/H^+ antiport activity, but it was able to complement the sodium sensitivity of the *E. coli* KNabc. This suggested that the Mrp antiporter of MrpG-P81A has

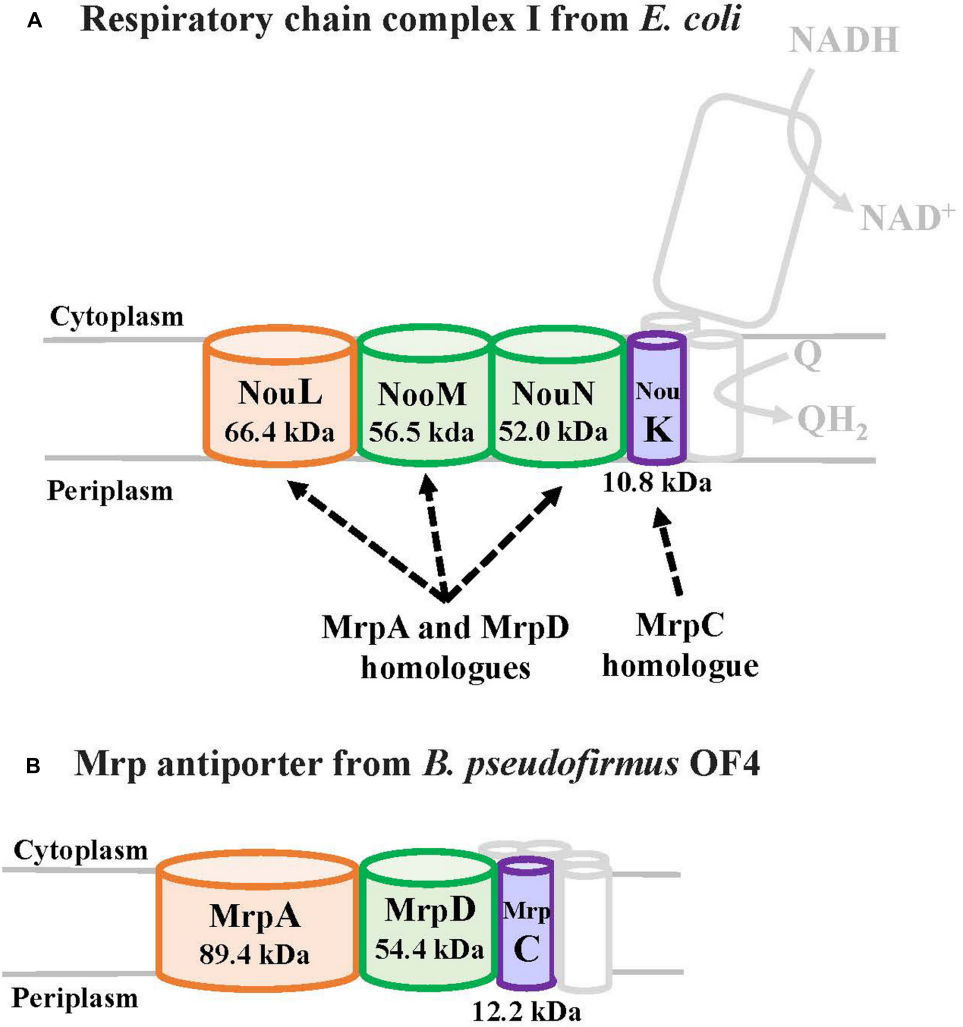

FIGURE 3 | The *E. coli* respiratory chain complex I subunit with homology to the Mrp subunit. **(A)** Schematic diagram of respiratory chain complex I. The NuoL, NuoM, and NuoN subunits of the *E. coli* respiratory chain complex I have homology with the MrpA and MrpD subunits of the Mrp antiporter, and the NuoK subunits also have partial homology with the MrpC subunit (Mathiesen and Hägerhäll, 2003). **(B)** Schematic diagram of Mrp antiporter.

Na^+ efflux capacity coupled with the transport of ions other than protons. For example, membrane potential-driven sodium ion excretion may occur concomitantly with the transport of anions. However, the phenotype of MrpG-P81A, including the possibility of having other transporting substrates, is only a hypothesis at this point; therefore, more detailed analyses are needed.

Functional Analysis of the Carboxyl-Terminal Region of the MrpA Subunit of the Bp–Mrp Antiporter

The C-terminal region of MrpA, which has similarity to the MrpB subunit, is conserved. This region of MrpA is not preserved in the respiratory chain complex I subunit; therefore, it is predicted to have unique functions and roles in the Mrp antiporter. Site-specific mutations involving substitutions at highly conserved amino acid residues located in the C-terminal region of Bp–MrpA were introduced (Morino et al., 2017). Two glutamic acid residues are conserved in the C-terminal region of MrpA, as has been reported by Kosono et al. (2006) using *B. subtilis* Mrp. In the Bp–Mrp antiporter, these acidic residues (MrpA-E687 and MrpA-E778) are also essential for Na^+/H^+ antiport activity. In addition, MrpA-P683G retained normal Na^+/H^+ antiport activity; however, the monomeric MrpABCDEFG complex could not be detected by BN-PAGE analysis. The fact that the same phenotype is also found in MrpB-P37G and MrpC-Q70A suggested that the C-terminal region of MrpA is a region through which interactions with low-molecular-weight Mrp subunits, MrpB and MrpC, occur. In addition, it was observed that Na^+/H^+ antiport activity decreased in MrpA-P702G and MrpA-R773A mutants, suggesting that the C-terminal region of MrpA has an important function in ion transport.

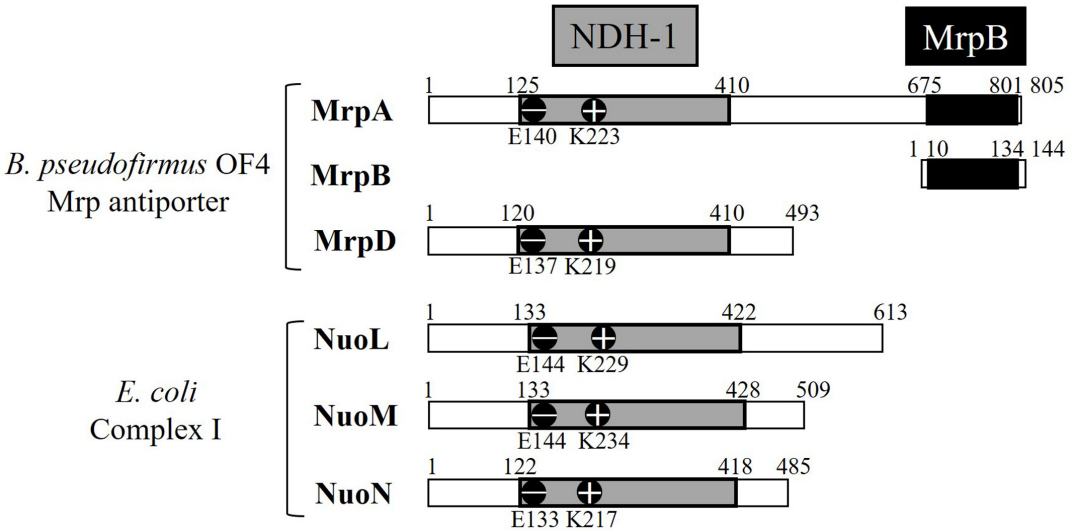

FIGURE 4 | Common regions preserved between the *B. pseudofirmus* OF4 Mrp antiporter and the *E. coli* complex I subunit. MrpA, MrpD, NuoL, NuoM, and NuoN proteins having homology to each other are described. The NDH-1 domains conserved among them are represented in gray. The glutamic acid residue (–) and the lysine residue (+) conserved in the NDH-1 region are shown in the schematic. The C-terminal region of MrpA, in black, has been found to be systematically related to the MrpB protein by PSI-Blast analysis (Mathiesen and Hägerhäll, 2003).

The above results also showed that the C-terminal region of MrpA has important functions not only in ion transport but also in interactions between subunits. Furthermore, the C-terminal region of MrpA is a region unique to the Mrp antiporter and is suggested to be involved in Na^+/H^+ antiport activity.

Purification and Reconstitution of the Bp–Mrp Antiporter

Reports have been published on structural analyses of various protein complexes by techniques such as single-particle analysis by the observation of high-purity samples under an electron microscope. For example, in the respiratory chain complex I, an L-shaped structure has been observed under an electron microscope (Holt et al., 2003). The structure of very large macromolecules, such as the H-ring, which is a component of the basal body of bacterial flagella, has also been clarified by microscopic observation (Terashima et al., 2010). High-purity samples of target proteins and complexes thereof are indispensable for such advanced structural analysis. As such, purification of the Mrp antiporter derived from *B. pseudofirmus* OF4 was investigated. The Mrp antiporter expressed in *E. coli* was purified by TALON resin and reconstituted into an artificial lipid membrane for further confirmation of its Na^+/H^+ antiport activity. In the reconstituted membrane, the proton motive force required for Mrp antiporter activation was generated by F_oF_1-ATPase derived from *Bacillus* sp. PS3, which was simultaneously reconstituted. This report is the first to describe the successful reconstitution of purified bacterial-derived Mrp antiporter into proteoliposomes retaining Na^+/H^+ antiport activity (Morino et al., 2014).

Mrp ANTIPORTERS FROM GRAM-POSITIVE BACTERIA OTHER THAN ALKALIPHILIC *Bacillus* spp.

It was shown that the *mrp* (alias *sha*) gene cluster of *B. subtilis* encodes a Na^+/H^+ antiporter and plays a major role in the mechanism of sodium tolerance of *B. subtilis* (Ito et al., 1999; Kosono et al., 1999). Various *mrp*-deficient strains have been produced in *B. subtilis*, and it has been reported from their analysis that the *mrpF* gene contributes to bile acid tolerance (Ito et al., 1999). Furthermore, it has been reported that sodium efflux capacity is retained in a *mrpE* gene-deficient strain (Yoshinaka et al., 2003; Morino et al., 2008). *S. aureus* Mrp is expected to be a target protein of a novel antibiotic because since growth inhibition of *S. aureus* is suppressed by inhibiting translation of the *mrpD* gene using antisense RNA (Ji et al., 2001).

Polyextremophiles such as *Natranaerobius thermophilus* are halophilic, alkaliphilic, and thermophilic bacteria that grow optimally at 3.5 M Na^+, pH 9.5, and 53°C–55°C (Mesbah et al., 2009). This bacterium has at least eight electrogenic $Na^+(K^+)/H^+$ antiporters. One of them, Nt-Nha, has homology with MrpA and MrpD, the two large subunits of group 1. In previous studies, none of the Mrp antiporters exhibited antiport activity with MrpA or MrpD alone. However, this Nt-Nha alone showed Na^+ $(K^+)/H^+$ antiport activity. This supports the suggestion that MrpA and MrpD are critical for the ion transport pathway for antiporters in the CPA 3 family (Krulwich et al., 2009). Recently, study of the Mrp complex of *Methanosarcina acetivorans* from the archaeal domain suggested that MrpA is essential for antiport activity and that the MrpA/MrpD subcomplex is critical for catalyzing Na^+/H^+ antiport activity (Jasso-Chavez et al., 2017). This is the second example showing that the Mrp complex

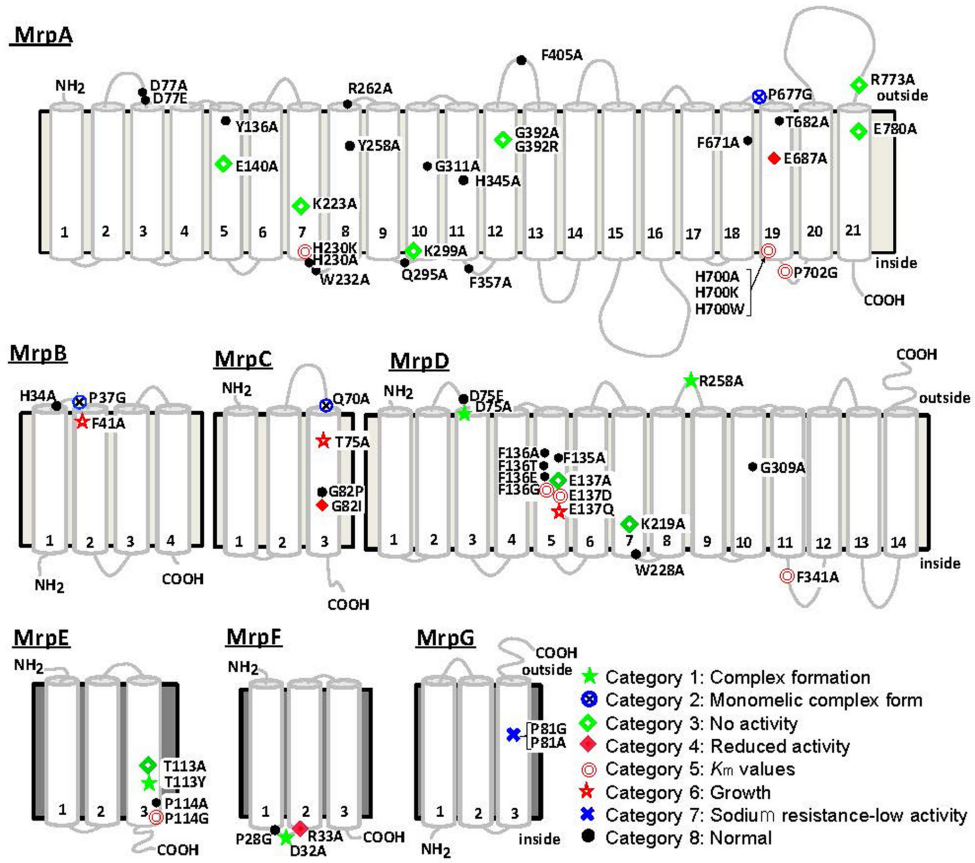

FIGURE 5 | Transmembrane topology of Bp–Mrp proteins and positions of mutations. Transmembrane segments predicted by ConPred II, HMMTOP, and TMHMM (available online) were used in the analyses of the secondary structure predictions for each Mrp subunit. ●, positions at which the mutations complemented an antiporter-deficient *E. coli* KNabc transformant and exhibited normal Na^+/H^+ antiport activity; ★, mutations that affected the level of Mrp proteins in the membrane; ◊, mutations that led to loss of the Na^+/H^+ antiport activity and loss of Na^+ tolerance; ♦, mutations that decreased the Na^+/H^+ antiport activity, without an effect on growth of the *E. coli* transformant; ⊚, mutations that affected the K_m values of Mrp-dependent antiport activity; ☆, mutations that affected transformant cell growth; ⊗, mutations that affected Mrp complex formation; × , the two mutants in MrpG-P81 that had a unique phenotype.

exhibits antiport activity even without all its subunits. The consequence of this observation is discussed in Section "Mrp Antiporters from Archaea".

Mrp ANTIPORTERS FROM GRAM-NEGATIVE BACTERIA

Sinorhizobium meliloti has two sets of *mrp* (*pha*) gene clusters, one belongs to Group 1 (Pha2) and the other belongs to Group 2 (Pha1). The *pha1* gene cluster (SMc03179 to 03184) was identified as a mutation insertion site in a potassium-sensitive strain of the root nodule bacterium *Sinorhizobium meliloti* (Putnoky et al., 1998). *Sinorhizobium*, a symbiotic bacterium, retains potassium-dependent alkaline pH homeostasis ability; however, *pha1* deficiency reportedly causes a loss of alkaline environmental adaptability (Putnoky et al., 1998). Detailed analysis revealed that the *pha1* gene cluster derived from *Sinorhizobium* encodes a K^+ (Na^+)/H^+ antiporter (Putnoky et al., 1998; Yamaguchi et al., 2009).

The *mrp* (*sha*) gene cluster has also been found in *Pseudomonas aeruginosa,* and it reportedly encodes a Na^+/H^+ antiporter. Furthermore, inactivation of the *mrp* gene cluster in *P. aeruginosa* PAO1 has been reported to cause reduced pathogenicity (Kosono et al., 2005).

In a study of the group 2 Mrp antiporter of *Vibrio cholerae*, expressed in a major Na^+/H^+ antiporter-deficient *E. coli* strain, EP432, this antiporter had Na^+ (Li^+, K^+)/H^+ antiport activity with optimal pH at pH 9–9.5 and also showed bile acid resistance in *E. coli* (Dzioba-Winogrodzki et al., 2009). A deletion mutant of the group 2 *mrp* gene cluster from *V. cholerae* revealed mutant physiological defects in nitrogen metabolism, cell motility, and biofilm formation (Aagesen et al., 2016).

In a study of the group 1 Mrp antiporter of *Thermomicrobium roseum* expressed in a Na^+/H^+ antiporter-deficient *E. coli* strain, KNabc, it was surprisingly found that this antiporter does not catalyze monovalent cation/proton antiport similar to the Mrp antiporters studied to date but catalyzes Ca^{2+}/H^+ antiport in *E. coli* membrane vesicles (Morino and Ito, 2012). This bacterium was isolated from an alkaline

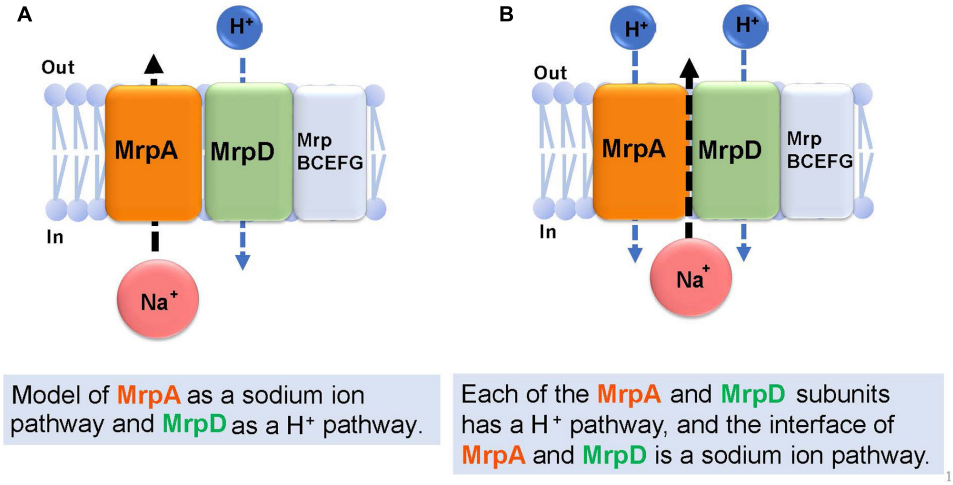

FIGURE 6 | Ion transport pathway model of the Mrp antiporter. Based on previous studies, there are two kinds of ion transport models for the Mrp antiporter. The first model **(A)** proposes MrpA as a Na^+ pathway and MrpD as a H^+ pathway (Moparthi et al., 2011). The second model **(B)** proposes that each of the MrpA and MrpD subunits has a H^+ pathway, and the interface of MrpA and MrpD is a Na^+ pathway (Sazanov, 2014).

hot spring in Yellowstone National Park (Jackson et al., 1973).

The gene cluster of a halotolerant cyanobacterium, *Aphanothece halophytica mrp* (Ah-mrp), which belongs to group 3, has a characteristic genetic structure that retains two *mrpD* genes in an unusual gene order (*mrpCD1D2EFGAB*). Study of a sodium-sensitive mutant *E. coli* expressing Ah-mrp showed that the cyanobacterial Mrp antiporter functions as a Na^+/H^+ antiporter and also contributes to sodium tolerance (Fukaya et al., 2009). Another cyanobacterium, *Anabaena* sp. strain PCC 7120, has a group 1 Mrp antiporter. Growth and photosynthesis were inhibited in a *mrpA* mutant cyanobacterial strain (Blanco-Rivero et al., 2009).

It has been reported that the group 1 Mrp antiporters of the halotolerant alkaliphile *Halomonas* sp. Y2 and the halophilic and alkaliphilic *Halomonas zhadongensis* had Na^+ (Li^+, K^+)/H^+ antiporter functions under alkaline conditions (Meng et al., 2014; Cheng et al., 2016).

Mrp ANTIPORTERS FROM ARCHAEA

Many Mrp complexes are annotated not only from bacterial genomes but also from archaea (Swartz et al., 2005). The Mrp antiporter from the methanogen *Methanosarcina acetivorans* C2A is composed of a group 1 type of gene cluster comprising seven genes (*mrpABCDEFG*). This Mrp complex plays an essential role in efficient ATP synthesis and optimal growth under conditions with low concentrations of acetic acid in the environment (Jasso-Chavez et al., 2013). Deficiency of a major Na^+/H^+ antiporter in *E. coli* cells expressing only MrpA from *M. acetivorans* was still associated with Na^+/H^+ antiport activity, although the K_m value was as low as ca. 50 mM (Jasso-Chavez et al., 2017). The details of these transport mechanisms have not yet been reported.

In hyperthermophilic archaea, Mrp is reported to be involved in the metabolic system of hydrogen production (Kim et al., 2010; Lim et al., 2010, 2014; Schut et al., 2013; Boyd et al., 2014). It is known that a hydrogenase involved in hydrogen production of *Pyrococcus furiosus* and *Thermococcus onnurineus* NA1 is composed of a [NiFe] hydrogenase domain (Mbh) and Mrp type Na^+/H^+ antiporter domain. However, there have been no reports of measurement of Mrp antiport activity in these strains/species (Schut et al., 2013). Given the considerable interest in this issue, it is anticipated that the details of the Mrp antiporter that is involved in archaeal energy production will soon be clarified.

PREDICTION OF THE ION TRANSPORT ROUTE IN THE Mrp ANTIPORTER

Figure 6 describes the prediction of the ion transport pathway of the Mrp antiporter (Moparthi and Hägerhäll, 2011; Moparthi et al., 2011; Sazanov, 2015). Owing to homology with the respiratory chain complex I subunit, it is expected that the Mrp antiporter is involved in an ion transport pathway via the MrpA and MrpD subunits. MrpA has the closest homology to the NuoL subunit of complex I and MrpD has the closest homology to complex I NuoM and NuoN subunits. Because the *nuoL*-deficient strain does not transport Na^+, it was suggested that the NuoL subunit is involved in Na^+ transport (Marreiros et al., 2014). Moreover, Na^+ transport was previously demonstrated by the NuoL subunit (Steuber, 2003; Gemperli et al., 2007). Moparthi et al. (2011) reported that the phenotypes of an *mrpA*-deficient strain and *mrpD*-deficient strain of *B. subtilis* are complemented by expressing, respectively, NuoL and NuoN of the respiratory chain complex I of *E. coli*. These observations prompted them to propose that MrpA transports Na^+, whereas MrpD transports H^+ in the

opposite direction, resulting in antiport activity (Moparthi et al., 2011) (**Figure 6A**).

Sazanov reported that, at the interface between the transmembrane region (TM 5) of the MrpA subunit and the transmembrane region (TM 12) of the MrpD subunit, a Na^+ transport pathway forms, which was confirmed from a homology model of the MrpA and MrpD subunits constructed from the results of crystal structure analyses of NuoL, NuoM, and NuoN (Sazanov, 2015). This model proposes that highly conserved glutamic acid residues in the NDH-1 motif that is common to the NuoL, NuoM, NuoN, MrpA, and MrpD subunits, function as cation binding sites (**Figure 6B**).

PROSPECTS FOR THE FUTURE

It is expected that the details of Mrp antiporter complexes and their functional properties as revealed by recent studies will help to reveal the mechanisms of adaptation to environmental conditions not only in alkaliphilic bacteria but also in many other bacteria. The Mrp antiporter plays a major role in the environmental adaptation of a wide variety of bacteria, including pathogenic ones. Furthermore, because Mrp is only found in prokaryotes, studies may lead to the development of inhibitors of the roles of Mrp antiporters that are important in the host.

AUTHOR CONTRIBUTIONS

The idea for this review paper was proposed by MI, MM, and TK. The paper was written by MI and TK.

FUNDING

This work was supported in part by research grant GM28454 from the National Institute of General Medical Sciences (to TK) as well as JSPS KAKENHI Grant Number 15K07012 (to MI).

REFERENCES

Aagesen, A. M., Schubiger, C. B., Hobson, E. C., Dibrov, P., and Hase, C. C. (2016). Effects of chromosomal deletion of the operon encoding the multiple resistance and pH-related antiporter in *Vibrio cholerae*. *Microbiology* 162, 2147–2158. doi: 10.1099/mic.0.000384

Baranova, E. A., Morgan, D. J., and Sazanov, L. A. (2007). Single particle analysis confirms distal location of subunits NuoL and NuoM in *Escherichia coli* complex I. *J. Struct. Biol.* 159, 238–242. doi: 10.1016/j.jsb.2007.01.009

Blanco-Rivero, A., Leganes, F., Fernandez-Valiente, E., and Fernandez-Pinas, F. (2009). *mrpA* (all1838), a gene involved in alkali and Na^+ sensitivity, may also have a role in energy metabolism in the cyanobacterium *Anabaena* sp. strain PCC 7120. *J. Plant Physiol.* 166, 1488–1496. doi: 10.1016/j.jplph.2009.03.007

Boyd, E. S., Schut, G. J., Adams, M. W., and Perers, J. W. (2014). Hydrogen metabolism and the evolution of biological respiration. *Microbe* 9, 361–367. doi: 10.1128/microbe.9.361.1

Cheng, B., Meng, Y., Cui, Y., Li, C., Tao, F., Yin, H., et al. (2016). Alkaline response of a halotolerant alkaliphilic halomonas strain and functional diversity of its Na^+ (K^+)/H^+ antiporters. *J. Biol. Chem.* 291, 26056–26065. doi: 10.1074/jbc.M116.751016

Dibrov, P. (2005). The sodium cycle in *Vibrio cholerae*: riddles in the dark. *Biochemistry* 70, 150–153. doi: 10.1007/s10541-005-0094-3

Dzioba-Winogrodzki, J., Winogrodzki, O., Krulwich, T. A., Boin, M. A., Hase, C. C., and Dibrov, P. (2009). The *Vibrio cholerae* Mrp system: cation/proton antiport properties and enhancement of bile salt resistance in a heterologous host. *J. Mol. Microbiol. Biotechnol.* 16, 176–186. doi: 10.1159/000119547

Efremov, R. G., and Sazanov, L. A. (2011). Structure of the membrane domain of respiratory complex I. *Nature* 476, 414–420. doi: 10.1038/nature10330

Fujinami, S., Takeda, K., Onodera, T., Satoh, K., Sano, M., Narumi, I., et al. (2013). Draft genome sequence of sodium-independent alkaliphilic *Microbacterium* sp. strain TS-1. *Genome Announc.* 1:e01043-31. doi: 10.1128/genomeA.01043-13

Fukaya, F., Promden, W., Hibino, T., Tanaka, Y., Nakamura, T., and Takabe, T. (2009). An Mrp-like cluster in the halotolerant cyanobacterium *Aphanothece halophytica* functions as a Na^+/H^+ antiporter. *Appl. Environ. Microbiol.* 75, 6626–6629. doi: 10.1128/AEM.01387-09

Fuster, D. G., and Alexander, R. T. (2014). Traditional and emerging roles for the SLC9 Na^+/H^+ exchangers. *Pflugers Arch.* 466, 61–76. doi: 10.1007/s00424-013-1408-8

Gemperli, A. C., Schaffitzel, C., Jakob, C., and Steuber, J. (2007). Transport of Na^+ and K^+ by an antiporter-related subunit from the *Escherichia coli* NADH dehydrogenase I produced in *Saccharomyces cerevisiae*. *Arch. Microbiol.* 188, 509–521. doi: 10.1007/s00203-007-0272-3

Hamamoto, T., Hashimoto, M., Hino, M., Kitada, M., Seto, Y., Kudo, T., et al. (1994). Characterization of a gene responsible for the Na^+/H^+ antiporter system of alkalophilic *Bacillus* species strain C-125. *Mol. Microbiol.* 14, 939–946. doi: 10.1111/j.1365-2958.1994.tb01329.x

Hisamitsu, T., Nakamura, T. Y., and Wakabayashi, S. (2012). Na^+/H^+ exchanger 1 directly binds to calcineurin A and activates downstream NFAT signaling, leading to cardiomyocyte hypertrophy. *Mol. Cell. Biol.* 32, 3265–3280. doi: 10.1128/MCB.00145-12

Holt, P. J., Morgan, D. J., and Sazanov, L. A. (2003). The location of NuoL and NuoM subunits in the membrane domain of the *Escherichia coli* complex I: implications for the mechanism of proton pumping. *J. Biol. Chem.* 278, 43114–43120. doi: 10.1074/jbc.M308247200

Ito, M., Guffanti, A. A., Oudega, B., and Krulwich, T. A. (1999). *mrp*, a multigene, multifunctional locus in *Bacillus subtilis* with roles in resistance to cholate and to Na^+ and in pH homeostasis. *J. Bacteriol.* 181, 2394–2402.

Ito, M., Guffanti, A. A., Wang, W., and Krulwich, T. A. (2000). Effects of nonpolar mutations in each of the seven *Bacillus subtilis mrp* genes suggest complex interactions among the gene products in support of Na^+ and alkali but not cholate resistance. *J. Bacteriol.* 182, 5663–5670. doi: 10.1128/JB.182.20.5663-5670.2000

Ivey, D. M., Guffanti, A. A., Zemsky, J., Pinner, E., Karpel, R., Padan, E., et al. (1993). Cloning and characterization of a putative Ca^{2+}/H^+ antiporter gene from *Escherichia coli* upon functional complementation of Na^+/H^+ antiporter-deficient strains by the overexpressed gene. *J. Biol. Chem.* 268, 11296–11303.

Jackson, T. J., Ramaley, R. F., and Meinsche, W. G. (1973) *Thermomicrobium*, a new genus of extremely thermophilic bacteria. *Int. J. Syst. Bacteriol.* 23, 28–36. doi: 10.1099/00207713-23-1-28

Jasso-Chavez, R., Apolinario, E. E., Sowers, K. R., and Ferry, J. G. (2013). MrpA functions in energy conversion during acetate-dependent growth of *Methanosarcina acetivorans*. *J. Bacteriol.* 195, 3987–3994. doi: 10.1128/JB.00581-13

Jasso-Chavez, R., Diaz-Perez, C., Rodriguez-Zavala, J. S., and Ferry, J. G. (2017). Functional role of MrpA in the MrpABCDEFG Na^+/H^+ antiporter complex from the Archaeon *Methanosarcina acetivorans*. *J. Bacteriol.* 199:e00662-16. doi: 10.1128/JB.00662-16

Ji, Y., Zhang, B., Van Horn, S. F., Warren, P., Woodnutt, G., Burnham, M. K., et al. (2001). Identification of critical staphylococcal genes using conditional phenotypes generated by antisense RNA. *Science* 293, 2266–2269. doi: 10.1126/science.1063566

Kajiyama, Y., Otagiri, M., Sekiguchi, J., Kosono, S., and Kudo, T. (2007). Complex formation by the *mrpABCDEFG* gene products, which constitute a principal Na^+/H^+ antiporter in *Bacillus subtilis*. *J. Bacteriol.* 189, 7511–7514. doi: 10.1128/JB.00968-07

Kajiyama, Y., Otagiri, M., Sekiguchi, J., Kudo, T., and Kosono, S. (2009). The MrpA, MrpB and MrpD subunits of the Mrp antiporter complex in *Bacillus subtilis*

contain membrane-embedded and essential acidic residues. *Microbiology* 155, 2137–2147. doi: 10.1099/mic.0.025205-0

Kashyap, D. R., Botero, L. M., Lehr, C., Hassett, D. J., and Mcdermott, T. R. (2006). A Na^+:H^+ antiporter and a molybdate transporter are essential for arsenite oxidation in *Agrobacterium tumefaciens*. *J. Bacteriol.* 188, 1577–1584. doi: 10.1128/JB.188.4.1577-1584.2006

Kim, Y. J., Lee, H. S., Kim, E. S., Bae, S. S., Lim, J. K., Matsumi, R., et al. (2010). Formate-driven growth coupled with H_2 production. *Nature* 467, 352–355. doi: 10.1038/nature09375

Kosono, S., Haga, K., Tomizawa, R., Kajiyama, Y., Hatano, K., Takeda, S., et al. (2005). Characterization of a multigene-encoded sodium/hydrogen antiporter (*sha*) from *Pseudomonas aeruginosa*: its involvement in pathogenesis. *J. Bacteriol.* 187, 5242–5248. doi: 10.1128/JB.187.15.5242-5248.2005

Kosono, S., Kajiyama, Y., Kawasaki, S., Yoshinaka, T., Haga, K., and Kudo, T. (2006). Functional involvement of membrane-embedded and conserved acidic residues in the ShaA subunit of the multigene-encoded Na^+/H^+ antiporter in *Bacillus subtilis*. *Biochim. Biophys. Acta* 1758, 627–635. doi: 10.1016/j.bbamem.2006.04.012

Kosono, S., Morotomi, S., Kitada, M., and Kudo, T. (1999). Analyses of a *Bacillus subtilis* homologue of the Na^+/H^+ antiporter gene which is important for pH homeostasis of alkaliphilic *Bacillus* sp. C-125. *Biochim. Biophys. Acta* 1409, 171–175. doi: 10.1016/S0005-2728(98)00157-1

Kosono, S., Ohashi, Y., Kawamura, F., Kitada, M., and Kudo, T. (2000). Function of a principal Na^+/H^+ antiporter, ShaA, is required for initiation of sporulation in *Bacillus subtilis*. *J. Bacteriol.* 182, 898–904. doi: 10.1128/JB.182.4.898-904.2000

Krulwich, T. A., Hicks, D. B., and Ito, M. (2009). Cation/proton antiporter complements of bacteria: Why so large and diverse? *Mol. Microbiol.* 74, 257–260. doi: 10.1111/j.1365-2958.2009.06842.x

Krulwich, T. A., and Ito, M. (2013). "Prokaryotic alkaliphiles," in *The Prokaryotes*, 4th Edn, eds E. Rosenberg, E. F. Delong, F. Thompson, S. Lory, and E. Stackebrandt (New York, NY: Springer).

Krulwich, T. A., Sachs, G., and Padan, E. (2011). Molecular aspects of bacterial pH sensing and homeostasis. *Nat. Rev. Microbiol.* 9, 330–343. doi: 10.1038/nrmicro2549

Kudo, T., Hino, M., Kitada, M., and Horikoshi, K. (1990). DNA sequences required for the alkalophily of *Bacillus* sp. strain C-125 are located close together on its chromosomal DNA. *J. Bacteriol.* 172, 7282–7283. doi: 10.1128/jb.172.12.7282-7283.1990

Lewinson, O., Adler, J., Poelarends, G. J., Mazurkiewicz, P., Driessen, A. J., and Bibi, E. (2003). The *Escherichia coli* multidrug transporter MdfA catalyzes both electrogenic and electroneutral transport reactions. *Proc. Natl. Acad. Sci. U.S.A.* 100, 1667–1672. doi: 10.1073/pnas.0435544100

Lim, J. K., Kang, S. G., Lebedinsky, A. V., Lee, J. H., and Lee, H. S. (2010). Identification of a novel class of membrane-bound [NiFe]-hydrogenases in *Thermococcus onnurineus* NA1 by in silico analysis. *Appl. Environ. Microbiol.* 76, 6286–6289. doi: 10.1128/AEM.00123-10

Lim, J. K., Mayer, F., Kang, S. G., and Muller, V. (2014). Energy conservation by oxidation of formate to carbon dioxide and hydrogen via a sodium ion current in a hyperthermophilic archaeon. *Proc. Natl. Acad. Sci. U.S.A.* 111, 11497–11502. doi: 10.1073/pnas.1407056111

Marreiros, B. C., Batista, A. P., and Pereira, M. M. (2014). Respiratory complex I from *Escherichia coli* does not transport Na^+ in the absence of its NuoL subunit. *FEBS Lett.* 588, 4520–4525. doi: 10.1016/j.febslet.2014.10.030

Mathiesen, C., and Hägerhäll, C. (2003). The 'antiporter module' of respiratory chain complex I includes the MrpC/NuoK subunit – a revision of the modular evolution scheme. *FEBS Lett.* 549, 7–13. doi: 10.1016/S0014-5793(03)00767-1

Meng, L., Hong, S., Liu, H., Huang, H., Sun, H., Xu, T., et al. (2014). Cloning and identification of Group 1 mrp operon encoding a novel monovalent cation/proton antiporter system from the moderate halophile *Halomonas zhaodongensis*. *Extremophiles* 18, 963–972. doi: 10.1007/s00792-014-0666-5

Mesbah, N. M., Cook, G. M., and Wiegel, J. (2009). The halophilic alkalithermophile *Natranaerobius thermophilus* adapts to multiple environmental extremes using a large repertoire of Na^+ (K^+)/H^+ antiporters. *Mol. Microbiol.* 74, 270–281. doi: 10.1111/j.1365-2958.2009.06845.x

Moparthi, V. K., and Hägerhäll, C. (2011). "Recruitment of the antiporter module — a key event in complex I evolution," in *A Structural Perspective on Complex I*, ed. L. A. Sazanov (Berlin: Springer), 123–143.

Moparthi, V. K., Kumar, B., Al-Eryani, Y., Sperling, E., Gorecki, K., Drakenberg, T., et al. (2014). Functional role of the MrpA- and MrpD-homologous protein subunits in enzyme complexes evolutionary related to respiratory chain complex I. *Biochim. Biophys. Acta* 1837, 178–185. doi: 10.1016/j.bbabio.2013.09.012

Moparthi, V. K., Kumar, B., Mathiesen, C., and Hägerhäll, C. (2011). Homologous protein subunits from *Escherichia coli* NADH:quinone oxidoreductase can functionally replace MrpA and MrpD in *Bacillus subtilis*. *Biochim. Biophys. Acta* 1807, 427–436. doi: 10.1016/j.bbabio.2011.01.005

Morino, M., and Ito, M. (2012). Functional expression of the multi-subunit type calcium/proton antiporter from *Thermomicrobium roseum*. *FEMS Microbiol. Lett.* 335, 26–30. doi: 10.1111/j.1574-6968.2012.02634.x

Morino, M., Natsui, S., Ono, T., Swartz, T. H., Krulwich, T. A., and Ito, M. (2010). Single site mutations in the hetero-oligomeric Mrp antiporter from alkaliphilic *Bacillus pseudofirmus* OF4 that affect Na^+/H^+ antiport activity, sodium exclusion, individual Mrp protein levels, or Mrp complex formation. *J. Biol. Chem.* 285, 30942–30950. doi: 10.1074/jbc.M110.118661

Morino, M., Natsui, S., Swartz, T. H., Krulwich, T. A., and Ito, M. (2008). Single gene deletions of *mrpA* to *mrpG* and *mrpE* point mutations affect activity of the Mrp Na^+/H^+ antiporter of alkaliphilic *Bacillus* and formation of hetero-oligomeric Mrp complexes. *J. Bacteriol.* 190, 4162–4172. doi: 10.1128/JB.00294-08

Morino, M., Ogoda, S., Krulwich, T. A., and Ito, M. (2017). Differences in the phenotypic effects of mutations in homologous MrpA and MrpD subunits of the multi-subunit Mrp-type Na^+/H^+ antiporter. *Extremophiles* 21, 51–64. doi: 10.1007/s00792-016-0877-z

Morino, M., Suzuki, T., Ito, M., and Krulwich, T. A. (2014). Purification and functional reconstitution of a seven-subunit mrp-type Na^+/H^+ antiporter. *J. Bacteriol.* 196, 28–35. doi: 10.1128/JB.01029-13

Mourin, M., Schubiger, C. B., Resch, C. T., Hase, C. C., and Dibrov, P. (2017). Physiology of the Vc-NhaP paralogous group of cation-proton antiporters in *Vibrio cholerae*. *Mol. Cell. Biochem.* 428, 87–99. doi: 10.1007/s11010-016-2919-3

Nakamaru-Ogiso, E., Kao, M. C., Chen, H., Sinha, S. C., Yagi, T., and Ohnishi, T. (2010). The membrane subunit NuoL(ND5) is involved in the indirect proton pumping mechanism of *Escherichia coli* complex I. *J. Biol. Chem.* 285, 39070–39078. doi: 10.1074/jbc.M110.157826

Nakamaru-Ogiso, E., Sakamoto, K., Matsuno-Yagi, A., Miyoshi, H., and Yagi, T. (2003a). The ND5 subunit was labeled by a photoaffinity analogue of fenpyroximate in bovine mitochondrial complex I. *Biochemistry* 42, 746–754.

Nakamaru-Ogiso, E., Seo, B. B., Yagi, T., and Matsuno-Yagi, A. (2003b). Amiloride inhibition of the proton-translocating NADH-quinone oxidoreductase of mammals and bacteria. *FEBS Lett.* 549, 43–46.

Ohgaki, R., Van, I. S. C., Matsushita, M., Hoekstra, D., and Kanazawa, H. (2011). Organellar Na^+/H^+ exchangers: novel players in organelle pH regulation and their emerging functions. *Biochemistry* 50, 443–450. doi: 10.1021/bi101082e

Ohnishi, T., Nakamaru-Ogiso, E., and Ohnishi, S. T. (2010). A new hypothesis on the simultaneous direct and indirect proton pump mechanisms in NADH-quinone oxidoreductase (complex I). *FEBS Lett.* 584, 4131–4137. doi: 10.1016/j.febslet.2010.08.039

Orlowski, J., and Grinstein, S. (2004). Diversity of the mammalian sodium/proton exchanger SLC9 gene family. *Pflugers Arch.* 447, 549–565. doi: 10.1007/s00424-003-1110-3

Orlowski, J., and Grinstein, S. (2011). Na^+/H^+ exchangers. *Compr. Physiol.* 1, 2083–2100. doi: 10.1002/cphy.c110020

Padan, E. (2014). Functional and structural dynamics of NhaA, a prototype for Na^+ and H^+ antiporters, which are responsible for Na^+ and H^+ homeostasis in cells. *Biochim. Biophys. Acta* 1837, 1047–1062. doi: 10.1016/j.bbabio.2013.12.007

Padan, E., Bibi, E., Ito, M., and Krulwich, T. A. (2005). Alkaline pH homeostasis in bacteria: new insights. *Biochim. Biophys. Acta* 1717, 67–88. doi: 10.1016/j.bbamem.2005.09.010

Padan, E., and Landau, M. (2016). Sodium-proton (Na^+/H^+) antiporters: properties and roles in health and disease. *Met. Ions Life Sci.* 16, 391–458. doi: 10.1007/978-3-319-21756-7_12

Padan, E., and Schuldiner, S. (1994). Molecular physiology of the Na^+/H^+ antiporter in *Escherichia coli*. *J. Exp. Biol.* 196, 443–456.

Padan, E., Venturi, M., Gerchman, Y., and Dover, N. (2001). Na^+/H^+ antiporters. *Biochim. Biophys. Acta* 1505, 144–157. doi: 10.1016/S0005-2728(00)00284-X

Pang, T., Su, X., Wakabayashi, S., and Shigekawa, M. (2001). Calcineurin homologous protein as an essential cofactor for Na^+/H^+ exchangers. *J. Biol. Chem.* 276, 17367–17372. doi: 10.1074/jbc.M100296200

Preiss, L., Hicks, D. B., Suzuki, S., Meier, T., and Krulwich, T. A. (2015). Alkaliphilic bacteria with impact on industrial applications, concepts of early life forms, and bioenergetics of ATP synthesis. *Front. Bioeng. Biotechnol.* 3:75. doi: 10.3389/fbioe.2015.00075

Putnoky, P., Kereszt, A., Nakamura, T., Endre, G., Grosskopf, E., Kiss, P., et al. (1998). The *pha* gene cluster of *Rhizobium meliloti* involved in pH adaptation and symbiosis encodes a novel type of K^+ efflux system. *Mol. Microbiol.* 28, 1091–1101. doi: 10.1046/j.1365-2958.1998.00868.x

Resch, C. T., Winogrodzki, J. L., Hase, C. C., and Dibrov, P. (2011). Insights into the biochemistry of the ubiquitous NhaP family of cation/H^+ antiporters. *Biochem. Cell Biol.* 89, 130–137. doi: 10.1139/o10-149

Saier, M. H. Jr., Reddy, V. S., Tsu, B. V., Ahmed, M. S., Li, C., and Moreno-Hagelsieb, G. (2016). The transporter classification database (TCDB): recent advances. *Nucleic Acids Res.* 44, D372–D379. doi: 10.1093/nar/gkv1103

Saier, M. H. Jr., Yen, M. R., Noto, K., Tamang, D. G., and Elkan, C. (2009). The transporter classification database: recent advances. *Nucleic Acids Res.* 37, D274–D278. doi: 10.1093/nar/gkn862

Sazanov, L. A. (2014). The mechanism of coupling between electron transfer and proton translocation in respiratory complex I. *J. Bioenerg. Biomembr.* 46, 247–253. doi: 10.1007/s10863-014-9554-z

Sazanov, L. A. (2015). A giant molecular proton pump: structure and mechanism of respiratory complex I. *Nat. Rev. Mol. Cell Biol.* 16, 375–388. doi: 10.1038/nrm3997

Schut, G. J., Boyd, E. S., Peters, J. W., and Adams, M. W. (2013). The modular respiratory complexes involved in hydrogen and sulfur metabolism by heterotrophic hyperthermophilic archaea and their evolutionary implications. *FEMS Microbiol. Rev.* 37, 182–203. doi: 10.1111/j.1574-6976.2012.00346.x

Shijuku, T., Yamashino, T., Ohashi, H., Saito, H., Kakegawa, T., Ohta, M., et al. (2002). Expression of chaA, a sodium ion extrusion system of *Escherichia coli*, is regulated by osmolarity and pH. *Biochim. Biophys. Acta* 1556, 142–148. doi: 10.1016/S0005-2728(02)00345-6

Sperling, E., Gorecki, K., Drakenberg, T., and Hagerhall, C. (2016). Functional differentiation of antiporter-like polypeptides in complex I; a site-directed mutagenesis study of residues conserved in MrpA and NuoL but not in MrpD, NuoM, and NuoN. *PLOS ONE* 11:e0158972. doi: 10.1371/journal.pone.0158972

Steuber, J. (2003). The C-terminally truncated NuoL subunit (ND5 homologue) of the Na^+-dependent complex I from *Escherichia coli* transports Na^+. *J. Biol. Chem.* 278, 26817–26822. doi: 10.1074/jbc.M301682200

Swartz, T. H., Ikewada, S., Ishikawa, O., Ito, M., and Krulwich, T. A. (2005). The Mrp system: a giant among monovalent cation/proton antiporters? *Extremophiles* 9, 345–354.

Swartz T. H., Ito, M., Ohira, T., Natsui, S., Hicks, D. B., and Krulwich, T. A. (2007). Catalytic properties of *Staphylococcus aureus* and *Bacillus* members of the secondary cation/proton antiporter-3 (Mrp) family are revealed by an optimized assay in an *Escherichia coli* host. *J. Bacteriol.* 189, 3081–3090. doi: 10.1128/JB.00021-07

Terashima, H., Koike, M., Kojima, S., and Homma, M. (2010). The flagellar basal body-associated protein FlgT is essential for a novel ring structure in the sodium-driven *Vibrio* motor. *J. Bacteriol.* 192, 5609–5615. doi: 10.1128/JB.00720-10

Torres-Bacete, J., Nakamaru-Ogiso, E., Matsuno-Yagi, A., and Yagi, T. (2007). Characterization of the NuoM (ND4) subunit in *Escherichia coli* NDH-1: conserved charged residues essential for energy-coupled activities. *J. Biol. Chem.* 282, 36914–36922. doi: 10.1074/jbc.M707855200

Torres-Bacete, J., Sinha, P. K., Matsuno-Yagi, A., and Yagi, T. (2011). Structural contribution of C-terminal segments of NuoL (ND5) and NuoM (ND4) subunits of complex I from *Escherichia coli*. *J. Biol. Chem.* 286, 34007–34014. doi: 10.1074/jbc.M111.260968

Vimont, S., and Berche, P. (2000). NhaA, an Na^+/H^+ antiporter involved in environmental survival of *Vibrio cholerae*. *J. Bacteriol.* 182, 2937–2944. doi: 10.1128/JB.182.10.2937-2944.2000

Waditee, R., Hibino, T., Tanaka, Y., Nakamura, T., Incharoensakdi, A., and Takabe, T. (2001). Halotolerant cyanobacterium *Aphanothece halophytica* contains an Na^+/H^+ antiporter, homologous to eukaryotic ones, with novel ion specificity affected by C-terminal tail. *J. Biol. Chem.* 276, 36931–36938. doi: 10.1074/jbc.M103650200

Wakabayashi, S., Shigekawa, M., and Pouyssegur, J. (1997). Molecular physiology of vertebrate Na^+/H^+ exchangers. *Physiol. Rev.* 77, 51–74.

Yamaguchi, T., Tsutsumi, F., Putnoky, P., Fukuhara, M., and Nakamura, T. (2009). pH-dependent regulation of the multi-subunit cation/proton antiporter Pha1 system from *Sinorhizobium meliloti*. *Microbiology* 155, 2750–2756. doi: 10.1099/mic.0.028563-0

Yoshinaka, T., Takasu, H., Tomizawa, R., Kosono, S., and Kudo, T. (2003). A *shaE* deletion mutant showed lower Na^+ sensitivity compound to other deletion mutants in the *Bacillus subtilis* sodium/hydrogen antiporter (Sha) system. *J. Biosci. Bioeng.* 95, 306–309. doi: 10.1016/S1389-1723(03)80035-X

Zilberstein, D., Agmon, V., Schuldiner, S., and Padan, E. (1982). The sodium/proton antiporter is part of the pH homeostasis mechanism in *Escherichia coli*. *J. Biol. Chem.* 257, 3687–3691.

Conflict of Interest Statement: The authors declare that the research was conducted in the absence of any commercial or financial relationships that could be construed as a potential conflict of interest.

frontiers in Microbiology

ORIGINAL RESEARCH
published: 01 May 2018
doi: 10.3389/fmicb.2018.00810

The Surface Layer Homology Domain-Containing Proteins of Alkaliphilic *Bacillus pseudofirmus* OF4 Play an Important Role in Alkaline Adaptation via Peptidoglycan Synthesis

Shun Fujinami[1,2]* *and Masahiro Ito*[1,3]

[1] Bio-Nano Electronics Research Centre, Toyo University, Kawagoe, Japan, [2] Department of Chemistry, College of Humanities and Sciences, Nihon University, Tokyo, Japan, [3] Graduate School of Life Sciences, Toyo University, Tokyo, Japan

It is well known that the Na^+ cycle and the cell wall are essential for alkaline adaptation of Na^+-dependent alkaliphilic *Bacillus* species. In *Bacillus pseudofirmus* OF4, surface layer protein A (SlpA), the most abundant protein in the surface layer (S-layer) of the cell wall, is involved in alkaline adaptation, especially under low Na^+ concentrations. The presence of a large number of genes that encode S-layer homology (SLH) domain-containing proteins has been suggested from the genome sequence of *B. pseudofirmus* OF4. However, other than SlpA, the functions of SLH domain-containing proteins are not well known. Therefore, a deletion mutant of the *csaB* gene, required for the retention of SLH domain-containing proteins on the cell wall, was constructed to investigate its physiological properties. The *csaB* mutant strain of *B. pseudofirmus* OF4 had a chained morphology and alkaline sensitivity even under a 230 mM Na^+ concentration at which there is no growth difference between the parental strain and the *slpA* mutant strain. Ultra-thin section transmission electron microscopy showed that a *csaB* mutant strain lacked an S-layer part, and its peptidoglycan (PG) layer was disturbed. The *slpA* mutant strain also lacked an S-layer part, although its PG layer was not disturbed. These results suggested that the surface layer homology domain-containing proteins of *B. pseudofirmus* OF4 play an important role in alkaline adaptation via peptidoglycan synthesis.

Keywords: alkaliphiles, alkaline environmental adaptation mechanisms, peptidoglycan synthesis, S-layer protein, SLH domain, *Bacillus*

OPEN ACCESS

Edited by:
Andreas Teske, University of North Carolina at Chapel Hill, United States

Reviewed by:
Xiuzhu Dong, Institute of Microbiology (CAS), China
Isao Yumoto, National Institute of Advanced Industrial Science and Technology, Japan

***Correspondence:**
Shun Fujinami
fujinami.shun@nihon-u.ac.jp

Specialty section:
This article was submitted to Extreme Microbiology, a section of the journal Frontiers in Microbiology

Received: *15 December 2017*
Accepted: *10 April 2018*
Published: *01 May 2018*

Citation:
Fujinami S and Ito M (2018) The Surface Layer Homology Domain-Containing Proteins of Alkaliphilic Bacillus pseudofirmus OF4 Play an Important Role in Alkaline Adaptation via Peptidoglycan Synthesis. Front. Microbiol. 9:810. doi: 10.3389/fmicb.2018.00810

INTRODUCTION

The typical Na^+-dependent alkaliphilic *Bacillus* species require Na^+ for growth and motility (Krulwich et al., 2001, 2011; Ito et al., 2011). In *Bacillus pseudofirmus* OF4, the growth at pH 7.5 requires a higher Na^+ concentration (at least 25 mM and, optimally more than 50 mM) than growth at pH 10.5 (10 mM Na^+), and the motility at pH 7.0 also requires a higher Na^+ concentration (100 mM) than motility at pH 10 (5 mM Na^+) (Gilmour et al., 2000; Fujinami et al., 2007b). The well-characterized alkaline adaptation system, which is also called the Na^+ cycle, is composed of

Na^+ efflux (e.g., Na^+/H^+ antiporters) and influx (e.g., voltage-gated Na^+ channels, Na^+-dependent flagellar motor stators, and Na^+-dependent solute transporters) components (Ito et al., 2004a,b; Fujinami et al., 2007a,b; Morino et al., 2014).

Since protoplasts of Na^+-dependent alkaliphilic *Bacillus halodurans* C-125 are unstable in an alkaline environment, the cell wall is also considered to be important for alkaline adaptation (Aono et al., 1992). The cell wall of *B. halodurans* C-125 consist of peptidoglycan (PG) and non-peptidoglycan components. The PG is the A1γ type, identical to that of neutrophilic *B. subtilis* (Aono et al., 1984). The cell wall has two major kinds of acidic polymers called teichuronic acid (TUA) and teichuronopeptide (TUP) (Aono, 1985). TUP is a polymer in which an acidic polypeptide binds covalently to polyglucuronic acid. The abundance of the acidic surface polymers, as well as the accompanying high anionic charge and proton accumulation around the cell, are thought to prevent hydroxide ion penetration (Aono et al., 1992). Therefore, TUA and TUP are considered to contribute to cell adaptation to an alkaline environment. It was reported that the amounts of TUA and TUP are enhanced in cells grown at an alkaline pH, as compared to those grown at neutral pH (Aono, 1985), and the mutants deficient in TUA and TUP have lost alkaliphilicity (Aono and Ohtani, 1990; Aono et al., 1995, 1999; Ito and Aono, 2002).

In *B. pseudofirmus* OF4, the lag phase of a mutant deficient in the surface layer (S-layer) protein A (SlpA) was increased at pH 11, especially under low Na^+ concentrations (i.e., 5 mM), and lacked an S-layer region (Gilmour et al., 2000). A schematic diagram of the putative S-layer structure of *B. pseudofirmus* OF4 is shown in **Figure 1**. The genome sequence of *B. pseudofirmus* OF4 codes for 17 S-layer homology (SLH) domain-containing proteins, including SlpA (**Table 1**). Although these genes do not have an operon structure, their gene products are thought to be retained in the cell surface in the same manner via its SLH domain. Most of the gene products were presumed to have three SLH domains immediately after the N-terminal signal peptide or at the C-terminus. It was proposed that the SLH domain binds to secondary cell wall polymers (SCWPs) (Schäffer and Messner, 2005). The SlpA, which has three SLH domains, is the most abundant protein in the cell wall of *B. pseudofirmus* OF4. The isoelectric points (p*I*) of the extracellular and cell wall proteins of alkaliphiles are reported to be relatively low (Janto et al., 2011). The SlpA protein, which has a p*I* of 4.36 (without signal peptide), contains few arginine and lysine residues. It is thought that the SlpA protein also causes a proton accumulation and prevention of hydroxide ion penetration, similarly to TUA and TUP (Gilmour et al., 2000; Krulwich et al., 2011; Krulwich and Ito, 2013).

The functions of the SLH domain-containing proteins other than SlpA are not well known. We hypothesized that SLH domain-containing proteins, other than SlpA, involved in alkaline adaptation. However, investigating the effect of numerous SLH domain-containing proteins on alkaline adaptation one by one requires an enormous amount of time, and there is also the possibility that it will not appear as a phenotype unless multiple genes are deleted. Therefore, a *csaB* deletion mutant of *B. pseudofirmus* OF4 was constructed. CsaB itself does not contain the SLH domain, but it was reported to act as an SCWP modification polysaccharide pyruvyl transferase (Kern et al., 2010), and it is required for the retention of SLH domain-containing proteins to the SCWPs of the *Bacillus anthracis* cell wall (Mesnage et al., 2000). It is thought that the SLH domain binds to the CsaB-catalyzed pyruvylation moieties of SCWP. Therefore, even in *B. pseudofirmus* OF4, the CsaB mutant strain was considered to show the phenotype in the case where the cell wall had no SLH domain-containing proteins at all.

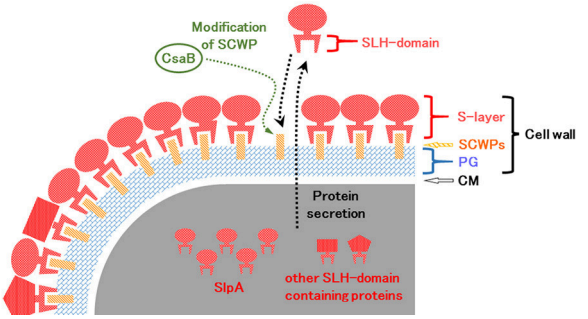

FIGURE 1 | Schematic diagram of the putative surface layer structure of *B. pseudofirmus* OF4. The cell wall of *B. pseudofirmus* OF4 is composed of PG, SCWPs, and an S-layer. It was suggested that the SLH domain-containing proteins are translated in the cytoplasm and secreted to the extracellular space by a protein secretion system. Secreted SLH domain-containing proteins are anchored to SCWPs that are modified by the polysaccharide pyruvyl transferase CsaB via the SLH domain. S-layer, surface layer; SLH, surface layer homology; SCWPs, secondary cell wall polymers; PG, peptidoglycan; CM, cytoplasmic membrane.

In this study, we report microscopic observations of the cell morphology, cell wall components, and cell growth at different pH values of *B. pseudofirmus* OF4 and its S-layer protein mutant strains to elucidate the effects of SLH domain-containing proteins on alkaline adaptation and cell morphology.

MATERIALS AND METHODS

Bacterial Strains and Media

The bacterial strains and plasmids used in this study are listed in **Table 2**. *Escherichia coli* strains were grown routinely in lysogeny broth (LB) medium (Sambrook et al., 1989). *B. pseudofirmus* OF4-811M and its derivative cells were grown in alkaline complex medium (pH 8.0, 9.0, 10, and 11) at 30°C with shaking at 200 rpm (Fujinami et al., 2007b). The Na^+ concentration of alkaline complex medium is 230 mM in all cases.

Construction of the *csaB* Deletion Strain CS54 and Its Restoration Strain CS54-R

A DNA fragment containing the upstream and downstream regions of the *csaB* gene was obtained by the gene SOEing (gene splicing by overlap extension) method (Horton, 1997) using the primers listed in **Table 3**. Two independent polymerase chain reactions (PCRs) were performed with *B. pseudofirmus* OF4-811M chromosomal DNA as the template and the primer pairs CS1F/CS2R-SS and CS3F-SS/CS4R. The two purified PCR

TABLE 1 | SLH domain-containing proteins of *B. pseudofirmus* OF4 suggested from the genome sequence.

Gene name		UniprotKB accession number	Protein function	Mass	Graphicval view of SLH domain
BpOF4_05935		D3FZK7	SLH domain-containing esterase	74,603	
BpOF4_16655	*ushA*	D3FQK4	Protein ushA (Two S-layer domains, UDP-sugar hydrolase, 5′-nucleotidase)	70,385	
BpOF4_06105	*lytC*	D3FZP1*	N-acetylmuramoyl-L-alanine amidase containing SLH domains	50,569	
BpOF4_05925		D3FZK5	5′-nucleotidase and SLH domain-containing protein	89,763	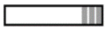
BpOF4_06055	*amyA*	D3FZN1	Alpha-amylase/pullulanase (1,4-alpha-D-glucan glucanohydrolase, Pullulanase) with SLH domain	293,461	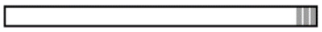
BpOF4_06130	*amyA2*	D3FZP6	Alpha-amylase/pullulanase (1,4-alpha-D-glucan glucanohydrolase, Pullulanase)	83,651	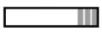
BpOF4_20104		D3G0Z4	SLH domain-containing hydrolase, putative beta-lactamase	59,025	
BpOF4_05815		D3FZI3*	SLH domain protein, peptidoglycan NAcGlcam'ase	71,137	
BpOF4_06075	slpA	D3FZN5	S-layer glycoprotein, contains three N-terminal SLH domains	96,883	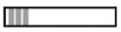
BpOF4_06080		D3FZN6*	Cell wall-associated hydrolase containing three SLH domains	36,064	
BpOF4_05835		D3FZI7	SLH domain, hydrolase	39,553	
BpOF4_06085		D3FZN7	Alkaline serine proteinase and SLH-domain protein	67,576	
BpOF4_05820		D3FZI4	SLH domain protein	82,212	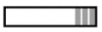
BpOF4_05825		D3FZI5	SLH-domain protein	24,467	
BpOF4_05940		D3FZK8	Uncharacterized protein	40,418	
BpOF4_21149		D3G1J9	S-layer like protein	45,236	
BpOF4_05920		D3FZK4	Putative S-layer protein	44,960	

This table was prepared from data extracted from UniprotKB.

**Putative SLH domain-containing peptidoglycan hydrolases The white box represents the putative gene product. The N-terminus is on the left side and the C-terminus is on the right side. Gray box shows the location of SLH domain in putative gene product.*

products were used as templates for a second PCR with the primer pair CS1F and CS4R. The purified product of this reaction was cloned into the *Sma*I digested plasmid pGEM7Zf(+), which yielded pGEMC1. The mutation-free pEMC1 insert was digested with the endonucleases *Kpn*I and *Bam*HI, and the purified inserted DNA fragment was cloned into the *Kpn*I- and *Bam*HI-digested plasmid pG$^+$host4, yielding pG4C4, which was then transformed into *B. pseudofirmus* OF4-811M protoplasts. The protocol of the protoplast transformation and isolation of single and double crossover candidates was previously reported (Ito et al., 1997; Fujinami et al., 2007a). Among the erythromycin-sensitive double crossover candidates, a *csaB* deletion was confirmed by PCR with the primer pairs CS0F/CS4R and CS1F/CS5R. The *csaB* deletion strain was designated CS54.

For restoration of the *csaB* gene at its native location, a DNA fragment containing the *csaB* gene was obtained by PCR with *B. pseudofirmus* OF4-811M chromosomal DNA as the template and the primer pair CS1F and CS4R. The purified product of this reaction was cloned into *Sma*I-digested pMW118, which yielded pMWCR. The mutation-free pMWCR insert was digested with endonucleases *Kpn*I and *Bam*HI and the purified *csaB* fragment was cloned into a *Kpn*I- and *Bam*HI-digested pG$^+$host4, yielding pG4CR, which was transformed into *B. pseudofirmus* OF4-CS54 protoplasts. The protocol for the isolation of single and double crossover candidates was previously reported (Ito et al., 1997). From the restoration strain candidates, which were grown in alkaline complex medium (pH10), *csaB* restoration at its native location was confirmed by PCR using the primer pairs CS0F/CS4R and CS1F/CS5R. The *csaB* restoration strain was designated CS54-R.

Microscopic Observation of Cell Wall Synthesis of *B. pseudofirmus* OF4 by Fluorescent Vancomycin Staining

Bacillus pseudofirmus OF4-811M and its derivative cells were grown at pH 8.0, as described above, and then stained with afluorescent vancomycin staining method (Tiyanont et al., 2006) modified for alkaliphilic *Bacillus* species cells, as described by Fujinami et al. (2011). Fluorescence microscopic images were obtained with a Leica FW4000 Fluorescence Workstation (Leica Microsystems AG, Heerbrugg, Switzerland) and processed with Photoshop CS software (Adobe Systems Incorporated, San Jose, CA, USA).

Sodium Dodecyl Sulfate Polyacrylamide Gel Electrophoresis (SDS-Page) of Proteins of *B. pseudofirmus* OF4

Bacillus pseudofirmus OF4-811M and its derivative cells were grown at pH 8.0, as described above. Then, 50 mL of culture

TABLE 2 | Bacterial strains and plasmids used in this study.

Strain and plasmid	Genotype and description	Source and reference
***E. coli* STRAINS**		
DH5αMCR	F- *mcrA*Δ*1 (mrr-hsd RMS-mcrBC) Φ80dlacZ* Δ*(lacZYAargF) U169 deoR recA1 endA1 supE44* λ*thi-1 gyr-496 relA1*	Stratagene
XL1-Blue MRF'	Δ*(mcrA)183* Δ*(mcrCB-hsdSMR-mrr)173 endA1 supE44 thi-1 recA1 gyrA96 relA1 lac [F'proAB lacIqZDM15 Tn10 (Tetr)]*	GIBCO/BRL
***BACILLUS PSEUDOFIRMUS* OF4 STRAINS**		
811M	wild-type, Met^-	Clejan et al., 1989
RG21	811MΔ*slpA*::Spc^R	Gilmour et al., 2000
CS54	811M, *csaB* deletion	This study
CS54-R	CS54, *csaB* restored at the native location	This study
PLASMIDS		
pGEM7Zf(+)	Cloning vector Amp^R	Promega
pGEMC1	pGEM7Zf(+)+Δ*csaB*	This study
pG^+host4	Temperature-sensitive vector Erm^R	Appligene
pG4C4	pG^+host4+Δ*csaB*	This study
pMW118	Cloning vector Amp^R	Nippon gene
pMWCR	pMW118+*csaB*	This study
pG4CR	pG^+host4+*csaB*	This study

TABLE 3 | Primers used in this study.

Primer	Sequence (5′-3′)	Accession number and corresponding sequence (nt)
CS0F	GAAGATAGAAATACCGGGGC	CP001878.2 [3417065→ 3417046 (minus strand)]
CS1F	ATAGACCTAGCATTAAAGGG	CP001878.2 [3416882→ 3416863 (minus strand)]
CS2R-SS	TCTTGGTCCTTTATATACCCT CCCGGGTCATCTATTCATCC ACCTCTT	CP001878.2 [3415087→ 3415107) CP001878.2 (3416163→ 3416183]
CS3F-SS	AAGAGGTGGATGAATAGATGA CCCGGGAGGGTATATAAAGG ACCAAGA	CP001878.2 [3416183→ 3416163 (minus strand)] CP001878.2 [3415107→ 3415087 (minus strand)]
CS4R	CCATCAATTAAGTTAATGGC	CP001878.2 (3414387→ 3414403)
CS5R	TATCCTAAGAATAAGGCCCC	CP001878.2 (3414195→ 3414214)

Extra nucleotides that were added to introduce restriction sites for other experiments are underlined.

was centrifuged at 7,000 g for 5 min at 4°C and separated into supernatant and cell fractions.

The remaining cells were removed from the supernatant fraction by centrifugation at 7,000 g for 5 min at 4°C. Then, the secreted proteins were precipitated with 10% trichloroacetic acid for 30 min on ice and then centrifuged at 16,000 g for 15 min. The precipitates were washed twice with ethanol and then suspended in 200 μL of homogenization buffer (50 mM NaCl, 2.5 mM $MgCl_2$, 25 mM K_2HPO_4, corrected to pH 7.0 with HCl).

From the cell fraction, protoplasts were prepared, as described by Aono et al. (1992). The cells were washed twice with 3 mL of a selective medium for the isolation of *Megasphaera* and *Pectinatus*, designated SMMP (Chang and Cohen, 1979). Then, 0.01 vol. of 1% (w/v) lysozyme solution was added to the suspension. Protoplast formation at 37°C was monitored microscopically. The protoplasts were centrifuged at 700 g for 10 min at 10°C and separated into cell wall and protoplast fractions. The remaining protoplasts were removed from the cell wall fraction by centrifugation at 700 g for 10 min at 4°C. Then, the cell wall proteins were precipitated with 10% trichloroacetic acid for 30 min on ice and centrifuged at 16,000 g for 15 min. The precipitates were washed twice with ethanol and then suspended in 200 μL of homogenization buffer.

Each protein solution was mixed with an equal volume of sample buffer. A 20-μL aliquot of each sample was separated by 7.5% Tricinre-SDS-PAGE (Schägger and von Jagow, 1987) and analyzed by Coomassie Brilliant Blue staining.

Ultrathin Section Transmission Electron Microscopy (TEM)

Bacillus pseudofirmus OF4-811M and its derivative cells were grown at pH 8.0, as described above. The thin section TEM methods described by others (Sleytr et al., 1988; Gilmour et al., 2000) were adapted for this study. Cells were pre-fixed in 1% osmium tetroxide in 0.1 M cacodylate buffer (CB) (pH 7.2) at 4°C for 2 h. The pre-fixed samples were washed three times with 0.1 M CB (pH 7.2) and then fixed with 2.5% glutaraldehyde-4% tannic acid in 0.1 M CB (pH 7.2) at 4°C for 2 h. The fixed samples were washed three times with 0.1 M CB (pH 7.2) and then embedded in 2% Noble agar. After solidification, the agar block was cut into small cubes (<1 mm^3) and post-fixed with 1% osmium tetroxide in 0.1 M CB (pH 7.2) at 4°C for 18 h. The post-fixed samples were washed twice with 0.1 M CB (pH 7.2) and then dehydrated stepwise according to the following procedures: 50% ethanol at 4°C for 5 min (twice), 70% ethanol at 4°C for 5 min (twice), 90% ethanol at room temperature for 5 min (twice), 95% ethanol at room temperature for 5 min (twice), 100% ethanol at room temperature for 10 min (twice), and propylene oxide at room temperature for 10 min (twice). The dehydrated samples were infiltrated with a 1:1 solution of propylene oxide: embedding medium for 3.5 h and then epoxy resin for 18 h at room temperature. The embedding medium consisted of 12.5 mL of Epon 812, 7.5 mL of Araldite M, 27.5 mL of dodecenylsuccinic anhydride, 1.5 mL of dibutyl phthalate, 0.75 mL of 2,4,6-tri(dimethylaminomethyl)phenol (Nisshin EM Co., Ltd., Tokyo, Japan). To embed the samples, each was transferred to an embedding capsule filled with the embedding medium and incubated at 40°C for 4 days and then at 60°C for 2 days. The blocks were trimmed and sectioned with an

ultramicrotome with diamond knives. The ultrathin sections were post-stained with TI blue (Nissin EM Co., Ltd.) at room temperature for 10 min and then washed four times with water. The ultrathin sections were further post-stained with 0.4% lead citrate staining solution at room temperature for 10 min and then washed four times with water. The prepared ultrathin sections were observed using a JEM-2100 electron microscope (JEOL Ltd., Tokyo, Japan) at an acceleration voltage of 100 kV.

The thicknesses of the S-layer, PG, and cell wall (S-layer plus PG) in the microphotograph were measured. The thickness of each cell wall component was measured 10 times at 10 nm intervals using three cells.

Relative Quantification of the Amount of DNA of *B. pseudofirmus* OF4-811M and Its Derivatives Cultured at Several pH Values

Bacillus pseudofirmus OF4-811M and its derivative cells were grown on alkaline complex medium (pH 8.0) overnight at 30°C with shaking at 200 rpm. A 1-mL aliquot of culture was then inoculated into 50 mL of fresh alkaline complex medium at pH 8.0, 9.0, 10, or 11 and grown at 30°C with shaking at 200 rpm for 16 h. The whole culture was thoroughly stirred with a vortex mixer, of which 2 mL was used for relative quantification of DNA, according to the method described by Ceriotti (1952). The values were ascertained as a ratio relative to that of *B. pseudofirmus* OF4-811M grown at pH 10, set as 1.0. All results are reported as the averages of three independent experiments.

RESULTS

The *B. pseudofirmus* OF4 *csaB* Mutant Shows Chained Morphology and Alkali-Sensitivity

To investigate the physiological functions of SLH domain-containing proteins of *B. pseudofirmus* OF4, a deletion mutant of the *csaB* gene (CS54 strain) and its restoration strain (CS54-R strain) were constructed, as described above. The parental 811M strain (wild type), *slpA* mutant RG21 strain (Gilmour et al., 2000), and CS54-R strain formed typical colonies on agar plates of alkaline complex medium (pH 8 and 10). On the other hand, the CS54 strain did not form colonies on agar plates of alkaline complex medium at pH 10 after overnight incubation, but rather lower viscosity colonies on agar plates of alkaline complex medium at pH 8. In liquid medium, the CS54 strain tended to grow as a macroscopically visible cluster of cells at pH 8.0 even with shaking at 200 rpm, and did not grow at pH 10 (Supplementary Figure S1). Therefore, the 811M strain and its derivative mutants were grown at pH 8.0, as described above. To analyze the details of the cell clusters, microscopic analyses were conducted, which revealed that the morphology of the 811M, RG21, and CS54-R strains were typically rod-shaped, while that of the CS54 strain was chained rod-shaped (Supplementary Figure S2). Nucleoids were observed in the chained rod-shaped cells of the CS54 strain (Supplementary Figure S3).

As shown in Supplementary Figures S1, S2, the CS54 strain grows in a chained rod-shaped in a liquid medium, and the colonies formed by spreading it on an agar medium are not considered to be derived from one cell. Therefore, it was thought that growth could not be compared by viable cell count. As shown in Supplementary Figure S3, it was suggested that chromosome partitioning occurred in each cells of the CS54 strain, and there was no anucleated cell. Therefore, it was thought that growth could be compared by the relative quantification of the amount of DNA. As shown in **Figure 2**, there was no significant difference in the amount of DNA among the 811M, RG21, and CS54-R strains at each pH value. In the CS54 strain, a significant decrease of the amount of DNA was observed at pH 9, 10, and 11.

A Deletion of the S-Layer and Disturbance of PG Synthesis Were Observed in the *B. pseudofirmus* OF4 *csaB* Mutant

To observe the cell wall of the 811M strain and its derivative cells, thin section TEM was carried out (**Figure 3**) and the thicknesses of the S-layer, PG, and cell wall (S-layer plus PG) were measured from the photographs (**Table 4**). The 811M and CS54-R strains have an S-layer as the outermost cell envelope component. The CS54 strain lacked an S-layer and its PG was disturbed, while the RG21 strain also lacked an S-layer but its PG was not affected.

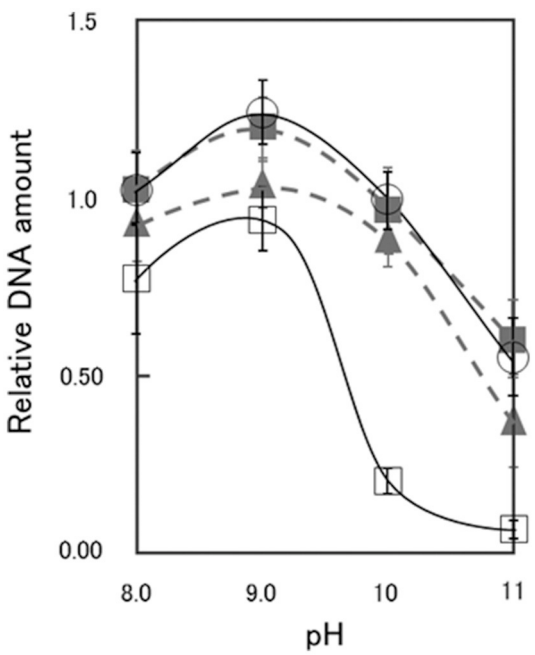

FIGURE 2 | Relative DNA amount of *B. pseudofirmus* OF4-811M and its derivatives grown at several pH values. *B. pseudofirmus* OF4-811M and its derivatives were grown for 16 h at several initial pH values and the DNA was quantified according to the method described by Ceriotti (1952).The black solid line and open circles show data for the 811M strain, the gray dashed line and filled triangles show data for the RG21 strain, the black solid line and open squares show data for the CS54 strain, and the gray dashed line and filled squares show data for the CS54-R strain. The values were ascertained as a ratio relative to that of *B. pseudofirmus* OF4-811M grown at pH 10, set as 1.0. All results are reported as the averages of three independent experiments. The error bars indicate the standard deviations of the values.

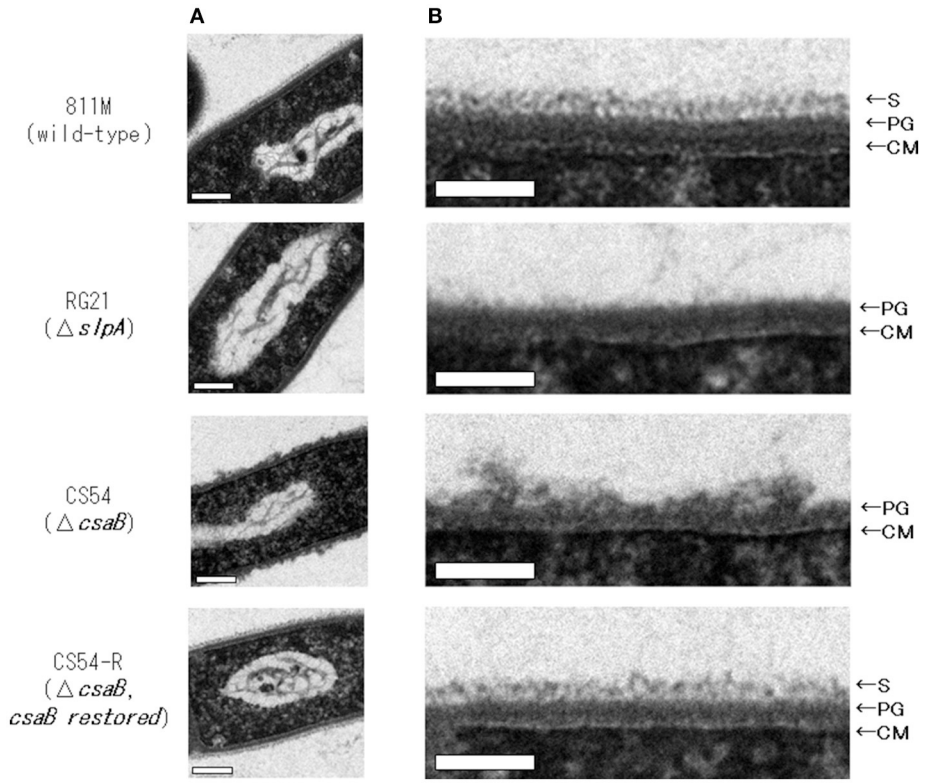

FIGURE 3 | Ultrathin section TEM of *B. pseudofirmus* OF4-811M and its derivative cells. *B. pseudofirmus* OF4-811M and its derivatives were grown at pH 8.0. Ultrathin sections were obtained, as described in the Materials and Methods section, and observed by TEM. Whole cell image **(A)** and an enlarged image of the cell surface region **(B)**. Representative images of the 811M, RG21, CS54, and CS54-R strains are shown. S-layer, surface layer; PG, peptidoglycan; CM, cytoplasmic membrane. Scale bar: 100 nm.

TABLE 4 | The thickness of each cell wall component in each of the strains.

	S-layer (nm)	Peptidoglycan (nm) (PG)	Cell wall (nm) (S-layer + PG)
811M	25 ± 3.4	31 ± 4.3	56 ± 5.2
RG21	N.D.	33 ± 3.2	33 ± 3.2
CS54	N.D.	53 ± 19	53 ± 19
CS54-R	25 ± 3.7	30 ± 4.0	55 ± 5.9

N.D., not detected.
The thickness of each cell wall component was measured 10 times at 10 nm intervals using three cells.

To confirm the insertion of new PG in the 811M strain and its derivative cells, the staining patterns of the cells were compared using fluorescent derivatives of the peptidoglycan-binding antibiotic vancomycin (**Figure 4**). If PG synthesis of strain CS54 was disturbed, the site of insertion of new PG was considered to be different from that of the 811M strain. Bright signals were observed at mid-cell and the poles of the cells in every strain. However, an additional bright signals, indicates the site where insertion of PG above the normal level occurs, as observed in the clustered cells of the CS54 strain.

SDS-Page Analysis Revealed That the Cell Wall of the CS54 Strain Does not Contain a Protein of About 94 kDa

To confirm expression of the SLH domain-containing proteins, the extracellular and cell wall protein fractions were obtained from the 811M strain and its derivatives, and analyzed by SDS-PAGE (**Figure 5**). In the 811M and CS54-R strains, strong bands were detected at about 94 kDa, in the cell wall protein fraction, corresponding to the size of the SlpA protein. These bands were also detected in the extracellular protein fraction. In the RG21 strain, no bands of about 94 kDa were detected in both fractions. In the CS54 strain, no bands of about 94 kDa were detected in cell wall fraction, and a weak band was detected at about 94 kDa in the extracellular protein fraction. In all cases, no bands of about 40 kDa, corresponding to the size of CsaB protein, were detected.

DISCUSSION

In this study, we constructed a deletion mutant of the *csaB* gene, required for the retention of SLH domain-containing proteins on the cell wall (Mesnage et al., 2000), of *B. pseudofirmus* OF4, and the results suggested that the SLH domain-containing protein,

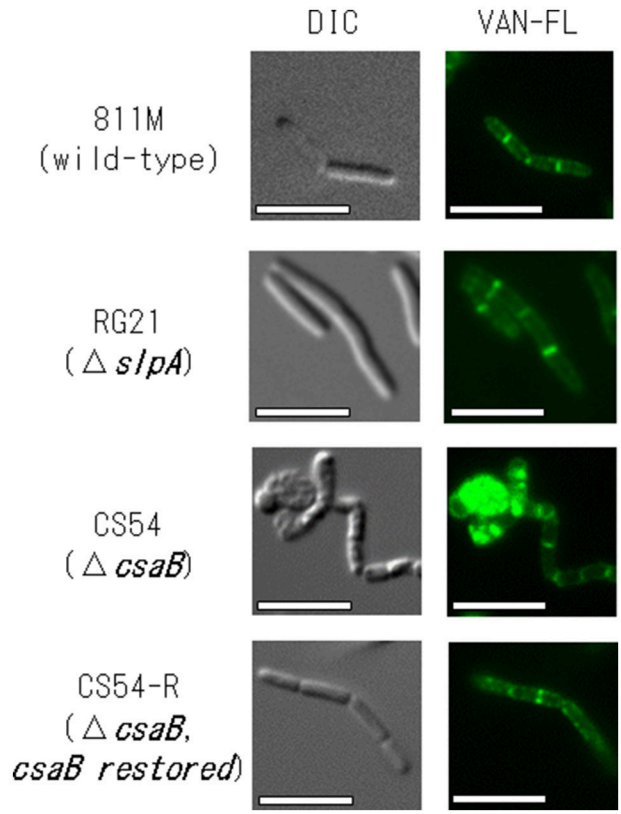

FIGURE 4 | Microscopic observation of the new peptidoglycan of *B. pseudofirmus* OF4-811M and its derivatives *B. pseudofirmus* OF4-811M and its derivatives were grown at pH 8.0. The insertion of new peptidoglycan was stained with FM4-64 and observed by fluorescence microscopy. Representative images of the 811M, RG21, CS54, and CS54-R strain are shown. DIC, differential-interference contrast microscopy; VAN-FL vancomycin, fluorescent vancomycin staining. Scale bar: 5 μm.

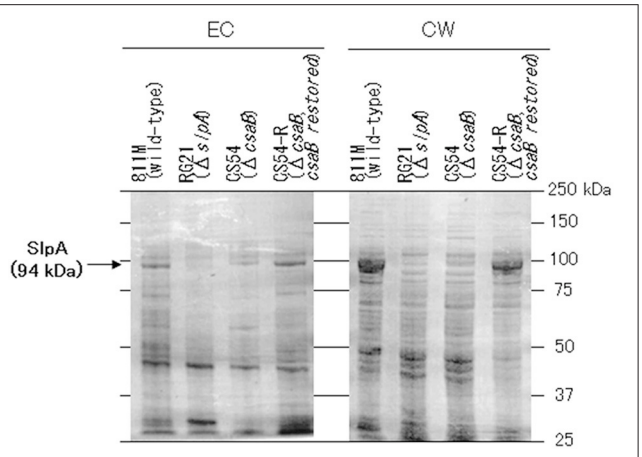

FIGURE 5 | SDS-PAGE of the extracellular and cell wall protein fractions of *B. pseudofirmus* OF4-811M and its derivatives. SDS-PAGE of the EC and CW fractions of *B. pseudofirmus* OF4-811M and its derivatives was performed. Proteins at about 94 kDa, corresponding to the size of SlpA, is indicated with arrows. EC, extracellular protein; CW, cell wall protein.

other than SlpA, plays an important role in alkaline adaptation via peptidoglycan synthesis (**Figures 2**, **3**).

The CS54 strain, a *csaB* gene deletion mutant of *B. pseudofirmus* OF4, grew as cell clusters in liquid medium and showed a chained morphology (Supplementary Figures S1, S2). Cell clustering also appeared to be more accelerated when cultured at a low shaking speed. These results strongly suggested that cells of the CS54 strain did not separate. A similar extraordinarily chained morphology has also been reported in *csaB* mutant strains of *B. anthracis* (Mesnage et al., 2000). It was reported that the SLH domain-containing PG hydrolase BslO mediates cell separation and is a determinant of *B. anthracis* chain length (Anderson et al., 2011). The putative SLH domain-containing PG hydrolase-encoding genes have been found in the genome of *B. pseudofirmus* OF4 (**Table 1**), suggesting that the cell separating PG hydrolase is delocalized from the cell wall in the CS54 strain, which causes a defect in cell separation leading to the chained morphology.

It has been reported that the *slpA* mutant RG21 strain has poorer growth than the parental 811M strain under conditions of an extremely high alkaline pH and low Na^+ concentration, such as pH 11 and 5 mM Na^+(Gilmour et al., 2000). Therefore, the growth of the CS54 strain was examined at several pH values. To investigate the growth of clustered cells, the amount of DNA was quantified (**Figure 2**). It has already been confirmed that chromosomal DNA is segregated, even in CS54 cells (Supplementary Figure S3), and the amount of DNA is proportional to the number of cells. There was no significant difference in the amount of DNA among the 811M, RG21, and CS54-R strains at each pH value, but the amount of the CS54 strain at pH 10 or higher was obviously smaller. These results suggest poorer growth of the CS54 strain than the 811M strain in an alkaline environment even under 230 mM $Na^{\pm}$ concentrations. The CS54 strain showed greater alkaline sensitivity than the RG21 strain, which strongly suggests that SLH domain-containing proteins, other than SlpA, are involved in the alkaline adaptation of *B. pseudofirmus* OF4.

Bands were detected at about 94 kDa in the cell wall protein fractions of the 811M and CS54-R strains by SDS-PAGE, corresponding to the size of the SlpA protein (**Figure 5**). These bands were also detected in the extracellular protein fractions. It has also been reported that the SLH domain-containing proteins were detected not only in the cell wall of *B. anthracis* but also in the medium (Lunderberg et al., 2013). The bands of about 94 kDa were not detected in the RG21 strain in both fractions, indicating defects of the SlpA protein. In the CS54 strain, no bands of about 94 kDa were detected in the cell wall fraction, and a weak band was detected at about 94 kDa in the extracellular protein fraction, indicating the possibility that SlpA protein is secreted into the medium but is not retained on the cell wall due to CsaB deficiency. In all cases, no bands of about 40 kDa, corresponding to the size of CsaB protein, were detected. Even in *B. anthracis*, CsaB protein was not detected by SDS-PAGE (Lunderberg et al., 2013), suggesting that the CsaB protein expressed at very low levels.

Next, ultrathin section TEM of the cell wall structure of *B. pseudofirmus* OF4 was performed (**Figure 3**) and the thicknesses of the S-layer, PG, and cell wall (S-layer + PG) were measured from the photograph (**Table 4**). The 811M and CS54-R strains had the S-layer as the outermost cell envelope component and homogeneous PG layers. The RG21 strain lacked an S-layer, but its PG was not affected, in accordance with the results of a previous study (Gilmour et al., 2000). On the other hand, the CS54 strain lacked an S-layer and its PG was heterogeneously disturbed. These results suggest that SlpA is a major protein of the S-layer and CsaB is necessary not only for *B. anthracis*, but also for *B. pseudofirmus* OF4 in order to maintain the SLH domain-containing proteins on the cell wall.

To investigate PG synthesis of the CS54 strain, the staining patterns of the cells were compared using fluorescent derivatives of the PG-binding antibiotic vancomycin (**Figure 4**). Bright signals were observed at mid-cell and the poles of the cells of every strain. Similar results have already been reported in *B. halodurans* C-125 and *B. subtilis* (Tiyanont et al., 2006; Fujinami et al., 2011). However, an additional bright signal was observed in the clustered CS54 cells, suggesting that the newly inserted PG was disturbed, which was considered to be responsible for the formation of the heterogeneous PG layer observed in **Figure 3**. It was suggested that the SLH domain-containing PG hydrolase, which is involved in PG metabolism, is also delocalized from the cell wall of the CS54 strain. It was reported that the cross-linking rate of PG of *B. halodurans* C-125 cells grown at pH 7.0 was lower than those grown at pH 10 (Aono and Sanada, 1994), indicating that incomplete PG is responsible for alkaline sensitivity.

The abundance of acidic polymers on the cell wall, such as SlpA of *B. pseudofirmus* OF4, has been thought to prevent hydroxide ion penetration, due to the high anionic charge, and promote proton accumulation around the cell (Krulwich, 1995; Gilmour et al., 2000; Fujinami and Fujisawa, 2010). In order to verify this hypothesis, measurement of the surface potential is necessary. However, it was reported that zeta potential does not accurately represent the surface potential of bacterial cells because of the Smoluchowski equation cannot be applied to a polymer-covered soft particle, such as bacterial cells (Morisaki et al., 1999). Therefore, we attempted to detect EPM (electrophoretic mobility) differences in the cells of each strain. Furthermore, since it is reported that flagella are a key factor that determines cell surface properties in *B. subtilis* (Okuda et al., 2003), we carried out a process to remove flagella from the cells by treatment with a syringe for 30 s before the measurement. As a result, no significant difference in EPM could be detected between the 811M strain and its derivatives, at least under this condition (Supplementary Figure S4).

It is not yet clear how SlpA contributes to alkaline adaptation. However, it was suggested that PG contributed more to alkaline adaptation than SlpA. In *B. subtilis*, PG hydrolases have been identified in cell separation and/or PG synthesis (Fukushima et al., 2006). In future studies, it is necessary to identify SLH domain-containing PG hydrolases involved in cell separation and /or PG synthesis in *B. pseudofirmus* OF4 and to find a PG hydrolase that plays a central role in cell morphology and/or alkaline adaptation.

AUTHOR CONTRIBUTIONS

SF and MI designed research. SF performed research. SF and MI analyzed data and wrote the paper.

ACKNOWLEDGMENTS

We wish to thank Ms. Kayoko Yamashita of Toyo University for technical assistance with observation by ultrathin section TEM and Dr. Arthur A. Guffanti for critical reading of the manuscript. This work was supported by a grant from Bio-Nano Electronics Research Centre, Toyo University, the Inoue Enryo Memorial Foundation for Promoting Science, Individual Research Expense of College of Humanities, and Science at Nihon University for 2016–2018 (to SF).

SUPPLEMENTARY MATERIAL

The Supplementary Material for this article can be found online at: https://www.frontiersin.org/articles/10.3389/fmicb.2018.00810/full#supplementary-material

REFERENCES

Anderson, V. J., Kern, J. W., McCool, J. W., Schneewind, O., and Missiakas, D. (2011). The SLH-domain protein BslO is a determinant of *Bacillus anthracis* chain length. *Mol. Microbiol.* 81, 192–205. doi: 10.1111/j.1365-2958.2011.07688.x

Aono, R. (1985). Isolation and partial characterization of structural components of the walls of alkalophilic bacillus strain C-125. *J. Gen. Microbiol.* 131, 105–111. doi: 10.1099/00221287-131-1-105

Aono, R., Horikoshi, K., and Goto, S. (1984). Composition of the peptidoglycan of alkalophilic *Bacillus* spp. *J. Bacteriol.* 157, 688–689.

Aono, R., Ito, M., and Horikoshi, K. (1992). Instability of the protoplast membrane of facultative alkaliphilic Bacillus sp. C-125 at alkaline pH values below the pH optimum for growth. *Biochem. J.* 285, 99–103. doi: 10.1042/bj2850099

Aono, R., Ito, M., Joblin, K. N., and Horikoshi, K. (1995). A high cell wall negative charge is necessary for the growth of the alkaliphile Bacillus lentus C-125 at elevated pH. *Microbiology* 141, 2955–2964. doi: 10.1099/13500872-141-11-2955

Aono, R., Ito, M., and Machida, T. (1999). Contribution of the cell wall component teichuronopeptide to pH homeostasis and alkaliphily in the alkaliphile Bacillus lentus C-125. *J. Bacteriol.* 181, 6600–6606.

Aono, R., and Ohtani, M. (1990). Loss of alkalophily in cell-wall-component-defective mutants derived from alkalophilic Bacillus C-125. Isolation and partial characterization of the mutants. *Biochem. J.* 266, 933–936.

Aono, R., and Sanada, T. (1994). Hyper-autolysis of the facultative alkaliphile *Bacillus* sp. C-125 cells grown at neutral pH: culture-pH dependent cross-linking of the peptide moieties of the peptidoglycan. *Biosci. Biotechnol. Biochem.* 58, 2015–2019. doi: 10.1271/bbb.58.2015

Ceriotti, G. (1952). A microchemical determination of desoxyribonucleic acid. *J. Biol. Chem.* 198, 297–303.

Chang, S., and Cohen, S. N. (1979). High frequency transformation of *Bacillus subtilis* protoplasts by plasmid DNA. *Mol. Gen. Genet.* 168, 111–115. doi: 10.1007/BF00267940

Clejan, S., Guffanti, A. A., Cohen, M. A., Krulwich, T.A. (1989). Mutation of Bacillus firmus OF4 to duramycin resistance results in substantial replacement

of membrane lipid phosphatidylethanolamine by its plasmalogen form. *J. Bacteriol.* 171, 1744–1746.

Fujinami, S., and Fujisawa, M. (2010). Industrial applications of alkaliphiles and their enzymes – past, present and future. *Environ. Technol.* 31, 845–856. doi: 10.1080/09593331003762807

Fujinami, S., Sato, T., and Ito, M. (2011). The relationship between a coiled morphology and Mbl in alkaliphilic *Bacillus halodurans* C-125 at neutral pH values. *Extremophiles* 15, 587–596. doi: 10.1007/s00792-011-0389-9

Fujinami, S., Sato, T., Trimmer, J. S., Spiller, B. W., Clapham, D. E., Krulwich, T. A., et al. (2007a). The voltage-gated Na+ channel NaVBP co-localizes with methyl-accepting chemotaxis protein at cell poles of alkaliphilic *Bacillus pseudofirmus* OF4. *Microbiology* 153, 4027–4038. doi: 10.1099/mic.0.2007/012070-0

Fujinami, S., Terahara, N., Lee, S., and Ito, M. (2007b). Na+ and flagella-dependent swimming of alkaliphilic *Bacillus pseudofirmus* OF4: a basis for poor motility at low pH and enhancement in viscous media in an "up-motile" variant. *Arch. Microbiol.* 187, 239–247. doi: 10.1007/s00203-006-0192-7

Fukushima, T., Afkham, A., Kurosawa, S., Tanabe, T., Yamamoto, H., and Sekiguchi, J. (2006). A new D,L-endopeptidase gene product, YojL (renamed CwlS), plays a role in cell separation with LytE and LytF in *Bacillus subtilis*. *J. Bacteriol.* 188, 5541–5550. doi: 10.1128/JB.00188-06

Gilmour, R., Messner, P., Guffanti, A. A., Kent, R., Scheberl, A., Kendrick, N., et al. (2000). Two-dimensional gel electrophoresis analyses of pH-dependent protein expression in facultatively alkaliphilic *Bacillus pseudofirmus* OF4 lead to characterization of an S-layer protein with a role in alkaliphily. *J. Bacteriol.* 182, 5969–5981. doi: 10.1128/JB.182.21.5969-5981.2000

Horton, R. M.,(1997). *In vitro* recombination and mutagenesis of DNA. SOEing together tailor-made genes. *Methods Mol. Biol.* 67, 141–149.

Ito, M., and Aono, R. (2002). Decrease in cytoplasmic pH-homeostastatic activity of the alkaliphile *Bacillus lentus* C-125 by a cell wall defect. *Biosci. Biotechnol. Biochem.* 66, 218–220. doi: 10.1271/bbb.66.218

Ito, M., Fujinami, S., and Terahara, N. (2011). "Bioenergetics: Cell motility and chemotaxis of extreme alkaliphiles," in *Extremophile Handbook*, ed K. Horikoshi (Tokyo: Springer), 141–162. doi: 10.1007/978-4-431-53898-1_8

Ito, M., Guffanti, A. A., Zemsky, J., Ivey, D. M., and Krulwich, T. A. (1997). Role of the nhaC-encoded Na+/H+ antiporter of alkaliphilic *Bacillus firmus* OF4. *J. Bacteriol.* 179, 3851–3857. doi: 10.1128/jb.179.12.3851-3857.1997

Ito, M., Hicks, D. B., Henkin, T. M., Guffanti, A. A., Powers, B. D., Zvi, L., et al. (2004a). MotPS is the stator-force generator for motility of alkaliphilic Bacillus, and its homologue is a second functional Mot in *Bacillus subtilis*. *Mol. Microbiol.* 53, 1035–1049. doi: 10.1111/j.1365-2958.2004.04173.x

Ito, M., Xu, H., Guffanti, A. A., Wei, Y., Zvi, L., Clapham, D. E., et al. (2004b). The voltage-gated Na+ channel NaVBP has a role in motility, chemotaxis, and pH homeostasis of an alkaliphilic Bacillus. *Proc. Natl. Acad. Sci. U.S.A.* 101, 10566–10571. doi: 10.1073/pnas.0402692101

Janto, B., Ahmed, A., Ito, M., Liu, J., Hicks, D. B., Pagni, S., et al. (2011). The genome of alkaliphilic *Bacillus pseudofirmus* OF4 reveals adaptations that suppot the ability to grow in an external pH range from 7.5 to 11.4. *Environ. Microbiol.* 13, 3289–3309. doi: 10.1111/j.1462-2920.2011.02591.x

Kern, J., Ryan, C., Faull, K., and Schneewind, O. (2010). *Bacillus anthracis* surface-layer proteins assemble by binding to the secondary cell wall polysaccharide in a manner that requires csaB and tagO. *J. Mol. Biol.* 401, 757–775. doi: 10.1016/j.jmb.2010.06.059

Krulwich, T. A. (1995). Alkaliphiles: "basic" molecular problems of pH tolerance and bioenergetics. *Mol. Microbiol.* 15, 403–410. doi: 10.1111/j.1365-2958.1995.tb02253.x

Krulwich, T. A., and Ito, M. (2013). "Prokaryotic alkaliphiles," in *The Prokaryotes*, *4th Edn.*, ed E. Rosenberg (Berlin; Heidelberg: Springer), 441–470. doi: 10.1007/978-3-642-30123-0_58

Krulwich, T. A., Ito, M., and Guffanti, A. A. (2001). The Na(+)-dependence of alkaliphily in Bacillus. *Biochim. Biophys. Acta* 1505, 158–168. doi: 10.1016/S0005-2728(00)00285-1

Krulwich, T. A., Liu, J., Morino, M., Fujisawa, M., Ito, M., and Hicks, D. B. (2011). "Adaptive mechanisms of extreme alkaliphiles," in *Extremophile Handbook*, ed K. Horikoshi (Tokyo: Springer), 119–139. doi: 10.1007/978-4-431-53898-1_7

Lunderberg, J. M., Nguyen-Mau, S.-M., Richter, G. S., Wang, Y. T., Dworkin, J., Missiakas, D. M., et al. (2013). *Bacillus anthracis* acetyltransferases PatA1 and PatA2 modify the secondary cell wall polysaccharide and affect the assembly of S-layer proteins. *J. Bacteriol.* 195, 977–989. doi: 10.1128/JB.01274-12

Mesnage, S., Fontaine, T., Mignot, T., Delepierre, M., Mock, M., and Fouet, A. (2000). Bacterial SLH domain proteins are non-covalently anchored to the cell surface via a conserved mechanism involving wall polysaccharide pyruvylation. *EMBO J.* 19, 4473–4484. doi: 10.1093/emboj/19.17.4473

Morino, M., Suzuki, T., Ito, M., and Krulwich, T. A. (2014). Purification and functional reconstitution of a seven-subunit mrp-type Na+/H+ antiporter. *J. Bacteriol.* 196, 28–35. doi: 10.1128/JB.01029-13

Morisaki, H., Nagai, S., Ohshima, H., Ikemoto, E., and Kogure, K. (1999). The effect of motility and cell-surface polymers on bacterial attachment. *Microbiology* 145, 2797–2802. doi: 10.1099/00221287-145-10-2797

Okuda, S., Igarashi, R., Kusui, Y., Kasahara, Y., and Morisaki, H. (2003). Electrophoretic mobility of *Bacillus subtilis* knockout mutants with and without flagella. *J. Bacteriol.* 185, 3711–3717. doi: 10.1128/JB.185.13.3711-3717.2003

Sambrook, J., Frisch, E. F., and Maniatis, T. (1989). *Molecular Cloning: A Laboratory Manual, 2nd Edn.*, New York, NY: Cold Spring Harbor Laboratory Press.

Schäffer, C., and Messner, P. (2005). The structure of secondary cell wall polymers: how Gram-positive bacteria stick their cell walls together. *Microbiology* 151, 643–651. doi: 10.1099/mic.0.27749-0

Schägger, H., and von Jagow, G. (1987). Tricine-sodium dodecyl sulfate-polyacrylamide gel electrophoresis for the separation of proteins in the range from 1 to 100 kDa. *Anal. Biochem.* 166, 368–379. doi: 10.1016/0003-2697(87)90587-2

Sleytr, U. B., Messner, P., and Pum, D. (1988). Analysis of crystalline bacterial surface layers by freeze-etching, metal shadowing, negative staining and ultrathin sectioning. *Methods. Microbiol.* 20, 29–60. doi: 10.1016/S0580-9517(08)70046-1

Tiyanont, K., Doan, T., Lazarus, M. B., Fang, X., Rudner, D. Z., and Walker, S. (2006). Imaging peptidoglycan biosynthesis in *Bacillus subtilis* with fluorescent antibiotics. *Proc. Natl. Acad. Sci. U.S.A.* 103, 11033–11038. doi: 10.1073/pnas.0600829103

Conflict of Interest Statement: The authors declare that the research was conducted in the absence of any commercial or financial relationships that could be construed as a potential conflict of interest.

frontiers in Microbiology

ORIGINAL RESEARCH
published: 02 May 2018
doi: 10.3389/fmicb.2018.00831

Critical Functions of Region 1-67 and Helix XIII in Retaining the Active Structure of NhaD Antiporter in *Halomonas* sp. Y2

*Zhou Yang, Yiwei Meng, Qi Zhao, Bin Cheng, Ping Xu and Chunyu Yang**

State Key Laboratory of Microbial Technology, Microbial Technology Institute, Shandong University, Jinan, China

NhaD-type antiporters are mainly distributed in various *Proteobacteria*, especially in marine microorganisms and human pathogens. This distribution as well as the pathogenic properties of these strains suggest that these antiporters contribute to the regulation of high osmoregulation and are potential drug targets. Two NhaD homologs, NhaD1 and NhaD2, from the halotolerant and alkaliphilic *Halomonas* sp. Y2 exhibits similar, high *in vitro* activity, but remarkably different *in vivo* functions. To search for critical domains or residues involved in these differences of physiological functions, various chimeras composed of NhaD1 and NhaD2 segments were generated. Two regions at residues 1–67 and 464–492 were found to be responsible for the robust *in vivo* function of NhaD2, and region 464–492 is also crucial to the pH response of the antiporter. In particular, the completely abolished activity of KNabc/N463r, highly recovered activity while very weakly recovered ion resistance of the KNabc/N463r-C7 chimera, suggested that transmembrane helix (TM) XIII is crucial for the robust ion resistance of NhaD2. Using site-directed mutagenesis, seven hydrophobic residues in TM XIII were identified as key residues for the ion translocation of NhaD2. Compared with the fluorescence resonance energy transfer (FRET) profile in the wild-type NhaD2, the reduced FRET efficiency of N463r chimeras provided solid evidence for conformational changes in the N463r fusion protein and consequently verified the structural functions of TM XIII in the pH activation and physiological functions of NhaD2.

Keywords: NhaD antiporter, *in vivo* activity, fusion protein, TM XIII, pH activation

OPEN ACCESS

Edited by:
Masahiro Ito,
Toyo University, Japan

Reviewed by:
Saori Kosono,
The University of Tokyo, Japan
Jun Liu,
Tianjin Institute of Industrial Biotechnology (CAS), China

****Correspondence:***
Chunyu Yang
ycy21th@sdu.edu.cn

Specialty section:
This article was submitted to Extreme Microbiology, a section of the journal Frontiers in Microbiology

Received: *22 January 2018*
Accepted: *11 April 2018*
Published: *02 May 2018*

Citation:
Yang Z, Meng Y, Zhao Q, Cheng B, Xu P and Yang C (2018) Critical Functions of Region 1-67 and Helix XIII in Retaining the Active Structure of NhaD Antiporter in Halomonas sp. Y2. Front. Microbiol. 9:831. doi: 10.3389/fmicb.2018.00831

INTRODUCTION

Sodium proton (Na^+/H^+) antiporters are secondary membrane protein transporters present in taxa belonging to all kingdoms. Over the last few decades, many putative Na^+/H^+ antiporters have been identified in a wide range of taxa and their critical functions have been characterized, e.g., in sodium, pH, and cell volume homeostasis; furthermore, they have been identified as potential drug targets in humans (Padan et al., 2001; Padan and Landau, 2016). Among these antiporters, NhaA from *Escherichia coli* (Ec-NhaA) has been extensively investigated with respect its structural properties, ion translocation activity, and pH regulatory effects (Maes et al., 2012). Since the crystal structure of downregulated Ec-NhaA was determined at pH 4.0, many biochemical and physiological studies have been performed and the pH-dependent features of Ec-NhaA have been

elucidated (Hunte et al., 2005; Krulwich et al., 2011). In particular, the pH- and Na^+-induced conformational changes and working model of Ec-NhaA have been monitored using various techniques, and these studies have provided solid evidence that environmental stress induces conformational changes of Ec-NhaA (Kozachkov et al., 2007; Tzubery et al., 2008; Appel et al., 2009; Herz et al., 2010; Mager et al., 2011).

Based on the TCDB[1] and PubMed databases, NhaD-type homologs have been exclusively found in the cell membranes of marine/haloalkaliphilic γ-*proteobacteria* and pathogenic strains, including *Vibrio cholera, Chlamydia trachomatis, Prevotella bergensis,* and *Campylobacter showae*. This distribution suggests a special mechanism for saline (alkaline) habitat adaptation and implies their potential application as drug targets (Kurz et al., 2006). However, only limited information of these antiporters are available from halotolerant or alkaliphilic species. Transport activity analyses of those antiporters from *Alkalimonas amylolytica*, *Halomonas*, and pathogenic *Vibrio* species have suggested that they are highly pH-dependent. In addition, these NhaD antiporters exhibited different pH profiles for Na^+ and Li^+ transport (Nozaki et al., 1998; Dzioba et al., 2002; Liu et al., 2005; Zhang et al., 2014), consistent with our previous findings for NhaD antiporters of the strain *Halomonas* sp. Y2 (Cui et al., 2016).

In the halotolerant and alkaliphilic *Halomonas* sp. Y2, we found Na^+/H^+ antiporters of different types working in concert to adapt to alkaline or saline stresses (Cheng et al., 2016). Among four antiporters investigated, two NhaD homologs (sequence identity, 72%) displayed substantially different physiological functions, i.e., NhaD2 exhibited robust physiological functions in both wild-type *Halomonas* sp. Y2 and antiporter-deficient *E. coli* strain KNabc, whereas very weak *in vivo* activity was detected for NhaD1 (Cui et al., 2016). Previously, we found that the N- and C-termini of these two NhaD antiporters functionally interact and play important roles in expelling ions (Meng et al., 2017), but the critical regions for these *in vivo* roles remain to be elucidated. In this study, to advance our understanding of the molecular mechanism underlying these physiological differences, critical regions and residues were identified by constructing a series of chimeras and mutants.

MATERIALS AND METHODS

Bacterial Strains, Plasmids, and Growth Conditions

The bacterial strains and plasmids used in this study are listed in **Table 1** and Supplementary Table S1. *E. coli* strain DH5α was used for routine cloning and cultivated at 37°C, in the Luria–Bertani (LB) medium containing 1.0% tryptone, 0.5% yeast extract, and 1.0% NaCl. The triple-antiporter deficient strain *E. coli* KNabc (Nozaki et al., 1998) was used as a host for the complementary assay and membrane vesicle preparation. Unless otherwise specified, *E. coli* KNabc transformants were grown aerobically at 37°C in the LBK medium, in which NaCl

[1]http://www.tcdb.org

TABLE 1 | Strains used or generated in this study.

Strain	Relevant phenotype or genotype	Reference
Halomonas sp. Y2	Moderate halophilic alkalophilic strain	Yang et al., 2010
E. coli C43	Competent cell for expression	
E. coli DH5α	Competent cell for cloning	
E. coli KNabc	Δ*nhaA*, Δ*nhaB*, and Δ*chaA*	Nozaki et al., 1998
NhaD1 chimerical strain		
KNabc/N40r	*E. coli* KNabc with N40r	This study
KNabc/N67r	*E. coli* KNabc with N67r	This study
KNabc/N129r	*E. coli* KNabc with N129r	This study
KNabc/N202r	*E. coli* KNabc with N202r	This study
KNabc/N267r	*E. coli* KNabc with N267r	This study
KNabc/N292r	*E. coli* KNabc with N292r	This study
KNabc/N358r	*E. coli* KNabc with N358r	This study
KNabc/N425r	*E. coli* KNabc with N425r	This study
KNabc/N463r	*E. coli* KNabc with N463r	This study
NhaD2 chimerical strain		
KNabc/N40	*E. coli* KNabc with N40	This study
KNabc/N67	*E. coli* KNabc with N67	This study
KNabc/N129	*E. coli* KNabc with N129	This study
KNabc/N202	*E. coli* KNabc with N202	This study
KNabc/N267	*E. coli* KNabc with N267	This study
KNabc/N292	*E. coli* KNabc with N292	This study
KNabc/N358	*E. coli* KNabc with N358	This study
KNabc/N425	*E. coli* KNabc with N425	This study
KNabc/N463	*E. coli* KNabc with N463	This study
KNabc/N463r-C7	*E. coli* KNabc with N463r-C7	This study
N463r-C7 mutant		
KNabc/N463r-C7-V466A	*E. coli* KNabc with N463r-C7-V466A	This study
KNabc/N463r-C7-A468V	*E. coli* KNabc with N463r-C7-A468V	This study
KNabc/N463r-C7-V474I	*E. coli* KNabc with N463r-C7-V474I	This study
KNabc/N463r-C7-A478I	*E. coli* KNabc with N463r-C7-A478I	This study
KNabc/N463r-C7-A479V	*E. coli* KNabc with N463r-C7-A479V	This study
KNabc/N463r-C7-M482W	*E. coli* KNabc with N463r-C7-M482W	This study
KNabc/N463r-C7-I483L	*E. coli* KNabc with N463r-C7-I483L	This study
***Halomonas* sp. Y2 strain**		
Y2/Δ*nhaD2*	Y2 with *nhaD2* deficiency	Cheng et al., 2016
Y2/NhaD2	Y2/Δ*nhaD2* with NhaD2	Cheng et al., 2016
Y2/N463r-C7	Y2/Δ*nhaD2* with N463r-C7	This study
Y2/N463r-C7-V466A	Y2/Δ*nhaD2* with N463r-C7-V466A	This study
Y2/N463r-C7-A468V	Y2/Δ*nhaD2* with N463r-C7-A468V	This study
Y2/N463r-C7-V474I	Y2/Δ*nhaD2* with N463r-C7-V474I	This study

(Continued)

TABLE 1 | Continued

Y2/N463r-C7-A478I	Y2/Δ*nhaD2* with N463r-C7-A478I	This study
Y2/N463r-C7-A479V	Y2/Δ*nhaD2* with N463r-C7-A479V	This study
Y2/N463r-C7-M482W	Y2/Δ*nhaD2* with N463r-C7-M482W	This study
Y2/N463r-C7-I483L	Y2/Δ*nhaD2* with N463r-C7-I483L	This study
***E. coli* C43 strains FRET analysis**		
C43/D2-CFP-YFP	*E. coli* C43 with D2-CFP-YFP	Meng et al., 2017
C43/N463r-CFP-YFP	*E. coli* C43 with N463r-CFP-YFP	This study

was replaced by 87 mM KCl and 100 μg ml^{-1} ampicillin was supplemented (Goldberg et al., 1987).

Chimera and Mutant Construction

The amino acid alignment between NhaD1 and NhaD2 was performed by Clustal_X (Thompson et al., 1997). For chimera generation (**Figure 1**), the gene splicing by overlap extension PCR (OE-PCR) was used for fusion fragments construction, by using NhaD1 and NhaD2 as templates, respectively. The primers used for fusion PCR was listed in Supplementary Table S2. These fused fragments were ligated into pEASY-blunt and transformed into *E. coli* DH5α for sequencing. After been confirmed for sequence fidelity, each fusion plasmids were transformed into *E. coli* KNabc for complementary growth and antiport activity measurement.

To recover the complementation ability of N463r, the three C-terminal residues of N463r (SMF) were replaced with seven C-terminal residues of NhaD2 (GSFSVYG), and a fusion protein of N463r-C7 was generated (**Figure 1**). Using the primers listed in Supplementary Table S2 and plasmid pEASYblunt-N463r-C7 as the template, seven mutants in transmembrane helix (TM) XIII were generated by PCR-based technique. Fidelity of all final mutated versions of *nhaD* in pEASY-blunt was verified by DNA sequencing. *E. coli* KNabc recombinants carrying the mutated plasmids were constructed as those of chimeras.

Growth of Constructed *E. coli* KNabc Variants

Complementary growth of a series of chimeras and mutants, together with KNabc/NhaD1 and KNabc/NhaD2, were tested in LBK medium supplemented with 200, 300 mM NaCl or 50, 100 mM LiCl, respectively. Recombinant carrying empty vector pEASY-blunt in *E. coli* KNabc was used as a negative control. Ampicillin was added to a final concentration of 100 μg ml^{-1}. After incubation at 37°C for 24 h, the growth of strains (OD_{600}) was measured.

Preparation of Reversed Membranes and Determination of Transport Activity

The KNabc mutants were cultured in LBK medium (100 μg ml^{-1} ampicillin) at 37°C to a concentration (OD_{600} = 0.6), and then IPTG (final concentration of 0.5 mM) was added for protein induction. Inside-out membrane vesicles from these cultures were prepared and the fluorescence-based activity was measured as previous described (Goldberg et al., 1987; Cheng et al., 2016). Protein concentration was determined by the Bradford protein assay (Bio-Rad). The antiport activity of around 60 μg vesicle was assayed in buffer B (140 mM choline chloride and 5 mM $MgCl_2$, 10 mM MES, 10 mM Tris, pH 8.5), by measuring the dequenching of fluorescence upon the subsequent addition of 10 mM of Na^+ or Li^+. The percent dequenching was calculated relative to the initial respiration-dependent quench. For the pH profile measurement, assay mixtures containing of 10 mM Tris-MES and 10 mM of Na^+ (Li^+) at different pH conditions were used (6.0–9.5). The concentration ranges of the cations tested was 0.1–100 mM at pH 8.5, and the apparent K_m values were calculated by linear regression of a Lineweaver–Burk plot.

Complementary Strain Construction in *Halomonas* sp. Y2/Δ*nhaD2*

N463r-C7 fused fragments, as well as its seven mutants were ligated with the shuttle vector pBBR1MCS-5, and transferred into the *nhaD2*-deficient strain of *Halomonas* sp. Y2 using the method we previously described (Cheng et al., 2016). The transformants were selected by LB plates with ampicillin (100 μg ml^{-1}) and gentamicin (50 μg ml^{-1}) supplementation, and confirmed by PCR and DNA sequencing.

The growth of eight complementary strains upon high alkalinity and salinity were measured in liquid LB-based medium that buffered with 50 mM Tris-HCl (pH 8.0) or 50 mM glycine-NaOH (pH 10.0), respectively. Based on the ion- and alkali-resistance of *Halomonas* sp. Y2, various concentrations of NaCl and LiCl were supplemented. For seed preparation, all cell suspensions were adjusted to 6.0 (OD_{600}) with Na^+-free LB medium and inoculated in a same inoculation volume. After 24 h incubation at 37°C, the cell growth (OD_{600}) was determined.

RNA Preparation and Quantitative Real-Time Reverse Transcription PCR (qRT-PCR) Analysis

The relative qPCR was performed to calculate the expression levels of N463r-C7 and its seven mutated proteins in helix XIII (TM XIII). Strains of KNabc/D1, D2, N463r-C7 and its mutants were cultured in LBK medium at 37°C to late exponential phase. Then, cells were harvested and used for RNA extraction, by using EasyPure RNA kit (Transgen). The cDNA was synthesized by the HiScript Q RT SuperMix for Qpcr (Vazyme Biotech) and used as the templates for qPCR analysis. Quantitative PCR was carried out in a MyiQ2^{TM} iCycler (two-color real-time PCR detection system) (Bio-Rad) with a Real Master mix kit (SYBR Green, Tiangen) according to the manufacturer's instructions. The primers used in this procedure are listed in Supplementary Table S2 and *16S rRNA* was used as an internal reference for each mutant. Three biological replicates were used for qPCR and at least four repeats for each sample, after which the average threshold cycle (Ct) was calculated for each sample. By using the

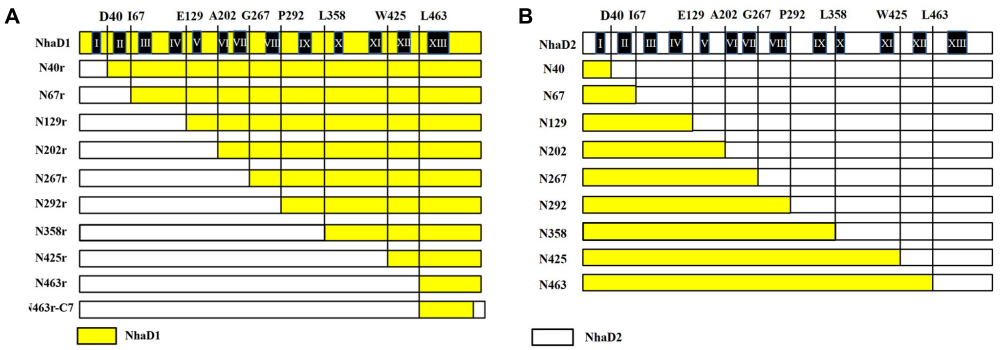

FIGURE 1 | Schematic representation of NhaD1 and NhaD2 chimeras. **(A)** NhaD1 chimeras that replaced N-terminal regions of NhaD1 with corresponding regions of NhaD2. **(B)** NhaD2 chimeras that replaced N-terminal regions of NhaD2 with corresponding regions of NhaD1. Regions from NhaD1 and NhaD2 are colored with yellow and white, respectively.

Ct values of *nhaD2* as a baseline, the relative fold changes in gene expression were calculated by $2^{-\Delta\Delta Ct}$ method. Statistical analysis was performed on $2^{-\Delta\Delta Ct}$ values using a paired Student's *t*-test.

Fluorescence Resonance Energy Transfer (FRET) Analysis for the Conformational Change

A previously construct of N39-CFP-C-YFP (designated as D2-CFP-YFP in this study) was also used as a template for generating mutant N463r-CFP-YFP (Meng et al., 2017), in which TM XIII was replaced with the corresponding region of NhaD1, CFP was fused after site 39 and YFP was fused at the C-terminal of N463r. In these two fusion proteins, CFP and YFP were fused after site 39 and C-terminus, respectively. *E. coli* KNabc carrying these plasmids were tested for antiport activities. After activity confirmation, *E. coli* C43 strains carrying these fusion plasmids were grown at 37°C in LB medium to a concentration (OD_{600} = 0.6–0.8) and induced by adding IPTG (final concentration of 0.5 mM), and cultivated at 20°C overnight. Cells were harvested and washed three times with the Tricine-KOH buffer solution (10 mM Tricine and 140 mM KCl, adjusted to pH 8.5 with KOH), and resuspended in the same buffer to an OD_{600} of 1.5. For fluorescence resonance energy transfer (FRET) analysis, a 2-ml cell suspensions of D2-CFP-YFP, N463r-CFP-YFP, or D2-CFP were irradiated at 433 nm to excite CFP, and recorded the fluorescence emission at 450–600 nm on a F-4600 spectrofluorophotometer (Hitachi). In the meanwhile, a 2-ml cell suspension of D2-CFP-YFP was also illuminated at 473 nm and recoded at 450–600 nm.

RESULTS

To identify the precise regions involved in the physiological differences, a series of chimeras were generated, as shown in **Figure 1**. The N-terminal region of NhaD1 and C-terminal sequence of NhaD2 were combined, or vice versa. As a result, two sets of chimeras from NhaD1 and NhaD2 were both generated.

E. coli KNabc Chimeras of NhaD1

The generated chimerical strains are shown in **Table 1**. To test their complementation abilities, growth was investigated in Luria–Bertani medium containing various concentrations of 200 or 300 mM NaCl. Similarly, all strains carrying NhaD1 chimeras, except KNabc/N67r, displayed identical ion resistance to that of KNabc/NhaD1 (**Table 2**). Moreover, these fusion proteins abolished transport activity in an everted membrane assay (**Figure 2**). In contrast, the KNabc/N67r fusion strain could tolerate up to 300 mM Na^+ and the protein N67r retained modest activities for Na^+ and Li^+ transport, with a similar pH profile to that of NhaD1 and maximum activity at pH 8.5–9.0 (**Figure 3**).

The substitution of residues 1–463 in NhaD1 with the corresponding region from NhaD2 (chimeric N463r, **Figure 1**) completely abolished the transport activity and complementation ability, indicating the importance of the C-terminal region of NhaD antiporters (**Figure 2**). To recover the complementation ability of N463r, the three C-terminal residues of N463r (SMF) were replaced with seven C-terminal residues of NhaD2 (GSFSVYG) (shown in the blue squares of **Figure 4**), and a fusion protein of N463r-C7 was generated (**Figure 1**). A weak ion resistance was obtained for the chimeric KNabc/N463r-C7 strain, with a slight growth observed (OD_{600} = 0.19) upon 300 mM Na^+ stress (**Table 2**). In contrast to the weak restored complementary growth, highly restored activities for Na^+ and Li^+ transport were detected in the everted membrane vesicle, with around 50% dequenching activities observed at pH 9.5. In addition, N463r-C7 exhibited a similar pH profile to that of NhaD2, in which the highest activity for $Na^+(Li^+)$ transport was observed at pH 9.5 or higher (**Figure 3**).

E. coli KNabc Chimeras of NhaD2

Compared to wild-type NhaD2, most chimeras displayed a remarkable reduction in growth complementation, with no growth detected in the presence of 300 mM NaCl. Differently, the *E. coli* KNabc strains carrying fusions of N67, N358, and N425 showed weak resistance to 300 mM NaCl (**Table 2**). In agreement with their impaired complementation, most fusion proteins abolished dequenching activities in the everted membrane assay,

TABLE 2 | Growth of constructed *E. coli* KNabc chimeras in the LBK medium.

Strain	NaCl (mM)		Strain	NaCl (mM)	
	200	300		200	300
KNabc/NhaD1	0.86 ± 0.05	0.05 ± 0.01	KNabc/NhaD2	1.62 ± 0.10	1.21 ± 0.11
KNabc/N40r	0.35 ± 0.02	0.07 ± 0.01	KNabc/N40	0.33 ± 0.01	0.06 ± 0.01
KNabc/N67r	1.20 ± 0.09	0.25 ± 0.02	KNabc/N67	0.83 ± 0.06	0.25 ± 0.04
KNabc/N129r	0.81 ± 0.06	0.07 ± 0.02	KNabc/N129	0.98 ± 0.09	0.05 ± 0.01
KNabc/N202r	0.73 ± 0.02	0.05 ± 0.01	KNabc/N202	0.83 ± 0.04	0.06 ± 0.01
KNabc/N267r	0.97 ± 0.03	0.06 ± 0	KNabc/N267	0.67 ± 0.07	0.06 ± 0.01
KNabc/N292r	0.58 ± 0.02	0.05 ± 0.01	KNabc/N292	0.89 ± 0.04	0.06 ± 0.01
KNabc/N358r	0.56 ± 0.04	0.04 ± 0	KNabc/N358	0.92 ± 0.05	0.19 ± 0.03
KNabc/N425r	0.74 ± 0.03	0.08 ± 0.01	KNabc/N425	0.80 ± 0.06	0.22 ± 0.01
KNabc/N463r	0.49 ± 0.05	0.03 ± 0.01	KNabc/N463	0.82 ± 0.03	0.06 ± 0.01
KNabc/N463r-C7	0.78 ± 0.02	0.19 ± 0.01	KNabc/pEASY	0.06 ± 0.01	0.05 ± 0.01

The medium contains indicated concentrations of NaCl or LiCl and measured at 600 nm (OD_{600}) after 24 h of cultivation. Each strain was tested in three replicates.

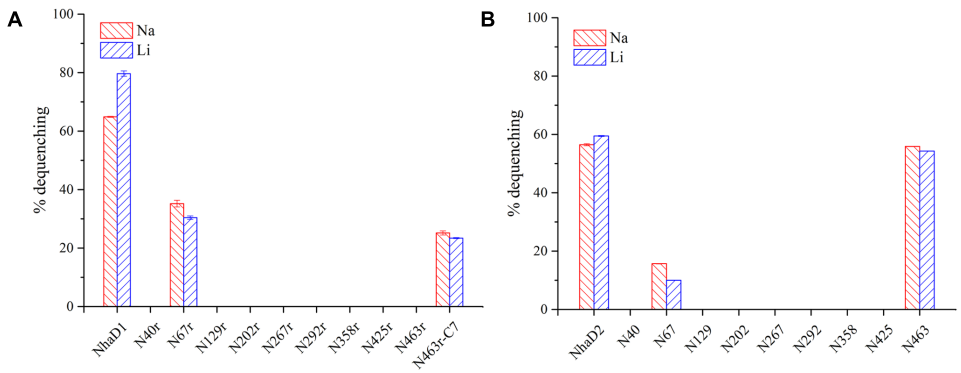

FIGURE 2 | Fluorescence-based antiport activities of chimerical proteins in sub-bacterial vesicles. **(A)** Na^+ and Li^+ antiport activities of NhaD1 chimerical proteins. **(B)** Na^+ and Li^+ antiport activities of NhaD2 chimerical proteins. The transport activities were measured in the assay buffer containing 10 mM Tris-MES (pH 8.5), 140 mM choline chloride, 5 mM $MgCl_2$, 1 μl acridine orange and 60 μg of vesicle protein. The antiporter activity was measured from the dequenching of fluorescence upon the subsequent addition of 10 mM of Na^+, or Li^+.

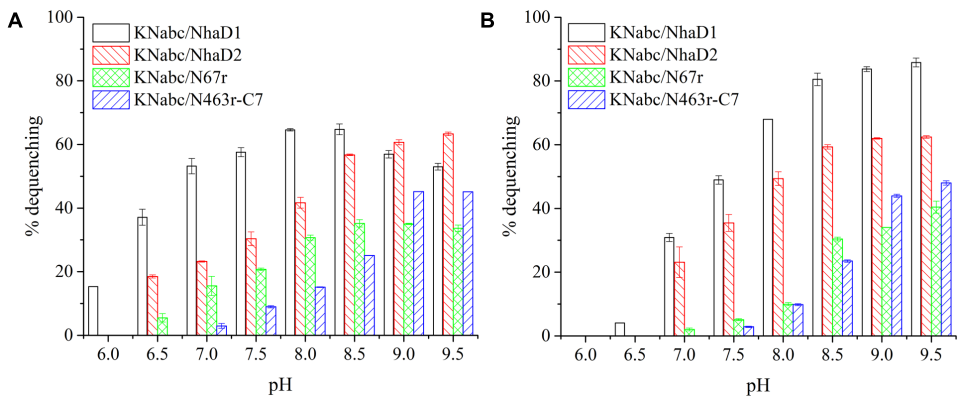

FIGURE 3 | Fluorescence-based antiport activities of NhaD1 chimerical proteins in sub-bacterial vesicles. **(A)** Transport activities of NhaD1 chimeric proteins with a supplementation of 10 mM NaCl at various pHs. **(B)** Transport activities of NhaD1 chimeric proteins with a supplementation of 10 mM LiCl at various pHs.

with only two exceptions, i.e., N67 and N463 chimeric proteins (**Figure 2**). Consistent with the weak growth complementation, modest Na^+ and Li^+ activities were detected in the everted membrane of N67, which exhibits a very similar pH-dependence to that of NhaD2. Interestingly, another active chimera of N463 retained full transport activity as well as a similar pH profile to

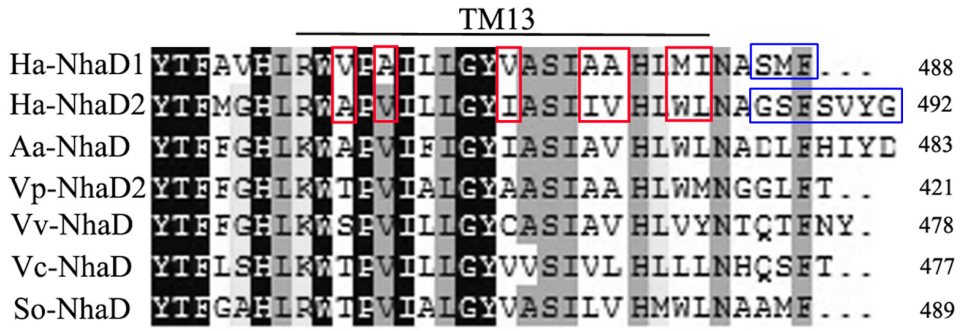

FIGURE 4 | Multiple alignment of the amino terminal sequences of various NhaD homologs by Clustal_X. Residues in blue squares are the replaced residues for chimera N463r-C7 construction; residues in TM XIII for mutation are shown in red squares. Amino acid sequence of NhaD2 was used as a query sequence for BlastP analysis. Homologous sequences from *Alkalimonas amylolytica* (Aa-NhaD, No. Q56EB3), *Vibrio parahaemolyticus* (Vp-NhaD), *Vibrio vulnificus* (Vv-NhaD, No. OJI52092), *Vibrio cholera* (Vc-NhaD, No. A5F120), and *Shewanella oneidensis* (So-NhaD, No. Q8EIA8) were selected for alignments.

that of NhaD2 (**Figures 5A,B**), albeit of its weak ion resistant abilities. Taken together, we proposed that the C-terminal region functions in both transport activity and the pH response of NhaD2.

Mutations in the TM XIII Region

As shown in **Figure 1**, the generated chimeric fragment of N463r-C7 comprises almost the full length of NhaD2 antiporter, except for the substitution of residues 463–485 with the corresponding region of NhaD1. Its weak complementation suggested that region 463–485 is indispensable for the robust complementation of NhaD2. Therefore, we compared this region in NhaD1 and NhaD2 to identify non-conserved residues for targeted site-directed mutagenesis (**Figure 4**). Using N463r-C7 as the template, seven residues were successively replaced with the corresponding residues of NhaD2, and their *E. coli* KNabc transformants were further evaluated for complementation ability and transport activity.

As expected, the last mutant KNabc/N463r-C7-I483L, which carried the NhaD2 sequence, exhibited identical complementation ability and dequenching activity to those of NhaD2. In addition, other than the A468V and M482W variants, all other mutants displayed obviously higher resistance to Na^+ and Li^+ ions than that of NhaD1 (**Figure 6A**). As shown in **Figures 6B,C**, NhaD1 exhibited high Na^+-expelling activity in acidic pH conditions, whereas other variants and NhaD2 were active at pH 9.0–9.5. In the vesicle assays, these seven variants showed an intermediate-type pH response between those of NhaD1 and NhaD2, but is closely related with that of NhaD2.

During the construction of seven variants, the recovery of growth complementation did not display an upward trend, as expected, from KNabc/N463r-C7 to KNabc/N463r-C7-I483L. Indeed, most of chimerical strains showed an obviously enhanced ion resistance than that of KNabc/N463r-C7, and the last mutant KNabc/N463r-C7-I483L restored the robust complementary ability of NhaD2. However, a remarkable exception at site 468 (A468V) was noticeable, which failed to complement the ion resistance of *E. coli* KNabc and completely abolished transport activity, although we constructed several chimeric clones for confirmation. Additionally, the mutant KNabc/N463r-C7-M482W possessed a relative weak resistance to both Na^+ and Li^+ (OD_{600} = 0.095 in the presence of 300 mM NaCl), as

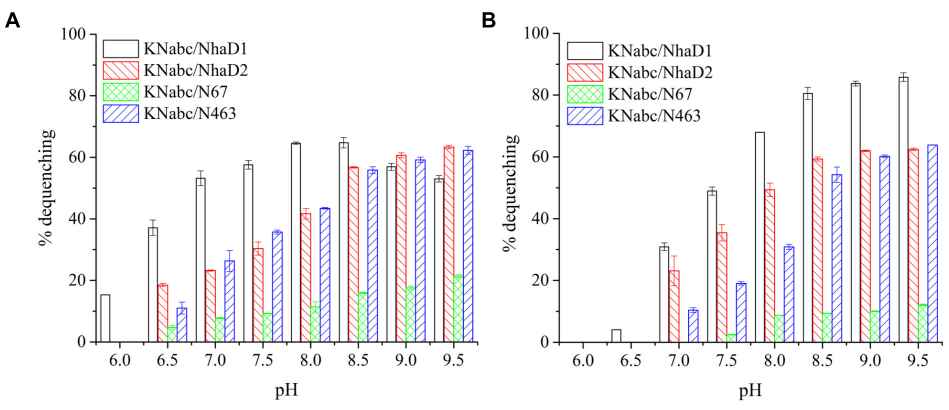

FIGURE 5 | Fluorescence-based antiport activities of NhaD2 chimerical proteins in sub-bacterial vesicles. **(A)** Transport activities of NhaD2 chimeric proteins with a supplementation of 10 mM NaCl at various pHs. **(B)** Transport activities of NhaD2 chimeric proteins with a supplementation of 10 mM LiCl at various pHs.

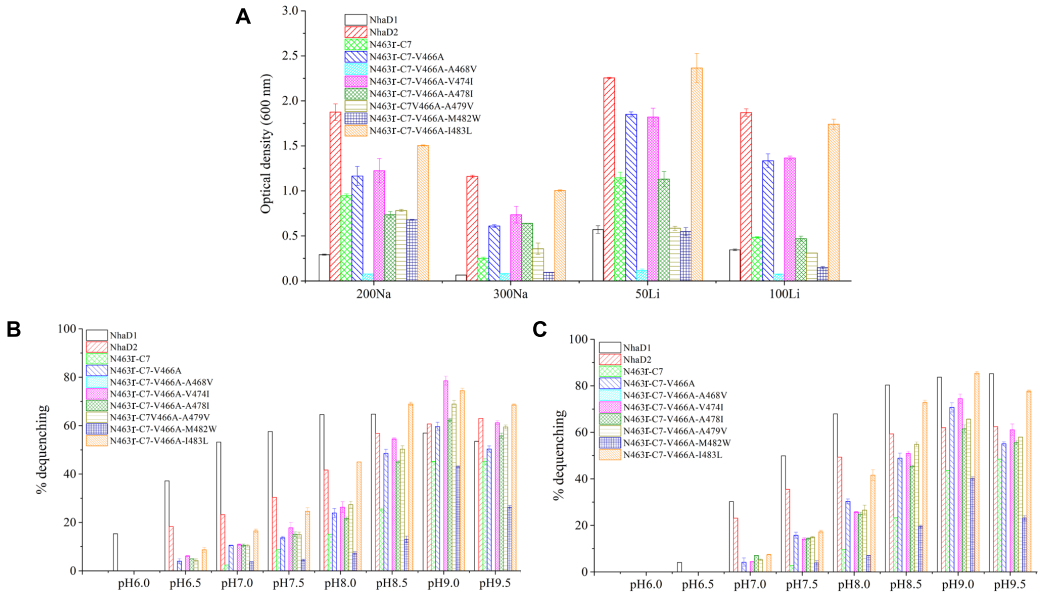

FIGURE 6 | Growth and antiport activities of N463r-C7 mutants in TM XIII. **(A)** Growth of mutants in the LBK medium containing indicated concentrations of NaCl or LiCl. **(B)** Fluorescence-based assays of mutants which initiated by 10 mM Na^+ and measured at different pH values. **(C)** Fluorescence-based assays of mutants which initiated by 10 mM Li^+ and measured at different pH values.

well as lower dequenching activities (13.0% and 19.5% for Na^+ and Li^+, pH 8.5). For explanation, qPCR was used to monitor the expression levels of these mutants, by using the expression level of *nhaD2* as a baseline. As a result, the expression levels of *nhaD1* and *nhaD2* are identical. Remarkably, the transcript levels of A468V and M482W showed a significant downregulation than those of other targeted genes (**Figure 7**), indicating that poor transport activities of these two mutants should be attributed to their decreased transcript levels in the KNabc strain.

To further assess the affinity of seven variants to alkali cations, the apparent K_m values were determined in their sub-bacterial vesicles (**Table 3**). The apparent K_m value of M482W for Na^+ and Li^+ binding was two to three times higher than that of wild-type NhaD2. The reduced binding affinity may also partially explain the decreased complementation of *E. coli* KNabc/M482W for Na^+ and Li^+ resistance. All other active mutants exhibited similar K_m values to that of NhaD2, indicating that ion binding was not affected by these site mutations.

Ion Resistance of Complementary Strains of *Halomonas* sp. Y2/Δ*nhaD2*

To verify the physiological functions of TM XIII in strain *Halomonas* sp. Y2, the seven mutated plasmids of N463r-C7 were transformed into the NhaD2-deficient strain we previously constructed (Cheng et al., 2016, designated Y2/Δ*nhaD2* in the text) and generated seven complementary strains (**Table 1**). For comparison, N463r-C7 was also inserted into Y2/Δ*nhaD2* and cultured under the same conditions. As shown in **Table 4**, the growth of the NhaD2-deficient strain was seriously inhibited by 15% NaCl at both tested pHs, whereas partial or completely restored growth was detected in the complementary strain Y2/*nhaD2*. In compared to NhaD2, the *nhaD1*-disrupted strain was merely modestly sensitive to 15% NaCl at pH 10.0. These results are consistent with our previous conclusions that NhaD2 plays important roles in the regulation of ion homeostasis (Cheng et al., 2016). Under high pH and ion concentrations, all complement strains except Y2/N463r-C7-A468V exhibited

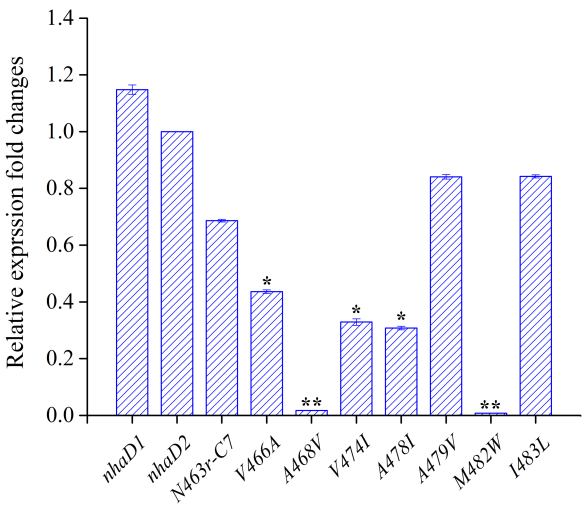

FIGURE 7 | Transcript levels of N463r-C7 mutants determined by qPCR analysis. The relative expression levels for each gene were calculated using the by $2^{-\Delta\Delta Ct}$ with normalization to *16S rRNA* genes. The significant differences (**$P < 0.001$, *$P < 0.05$, fold change ≥2 or fold change ≤0.5, Student's *t*-test) between the expression levels of mutated genes and *nhaD2* are indicated by asterisks.

TABLE 3 | Apparent K_m values of constructed fusion proteins in TM XIII.

Variants	Apparent K_m (mM)	
	Na^+	Li^+
NhaD1	0.89 ± 0.05	2.43 ± 0.12
NhaD2	0.47 ± 0.02	2.07 ± 0.11
N463r-C7	0.33 ± 0.01	1.44 ± 0.12
N463r-C7-V466A	0.49 ± 0.05	2.29 ± 0.08
N463r-C7-A468V	–	–
N463r-C7-V474I	0.48 ± 0.02	2.95 ± 0.06
N463r-C7-A478I	0.42 ± 0.03	2.82 ± 0.11
N463r-C7-A479V	0.37 ± 0.02	2.64 ± 0.14
N463r-C7-M482W	1.67 ± 0.06	5.00 ± 0.21
N463r-C7-I483L	0.59 ± 0.05	2.48 ± 0.08

The everted membrane activities of these proteins were measured in buffer B solution at pH 8.5, with different concentrations of NaCl or LiCl (0.01–100 mM) supplementation. "–" indicates no activity and not determined. The activity of each sample was determined in triplicate.

obviously greater growth than that of Y2/N463r-C7. Moreover, identical growth to that of wild-type *Halomonas* sp. Y2 was detected in the final strain (Y2/N463r-C7-I483L), with a similar OD_{600} values at pH 8.0 (OD_{600} = 2.17) and pH 10.0 (OD_{600} = 1.08), in the presence of 15% NaCl (**Table 4**). These *in situ* capacities for ion resistance are in good agreement with those of *E. coli* KNabc recombinants (**Figure 6A**), including the impaired ion resistance of A468V mutants. It is noticeable that the impaired growth was mainly observed in the highly alkaline and saline medium (15% NaCl, pH 10.0), in which Y2/N463r-C7-A468V showed a high similar growth to that of Y2/Δ*nhaD2*.

FRET Analysis for Conformational Changes of N463r Fusion

It is well accepted that FRET could be used to monitor protein–protein interactions, oligomerization, and conformational change of proteins (Stryer, 1978; Karasawa et al., 2005). Based on a previous FRET construct of N39-CFP-C-YFP (designed D2-CFP-YFP in this study, **Figure 8A**) as a template (Meng et al., 2017), we successfully replaced its C-terminal region (residues 464–492) with the corresponding fragment of NhaD1 and generated chimeric protein N463r-CFP-YFP (**Figures 8A,B**). After cultivation and induction, the suspended cells were subjected to the fluorescence scanning from 400 to 600 nm. Compared to D2-CFP-YFP, the fluorescence spectrum of N463r-CFP-YFP displayed a reduced signal at 528 nm (red arrow) when being excitated by 433 nm. This was identical to the negative control D2-N39-CFP, but much lower than that of D2-CFP-YFP (**Figure 8C**). These results suggest that the substitution of region 464–492 induced some conformational changes and prolonged the distance between TM I and C-terminus.

DISCUSSION

In this study, taking advantage of the high sequence identity of NhaD1 and NhaD2, various chimeric NhaD1 and NhaD2 fusions were constructed and alterations in transport activity were evaluated. As the major difference between NhaD1 and NhaD2 is their complementation ability, the growth of each *E. coli* KNabc chimera was first tested using different NaCl concentrations. Unexpectedly, most chimeras showed weak growth in the presence of 200 mM NaCl and completely lost their original activities. However, an interesting exception was found in the NhaD2-derived chimera N67, which contains 67 N-terminal residues of NhaD1 and the 68–492 fragment of NhaD2. When compared to NhaD2, it retained partial complementation ability and antiport activity, as well as a similar pH-dependent profile for Na^+ and Li^+ translocation. Its corresponding chimera N67r exhibited a slightly higher complementation ability than that of NhaD1, together with partial antiport activity and a similar pH profile and ion affinities to those of NhaD1. In combination with the lack of growth and activities observed for N40 and N40r, we speculate that (i) TMs I and II in the N-terminus functional interact to retain the active structure of NhaD; (ii) region 1–67 is partially responsible for the complementation ability of the antiporter, but is not directly involved in the catalytic center for pH sensitivity or ion binding; (iii) region 68–488 in NhaD1 (or 492 in NhaD2) is the catalytic center for pH sensitivity and ion translocation.

Another remarkable exception is two fusions at site 463, in which N463r completely abolished the transport activity and complementation abilities. We previously disclosed that the C-terminus of NhaD1 and NhaD2 is irreplaceable for their ion transport capacities (Meng et al., 2017), and consequently, the diminished activity of N463r was expected. In contrast, N463 retained a surprising high activity and similar pH profile as that of NhaD2. As shown in **Figure 1**, chimera N463 comprises almost the full length of NhaD1, except for the substitution of region 464–488 with the corresponding region (464–492) of NhaD2. Therefore, we suspected that the C-terminal region is directly involved in the pH sensitivity of these antiporters and structurally affects the transport activity. Contrast to robust dequenching activity, the KNabc strain carrying chimera N463 plasmid only displayed slightly complementation ability. Such gaps between the transport activity and ion complementary ability is similar to that of wild-type NhaD1. Possible explanation for such gaps would be the difference of *in vivo* and *in vitro* environments, i.e., the Tris-MES assay mixture is different from the physiological environment of the cells. In the pH-blocked structure of Ec-NhaA, the periplasmic passage is blocked by an ion barrier under some conditions (Karpel et al., 1988; Hunte et al., 2005). Thereby, different environments might affect the pH-activated conformational changes of these proteins and retard the ion translocation process. In combination with the alterations of pH profiles of those chimeras, we suspected that region 464–492 might be critical to the pH sensitivity and pH activation of NhaD2 antiporter.

To explore critical regions that are responsible for the strong physiological functions of NhaD2, N463r-C7 was further generated by replacing its four C-terminal amino acids with seven amino acids from NhaD2. Notably, the transport activity was significantly enhanced by this fusion; around 50% activity

TABLE 4 | Complementation growth of constructed mutants to the wild type *Halomonas* sp. Y2.

Strain	pH 8.0			pH 10.0	
	10% Na	15% Na	6% Li	10% Na	15% Na
Halomonas sp. Y2	5.71 ± 0.31	2.18 ± 0.07	0.91 ± 0.12	4.87 ± 0.19	1.23 ± 0.08
Y2/Δ*nhaD1*	5.57 ± 0.12	2.29 ± 0.02	0.89 ± 0.05	4.46 ± 0.11	0.65 ± 0.07
Y2/Δ*nhaD2*	4.26 ± 0.21	1.09 ± 0.02	0.78 ± 0.05	3.32 ± 0.12	0.24 ± 0.04
Y2/Δ*nhaD1*/*nhaD1*	5.01 ± 0.23	2.05 ± 0.10	0.95 ± 0.03	4.69 ± 0.17	1.02 ± 0.06
Y2/Δ*nhaD2*/*nhaD2*	5.59 ± 0.19	1.76 ± 0.11	0.90 ± 0.12	4.90 ± 0.15	0.93 ± 0.08
Y2/N463r-C7	4.01 ± 0.14	0.66 ± 0.03	0.42 ± 0.04	4.50 ± 0.17	0.14 ± 0.01
Y2/N463r-C7-V466A	4.59 ± 0.17	1.23 ± 0.12	0.34 ± 0.02	4.06 ± 0.09	0.29 ± 0.02
Y2/N463r-C7-A468V	4.98 ± 0.20	1.41 ± 0.09	0.36 ± 0.06	4.35 ± 0.04	0.20 ± 0.02
Y2/N463r-C7-V474I	4.30 ± 0.21	1.47 ± 0.10	0.68 ± 0.11	4.18 ± 0.20	0.54 ± 0.03
Y2/N463r-C7-A478I	4.47 ± 0.14	1.54 ± 0.12	0.69 ± 0.08	4.41 ± 0.15	0.41 ± 0.06
Y2/N463r-C7-A479V	4.90 ± 0.17	1.50 ± 0.08	0.48 ± 0.07	4.38 ± 0.12	0.58 ± 0.09
Y2/N463r-C7-M482W	4.44 ± 0.16	1.65 ± 0.18	0.82 ± 0.12	3.38 ± 0.18	0.51 ± 0.07
Y2/N463r-C7-I483L	5.10 ± 0.22	2.17 ± 0.21	0.84 ± 0.08	4.49 ± 0.21	1.08 ± 0.12

The mutated fragments were from plasmid N463r-C7 and transformed into strain Halomonas sp. Y2 with NhaD2 deficiency (Y2/ ΔnhaD2). After 24-h incubation in the LB medium with various concentrations of NaCl and LiCl, OD_{600nm} were determined. Each strain was tested in three replicates.

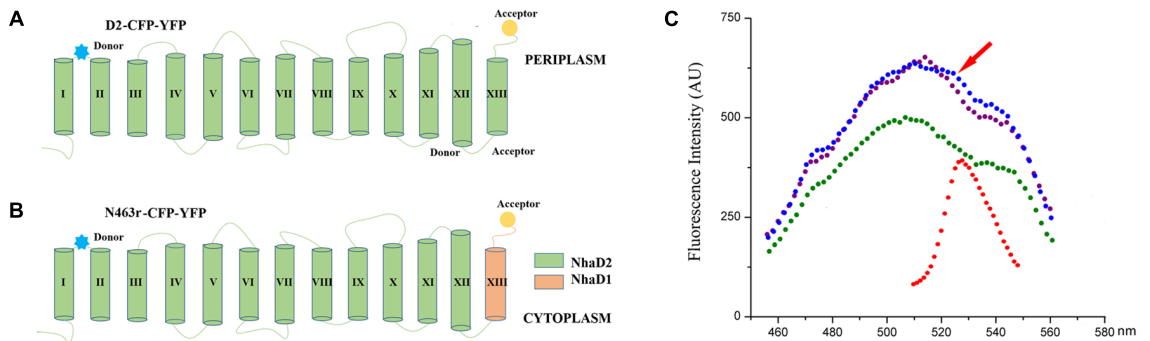

FIGURE 8 | Schematic representation and fluorescence spectra of cell suspensions containing N39 fusions for FRET analysis. **(A)** NhaD2 fusion protein with CFP fused at site 39 and YFP at the C terminus. **(B)** N463r fusion protein with CFP fused at site 39 and YFP at the C terminus. **(C)** Fluorescence spectra of CFP and YFP constructs. Fluorescence emissions upon excitation by 433 nm for CFP or 473 nm for YFP were measured in the cells that resuspending in Tricine-KOH buffer (pH 8.5). Fluorescence emission upon 473 nm excitation of D2-CFP-YFP was recorded as red; fluorescence emission of D2-CFP fusion cells that excited by 433 nm was recorded as green; fluorescence emission upon 433 nm excitation of D2-CFP-YFP was presented as blue; and fluorescence emission upon 433 nm excitation of N463r-CFP-YFP was presented as purple.

was observed at pH 9.5 in the everted membrane of N463r-C7 (**Figure 3**). These recoveries agree well with our previous conclusion that the C-terminus of NhaD functionally interacts with the N-terminus (Meng et al., 2017). However, strains of *E. coli* KNabc and *Halomonas* sp. Y2/Δ*nhaD2* carrying N463r-C7 merely displayed a weakly restored ion resistance (**Tables 2**, **4**). As shown in **Figure 1**, the majority of the N463r-C7 fragment was from NhaD2, whereas only residues 464–485 were replaced with the corresponding sequence in NhaD1. Therefore, the weakly recovered complementation ability implies that region 464–485 is important to the robust *in vivo* functions of NhaD2.

Based on the constructed topological model of NhaD2 (Meng et al., 2017), residues 464–485 are mainly located in the last helix of TM XIII, which raises the possibility that TM XIII is a key region for the physiological functions of NhaD2. Seven mutated N463r-C7 plasmids were then constructed and transformed into *E. coli* KNabc or *Halomonas* sp. Y2/Δ*nhaD2*. Compared to KNabc/N463r-C7 and Y2/Δ*nhaD2*/N463r-C7, the ion resistances of these mutants were significantly improved. Considering the seriously impaired FRET efficiency of N463r-CFP-YFP, we proposed that the substitution of region 464–482 caused a conformational change in NhaD2 and seriously blocked its ion translocation function. Further mutations in TM XIII verified our supposition, in which seven mutants recovered the robust transport activities of NhaD2 gradually. Since the pioneering work resolving the crystal structure of Ec-NhaA, structures of other bacterial ion-coupled transporters have been determined (Hunte et al., 2005). These include some ATPases (Morth et al., 2007; Olesen et al., 2007), secondary transporters of Na^+/galactose (Faham et al., 2008), Na^+/bile acid (Hu et al., 2011), and Na^+/citrate (Mancusso et al., 2014). These antiporters share little or no similarity to Ec-NhaA, but also include inverted topological repeats containing an interrupted helix where the ion-binding site is located (Screpanti and Hunte, 2007). A series of

charged/polar mutations in Vc-NhaD also suggested that NhaD antiporters may share common structural features and catalytic modes with other reports (Habibian et al., 2005). Based on these resolved structures, the last helix is not directly involved in ion translocation. Similar to those of Ec-NhaA, TMs IV, V, VI, and X-XII in Vc-NhaD are suggested to form a transmembrane relay involved in the attraction, coordination, and translocation of transported cations (Habibian et al., 2005). We speculated that NhaD1 and NhaD2 contain a similar relay as that of NhaA, and TM XIII is not directly involved in the catalytic cavity but conformational affects the ion barrier and pH activation of NhaD antiporters. In the physiological environments, the conformational activations of NhaD1 and N463 were affected and thereby retards the *in vivo* transport ability.

CONCLUSION

Taken together, high *in vitro* activities of NhaD1 and NhaD2 and the remarkable difference of *in vivo* ion resistance provided an interesting starting point for studying the transport mechanism of NhaD-type antiporters. It is likely that the mechanism underlying the robust physiological function of NhaD2 includes multiple components, but the N and C terminal regions, especially TM XIII, is indispensable. We suspected that TM XIII is in close proximity to the periplasmic catalytic center of NhaD2, and consequently influences the conformational change of the pH-activated or ion-translocating states that observed in Ec-NhaA or $MjNhaP_1$ (Olkhova et al., 2006; Schushan et al., 2012; Cristina and Werner, 2014).

AUTHOR CONTRIBUTIONS

CY designed the experiments and analyzed the data. CY and PX prepared the manuscript. ZY, YM, QZ, and BC conducted the experiments.

FUNDING

Funding for this project was provided from the National Natural Science Foundation of China (31670109 and 31370153).

ACKNOWLEDGMENTS

The authors thank Dr. T. A. Krulwich (Icahn School of Medicine at Mount Sinai, New York, NY, United States) for kindly providing strain *E. coli* KNabc.

SUPPLEMENTARY MATERIAL

The Supplementary Material for this article can be found online at: https://www.frontiersin.org/articles/10.3389/fmicb.2018.00831/full#supplementary-material

REFERENCES

Appel, M., Hizlan, D., Vinothkumar, K. R., Ziegler, C., and Kühlbrandt, W. (2009). Conformations of NhaA, the Na^+/H^+ exchanger from *Escherichia coli*, in the pH-activated and ion-translocating states. *J. Mol. Biol.* 386, 351–365. doi: 10.1016/j.jmb.2008.12.042

Cheng, B., Meng, Y. W., Cui, Y. B., Li, C. F., Tao, F., Yin, H. J., et al. (2016). Alkaline response of a halotolerant alkaliphilic *Halomonas* strain and functional diversity of its $Na^+(K^+)/H^+$ antiporters. *J. Biol. Chem.* 291, 26056–26065. doi: 10.1074/jbc.M116.751016

Cristina, P., and Werner, K. (2014). pH- and sodium-induced changes in a sodium/proton antiporter. *eLife* 3:e01412. doi: 10.7554/eLife.01412

Cui, Y. B., Cheng, B., Meng, Y. W., Li, C. F., Yin, H. J., Xu, P., et al. (2016). Expression and functional analysis of two NhaD type antiporters from the halotolerant and alkaliphilic *Halomonas* sp. Y2. *Extremophiles* 20, 631–639. doi: 10.1007/s00792-016-0852-8

Dzioba, J., Ostroumov, E., Winogrodzki, A., and Dibrov, P. (2002). Cloning, functional expression in *Escherichia coli* and primary characterization of a new Na^+/H^+ antiporter, NhaD, of *Vibrio cholerae*. *Mol. Cell. Biochem.* 229, 119–124. doi: 10.1023/A:1017932829927

Faham, S., Watanabe, A., Besserer, G. M., Cascio, D., Specht, A., Hirayama, B. A., et al. (2008). The crystal structure of a sodium galactose transporter reveals mechanistic insights into Na^+/sugar symport. *Science* 321, 810–814. doi: 10.1126/science.1160406

Goldberg, E. B., Arbel, T., Chen, J., Karpel, R., Mackie, G. A., Schuldiner, S., et al. (1987). Characterization of a Na^+/H^+ antiporter gene of *Escherichia coli*. *Proc. Natl. Acad. Sci. U.S.A.* 84, 2615–2619. doi: 10.1073/pnas.84.9.2615

Habibian, R., Dzioba, J., Barrett, J., Galperin, M. Y., Loewen, P. C., and Dibrov, P. (2005). Functional analysis of conserved polar residues in Vc-NhaD, Na^+/H^+ antiporter of *Vibrio cholerae*. *J. Biol. Chem.* 280, 39637–39643. doi: 10.1074/jbc.M509328200

Herz, K., Rimon, A., Olkhova, E., Kozachkov, L., and Padan, E. (2010). Transmembrane segment II of NhaA Na^+/H^+ antiporter lines the cation passage, and Asp65 is critical for pH activation of the antiporter. *J. Biol. Chem.* 285, 2211–2220. doi: 10.1074/jbc.M109.047134

Hu, N. J., Iwata, S., Cameron, A. D., and Drew, D. (2011). Crystal structure of a bacterial homologue of the bile acid sodium symporter ASBT. *Nature* 478, 408–411. doi: 10.1038/nature10450

Hunte, C., Screpanti, M., Venturi, M., Rimon, A., Padan, E., and Michel, H. (2005). Structure of a Na^+/H^+ antiporter and insights into mechanism of action and regulation by pH. *Nature* 534, 1197–1202. doi: 10.1038/nature03692

Karasawa, A., Tsuboi, Y., Inoue, H., Kinoshita, R., Nakamura, N., and Kanazawa, H. (2005). Detection of oligomerization and conformational changes in the Na^+/H^+ antiporter from *Helicobacter pylori* by fluorescence resonance energy transfer. *J. Biol. Chem.* 280, 41900–41911. doi: 10.1074/jbc.M510795200

Karpel, R., Olami, Y., Taglicht, D., Schuldiner, S., and Padan, E. (1988). Sequencing of the gene ant which affects the Na^+/H^+ antiporter activity in *Escherichia coli*. *J. Biol. Chem.* 263, 10408–10414.

Kozachkov, L., Herz, K., and Padan, E. (2007). Functional and structural interactions of the transmembrane domain X of NhaA, Na^+/H^+ antiporter of *Escherichia coli*, at physiological pH. *Biochemistry* 46, 2419–2430. doi: 10.1021/bi602393s

Krulwich, T. A., Sachs, G., and Padan, E. (2011). Molecular aspects of bacterial pH sensing and homeostasis. *Nat. Rev. Microbiol.* 9, 330–343. doi: 10.1038/nrmicro2549

Kurz, M., Brünig, A. N., and Galinski, E. A. (2006). NhaD type sodium/proton-antiporter of *Halomonas elongata*: a salt stress response mechanism in marine habitats? *Saline Systems* 2:10. doi: 10.1186/1746-1448-2-10

Liu, J., Xue, Y., Wang, Q., Wei, Y., and Swartz, T. H. (2005). The activity profile of the NhaD-type $Na^+(Li^+)/H^+$ antiporter from the soda lake haloalkaliphile *Alkalimonas amylolytica* is adaptive for the extreme environment. *J. Bacteriol.* 187, 7589–7595. doi: 10.1128/JB.187.22.7589-7595.2005

Maes, M., Rimon, A., Kozachkov-Magrisso, L., Friedler, A., and Padan, E. (2012). Revealing the ligand binding site of NhaA Na^+/H^+ antiporter and its pH dependence. *J. Biol. Chem.* 287, 38150–38157. doi: 10.1074/jbc.M112.391128

Mager, T., Rimon, A., Padan, E., and Fendler, K. (2011). Transport mechanism and pH regulation of the Na^+/H^+ antiporter NhaA from *Escherichia coli*: an electrophysiological study. *J. Biol. Chem.* 286, 23570–23581. doi: 10.1074/jbc.M111.230235

Mancusso, R., Gregorio, G. G., Liu, Q., and Wang, D. N. (2014). Structure and mechanism of a bacterial sodium-dependent dicarboxylate transporter. *Nature* 491, 622–626. doi: 10.1038/nature11542

Meng, Y., Yang, Z., Cheng, B., Nie, X. Y., Li, S. N., Yin, H. J., et al. (2017). Functional interaction between the N- and C-termini of NhaD antiporters from *Halomonas* sp. Y2. *J. Bacteriol.* 199, 1–11. doi: 10.1128/JB.00302-17

Morth, J. P., Pedersen, B. P., Toustrup-Jensen, M. S., Sorensen, T. L., Petersen, J., Andersen, J. P., et al. (2007). Crystal structure of the sodium-potassium pump. *Nature* 450, 1043–1049. doi: 10.1038/nature06419

Nozaki, K., Kuroda, T., Mizushima, T., and Tsuchiya, T. (1998). A new Na^+/H^+ antiporter, NhaD, of *Vibrio parahaemolyticus*. *Biochim. Biophys. Acta* 1369, 213–220. doi: 10.1016/S0005-2736(97)00223-X

Olesen, C., Picard, M., Winther, A. M., Gyrup, C., Morth, J. P., Oxvig, C., et al. (2007). The structural basis of calcium transport by the calcium pump. *Nature* 450, 1036–1042. doi: 10.1038/nature06418

Olkhova, E., Hunte, C., Screpanti, E., Padan, E., and Michel, H. (2006). Multiconformation continuum electrostatics analysis of the NhaA Na^+/H^+ antiporter of *Escherichia coli* with functional implications. *Proc. Natl. Acad. Sci. U.S.A.* 103, 2629–2634. doi: 10.1073/pnas.0510914103

Padan, E., and Landau, M. (2016). Sodium-proton (Na^+/H^+) antiporters: properties and roles in health and disease. *Met. Ions Life Sci.* 16, 391–458.

Padan, E., Venturi, M., Gerchman, Y., and Dover, N. (2001). Na^+/H^+ antiporters. *Biochim. Biophys. Acta* 1505, 144–157. doi: 10.1016/0304-4173(83)90011-3

Schushan, M., Rimon, A., Haliloglu, T., Forrest, L. R., Padan, E., and Ben-Tal, N. (2012). A model-structure of a periplasm-facing state of the NhaA antiporter suggests the molecular underpinnings of pH-induced conformational changes. *J. Biol. Chem.* 287, 18249–18261. doi: 10.1074/jbc.M111.336446

Screpanti, E., and Hunte, C. (2007). Discontinuous membrane helices in transport proteins and their correlation with function. *J. Struct. Biol.* 159, 261–267. doi: 10.1016/j.jsb.2007.01.011

Stryer, L. (1978). Fluorescence energy transfer as a spectroscopic ruler. *Annu. Rev. Biochem.* 47, 819–846. doi: 10.1146/annurev.bi.47.070178.004131

Thompson, J. D., Gibson, T. J., Plewniak, F., Jeanmougin, F., and Higgins, D. G. (1997). The CLUSTAL_X windows interface: flexible strategies for multiple sequence alignment aided by quality analysis tools. *Nucleic Acids Res.* 25, 4876–4882. doi: 10.1093/nar/25.24.4876

Tzubery, T., Rimon, A., and Padan, E. (2008). Structure based functional study reveals multiple roles of transmembrane segment IX and loop VIII–IX in NhaA Na^+/H^+ antiporter of *Escherichia coli* at physiological pH. *J. Biol. Chem.* 283, 15975–15987. doi: 10.1074/jbc.M800482200

Yang, C., Wang, Z., Li, Y., Niu, Y., Du, M., He, X., et al. (2010). Metabolic versatility of halotolerant and alkaliphilic strains of *Halomonas* isolated from alkaline black liquor. *Bioresour. Technol.* 101, 6778–6784. doi: 10.1016/j.biortech.2010.03.108

Zhang, H., Wang, Z., Wang, L., Mu, R., Zou, Z., Yuan, K., et al. (2014). Cloning and identification of a novel NhaD-type Na^+/H^+ antiporter from metagenomic DNA of the halophilic bacteria in soil samples around Daban Salt Lake. *Extremophiles* 18, 89–98. doi: 10.1007/s00792-013-0600-2

Conflict of Interest Statement: The authors declare that the research was conducted in the absence of any commercial or financial relationships that could be construed as a potential conflict of interest.

frontiers in Microbiology

ORIGINAL RESEARCH
published: 28 August 2018
doi: 10.3389/fmicb.2018.01994

A Hydrophobic Small Protein, BpOF4_01690, Is Critical for Alkaliphily of Alkaliphilic *Bacillus pseudofirmus* OF4

*Tetsuaki Takahashi[1], Terry A. Krulwich[2] and Masahiro Ito[1,3]**

[1] Graduate School of Life Sciences, Toyo University, Gunma, Japan, [2] Department of Pharmacological Sciences, Icahn School of Medicine at Mount Sinai, New York, NY, United States, [3] Bio-Nano Electronics Research Centre, Toyo University, Kawagoe, Japan

A monocistronic small protein, BpOF4_01690, was annotated in alkaliphilic *Bacillus pseudofirmus* OF4. It comprises 59 amino acids and is hydrophobic. Importantly, homologs of this protein were identified only in alkaliphiles. In this study, a mutant with a BpOF4_01690 gene deletion (designated Δ01690) exhibited weaker growth than that of the wild type in both malate-based defined and glucose-based defined media under low-sodium conditions at pH 10.5. Additionally, the enzymatic activity of the respiratory chain of Δ01690 was much lower than that of the wild type. These phenotypes were similar to those of a *ctaD* deletion mutant and an *atpB-F* deletion mutant. Therefore, we hypothesize that BpOF4_01690 plays a critical role in oxidative phosphorylation under highly alkaline conditions.

Keywords: alkaliphiles, small protein, *Bacillus pseudofirmus,* respiratory chain, pH homeostasis, alkaliphily

OPEN ACCESS

Edited by:
Philippe M. Oger, UMR5240 Microbiologie, Adaptation et Pathogenie (MAP), France

Reviewed by:
James A. Coker, University of Maryland University College, United States
Dong-Woo Lee, Yonsei University, South Korea
Satyanarayana Tulasi, University of Delhi, India

***Correspondence:**
Masahiro Ito
masahiro.ito@toyo.jp

Specialty section:
This article was submitted to Extreme Microbiology, a section of the journal Frontiers in Microbiology

Received: *01 May 2018*
Accepted: *08 August 2018*
Published: *28 August 2018*

Citation:
Takahashi T, Krulwich TA and Ito M (2018) A Hydrophobic Small Protein, BpOF4_01690, Is Critical for Alkaliphily of Alkaliphilic Bacillus pseudofirmus OF4. Front. Microbiol. 9:1994. doi: 10.3389/fmicb.2018.01994

INTRODUCTION

Alkaliphilic microorganisms usually grow vigorously in highly alkaline environments and require Na^+ for their growth (Horikoshi, 1991; Krulwich et al., 2011; Preiss et al., 2015). Na^+ cycling was found to be critical for the alkaline pH adaptation of alkaliphilic bacteria (Ito et al., 2004a,b) (**Figure 1**). Although it is extremely difficult to produce and utilize a proton-motive force (PMF) at highly alkaline pH, ATP synthesis by oxidative phosphorylation (OXPHOS) using F_1F_o-ATP synthase is driven by PMF in alkaliphilic *Bacillus* species (Guffanti and Krulwich, 1994). Therefore, some effective ATP synthesis mechanisms are expected to operate in these bacteria in their highly alkaline environment. It has been suggested that accumulation of protons on the outer surface of the cytoplasmic membrane (Yoshimune et al., 2010) facilitates energy coupling that is more efficient than usual, thereby increasing the feasibility of ATP synthesis in a highly alkaline pH environment (Krulwich, 1995). The alkaliphilic *Bacillus clarkia* K24-1U was also proposed to efflux protons by the respiratory chain, accumulating them on the outer surface of the cytoplasmic membrane (Cherepanov et al., 2003; Mulkidjanian, 2006). Another possibility is the activity of an unidentified proton carrier that depends on the dielectric properties of the membrane potential (Liu et al., 2007). Thus, the outer surface vicinity of the cytoplasmic membrane is locally acidified, and enough PMF necessary for the synthesis of ATP is provided despite the alkaline environment. Fast cardiolipin-mediated proton translocation from the respiratory chain pumps to ATP synthase by OXPHOS was also hypothesized. However, the mutational loss of membrane cardiolipin did not significantly affect alkaliphile ATP synthesis in alkaliphilic *B. pseudofirmus* OF4 (Liu et al., 2014).

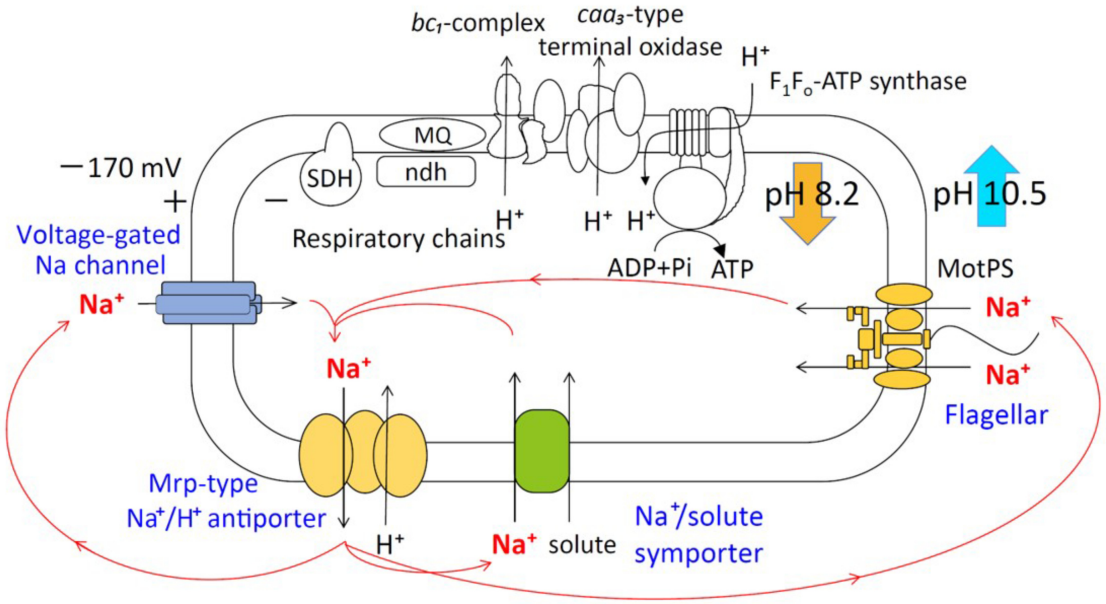

FIGURE 1 | Schematic diagram of the Na^+ cycle of alkaliphilic *Bacillus pseudofirmus* OF4. Alkaliphilic *B. pseudofirmus* OF4 grows well around pH 10, and the intracellular pH is maintained around 8.2. The Mrp-type Na^+/H^+ antiporter performs a crucial role in the maintenance of intracellular ion concentrations and pH homeostasis. Na^+/H^+ antiporters catalyze proton accumulation in the cytoplasm while cells are extruding H^+ during respiration. Na^+ re-entry in support of pH homeostasis is achieved by Na^+: solute symporters. When Na^+ entry is limited, e.g., at low [Na^+] concentrations or a lack of symporter substrates, the voltage-gated Na channel operates as a physiologically important ensuring a re-entry route for Na^+. The Na^+-driven flagellar motor (MotPS channel) functions as a secondary pathway. SDH, succinate dehydrogenase; MQ, menaquinone; Ndh-II, type II NADH:quinone oxidoreductase.

Descriptions of a unique "alkaliphily" motif in the *c*-ring of ATP synthase from alkaliphilic *B. pseudofirmus* OF4 had been noted in earlier studies of alkaliphilic bacteria (Liu et al., 2009; Fujisawa et al., 2010). This alkaliphile OXPHOS motif could underpin the efflux of protons by the respiratory chain. Nonetheless, the amount of protons is not in equilibrium with that of the external environment. Consequently, during ATP synthesis, protons are directly transferred to F_1F_o-ATP synthase through the cytoplasmic membrane. Results of differential scanning calorimetry analysis and saturation transfer electron spin resonance provided indirect evidence for the interaction between the caa_3-type terminal oxidase and F_1F_o-ATP synthase in the proteoliposome (Liu et al., 2007). However, no reports demonstrate the presence of a direct interaction between caa_3-type oxidase and F_1F_o-ATP synthase.

The hypothetical small protein BH2819 containing 62 amino acids was identified as a complementation gene product of an alkaline pH-sensitive mutant, which was isolated from alkaliphilic *B. halodurans* C-125 by chemical mutagenesis using ethyl methanesulfonate (Aono et al., 1993). Since the BH2819 mutants showed both decreased NADH oxidase activity and loss of growth at a highly alkaline pH, the potential involvement of the BH2819 protein in alkali mechanisms attracted scientific interest, particularly regarding the respiratory chain complexes. The previous evidence of a lack of genetic accessibility of the target gene disruption technique of *B. halodurans* C-125 genomic DNA, whole genome sequencing of *B. pseudofirmus* OF4, a closely related species to *B. halodurans* C-125, was performed. The result revealed a homologous protein of BH2819, designated BpOF4_01690, a monocistronic small protein, which was unique and found mostly in alkaliphilic *Bacillus* species (**Figure 2**) (Janto et al., 2011). BpOF4_01690 is a low-molecular-weight protein that, similarly to the BH2819 protein, consists of only 59 amino acids (GenBank accession no. ADC48406.1).

In major studies on small proteins reported by Hobbs et al. (2011) and Storz et al. (2014), this type of protein was defined as proteins made up of <50 amino acids (aa's). However, we encountered a somewhat larger protein in alkaliphilic *B. pseudofirmus* OF4: BpOF4_01690 with 59 aa's and a similar protein from *B. halodurans* C-125, BH2819 with 62 aa's. While not quite as small as the "small proteins" studied by others, they appeared to be sufficiently small to be worthwhile examining in this context.

Many small proteins studied to date are classified as integral membrane proteins. The function of small proteins is diverse, including spore formation, cell division, transport, and the activities of membrane-bound enzymes, such as we were studying, as well as protein kinases, and signal transduction systems (Su et al., 2013; Storz et al., 2014). It has been reported that the small protein Rcf1 plays an important role in the formation of respiratory chain supercomplexes of mitochondria (Chen et al., 2012). Rcf1 is interposed between complex III and IV, and its function is to promote the formation of the supercomplex. Consequently, respiratory failure occurs in the mitochondrial respiratory chains of Rcf1-defective mutants.

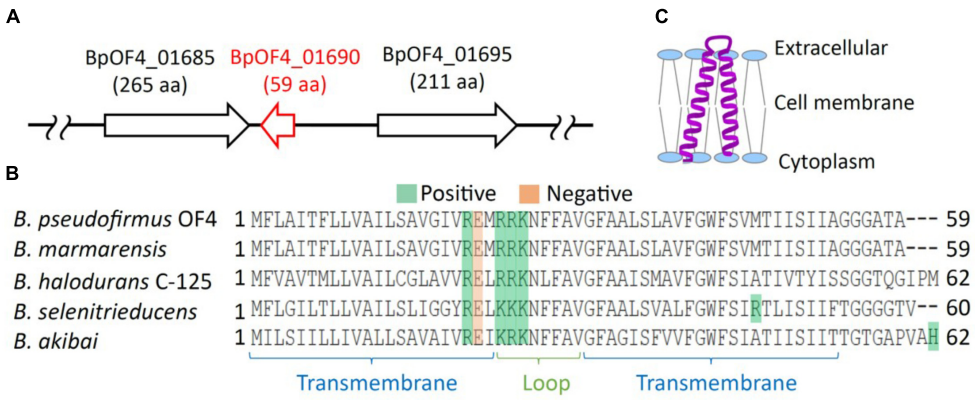

FIGURE 2 | Features of BpOF4_01690. **(A)** The arrangement of BpOF4_01690 and the surrounding genes. **(B)** Multiple alignment analysis of BpOF4_01690 and its homologous proteins was performed using Uniprot (http://www.uniprot.org/). The positively charged amino acid residues are denoted in green, whereas the negatively charged amino acid residues are shown in pink. Transmembrane region prediction was performed using SOSUI (http://harrier.nagahama-i-bio.ac.jp/sosui/) and TMHMM server ver. 2 (http://www.cbs.dtu.dk/services/TMHMM/). **(C)** Estimated schematic diagram of BpOF4_01690 from the secondary protein structure prediction and hydropathy profile.

In the present study, we used *B. pseudofirmus* OF4, which was successfully subjected to genome engineering. First, a BpOF4_01690-deleted strain (named Δ01690) was constructed from *B. pseudofirmus* OF4. Then, growth experiments at neutral and alkaline pH and several Na^+ concentrations were conducted. In addition, media with different carbon sources were examined in the wild type *B. pseudofirmus* OF4-811M and in the Δ01690 mutant. The activities of the respiratory chain complexes of the wild type and Δ01690 mutant were also compared. This investigation is aimed at identifying the physiological role of small protein BpOF4_01690 at highly alkaline pH.

MATERIALS AND METHODS

Bacterial Strains and Plasmids

The bacterial strains and plasmids used in the present study are listed in **Table 1**, and the primers utilized in our investigation are available on request. The wild type strain was alkaliphilic *B. pseudofirmus* OF4 (Clejan et al., 1989), whose whole genome had been previously sequenced (Janto et al., 2011). The BpOF4_01690 gene and *ctaD* (accession no. BpOF4_00910) deletion mutant were individually constructed in the native alkaliphile host as described previously (Liu et al., 2013). Briefly, to construct the Δ01690 strain, upstream and downstream flanking regions of the BpOF4_01690 gene of approximately 800 bp were amplified using *B. pseudofirmus* OF4 genomic DNA as the template and subsequently cloned into pGEM7Zf(+) (Promega) and pG^+host4 (Appligene, Pleasanton, CA, United States) sequentially. The resulting pG^+host4 construct was transformed into the *B. pseudofirmus* OF4 strain by protoplast transformation (Ito et al., 1997). The Δ01690 strain was constructed after a single crossover step and a double crossover recombination step. The deletion region was verified by DNA sequencing performed by Eurofins Genomics K.K. (Tokyo, Japan). Restoration of a functional BpOF4_01690 gene in the mutant strain Δ01690 was achieved by applying a similar strategy to replace the region that was disrupted in the mutants with the sequence of the wild type. The Δ*ctaD* strain was constructed in a similar way. The deleted *atpBEF* (a, c, and b subunit of the F_o part of ATPase, accession no. BpOF4_06880, BpOF4_06875, and BpOF4_06870) of *B. pseudofirmus* OF4 was used for the development of the ΔF_o strain (Wang et al., 2004). The β-His strain of *B. pseudofirmus* OF4 containing a six-codon addition encoding 6-His just after the N-terminal methionine of the β-subunit of F_1 part of ATPase (AtpD, accession no. BpOF4_06850) was used for immune blotting and pull-down assay (Fujisawa et al., 2010).

Growth Media and Conditions

Two types of media were used for the experiments; they were buffered at pH 7.5 and 10.5. Either malate (to 50 mM) was used as the carbon source to support non-fermentative growth or glucose (to 50 mM) to promote fermentative growth. The semi-defined media with the above-mentioned respective carbon sources were referred to as KMYE (potassium malate-yeast extract) and KGYE (potassium glucose-yeast extract) media (Wang et al., 2004). The KMYE medium (pH 10.5) contained 6.70 g of malic acid, 1 g of Yeast Extract, 12.44 g of K_2CO_3, 1 g of $KHCO_3$, 0.136 g of K_2HPO_4, 0.025 g of $MgSO_4{\cdot}7H_2O$, and 1% (v/v) trace elements per liter of deionized water. The pH was adjusted to 10.5 with potassium hydroxide solution. The KMYE medium (pH 7.5) contained 6.70 g of malic acid, 1 g of Yeast Extract, 16.37 g of K_2HPO_4, 0.8 g of KH_2PO_4, 0.025 g of $MgSO_4{\cdot}7H_2O$, and 1% (v/v) trace elements per liter of deionized water. The pH was adjusted to 7.5 with potassium hydroxide solution. KGYE medium contained the same composition as that of the KMYE medium except for the carbon source which was 9 g of glucose. MYE medium (pH 10.5) was used for growth of the β-His strain. The MYE medium contained 6.70 g of malic acid, 1 g of yeast extract, 9.54 g of Na_2CO_3, 0.84 g of $NaHCO_3$, 0.136 g of K_2HPO_4, 0.025 g of $MgSO_4{\cdot}7H_2O$, and 1% (v/v) trace elements per liter

TABLE 1 | Bacterial strains and plasmids used in this study.

Strain and plasmid	Genotype and description	Source and reference
***E. coli* strains**		
DH5αMCR	F-*mcrA*Δ*1 (mrr-hsd RMS-mcrBC) Φ80dlacZ* Δ*(lacZYAargF) U169 deoR recA1 endA1 supE44* λ*thi-1 gyr-496 relA1*	Stratagene
XL1-Blue MRF'	Δ*(mcrA)183* Δ*(mcrCB-hsdSMR-mrr)173 endA1 supE44 thi-1 recA1 gyrA96 relA1 lac [F'proAB lacIqZDM15 Tn10 (Tetr)]*	GIBCO/BRL
***Bacillus pseudofirmus* OF4 strains**		
811M	Wild type, Met^-	Clejan et al., 1989
Δ01690	811M, ΔBpOF4_01690	This study
Δ01690-R	Δ01690, BpOF4_01690 restored at the native location	This study
Δ01690-R-His_6	Δ01690, BpOF4_01690 with 6xHis-tag at C-terminal side restored at the native location	This study
Δ*ctaD*	811M, Δ*ctaD*	This study
ΔF_o	811M, Δ*atpBEF*	Wang et al., 2004
β-His	811M, AtpD with 6xHis-tag at N-terminal side	Fujisawa et al., 2010
Plasmids		
pGEM7Zf(+)	Cloning vector Amp^R	Promega
pGEM7zf(+)_Δ01690	pGEM7zf(+) plus BpOF4_Δ01690 fragment	This study
pMW118	Cloning vector Amp^R	Nippon Gene
pMW118_01690-R	pMW118+BpOF4_01690 fragment	This study
pG^+host4	Temperature-sensitive vector, Erm^R	Appligene
pG^+host4_Δ01690	pG^+host4 + BpOF4_Δ01690 fragment	This study
pG^+host4_01690-R	pG^+host4 + BpOF4_01690 fragment	This study
pG^+host4_01690-R-His_6	pG^+host4 + BpOF4_01690 with 6xHis-tag at C-terminal side fragment	This study
pG^+host4_ΔctaD	pG^+host4 + Δ*ctaD* fragment	This study

of deionized water (pH 10.5). The pH was adjusted to 10.5 with sodium hydroxide solution. An *E. coli* strain was grown at 30°C for derivatives of pG^+host4 or 37°C for another plasmid in LB medium. When antibiotics are required for growth selection, the particular medium was supplemented with erythromycin (0.3–0.6 μg/ml for *B. pseudofirmus* and 150–300 μg/ml for *E. coli*) or ampicillin (100 μg/ml). The cells were grown at 37°C with shaking. Their growth was monitored by measuring the absorbance at 600 nm using a spectrophotometer.

Alignment of the Small Protein With Homologous Proteins of Several Bacterial Species

The amino acid sequences of BpOF4_01690 and several homologs were obtained using the BLASTP algorithm at NCBI[1]. Selected amino acid residues in the alignment were analyzed using ClustalW[2].

Isolation of Everted Membrane Vesicles and ATPase Assays

Everted membrane vesicles were prepared from overnight cultures grown under several conditions as described previously (Liu et al., 2014). Protein content was determined by the Lowry method using lysozyme as the standard (Lowry et al., 1951). Octylglucoside-stimulated ATPase assays were performed for 3 min at 37°C and pH 8.0 in a 0.5-ml volume, containing 20 mM Tricine-NaOH, 5 mM ATP (sodium salt, Sigma), 2.5 mM $MgCl_2$, 30 mM octylglucoside, 50 mM Na_2SO_3, and 20 μg membrane protein (Liu et al., 2014). Subsequently, a 0.5-ml volume of Pi detection solution containing 0.3 ml of LeBel reagent was added, which comprised 1% sodium sulfate, 0.4% 4-(methylamino) phenol, and 1% ammonium molybdate. The reactions were incubated for 5 min at room temperature and terminated by a 0.1-ml volume of 34% sodium citrate. The precipitated protein was removed by centrifugation, and the liberated P_i in the supernatants was measured at 750 nm according to Lebel et al. (1978).

Assays of Respiratory Chain Components

All enzyme assays were performed at room temperature using a Shimadzu UV-1800 UV-Visible spectrophotometer. Tris-HCl (50 mM, pH 8) was utilized as the assay buffer, and 1 ml of 50 or 100 μg of everted membrane vesicle protein was used as the assay volume. NADH oxidase assays were performed by monitoring the decrease of A_{340} over time in the presence of 0.2 mM NADH. The NADH-ferricyanide oxidoreductase activity was measured at 420 nm in a buffer containing 1 mM NADH, 1 mM $K_3Fe(CN)_6$, and 10 mM KCN, as described previously (Swartz et al., 2007). Succinate dehydrogenase activity was monitored by following the phenazine methosulfate-coupled reduction of 2,6-dichloroindophenol at 600 nm (Hatefi, 1978). The reaction mixture, consisting of 10 mM succinate, 50 μg

[1]https://blast.ncbi.nlm.nih.gov/Blast.cgi?PROGRAM=blastp&PAGE_TYPE=BlastSearch&LINK_LOC=blasthome

[2]https://www.genome.jp/tools-bin/clustalw

vesicles, and 10 mM KCN, was preincubated for 5 min at room temperature. Then, 0.07 mM 2,6-dichloroindophenol and 1.625 mM phenazine methosulfate were added to initiate the reaction. The *N*,*N*,*N*′,*N*′-tetramethyl-*p*-phenylenediamine (TMPD) oxidase level was determined by monitoring the increase in A_{562} in the presence of 0.25 mM TMPD (Sakamoto et al., 1996). The extinction coefficients (mM^{-1} cm^{-1}) used for activity calculations were as follows: 6.2 at 340 nm, 1 at 420 nm, 21 at 600 nm, and 10.5 at 562 nm. One unit (U) was defined as 1 μmol of substrate reduced or oxidized per minute per mg of protein.

Immunoblot Analysis of BpOF4_01690-6xHis Protein in Strain Δ01690-R-His$_6$ Membrane Fractions

Five microliters of membrane suspension (4 μg of membrane protein/μl) from each sample was used for one-dimensional sodium dodecyl sulfate (SDS)-PAGE analyses of the membrane samples. The same volume of SDS loading buffer was added to each sample, after which the proteins were separated on 12% polyacrylamide SDS gels. Next, the gels were electrophoretically transferred to nitrocellulose filters (Bio-Rad) by the application of 60 V for 3 h in Tris-glycine-methanol buffer [25 mM Tris, 192 mM glycine, and 20% (v/v) methanol (pH 8.3)]. The BpOF4_01690-His$_6$ protein was detected by anti-His antibody HRP conjugate (Qiagen). ECL solution (Promega) was the usual detection reagent. A quantitative imaging system, Pluor-S MAX (Bio-Rad), was used for the detection and analysis of chemiluminescence images.

Heme Staining Analysis of Cytochrome Content

For heme staining and subsequent analyses, 30 μg of everted membrane vesicle protein was separated by native 12% PAGE (Schagger and Von Jagow, 1987). The gels were immersed for 30 min at room temperature in the dark in 25 ml of staining solution (pH 4.7) containing 0.5 mg/ml 3,3′,5,5′-tetramethylbenzidine, 50% methanol, and 1 M sodium acetate (Guikema and Sherman, 1981), with slow shaking, after which H_2O_2 was added to 0.5%. The stained bands appeared in 5 min, after which the gels were scanned. The bands were quantified by ImageJ 1.47 software and described as % of WT, with WT set at 100%.

Solubilization of Membrane Proteins From the β-His Strain

Membrane vesicles were prepared from overnight cultures grown in MYE medium at pH 10.5 as described previously (Liu et al., 2009). 10 mg/mL membrane proteins from the β-His strain were solubilized by an extraction solution which contains 200 mM NaCl, 1%(w/v) dodecyl maltoside (DDM), 3 mM HEPES, 15 mM $MgCl_2$ and 3% glycerol (pH 8.0). The pH was adjusted to 8.0 with sodium hydroxide solution. The solution was gently mixed with a nutator at 4°C for 1 h. Ultracentrifugation (Beckman Coulter Optima TL 100) was performed at 45,000 rpm at 4°C for 1 h to remove insoluble proteins.

Sucrose Density Gradient Ultracentrifugation

The Ultra-clear™ centrifuge tube was first filled with 4 ml of 20% sucrose and then 4 ml of 30% sucrose buffer was carefully filled into the bottom of the tube using a needle-long syringe to keep the interface of the buffer as stable as possible. Sucrose buffer contains 2.38 g of HEPES, 10.17 g of $MgCl_2 \cdot 6H_2O$, 200 g (20%) or 300 g (30%) of sucrose, and 0.15% DDM per liter of deionized water (pH 8.0). The pH was adjusted to 8.0 with sodium hydroxide solution. The tube was capped with parafilm and allowed to stand at room temperature for 2 h in a tilted state to form a sucrose density gradient. Thereafter, it was left for 1 h at 4°C. One milliliter of solubilized membrane protein (10 mg/ml) solubilized from the β-His strain was carefully overlaid on the sucrose density gradient. Ultracentrifugation was performed using OptimaTML-80XP and an SW40 Ti Rotor (Beckman coulter) at 40,000 rpm at 4°C for 16 h. After ultracentrifugation, 400 μl of the fraction was carefully separated from the upper layer of the tube, and A_{280} of each fraction was measured with NANO DROP 200c (Thermo Fisher Scientific). Fractions in which cytochrome oxidase activity was observed using TMPD were used for the next analysis.

Immunoblot Analysis of the β Subunit of F_1-ATPase and CtaC Subunit of *caa*$_3$-Type Terminal Cytochrome Oxidase From Fractions Separated by Sucrose Density Gradient Ultracentrifugation

A 15% acrylamide gel was prepared, and a sample buffer was added to each of 23 fractions in which cytochrome oxidase activity was observed and electrophoresed at 30 mA. Blue Star Prestained Protein Marker (NIPPON Genetics) was used as a marker. Proteins in the gel were transferred to nitrocellulose filters (Bio-Rad) by applying electricity at 20 V for 16 h in Tris-glycine-methanol buffer [25 mM Tris, 192 mM glycine, and 20% (v/v) methanol (pH 8.3)] using a Mini Trans-Blot® Cell manufactured (Bio-Rad). Western blots were performed as described previously (Morino et al., 2008). The β subunit-His$_6$ protein of ATP synthase was detected by anti-His antibody HRP conjugate (Qiagen). For detection of the CtaC protein, rabbit anti-CtaC polyclonal antibody (Eurofins Genomics) was used as a primary antibody and goat anti-rabbit IgG-HRP conjugate (Abcam) was used as a secondary antibody. ECL solution (Promega) was the usual detection reagent. A quantitative imaging system, ChemiDoc™ XRS$^+$ (Bio-Rad) and a PC application software, Quantity One were used for the detection and analysis of chemiluminescence images.

Pull Down Assay and Immunoblot Analysis

One milliliter of Ni-NTA resin (QIAGEN) was packed in the column. One column volume is 0.5 ml. Two to four column volumes of distilled water were passed through the resin and

TABLE 2 | Result of protein BLAST analysis against BpOF4_01690.

Strain	Protein names	GenBank accession no.	Length	Identity (%)
Bacillus pseudofirmus OF4	BpOF4_01690	ADC48406.1	59	100
Bacillus marmarensis DSM 21297	A33I_13875	ERN53048.1	59	100
Bacillus halodurans C-125	BH2819	BAB06538.1	62	66
Bacillus selenitrieducens ATCC 700615	Bsel_2302	ADH99805.1	60	69
Bacillus akibai JCM 9157	JCM9157_3465	GAE36304.1	62	69
Bacillus hemicellulosilyticus JCM 9152	JCM9152_3343	GAE31848.1	60	63
Bacillus sp. TS-2	BTS2_0672	GAF63780.1	63	67
Bacillus cellulosilyticus DSM 2522	Bcell_1668	ADU29931.1	60	67
Bacillus alcalophilus ATCC 27647	BALCAV_0219525	KGA95903.1	61	62
Bacillus wakoensis JCM 9140	JCM9140_4660	GAE28435.1	62	62

As a result of the BLAST search analysis using Uniprot, it was found that 250 strains belonging to the Firmicutes have homologous proteins of BpOF4_01690. Ten strains with top 10 scores (values considering similarity and expectation values) were extracted in order. All 10 strains were alkaliphilic Bacillus spp.

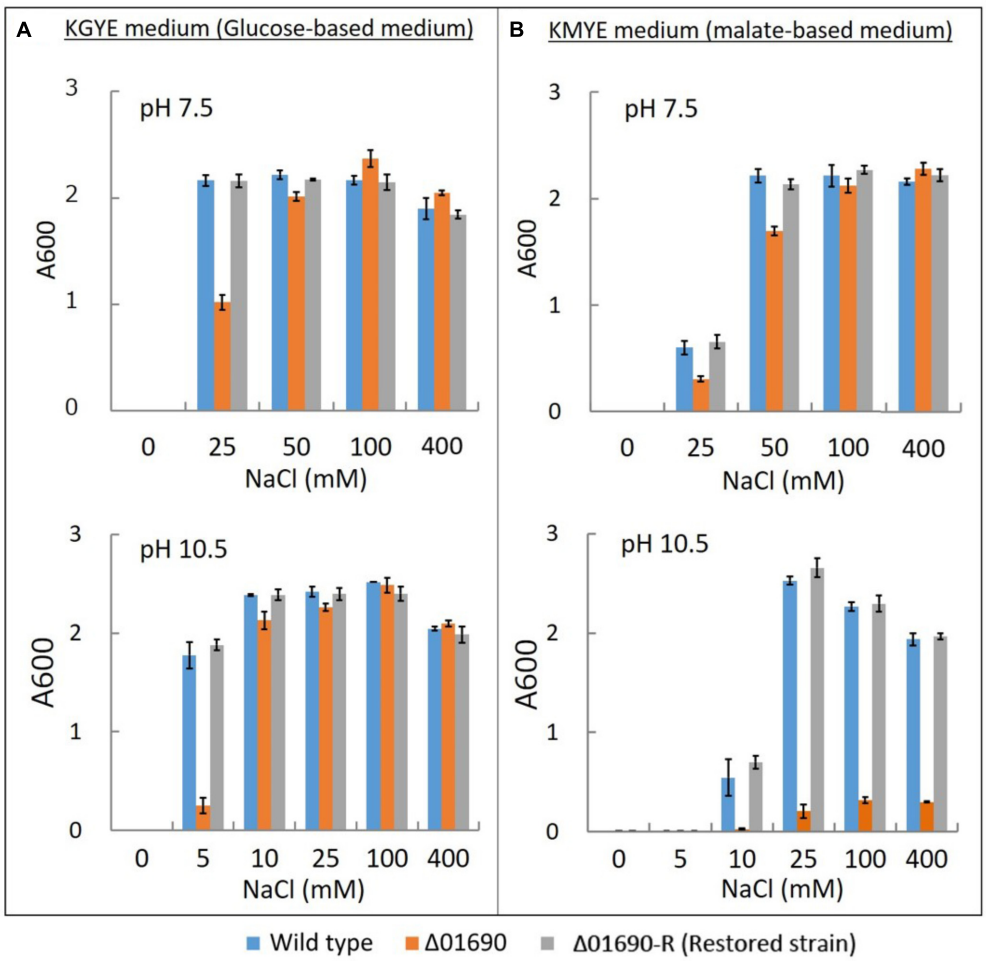

FIGURE 3 | Growth of *B. pseudofirmus* OF4 (wild type), Δ01690, and Δ01690-R under various sodium concentrations. As preculture, each cell was grown in a GYE medium (pH 7.5) overnight at 37°C. Absorbance at A_{600} of each preculture was measured, and the A_{600} of each preculture was adjusted to 1.0. Next, each preculture was harvested by centrifugation and resuspended using the same medium as in the culture so that the glucose and Na^+ were not transferred from the preculture to the culture. **(A,B)** Preculture (2 μl) was added to 2 ml of KGYE medium (pH 7.5), KGYE medium (pH 10.5), KMYE medium (pH 7.5), and KMYE medium (pH 10.5) with various concentrations of NaCl and grown aerobically at 37°C for 16 h. The A_{600} of the cultures was then measured. The error bars indicate standard deviations for the results from duplicate cultures in three independent experiments.

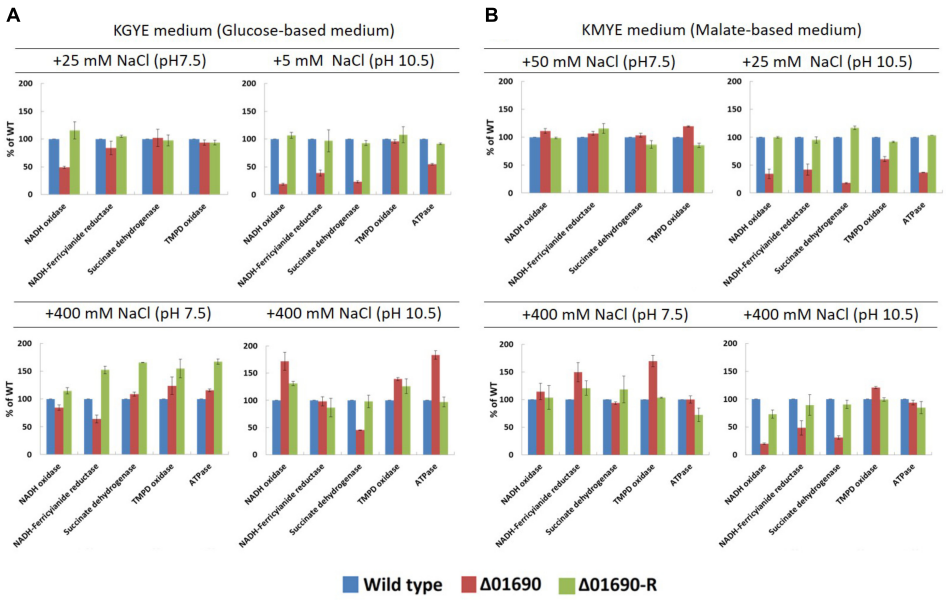

FIGURE 4 | Measurements of various respiratory chain activates of *B. pseudofirmus* OF4 (wild type), Δ01690, and Δ01690-R under various growth conditions (**A**: KGYE medium, **B**: KMYE medium) at pH 7.5 and 10.5. Based on the specific activity of the wild type, referred to as 100%, the specific activities of Δ01690 and Δ01690-R (restored strain) are shown as relative activities (%). The error bars indicate standard deviations for the results from three independent experiments. The details of the experiment are described in the "Materials and Methods" section.

subsequently 10 column volumes of wash buffer (10 mM HEPES, 5 mM $MgCl_2$, 20 mM imidazole, 20 mM NaCl and 0.15% DDM, pH 8.0) were applied to the column to wash the resin. Imidazole was added to the membrane protein of the β-His strain solubilized by DDM to a final concentration of 20 mM and this was applied to the resin. The resin and solubilized membrane protein were well mixed, transferred to a 15 ml tube, and shaken at 4°C for 1 h with a nutator at low speed. Mixed resin and membrane protein were passed through the column to obtain a non-adsorbed fraction. Subsequently, 1 ml of wash buffer was passed through the column to obtain a washed fraction. Finally, 1 ml of elution buffer (10 mM HEPES, 5 mM $MgCl_2$, 200 mM imidazole, 20 mM NaCl and 0.15% DDM, pH 8.0) was passed through the column, and the eluted fraction was obtained.

The solubilized fraction, non-adsorbed fraction, washed fraction, and eluted fraction obtained by the pull-down assay were used for immunoblotting analysis which was performed in the same manner as described above.

RESULTS AND DISCUSSION

Verification of the Interaction Between Cytochrome *caa*$_3$-Type Terminal Oxidase and F_1F_o-ATP Synthase

Sucrose density gradient ultracentrifugation and pull-down assays were carried out to verify the direct interaction between F_1F_o-ATP synthase and cytochrome *caa*$_3$ type terminal oxidase involved in OXPHOS. Indirect interaction between F_1F_o-ATP synthase and cytochrome *caa*$_3$ type terminal oxidase of *B. pseudofirmus* OF4 has been demonstrated by using saturated mobile electron spin resonance and differential scanning calorimetry analysis (Liu et al., 2007). However, there is no direct report that the two proteins form a complex. Sucrose density gradient centrifugation and pull-down assay were conducted to confirm the interaction of proteins under mild conditions to verify whether these two complexes form a complex in the cell membrane.

From the results of sucrose density gradient ultracentrifugation and its immunoblot analysis, monomeric cytochrome *caa*$_3$ type terminal oxidase was detected in low molecular weight fractions, and F_1F_o-ATP synthase and cytochrome *caa*$_3$ type terminal oxidase were simultaneously detected in the high molecular weight fractions (**Supplementary Figure S1**). This result suggested the possibility of interaction between these two protein complexes. Subsequently, we attempted a pull-down assay to detect direct interactions between them (**Supplementary Figure S2**). However, the cytochrome *caa*$_3$-type terminal oxidase was not purified together with the F_1F_o-ATP synthase. This result suggests that interaction between the two complexes is not strong in the cell membrane, i.e., may be a weak protein interaction. It is also possible that there may be another membrane protein that mediates between the two complexes.

Bioinformatics Analysis of BpOF4_01690

The results of the BLAST sequence analysis[3] showed that the homologous small proteins of BpOF4_01690 are present

[3]http://blast.ncbi.nlm.nih.gov/Blast.cgi

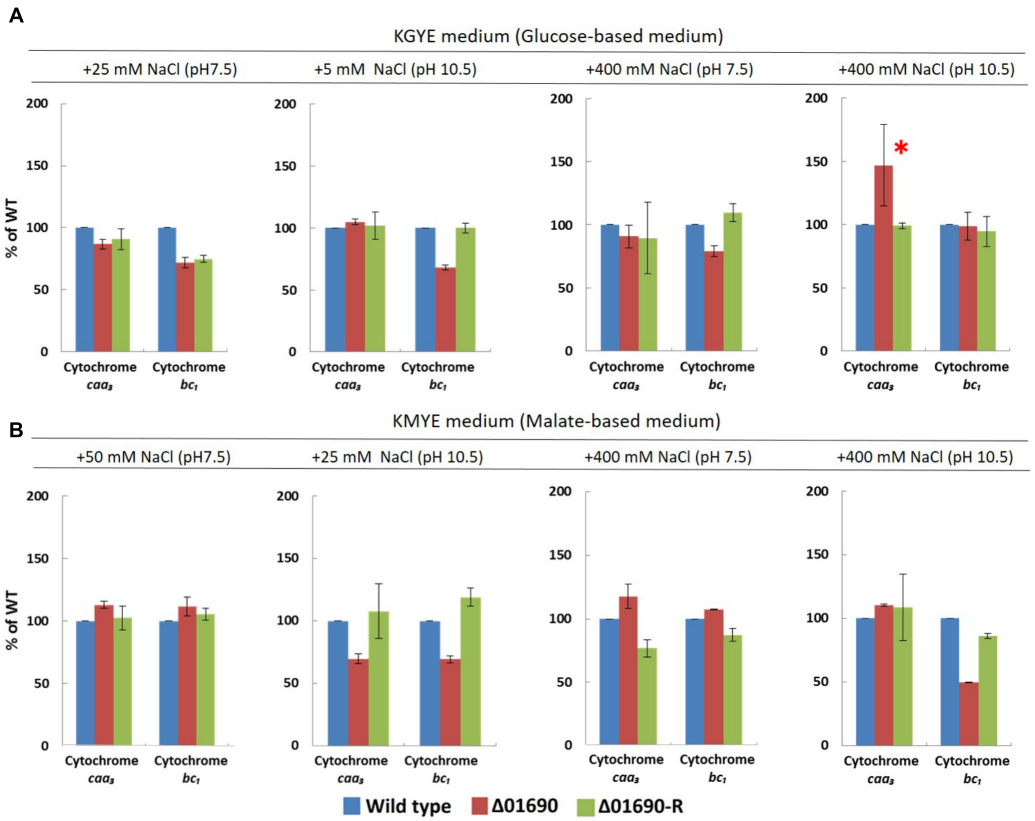

FIGURE 5 | Expression levels of cytochrome caa_3 and cytochrome bc_1 of *B. pseudofirmus* OF4 (wild type), Δ01690, and Δ01690-R under various growth conditions (**A**: KGYE medium, **B**: KMYE medium) at pH 7.5 and 10.5. Based on the expression level of the wild type, referred to as 100%, the expression levels of Δ01690 and Δ01690-R (restored strain) are shown as relative activities (%). The error bars indicate standard deviations for the results from three independent experiments. The detailed description of the experiment is presented in the "Materials and Methods" section.

predominantly in alkaliphilic *Bacillus* species (**Table 2**). The secondary protein structure prediction and hydropathy profile of BpOF4_01690 and its homologs indicated that each protein has two transmembrane-spanning segments and there are highly conserved charged amino acid residues in the loop region between the transmembrane segments (**Figures 2B,C**). However, no functional motif and domain were identified, and its physiological function remains unknown.

Growth of the Wild Type, Δ01690, and Δ01690-R Under Low-Sodium Conditions

KGYE (potassium glucose-yeast extract) and KMYE (potassium malate-yeast extract) were used as growth media, in which K^+ was used instead of Na^+ at pH 7.5 and 10.5 (Wang et al., 2004). The major carbon sources in the KGYE and KMYE media were D-glucose and L-malic acid, respectively. In the KGYE medium, glucose was metabolized via the glycolytic pathway, and ATP was synthesized by OXPHOS and substrate-level phosphorylation. In contrast, in the KMYE medium, malic acid was metabolized via the TCA cycle, and ATP was synthesized predominantly by OXPHOS (**Supplementary Figure S3**).

Alkaliphilic bacteria generally require Na^+ for growth. Reportedly, Na^+ in the medium is utilized as a source of coupling ions for flagellar rotation, uptake of various substrates, Na^+/H^+ antiporters, voltage-gated sodium channel, etc. (Krulwich and Ito, 2013; Preiss et al., 2015; Ito et al., 2017; Morino et al., 2017). Therefore, ensuring optimal Na^+ concentration is critical for the provision of favorable growth conditions. Earlier reports showed that higher NaCl concentrations were required at pH 7.5 than at pH 10.5 to support optimal growth rates (Ito et al., 1997). Thus, to determine the effect of Na^+, K^+ was used as a substitute for Na^+ in the KGYE and KMYE media. Then, growth experiments with various concentrations of added Na^+ were conducted (**Figure 3**) (Terahara et al., 2012).

The growth of the wild type, Δ01690, and Δ01690-R in the KGYE medium at pH 7.5 was almost identical to the growth with the addition of 50 mM Na^+. However, 50% of the growth of Δ01690 was observed at 25 mM Na^+ compared with wild type and Δ01690-R (**Figure 3A**). Moderate decline in growth of Δ01690 in the KMYE medium at pH 7.5 was observed under 25 mM and 50 mM Na^+ conditions compared to wild type and Δ01690-R (**Figure 3B**). In contrast, the growth of the wild type, Δ01690, and Δ01690-R in the KGYE medium at pH 10.5 was almost identical to that in the medium with the addition of

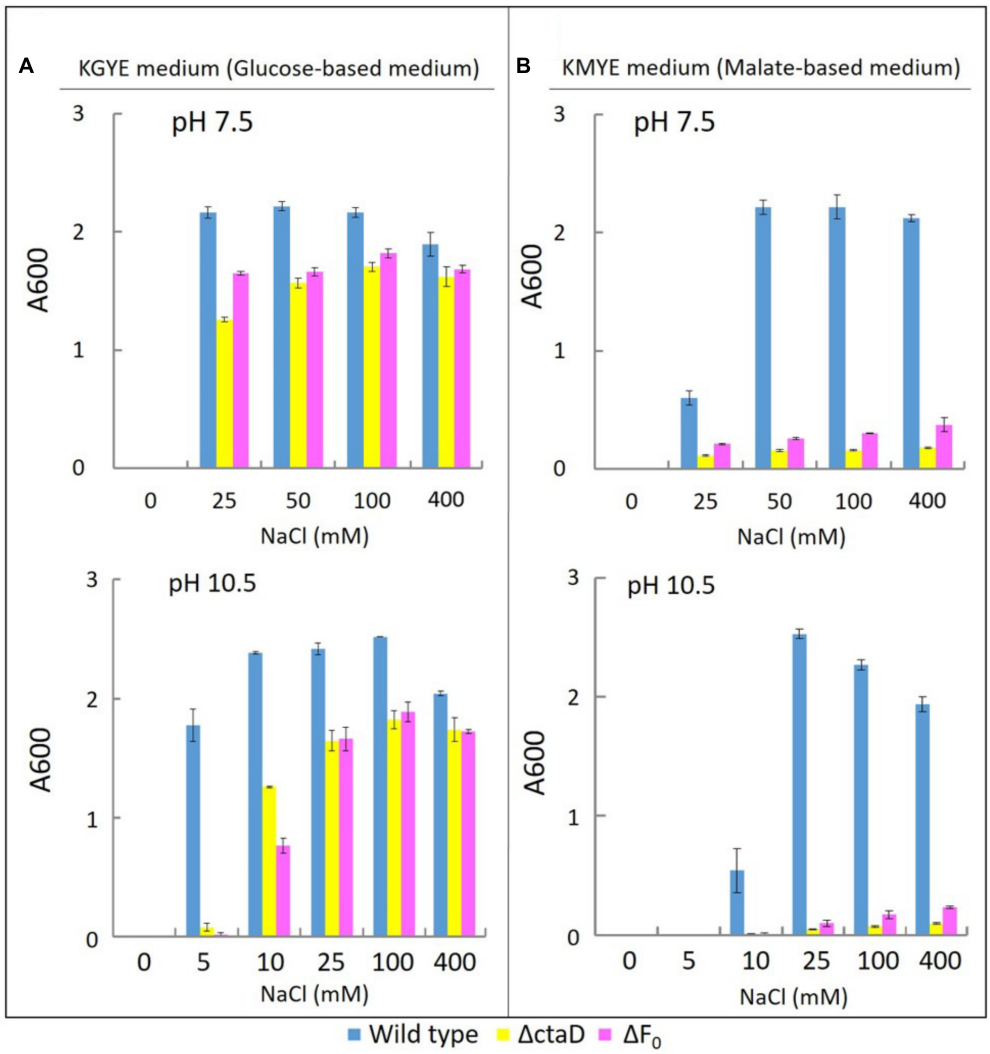

FIGURE 6 | Growth of *B. pseudofirmus* OF4 (wild type), Δ*ctaD*, and ΔF_o under various Na^+ concentrations (**A**: KGYE medium, **B**: KMYE medium). The experimental method used is the same as that outlined in the legend of **Figure 3**.

10 mM Na^+. Nevertheless, at 5 mM Na^+, the growth of Δ01690 was poorer than that in the wild type and Δ01690-R (**Figure 3A**). Poor growth of Δ01690 was observed under all tested conditions in the KMYE medium at pH 10.5. Both the wild type and Δ01690 grew well in NaCl concentrations over 25–400 mM (**Figure 3B**).

Comparison of the Expression Level of Protein BpOF4_01690 Under Different Growth Conditions

The expression level of BpOF4_01690 fused with 6xHis-tag in the strain Δ01690-R-His_6 cultured in KMYE and KGYE media at pH 10.5 was detected by western blotting (**Supplementary Figure S4**). The highest expression level was detected when the cells were grown on KMYE medium containing 25 mM Na^+ at pH 10.5. However, no dramatic increase or decrease in the protein expression was detected under either condition.

Measurements of Diverse Respiratory Chain Activities and Expression Levels of Cytochrome bc_1 of the Wild Type, Δ01690, and Δ01690-R

Under the condition that the growth of Δ01690 is worse than that of the wild type, enzymatic activities of various respiratory chain complexes of the wild type were measured in both Δ01690 and Δ01690-R under high- and low-sodium conditions at pH 7.5 and 10.5 (**Figure 4**). The activities of NADH oxidase, NADH ferricyanide reductase, succinate dehydrogenase, TMPD oxidase, and F_1F_o-ATPase were lower than those in the wild type in the KMYE medium plus 25 mM NaCl at pH 10.5 (**Figure 4B**, upper right). The high NaCl concentration (400 mM) in the KMYE medium at pH 10.5 enabled recovery of the activity of TMPD oxidase and ATPase (**Figure 4B**, bottom right). Both KGYE medium plus 5 mM NaCl at pH 10.5

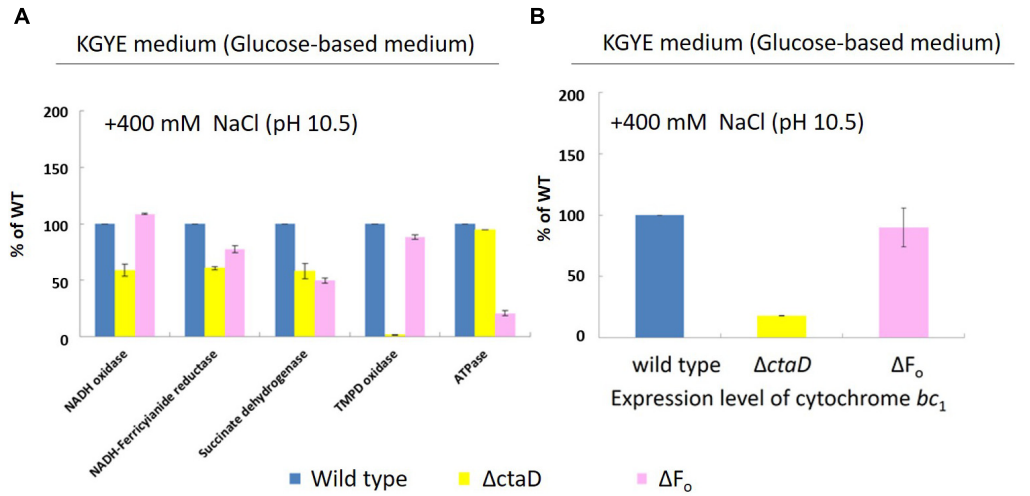

FIGURE 7 | Measurements of various respiratory chain activities **(A)** and the expression level of cytochrome bc1 **(B)** of *B. pseudofirmus* OF4 (wild type), Δ*ctaD*, and ΔF_o in the KGYE medium plus 400 mM Na^+ at pH 10.5. Based on the specific activity of the wild type, referred to as 100%, the specific activities of Δ*ctaD* and ΔF_o are displayed as relative activities (%). The error bars indicate standard deviations for the results from three independent experiments. The details of the experiment are described in the "Materials and Methods" section.

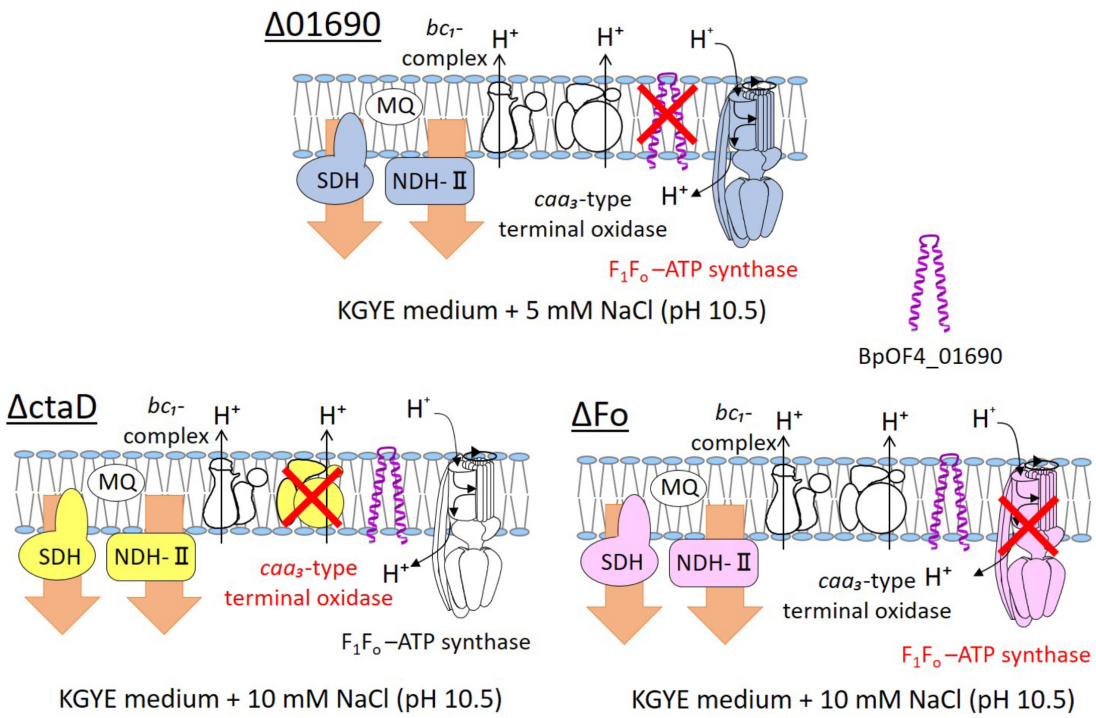

FIGURE 8 | Thematic diagram of the phenotype summaries of the respiratory chain complexes of Δ01690, Δ*ctaD*, and ΔF_o. Based on the results depicted in **Figures 4A**, **7A**, the respiratory chain enzymes and ATP synthase of Δ01690, ΔctaD, and ΔF_o in the KGYE medium plus 5 mM NaCl (pH 10.5) are shown. The ΔctaD strain is a defective mutant of caa_3-type terminal oxidase. The ΔF_o strain is a defective mutant of F_1F_o-ATP synthase. A common phenotype of all three strains was the decreased activity of SDH and NDH-II. BpOF4_01690 is shown as a purple structure.

and KMYE medium plus 25 mM NaCl at pH 10.5 showed similar phenotype except TMPD oxidase activity (**Figure 4A**, upper right and **Figure 4B**, upper right). The high NaCl concentration (400 mM) in the KGYE medium at pH 10.5, the activity of NADH oxidase, TMPD oxidase and ATPase exhibited increased up to 172% ± 17%, 139% ± 3% and 183% ± 8%, respectively, compared with wild type (**Figure 4A**, bottom right). On the other hand, the activity of succinate

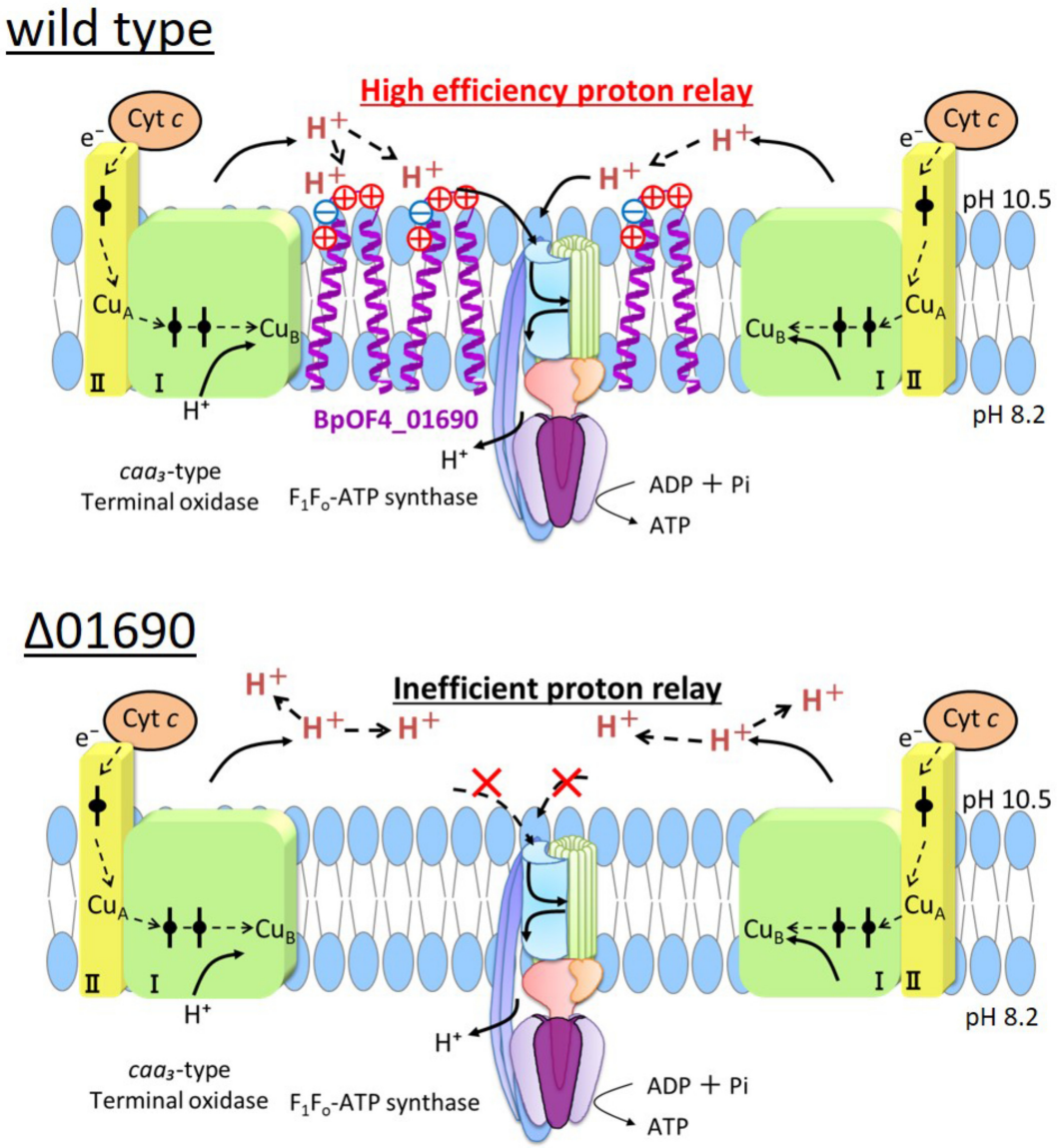

FIGURE 9 | Model diagram of ATP synthesis by OXPHOS in the wild type and Δ01690 under highly alkaline conditions. In the wild type strain, OXIPHOS is conducted by efficient proton delivery between the respiratory chain and F_1F_o-ATPase due to the presence of BpOF4_01690. In contrast, OXIPHOS does not work well in the Δ01690 strain because protons from the respiratory chain are not transferred efficiently to F_1F_o-ATPase. Due to this negative influence, the growth in the KMYE medium was extremely poor. It is, therefore, inferred that BpOF4_01690 mediates this efficient proton delivery.

dehydrogenase was decreased to 45% ± 1% compared with wild type. These results suggest that at highly alkaline pH, the protein BpOF4_01690 affects both the respiratory chain and ATP synthesis by OXPHOS.

The expression levels of cytochrome bc_1 and cytochrome caa_3 of everted membrane vesicles prepared from the wild type, Δ01690, and Δ01690-R in the KGYE and KMYE media with low or high Na^+ concentrations at pH 10.5 were determined by heme staining and compared (**Figure 5**). In the KGYE medium with 5 mM Na^+ and pH 10.5, the expression level of cytochrome bc_1 of Δ01690 was reduced to 68% ± 2% of that of the wild type (**Figure 5A**). In contrast, in the KGYE medium with 400 mM Na^+ and pH 10.5, the expression level of cytochrome caa_3 of Δ01690 increased to 147% ± 32% of that of the wild type (**Figure 5A**). However, under an identical condition, there was no indication that the growth of Δ01690 was more intensive than that of the wild type (**Figure 3A**, bottom). In the KMYE medium with 25 mM Na^+ and pH 10.5, the expression levels of cytochrome caa_3 and cytochrome bc_1 of Δ01690 were reduced up to 70% ± 4% and 69% ± 3% of those of the wild type, respectively (**Figure 5B**). In contrast, in the KMYE medium with 400 mM

Na^+ and pH 10.5, the expression level of cytochrome bc_1 of Δ01690 decreased to 49% ± 0% of that of the wild type (**Figure 5B**). These findings suggest that the deletion of BpOF4_01690 negatively affects the expression level of cytochrome caa_3 in the KMYE medium with a low Na^+ concentration and high pH; the expression level of cytochrome bc_1 under all tested conditions was also influenced at high pH, except in the KGYE medium with 400 mM Na^+ at pH 10.5.

Growth of Strains Δ*ctaD* and ΔF_o Mutants Under Low-Sodium Conditions

To compare the phenotype of Δ01690 with other respiratory chain and OXPHOS-related mutants, the Δ*ctaD* mutant in which disruption was caused in the *ctaD* of caa_3-type terminal oxidase operon and the ΔF_o mutant with the deleted F_o part (*atpB-F*) of *unc* operon were used as reference and comparative strains. The growth of the wild type and these two mutants was measured in the KGYE and KMYE media at pH 7.5 and 10.5 (**Figure 6**).

The growth of the wild type, Δ*ctaD*, and ΔF_o in the KGYE medium at pH 7.5 and 10.5, was compared as a function of NaCl concentration (**Figure 6A**). The wild type had optimal growth at 25–400 mM NaCl at pH 7.5 and at 5–400 mM NaCl at pH 10.5, whereas both Δ*ctaD* and ΔF_o mutants had a significantly lower level of growth at 10 mM NaCl at pH 10.5 (**Figure 6A**). The poor growth of both Δ*ctaD* and ΔF_o mutants was observed in the KGYE medium with 5 mM NaCl and pH 10.5 and compared to that of the wild type (**Figure 6A**). Meanwhile, the growth of both Δ*ctaD* and ΔF_o mutants in the KMYE medium at both pH values was poor under all examined conditions, even at concentrations above 25 mM Na^+, in which the wild type grew actively (**Figure 6B**).

Measurements of Various Respiratory Chain Activities and Expression Levels of Cytochrome bc_1 of Δ*ctaD* and ΔF_o Mutants

Measurements were performed of the activities of various respiratory chain complexes and the expression levels of cytochrome bc_1 of the wild type, Δ*ctaD*, and ΔF_o in the KGYE medium with 400 mM Na^+ and pH 10.5 (**Figure 7A**), followed by comparative assessments. The enzymatic activity of NADH oxidase, NADH-ferricyanide reductase, succinate dehydrogenase, and TMPD oxidase, as well as the expression level of cytochrome bc_1 in Δ*ctaD*, were lower than those of the wild type. In particular, the activity of TMPD oxidase was hardly detected. In contrast, the ATP hydrolysis activity of Δ*ctaD* was almost identical to that of the wild type.

For strain ΔF_o, the enzymatic activities of NADH-ferricyanide reductase, succinate dehydrogenase, and ATPase were lower than those of the wild type. In particular, the ATPase activity was drastically reduced. In contrast, the enzymatic activity of NADH oxidase and TMPD oxidase, as well as the expression level of cytochrome bc_1, were almost identical to those of the wild type.

The expression level of cytochrome bc_1 of Δ*ctaD* and ΔF_o mutants, one of the terminal oxidases indicated that the Δ*ctaD* mutant was much lower in activity compared with the wild type and the ΔF_o, which showed little activity loss (**Figure 7B**).

We presumed that Δ*ctaD* influences the activities of multiple enzymes of the respiratory electron transport system. In contrast, ΔF_o displayed poor ATPase activity and reduced levels of both NADH dehydrogenase and succinate dehydrogenase. The levels of Δ*ctaD* and ΔF_o were indirectly influenced by the actions of multiple enzymes of the respiratory electron transport system. A thematic diagram of the phenotypes of the respiratory chain complexes of Δ01690, Δ*ctaD*, and ΔF_o at high pH is illustrated in **Figure 8**. Importantly, a deletion of either Δ*ctaD* or ΔF_o reduced the expression of the electron transfer enzymes, SDH and NDH-II. Moreover, the deletion of *ctaD* also led to the loss of caa_3-type terminal oxidase activity.

In view of the observations recorded above, similarly to Δ*ctaD* and ΔF_o mutants, the negative effect of the enzymatic activity of respiratory chain complexes of Δ01690 might have been due to independently exerted effects that directly influenced the caa_3-type terminal oxidase or F_1F_o-ATP synthase (**Figure 8**). Therefore, we suggest that the deletion of BpOF4_01690 influences the activity of the respiratory chain-related enzymes and ATP synthesis by OXPHOS. Moreover, the small protein BpOF4_01690 may also play a critical role under lower sodium motive force conditions.

Highly conserved charged amino acid residues are present in the loop region between the transmembrane segments of BpOF4_01690 and its homologous proteins. Thus, we hypothesize that the negatively charged amino acid residue BpOF4_01690-E21 has a functionally critical role in the surrounding conserved positively charged amino acid residues (**Figure 2B**). We propose a working model describing the function of BpOF4_01690 (**Figure 9**). Some of the protons effluxed from the proton pump of the respiratory chain bind to negatively charged sites of the side chain of the glutamic acid residue of BpOF4_01690 at the outer surface of the cell membrane. Then, the protons are efficiently transferred to F_1F_o-ATP synthase, which is present in the proton pump of the terminal oxidase and BpOF4_01690 in the vicinity of a highly alkaline environment.

CONCLUSION

In conclusion, the small protein BpOF4_01690 appears to play a central role in the energy-coupled retention of protons needed for ATP synthesis via OXPHOS of alkaliphilic *Bacillus* species in highly alkaline environments. This finding is very interesting while considering that alkaliphiles acquired BpOF4_01690 in the process of evolution to adapt to OXPHOS in alkaline environment.

AUTHOR CONTRIBUTIONS

TK and MI designed the research. TT performed the research with experimental work. TT, TK, and MI analyzed the data. TK and MI wrote the paper.

FUNDING

This work was supported in part by research grant GM28454 from the National Institute of General Medical Sciences (to TK) as well as a grant from Bio-Nano Electronics Research Centre, Toyo University (to MI).

ACKNOWLEDGMENTS

We thank Dr. David B. Hicks of Icahn School of Medicine at Mount Sinai and Ms. Yuko Nakano of Graduate School of Life Sciences, Toyo University for technical assistance and Dr. Arthur A. Guffanti for critical reading of the manuscript.

SUPPLEMENTARY MATERIAL

The Supplementary Material for this article can be found online at: https://www.frontiersin.org/articles/10.3389/fmicb.2018.01994/full#supplementary-material

REFERENCES

Aono, R., Hayakawa, A., Hashimoto, M., Kaneko, H., Nakamura, S., and Horikoshi, K. (1993). Cloning of a gene required for the alkaliphily of alkaliphilic *Bacillus* sp. strain C-125. *Nucleic Acids Symp. Ser.* 29, 139–140.

Chen, Y. C., Taylor, E. B., Dephoure, N., Heo, J. M., Tonhato, A., Papandreou, I., et al. (2012). Identification of a protein mediating respiratory supercomplex stability. *Cell Metab.* 15, 348–360. doi: 10.1016/j.cmet.2012.02.006

Cherepanov, D. A., Feniouk, B. A., Junge, W., and Mulkidjanian, A. Y. (2003). Low dielectric permittivity of water at the membrane interface: effect on the energy coupling mechanism in biological membranes. *Biophys. J.* 85, 1307–1316. doi: 10.1016/S0006-3495(03)74565-2

Clejan, S., Guffanti, A. A., Cohen, M. A., and Krulwich, T. A. (1989). Mutation of *Bacillus firmus* OF4 to duramycin resistance results in substantial replacement of membrane lipid phosphatidylethanolamine by its plasmalogen form. *J. Bacteriol.* 171, 1744–1746. doi: 10.1128/jb.171.3.1744-1746.1989

Fujisawa, M., Fackelmayer, O. J., Liu, J., Krulwich, T. A., and Hicks, D. B. (2010). The ATP synthase a-subunit of extreme alkaliphiles is a distinct variant: mutations in the critical alkaliphile-specific residue Lys-180 and other residues that support alkaliphile oxidative phosphorylation. *J. Biol. Chem.* 285, 32105–32115. doi: 10.1074/jbc.M110.165084

Guffanti, A. A., and Krulwich, T. A. (1994). Oxidative phosphorylation by ADP + Pi-loaded membrane vesicles of alkaliphilic *Bacillus firmus* OF4. *J. Biol. Chem.* 269, 21576–21582.

Guikema, J. A., and Sherman, L. A. (1981). Electrophoretic profiles of cyanobacterial membrane polypeptides showing heme-dependent peroxidase activity. *Biochim. Biophys. Acta* 637, 189–201. doi: 10.1016/0005-2728(81)90157-2

Hatefi, Y. (1978). Resolution of complex II and isolation of succinate dehydrogenase (EC 1.3.99.1). *Methods Enzymol.* 53, 27–35. doi: 10.1016/S0076-6879(78)53009-7

Hobbs, E. C., Fontaine, F., Yin, X., and Storz, G. (2011). An expanding universe of small proteins. *Curr. Opin. Microbiol.* 14, 167–173. doi: 10.1016/j.mib.2011.01.007

Horikoshi, K. (1991). *Microorganisms in Alkaline Environments*. New York, NY: VCH Publishers Inc.

Ito, M., Guffanti, A. A., Zemsky, J., Ivey, D. M., and Krulwich, T. A. (1997). Role of the nhaC-encoded Na^+/H^+ antiporter of alkaliphilic *Bacillus firmus* OF4. *J. Bacteriol.* 179, 3851–3857. doi: 10.1128/jb.179.12.3851-3857.1997

Ito, M., Hicks, D. B., Henkin, T. M., Guffanti, A. A., Powers, B., Zvi, L., et al. (2004a). MotPS is the stator-force generator for motility of alkaliphilic *Bacillus* and its homologue is a second functional Mot in *Bacillus subtilis*. *Mol. Microbiol.* 53, 1035–1049. doi: 10.1111/j.1365-2958.2004.04173.x

Ito, M., Xu, H., Guffanti, A. A., Wei, Y., Zvi, L., Clapham, D. E., et al. (2004b). The voltage-gated Na^+ channel NavBP has a role in motility, chemotaxis, and pH homeostasis of an alkaliphilic *Bacillus*. *Proc. Natl. Acad. Sci. U.S.A.* 101, 10566–10571. doi: 10.1073/pnas.0402692101

Ito, M., Morino, M., and Krulwich, T. A. (2017). Mrp antiporters have important roles in diverse bacteria and Archaea. *Front. Microbiol.* 8:2325. doi: 10.3389/fmicb.2017.02325

Janto, B., Ahmed, A., Ito, M., Liu, J., Hicks, D. B., Pagni, S., et al. (2011). Genome of alkaliphilic *Bacillus pseudofirmus* OF4 reveals adaptations that support the ability to grow in an external pH range from 7.5 to 11.4. *Environ. Microbiol.* 13, 3289–3309. doi: 10.1111/j.1462-2920.2011.02591.x

Krulwich, T. A. (1995). Alkaliphiles: 'basic' molecular problems of pH tolerance and bioenergetics. *Mol. Microbiol.* 15, 403–410. doi: 10.1111/j.1365-2958.1995.tb02253.x

Krulwich, T. A., and Ito, M. (2013). "Prokaryotic alkaliphiles," in *The Prokaryotes*, 4th Edn, eds E. Rosenberg, E. F. Delong, F. Thompson, S. Lory, and E. Stackebrandt (New York, NY: Springer), 441–469. doi: 10.1007/978-3-642-30123-0_58

Krulwich, T. A., Liu, J., Morino, M., Fujisawa, M., Ito, M., and Hicks, D. B. (2011). "Adaptive mechanisms of extreme alkaliphiles," in *Extremophiles Handbook*, ed. K. Horikoshi (Berlin: Springer), 119–139. doi: 10.1007/978-4-431-53898-1_7

Lebel, D., Poirier, G. G., and Beaudoin, A. R. (1978). A convenient method for the ATPase assay. *Anal. Biochem.* 85, 86–89. doi: 10.1016/0003-2697(78)90277-4

Liu, J., Fujisawa, M., Hicks, D. B., and Krulwich, T. A. (2009). Characterization of the functionally critical AXAXAXA and PXXEXXP motifs of the ATP synthase c-subunit from an alkaliphilic *Bacillus*. *J. Biol. Chem.* 284, 8714–8725. doi: 10.1074/jbc.M808738200

Liu, J., Hicks, D. B., and Krulwich, T. A. (2013). Roles of AtpI and two YidC-type proteins from alkaliphilic *Bacillus pseudofirmus* OF4 in ATP synthase assembly and nonfermentative growth. *J. Bacteriol.* 195, 220–230. doi: 10.1128/JB.01493-12

Liu, J., Ryabichko, S., Bogdanov, M., Fackelmayer, O. J., Dowhan, W., and Krulwich, T. A. (2014). Cardiolipin is dispensable for oxidative phosphorylation and non-fermentative growth of alkaliphilic *Bacillus pseudofirmus* OF4. *J. Biol. Chem.* 289, 2960–2971. doi: 10.1074/jbc.M113.536193

Liu, X., Gong, X., Hicks, D. B., Krulwich, T. A., Yu, L., and Yu, C. A. (2007). Interaction between cytochrome caa3 and F1F0-ATP synthase of alkaliphilic *Bacillus pseudofirmus* OF4 is demonstrated by saturation transfer electron paramagnetic resonance and differential scanning calorimetry assays. *Biochemistry* 46, 306–313. doi: 10.1021/bi0619167

Lowry, O. H., Rosebrough, N. J., Farr, A. L., and Randall, R. J. (1951). Protein measurement with the Folin phenol reagent. *J. Biol. Chem.* 193, 265–275.

Morino, M., Natsui, S., Swartz, T. H., Krulwich, T. A., and Ito, M. (2008). Single gene deletions of *mrpA* to *mrpG* and *mrpE* point mutations affect activity of the Mrp Na^+/H^+ antiporter of alkaliphilic *Bacillus* and formation of hetero-oligomeric Mrp complexes. *J. Bacteriol.* 190, 4162–4172. doi: 10.1128/JB.00294-08

Morino, M., Ogoda, S., Krulwich, T. A., and Ito, M. (2017). Differences in the phenotypic effects of mutations in homologous MrpA and MrpD subunits of the multi-subunit Mrp-type $Na(^+)/H(^+)$ antiporter. *Extremophiles* 21, 51–64. doi: 10.1007/s00792-016-0877-z

Mulkidjanian, A. Y. (2006). Proton in the well and through the desolvation barrier. *Biochim. Biophys. Acta* 1757, 415–427. doi: 10.1016/j.bbabio.2006.04.023

Preiss, L., Hicks, D. B., Suzuki, S., Meier, T., and Krulwich, T. A. (2015). Alkaliphilic bacteria with impact on industrial applications, concepts of early life forms, and bioenergetics of ATP synthesis. *Front. Bioeng. Biotechnol.* 3:75. doi: 10.3389/fbioe.2015.00075

Sakamoto, J., Matsumoto, A., Oobuchi, K., and Sone, N. (1996). Cytochrome bd-type quinol oxidase in a mutant of *Bacillus stearothermophilus* deficient in caa3-type cytochrome c oxidase. *FEMS Microbiol. Lett.* 143, 151–158. doi: 10.1111/j.1574-6968.1996.tb08474.x

Schagger, H., and Von Jagow, G. (1987). Tricine-sodium dodecyl sulfate-polyacrylamide gel electrophoresis for the separation of proteins in the range from 1 to 100 kDa. *Anal. Biochem.* 166, 368–379. doi: 10.1016/0003-2697(87)90587-2

Storz, G., Wolf, Y. I., and Ramamurthi, K. S. (2014). Small proteins can no longer be ignored. *Annu. Rev. Biochem.* 83, 753–777. doi: 10.1146/annurev-biochem-070611-102400

Su, M., Ling, Y., Yu, J., Wu, J., and Xiao, J. (2013). Small proteins: untapped area of potential biological importance. *Front. Genet.* 4:286. doi: 10.3389/fgene.2013.00286

Swartz, T. H., Ito, M., Ohira, T., Natsui, S., Hicks, D. B., and Krulwich, T. A. (2007). Catalytic properties of *Staphylococcus aureus* and *Bacillus* members of the secondary cation/proton antiporter-3 (Mrp) family are revealed by an optimized assay in an *Escherichia coli* host. *J. Bacteriol.* 189, 3081–3090. doi: 10.1128/JB.00021-07

Terahara, N., Sano, M., and Ito, M. (2012). A *Bacillus* flagellar motor that can use both Na^+ and K^+ as a coupling ion is converted by a single mutation to use only Na^+. *PLoS One* 7:e46248. doi: 10.1371/journal.pone.0046248

Wang, Z., Hicks, D. B., Guffanti, A. A., Baldwin, K., and Krulwich, T. A. (2004). Replacement of amino acid sequence features of a- and c-subunits of ATP synthases of alkaliphilic *Bacillus* with the *Bacillus* consensus sequence results in defective oxidative phosphorylation and non-fermentative growth at pH 10.5. *J. Biol. Chem.* 279, 26546–26554. doi: 10.1074/jbc.M401206200

Yoshimune, K., Morimoto, H., Hirano, Y., Sakamoto, J., Matsuyama, H., and Yumoto, I. (2010). The obligate alkaliphile *Bacillus clarkii* K24-1U retains extruded protons at the beginning of respiration. *J. Bioenerg. Biomembr.* 42, 111–116. doi: 10.1007/s10863-010-9278-7

Conflict of Interest Statement: The authors declare that the research was conducted in the absence of any commercial or financial relationships that could be construed as a potential conflict of interest.

frontiers in Microbiology

REVIEW
published: 18 September 2018
doi: 10.3389/fmicb.2018.02196

Microbial Communities Associated With Indigo Fermentation That Thrive in Anaerobic Alkaline Environments

*Keiichi Aino[1,2], Kikue Hirota[1], Takahiro Okamoto[3], Zhihao Tu[1,2], Hidetoshi Matsuyama[3] and Isao Yumoto[1,2]**

[1] Bioproduction Research Institute, National Institute of Advanced Industrial Science and Technology, Sapporo, Japan, [2] Department of Bioscience and Technology, School of Biological Science and Engineering, Tokai University, Hiratsuka-shi, Japan, [3] Graduate School of Agriculture, Hokkaido University, Sapporo, Japan

Indigo fermentation, which depends on the indigo-reducing action of microorganisms, has traditionally been performed to dye textiles blue in Asia as well as in Europe. This fermentation process is carried out by naturally occurring microbial communities and occurs under alkaline, anaerobic conditions. Therefore, there is uncertainty regarding the fermentation process, and many unknown microorganisms thrive in this unique fermentation environment. Until recently, there was limited information available on bacteria associated with this fermentation process. Indigo reduction normally occurs from 4 days to 2 weeks after initiation of fermentation. However, the changes in the microbiota that occur during the transition to an indigo-reducing state have not been elucidated. Here, the structural changes in the bacterial community were estimated by PCR-based methods. On the second day of fermentation, a large change in the redox potential occurred. On the fourth day, distinct substitution of the genus *Halomonas* with the aerotolerant genus *Amphibacillus* was observed, corresponding to marked changes in indigo reduction. Under open-air conditions, indigo reduction during the fermentation process continued for 6 months on average. The microbiota, including indigo-reducing bacteria, was continuously replaced with other microbial communities that consisted of other types of indigo-reducing bacteria. A stable state consisting mainly of the genus *Anaerobacillus* was also observed in a long-term fermentation sample. The stability of the microbiota, proportion of indigo-reducing microorganisms, and appropriate diversity and microbiota within the fluid may play key factors in the maintenance of a reducing state during long-term indigo fermentation. Although more than 10 species of indigo-reducing bacteria were identified, the reduction mechanism of indigo particle is riddle. It can be predicted that the mechanism involves electrons, as byproducts of metabolism, being discarded by analogs mechanisms reported in bacterial extracellular solid Fe^{3+} reduction under alkaline anaerobic condition.

Keywords: indigo fermentation, *Alkalibacterium*, *Amphibacillus*, *Polygonibacillus*, *Fermentibacillus*, *Paralkalibacillus*, *Anaerobacillus*

OPEN ACCESS

Edited by:
Masahiro Ito,
Toyo University, Japan

Reviewed by:
Kengo Inoue,
University of Miyazaki, Japan
Masahiro Kamekura,
Halophiles Research Institute, Japan

***Correspondence:**
Isao Yumoto
i.yumoto@aist.go.jp

Specialty section:
This article was submitted to Extreme Microbiology, a section of the journal Frontiers in Microbiology

Received: *31 May 2018*
Accepted: *28 August 2018*
Published: *18 September 2018*

Citation:
Aino K, Hirota K, Okamoto T, Tu Z, Matsuyama H and Yumoto I (2018) Microbial Communities Associated With Indigo Fermentation That Thrive in Anaerobic Alkaline Environments. Front. Microbiol. 9:2196. doi: 10.3389/fmicb.2018.02196

INTRODUCTION

Ancient human beings developed a number of environmentally friendly and renewable bioprocesses to benefit their communities. Hence, reexamining these procedures and understanding their scientific bases will aid the development of environmentally friendly procedures. In addition, these techniques can be modified for the development of highly sophisticated procedures. In this review, we discuss the molecular and microbiological bases for the traditional procedure for dyeing textiles and reconsider these procedures for the design of environmentally friendly bioprocesses.

Since ancient times, humans have dyed textiles with pigments, mainly plant pigments. Indigo is one of the oldest dyes and has been used since the Neolithic period (Clark et al., 1993). Textiles pigmented using indigo plants were discovered on an Egyptian mummy from 2500 BC (Balfour-Paul, 2000; Gilbert and Cooke, 2001). Recently, evidence for the earliest use of indigo, dating back to approximately 4000 BC, was obtained from Huaca Prieta, in contemporary Peru (Splitstoser et al., 2016). The polygonaceous Japanese indigo plant (*Polygonum tinctorium* Lour.) has been used in China, Korea, and Japan. Ryukyu-Ai (*Strobilanthes cusia*) has been used in the Ryukyu Islands (in contemporary Okinawa Prefecture), Japan. Indigofera (*Indigofera tinctoria* L. and *Indigofera suffruticosa* Mill.) and woad (*Isatis tinctoria* L.) have been employed in India and Europe (Hurry, 1930; Clark et al., 1993), respectively.

Several processing procedures for the preservation and transportation of indigo dye-containing plants have been used worldwide. Indigo can be extracted from indigo dye-containing plants with water and is processed by intrinsic enzymatic reactions carried out by β-glucosidase in chloroplasts (Minami et al., 1997; Song et al., 2010), which transforms indican (no color) to indoxyl (no color) and produces indigo dye via oxidation (when exposed to air). The original state of indigo dye is always indican (**Figure 1**). Therefore, transformation of indican to indoxyl is necessary for the production of indigo dye for dyeing textiles. The extracted indigo dye is oxidized by aeration, heated, and air dried or used to make a paste with lime hydrate ($Ca(OH)_2$). The former method is popular in India. The latter method is popular in Okinawa Prefecture in Japan, the northeastern part of India (a mountainous region), southeast Asia, and southern China. Alternatively, indigo-containing plants are composted by microorganisms, and indican is transformed to indigo via the formation of indoxyl during this process (**Figure 1**). This procedure is performed in Japan, Europe, northeastern India, and West Africa. However, the composting procedure and plant material differ depending on the country.

Indigo extraction from indigo-containing leaves is quite an effective method for enrichment of indigo dye. However, if the collected indigo dye is heated to destroy microorganisms for preservation, direct fermentation might be difficult in the subsequent step of indigo reduction by microorganisms. The reducing power of the plant *Cassia tora* has been previously used in such a scenario. On the other hand, the composting procedure sustains microorganisms for subsequent indigo reduction (indigo → leucoindigo) (**Figure 1**). In Europe, a composting procedure that uses woad was developed in the Middle Ages. Harvested woad leaves are cut into very small pieces and gathered into a ball that fits in the palm of a hand. These prepared balls are then fermented for a short period under appropriate moisture conditions and dried completely to produce dried woad balls. Then, the balls are crushed, and the products are fermented over a long period via the addition of water to produce appropriate conditions for microbial activation, including an increase in the temperature to 55°C. After approximately 2 weeks of being subjected to microbial degradation, the "couched woad" is allowed to dry (Padden et al., 2000). Subsequently, the obtained product is transferred to the woad vat, which is maintained at 50°C, for a second fermentation to induce indigo reduction.

In Japan, a method for composting indigo-containing plants has been developed in Tokushima Prefecture, Shikoku, Japan (34°04′ N, 134°31′ E). The production of *sukumo*, the composted Japanese indigo plant, was developed not only for the preservation and transportation of indigo dye but also for enrichment of the indigo dye in the plant. In addition, the remaining microorganisms serve as inocula for the culture in next fermentation step, and the microorganisms present in *sukumo* can survive for at least 5 years. Furthermore, the remaining plant materials can be used as nutrient sources for microbial growth in the next fermentation step and may aid the attachment of the essential microorganisms to the debris.

Indigo is transformed to leucoindigo by the action of indigo-reducing bacteria (indigo → leucoindigo) (**Figure 1**). Although indigo is not soluble in water, leucoindigo is soluble in water. Therefore, leucoindigo penetrates textiles dipped in indigo fermentation fluid, followed by a brief exposure to air to oxidize leucoindigo (leucoindigo → indigo). Thus, indigo fixed in the textile. Traditional indigo fermentation is difficult to initiate, and long-term maintenance of the fermentation fluid in an indigo-reducing state (leucoindigo) is also challenging because the presence of the microorganisms depends on their natural occurrence and on appropriate maintenance procedures (i.e., stirring once a day, maintaining the pH, appropriately timing the feeding of the microorganisms), which requires much experience. Therefore, the fermentation procedure has been replaced with chemical reduction using sodium dithionite ($Na_2S_2O_2$). However, the addition of $Na_2S_2O_2$ produces environmentally unfavorable products, which leads problems in the disposal of the dye waste (Bechtold et al., 1993; Božič and Kokol, 2008). Sodium dithionite is ultimately oxidized to toxic derivatives such as sodium sulfate (Na_2SO_4), sulfite ions (SO_3^{2-}), and thiosulfate ($S_2O_3^{2-}$). When sodium dithionite is dumped into a water treatment system, these chemical damages the activated sludge due to its strong reducing power.

Thus, the development of conventional procedures, including management systems that do not involve the use of chemical reagents, is indispensable for the reemerging of the technique of indigo reduction by microorganisms. To achieve this goal, it may be helpful to identify the microorganisms responsible for indigo reduction and the mechanisms of indigo reduction during both the initial transitional changes and the stable state in the fermentation process. In addition, it is important to elucidate the maintenance mechanisms of the microbiota under

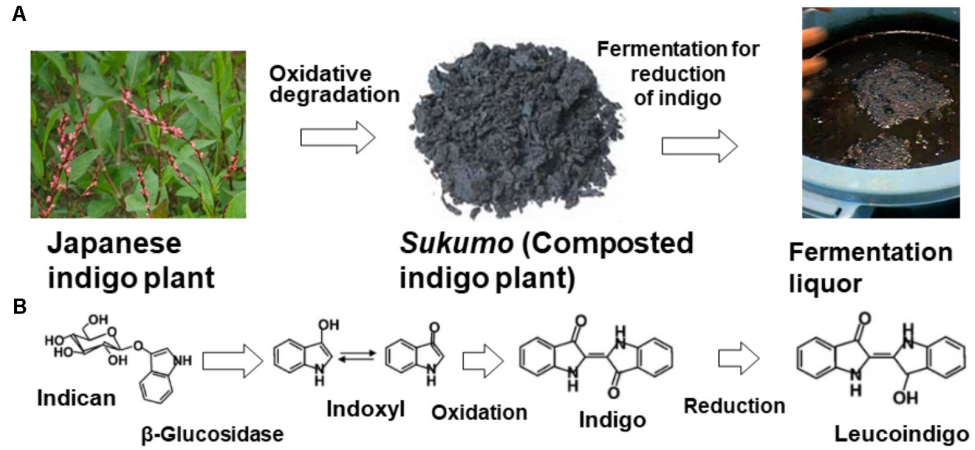

FIGURE 1 | Scheme for indigo dyeing via the traditional fermentation method using indigo plant leaves **(A)** and the concomitant chemical changes in the dye **(B)**. The origin of the dye is indican, present in the Japanese indigo plant. Indican is transformed during the production of *sukumo*. Indigo is reduced by the action of indigo-reducing bacteria and is transformed to leucoindigo.

open-air conditions and the mechanisms of deterioration toward the end of fermentation. Currently, craftspeople employ specific procedures that they have developed themselves. Therefore, there are likely many possible appropriate procedures. Analysis of many kinds of fermentation fluids in various fermentation stages is necessary for elucidation of the core mechanisms associated with the transitional changes in the microbiota during indigo fermentation.

TRADITIONAL PROCEDURES FOR INDIGO DYEING IN JAPAN

The polygonaceous Japanese indigo plant harvested during summer is cut to a length of 1.5 cm. The following day, the obtained product is air dried and separated into leaves and stem, and the leaves are placed in a straw bag. At the beginning of September, the leaves are piled on an earthen floor (an indoor ground place; approximate size: 5 × 5 m) to a thickness of approximately 1 m and appropriately wetted to induce decomposition by microorganisms. Fermentation begins after approximately 4–5 days, and produces ammonia, which is identifiable by its odor, at a temperature of 70°C. Fermentation of the indigo leaves is promoted by appropriate regulation of the moisture content to maintain aerobic conditions and high temperatures by adjusting the turnover frequency and adding water; this process requires the technical skills of a trained and well-experienced craft person. This fermentation step is continuously performed through the end of December, and the product, referred to as *sukumo* (**Figure 1**), is then covered with a straw mat. The production of *sukumo* is difficult to manage. In addition, there are only a few craftspeople who can produce *sukumo*. Therefore, to maintain an environmentally friendly indigo-reducing procedure, alternative procedures for the traditional production of *sukumo* should be developed in the near future.

In the liquid fermentation step for reduction of the indigo contained in *sukumo*, the insoluble oxidized state of indigo in *sukumo* is solubilized by indigo-reducing microorganisms (**Figure 1**). First, *sukumo* is wetted with hot wood ash extract (80°C) and mixed well in a container. The obtained clay-like product is subsequently kneaded well, added to a small amount of Japanese rice wine, and allowed to settle overnight at room temperature. Next, hot wood ash extract is added at up to one-third of the final volume. After indigo reduction occurs, fermentation liquid is added at up to two-thirds of the final volume. The effective reduction of indigo is then verified, and fermentation fluid is added to obtain the final volume (**Figure 2C**). The resulting indigo-reduced fermentation mixture is maintained at a pH greater than 10.3–10.5 by adding lime hydrate ($Ca(OH)_2$) and is stirred once daily. Based on the dyeing intensity (determined by checking the staining of cotton cloth), wheat bran is added as a substrate for the indigo-reducing microorganisms.

Indigo reduction is initiated by spontaneously occurring microbes that probably originate from the *sukumo*. Therefore, the period between the initiation of the fermentation and the appearance of indigo (from 3 to 4 days to greater than 2–3 weeks) varies depending on the quality of the *sukumo* and the preparation procedure. This uncertainty in the reduction leads many people to add chemical reducing agents. The indigo-reducing state during liquid fermentation is sustained by the microbiota. Therefore, if the microbiota in the fermentation mixture becomes imbalanced, the indigo-reducing state of the fermentation mixture is not maintained, which is why long-term fermentation for indigo dyeing is difficult to maintain. The liquid fermentation period changes depending on the capacity of the fermentation vat, the initial microbiota, the shape of the container, the maintenance procedure, and the frequency of dyeing. The indigo-reducing state is maintained for an average of approximately 6 months under conditions that introduce the risk of contamination by unfavorable microorganisms, especially

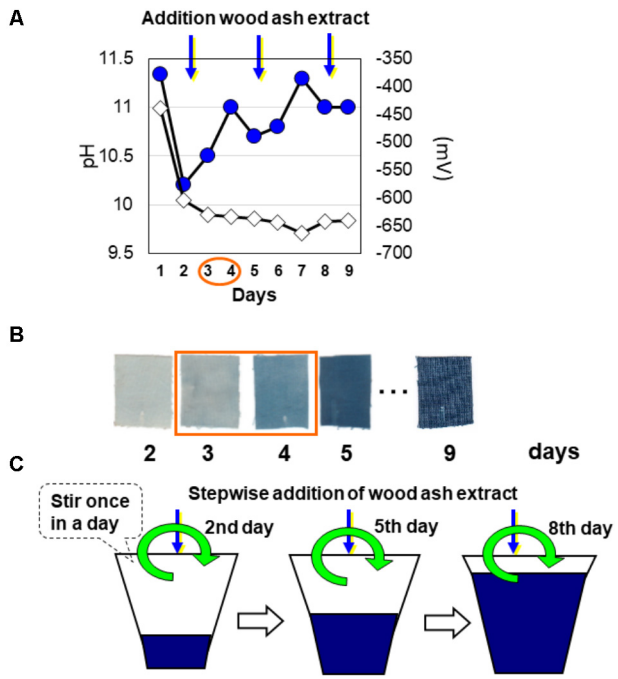

FIGURE 2 | Changes in abiotic parameters in the preparation of indigo fermentation systems and the preparation scheme. The measured parameters were pH (filled circles) and ORP (open diamond) **(A)**. The textile dyeing intensity **(B)** was estimated by dipping a strip of textile. Scheme of preparation for initiation via stepwise addition of wood ash extract **(C)** to the fermentation liquor used for indigo dyeing during the initial incubation period. The indigo fermentation batch was prepared in the laboratory. This figure was reproduced from a figure in Aino et al. (2011) with some modifications. This reproduction was permitted by Oxford University Press.

during the dyeing occasion (i.e., contaminants introduced by the dipping of textiles and by hands). Although the fermentation mixture has a high pH and presents unfavorable conditions for ordinary microorganisms to thrive, neutralophilic microorganisms can survive under such conditions due to the existence of localized niches that exhibit lower pH values than the bulk environment. Such localized niches could be generated by acid-producing bacteria. In fact, some indigo-reducing bacteria, such as *Alkalibacterium* spp., produce lactic acid (Yumoto et al., 2014). Therefore, it is considered that stirring once a day is important to prevent the spread of small, localized, neutral niches in the fermentation fluid.

AN EARLY STUDY ON INDIGO-REDUCING BACTERIA

Identification and application of indigo-reducing bacteria are essential for the improvement of indigo fermentation. The first indigo-reducing bacterium was discovered by Takahara and Tanabe (1960). Based on phenotypic characterization, they identified the isolate as belonging to the genus *Bacillus*. Given its novel characteristics, the isolate was considered a new species, which they named '*Bacillus alkaliphiles*.' The cell size of this bacterium is 0.9–1.0 × 2.5–3.5 μm, and it occurs both singly and in pairs. This motile, Gram-negative bacterium grows at a high pH (e.g., pH 10) and exhibits a strong ability to reduce the redox potential of indigo fermentation fluid. The optimum pH for the growth of this bacterium is 10–11.5. This species grows at temperatures between 10 and 50°C, with an optimum temperature of 30°C. However, the growth rate of this bacterium decreased at temperatures greater than 36°C. This bacterium is a facultative anaerobe and requires a growth factor that consists of seven amino acids. This species produces spores, is catalase positive, and hydrolyzed gelatin and starch. Since Takahara and Tanabe did not deposit the '*B. alkaliphiles*' strain in a culture collection, it is impossible to compare directly '*B. alkaliphiles*' with recently isolated indigo-reducing bacteria.

STUDIES ON WOAD DYE FERMENTATION VATS

In 1998, the indigo-reducing *Clostridium isatidis* was isolated from a couched woad vat prepared by a traditional medieval European procedure (Padden et al., 1998a,b, 2000). This bacterium was isolated in a medium at pH 9.0 that was incubated at 47°C. The cell size of this species is 0.3–0.6 × 1.8–9.1 μm. *C. isatidis* is Gram positive and aerotolerant but strictly anaerobic for growth. This moderate thermophilic bacterium occurs singly, in pairs, or in chains; and produces terminal endospores. The pH range for the growth of this bacterium is 5.9–9.9, with an optimum pH of 7.2 (at 50°C). The temperature range for the growth of this bacterium is 30–55°C, with an optimum temperature of 49–52°C (at pH 7.2). This strain produces a large amount of gas, which consists of carbon dioxide and hydrogen. This strain also produces acids, mainly acetic, lactic, and formic acids. In addition, three more strains to remove oxygen were identified. Two strains, *Bacillus pallidus* and *Ureibacillus thermosphaericus*, which have already mentioned in relation to the couching process and *Bacillus thermoamylovorans* probably consume oxygen through respiration (Cardon, 2007). The fermentation conditions for this strain differ from those for the method using *sukumo* in terms of pH and temperature. *C. isatidis* is assumed to be a specific indigo-reducing bacterium that is present in couched woad. Although the pH level during fermentation with this strain is not sufficiently stringent to exclude neutralophilic bacteria, the fermentation temperature is higher than that of the Japanese procedure. Therefore, it can be assumed that the pH combined with the temperature is stringent enough to exclude commonly existing bacteria. The microbiota of the couched woad fermentation fluid differs from that of the Japanese method that uses *sukumo* as will be discussed below.

The indigo reduction mechanism was studied using *C. isatidis* (Nicholson and John, 2005). The diameter of the indigo particles was at least 50 times that of the bacterial cells (Compton et al., 2000). Therefore, it can be presumed that indigo-reducing bacteria solubilize solid matter that is much larger than the bacterial cells for reduction. Comparative studies of the indigo-reducing *C. isatidis* and four other *Clostridium* species showed that the indigo-reducing ability of this strain was not shared

by the other species. The culture supernatant from *C. isatidis* decreased the indigo particle size to one-tenth of the initial diameter, which was not observed with the other species. An electron mediator, anthraquinone-2,6-disulfonic acid (AQDA), stimulated indigo reduction by *C. isatidis*. *C. isatidis* exhibited a greater ability to reduce ambient redox potential than the other strains used in this study. The redox potential of *C. isatidis* culture was −600 mV, which was 100 mV lower than the redox potentials of the other four *Clostridium* spp. Although the authors mentioned that quinone probably acts by modifying the surfaces of the bacteria or indigo particles, it is possible that quinone acts as an electron mediator in the reduction of indigo because the addition of quinone accelerates indigo reduction. The decrease in indigo particle size caused by the culture supernatant of *C. isatidis* suggested that the electron-retaining quinone from woad reduced the indigo particle. Thus, as an electron mediator, quinone is considered to be very important for indigo reduction in woad dye vats. On the other hand, direct electron transfer between *C. isatidis* cells and carbon electrodes has been demonstrated (Compton et al., 2000). Although the report indicated that *C. isatidis* could transfer electrons to the solid material, it was not determined whether the bacterium can reduce indigo particles directly.

Two broth media, containing either yeast extract (extracted from baker's yeast; 30 g L^{-1}) or corn steep liquor (CSL; 10 g L^{-1}), were used for their capacity to sustain the growth and reducing activity of *C. isatidis* (Osimani et al., 2012). A relatively high viable cell count and low oxidation-reduction potential (ORP) value were observed in the CSL-containing broth. Subsequently, in order to examine sustainability, CSL broth treated with 140 g L^{-1} woad powder and 2.4 g L^{-1} indigo dye under sterilized conditions was fermented under anaerobic or microaerobic conditions. In all the fermentation batches, sufficiently low ORP values for reducing indigo were attained within 24 h and were maintained for up to 9 days. However, the total counts of vegetative cells and spores were higher under anaerobic conditions. In addition, rapid indigo dye reduction was observed under strictly anaerobic conditions. This observation indicates the superiority of the original woad system compared to the indigo dye system for indigo reduction in CSL broth, as the original system did not require the introduction of N_2. This suggest that microbiota containing in the original woad system have a role to accelerate in the fermentation vat under atmospheric condition.

The microbiota of woad vat fermentation liquor aged for 12 months has been examined via PCR-DGGE (denaturing gradient gel electrophoresis) and pyrosequencing (Milanović et al., 2017). Bands corresponding to *Paenibacillus lactis* (98–99% identity) and *B. thermoamylovorans* (99%) were frequently observed in these assays. Bands corresponding to *Bacillus pumilus* (92–94%), *Sporosarcina koreensis* (99%), and *Bacillus licheniformis* (99%) were also observed. These bacterial members are rarely observed in the Japanese procedure that uses *sukumo*. This indicates that the fermentation conditions of this method have a lower pH and higher temperature than those of the *sukumo*-using method.

By pyrosequencing analysis, *Clostridium ultunense*, *Alcaligenes faecalis*, and *Tissierella* spp. were observed to be the predominant members of the dyeing fluid (Milanović et al., 2017). *Virgibacillus pantothenticus* and *Virgibacillus* spp. were also detected as minor constituents. Unidentified Bacillaceae and Clostridia, including moderately thermophilic bacteria, lactic acid bacteria, and photosynthetic bacteria, were observed among the subdominant components. These results suggest that the reported indigo-reducing bacteria are not major members of this fermentation fluid. However, all the indigo-reducing bacteria have not been identified yet. Therefore, there is a possibility that some of the detected members are indigo-reducing bacteria. Furthermore, there is a possibility that this pyrosequencing analysis could not detect indigo-reducing bacteria because pyrosequencing analysis results can vary depending on bacterial community structure, sequencing technology, and PCR bias (Aird et al., 2011; Klindworth et al., 2012; Lee et al., 2012; Luo et al., 2012; Pinto and Raskin, 2012; Wu et al., 2012; O'Donnell et al., 2016).

INDIGO-REDUCING ENZYMES

An indigo-carmine (**Figure 3**)-reducing enzyme from a *Bacillus cohnii* strain that was isolated from an indigo fermentation system has been purified and characterized (Nii et al., 2006). The enzyme was purified from disrupted cells, and the enzymatic activity was determined using NADH and indigo carmine as the electron donor and acceptor, respectively. The optimum pH for the activity is pH 7.5, and the enzyme is stable at pH 3.5–9.5. The optimum temperature for the activity is 30°C, and the enzyme is stable at temperatures up to 30°C. The activity increases substantially when 2,6-dichlorophenol-indophenol is used as the electron acceptor instead of indigo carmine. The molecular mass was determined to be 74 kDa by gel filtration.

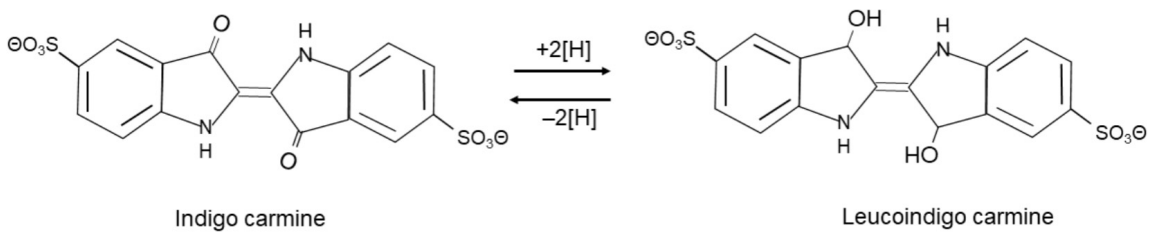

FIGURE 3 | Chemical structure of indigo carmine and its reduction/oxidation.

The reported enzyme is considered to be a kind of azoreductase. A few azoreductases have been reported in *Bacillus* spp. (e.g., *Bacillus* sp. and *Bacillus cereus*) (Ooi et al., 2007; Pricelius et al., 2007). These azoreductases are thought to react with soluble substrates such as indigo carmine. It is considered that it is unlikely that these azoreductase-like enzymes react directly with solid substrates that have diameters at least 50 times larger than those of the bacterial cells. However, an azoreductase which oxidized NADH in presence of indigo was reported by Suzuki et al. (2018). Large indigo particles may also react with electron mediators such as quinone or by electrically conductive pilus-like "nanowires." However, it has been considered that azoreductases from *Bacillus* spp. will contribute to the maintenance of indigo in the reduced state.

EXTRACELLULAR REDUCTION IN ALKALIPHILES

If an alkaliphile that is present in indigo dye vats has the ability to reduce extracellular substances, it is possible that the microorganism has the ability to reduce indigo particles. Ma et al. (2012) isolated an alkaliphilic *Bacillus*, namely, *Bacillus pseudofirmus* MC02, that can transfer electrons to anthraquinone-2,6-disulfonate (AQDS), humic acids (HAs), and Fe(III) oxides as representative electron acceptors. This strain could effectively perform Fe(III) oxide reduction coupled with sucrose fermentation when AQDS was added as an electron mediator. In addition, this bacterium can decolorize azo dyes in alkaline conditions. Although it has not been determined whether *B. pseudofirmus* MC02 can reduce water-insoluble indigo, this bacterium occupies the same branch as the indigo-reducing bacterium *Paralkalibacillus indicireducens* (**Figure 4**). *Anaerobacillus arsenicoselenatis* and *Anaerobranca californiensis* have been reported as exhibiting Fe(III) reduction (Blum et al., 1998; Gorlenko et al., 2004). As described below, *Anaerobacillus* spp. and *Anaerobranca* spp. are frequently observed in indigo fermentation vats. While the *Anaerobacillus* and *Anaerobranca* strains mentioned above were examined using soluble Fe^{3+} as an electron accepter, *B. pseudofirmus* MC02 could reduce both soluble Fe^{3+} and solid-phase Fe(III) oxides.

EFFECT OF REDOX POTENTIAL

Addition of AQDA (0.003–0.01%) stimulates indigo reduction. However, it is considered that AQDA does not contribute directly to reduction of the redox potential in bacterial cultures in that study, due to its higher midpoint redox potential than that of indigo (Nicholson and John, 2005). The midpoint redox potential (E'^0) of AQDS is −184 mV at pH 7 (Clark, 1960) or −290 mV at pH 9 (Chatterjee et al., 1998). The midpoint potential of indigo is difficult to estimate due to the insolubility of the oxidized form of this compound. An indicative value of −474 mV [versus a saturated calomel electrode (SCE)] in water at 50°C was determined in the presence of solid indigo (Vickerstaff, 1954). However, an even lower redox potential (−600 mV) is considered to be required for indigo reduction in industrial practice (Bechtold et al., 1993). Although theoretical electron transfer from AQDS is difficult, the finding of acceleration of indigo reduction by AQDS indicates that the difference in redox potential between AQDA and an indigo particle at the surfaces of the indigo particle may be different from the bulk redox potential that is necessary to reduce indigo in the absence of electron mediators.

INDIGO-REDUCING BACTERIA BELONGING TO THE GENUS *ALKALIBACTERIUM*

We attempted to isolate indigo-reducing bacteria from an enrichment culture using a conventional broth medium (pH 10) under anaerobic conditions with fermentation fluid obtained from the craft center. Commercially available indigo powder, which is insoluble in water, was used as an indicator of indigo reduction. This enrichment culture was repeated five times and then transferred to conventional agar medium. By this procedure, we isolated the strain IDR2-2^T, which can reduce indigo (Yumoto et al., 2004). This strain was identified as a member of the genus *Alkalibacterium* by 16S rRNA gene sequence analysis (**Figure 4**). This strain was identified as a new species because it differed from the only species of this genus that had been discovered up to that point, namely, *Alkalibacterium olivapovliticus*. Therefore, we named this strain *Alkalibacterium psychrotolerans* (Yumoto et al., 2004; **Table 1**). This strain grew equally well under both aerobic and anaerobic conditions and produced L-lactic acid. In addition to *Alkali. psychrotolerans*, *Alkalibacterium iburiense* (Nakajima et al., 2005; **Table 1**) and *Alkalibacterium indicireducens* (Yumoto et al., 2008; **Table 1**) were subsequently isolated and characterized (**Figure 4**). All the strains of *Alkali. psychrotolerans* and *Alkali. iburiense* were isolated from fermentation fluid obtained from Date City, Hokkaido, Japan, whereas *Alkali. indicireducens* was isolated from an indigo fermentation fluid sample obtained from Tokushima Prefecture, Shikoku, Japan. Although these species have similar characteristics to *A. psychrotolerans*, they differ from one another. For example, *A. psychrotolerans* grows faster than the other two species. In addition, *Alkali. psychrotolerans* and *Alkali. iburiense* produce acid from a number of carbohydrates, whereas *Alkali. indicireducens* did not produce acid from several tested carbohydrates. Although the preparation and maintenance procedures differed from the Japanese procedure, *Alkalibacterium* sp. has been isolated from a natural fermentation system used for 6 years for dyeing cotton textiles in Korea (Park et al., 2012).

TRANSITIONAL CHANGE IN THE EARLY PHASE OF INDIGO FERMENTATION

Initiation of indigo reduction is expected to be associated with transitional changes in the microbiota in indigo fermentation vats under anaerobic alkaline conditions. Changes in the composition of the microbiota upon initiation of indigo reduction were examined via PCR-DGGE (Aino et al., 2011). Wood ash extract

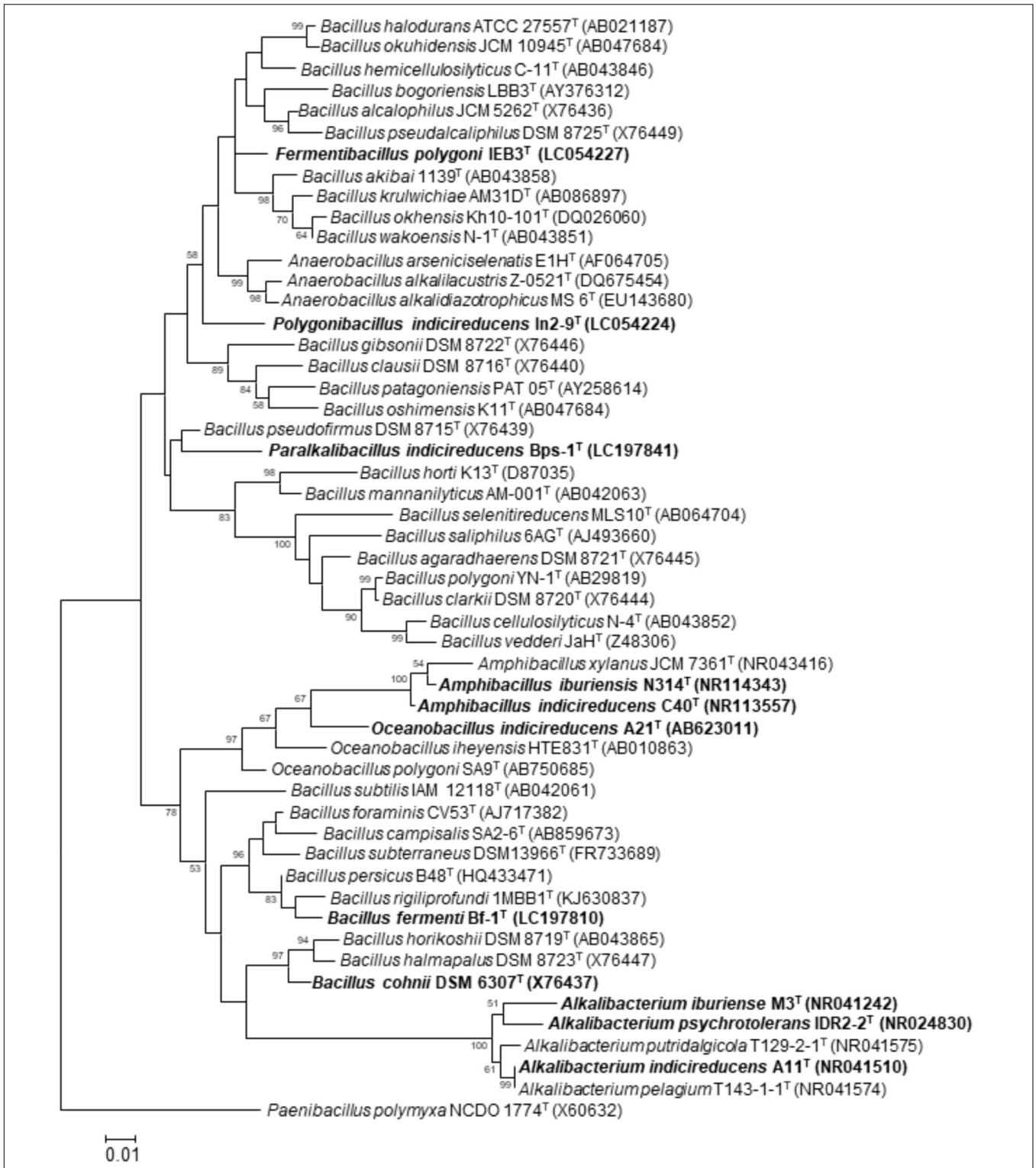

FIGURE 4 | Maximum-likelihood phylogenetic tree derived from 16S rRNA gene sequences, showing the phylogenetic positions of the isolated indigo-reducing bacteria. To construct the phylogenetic tree, the sequences were aligned with the sequences of neighboring species, and the consensus sequence was determined by CLUSTAL W (Thompson et al., 1994). The evolutionary history was inferred by using the maximum-likelihood method (Guindon and Gascuel, 2003) in MEGA 7 (Kumar et al., 2016). The evolutionary distance matrix was calculated by using Kimura's two-parameter model (Kimura, 1980). Bold letters indicate the indigo-reducing bacteria. Although *B. cohnii* DSM 6307^T was not one of our isolates, strains belonging to this species that reduced indigo were isolated from indigo fermentation fluid. Bootstrap percentages (based on 1000 replicates) >50% are shown at branch points. Scale bars = 0.01 substitutions per nucleotide position.

TABLE 1 | Characteristics of indigo-reducing bacteria found in indigo fermentation fluid.

	1	2	3	4	5	6	7	8	9	10	11
Cell shape	Rod	Rod	Rod	Rod	Rod	Rod	Rod	Rod	Rod	Rod	Rod
Gram stain	+	+	+	+	+	+	+	+	+	+	+
Cell size (μm)	0.4–0.9 × 0.7–3.1	0.3–0.4 × 1.7–3.0	0.4–1.2 × 1.7–3.7	0.3–0.5 × 1.0–3.0	0.3–0.4 × 1.7–3.0	0.4–0.9 × 1.7–2.6	0.6–1.0 × 1.3–4.5	0.7–0.8 × 2.0–6.4	0.5–0.8 × 1.1–2.0	0.8–1.2 × 2.2–3.8	ND
Aerotolerant anaerobic*	Y	Y	Y	Y	Y	N	N	N	N	N	N
Facultatively anaerobic*	N	N	N	N	N	Y	Y	Y	Y	Y	Y
Oxidase	–	–	–	–	–	+	+	+	+	+	+
Catalase	–	–	–	–	–	+	+	+	+	+	+
Spore location[§]	No spore	No spore	No spore	T	T	STC	STC	STC	T	STC	T
Flagella[¶]	Per	Per	Per	Per	Per	Per	Pair of subpolar	Per	Pair of subpolar and center side	Pair of subpolar	Per
Growth pH range	9–12	9–12	9–12.3	9–12	8–9.1[‡]	7–12	7.5–12	8–12	8–11	8–12	ND
Optimum growth pH	9.5–10.5	9.5–10.5	9.5–11.5	10	8.9–9.0[‡]	10	9 or 10	10	9–10	9–10	ND
Growth NaCl concentration range (%)	0–17	0 to 14–16	0 to 14–15	0–7	0–7	0–10	0–5 or 0–10	0–10	0–10	0–7	ND
Optimum growth NaCl concentration (%)	2–12	3–13	1–11	0–1	0–3	1–11	0	3	7	0–3	ND
Growth temperature range (°C)	5–45	5–45	15–40	17–39	26–39	18–48	12–40	10–45	18–40	15–45	10–47
Optimum growth temperature (°C)	34	30–37	20–30	35	36	39	30–33	35–37	33	33–40	ND
Isoprenoid quinone	No quinone	No quinone	No quinone	No quinone	No quinone	No quinone	MK-7	MK-6	MK-7	MK-7	MK-7
DNA G+C content (mol%)	40.6	42.6–43.2	47.0–47.8	37.5–37.7	38.4	39.7	39.0	39.4	40.3	41.7	33.5–35.0
Hydrolysis of cellulose and xylan	+	+	+	+	+	–	–	–	–	–	ND
Origin	Fermentation fluid prepared in a craft center	Fermentation fluid prepared in a craft center	Fermentation fluid prepared in a craft center	10-month-old aged fermentation fluid obtained from a craft center	10-month-old aged fermentation fluid obtained from a craft center	4th-day fermentation fluid prepared in a laboratory	Fermentation fluid prepared in a laboratory	Aged fermentation fluid obtained from a craft center	Aged fermentation fluid obtained from a craft center	Aged fermentation fluid obtained from a craft center	Aged fermentation fluid obtained from a craft center

*Strains: 1, Alkalibacterium psychrotolerans; 2, Alkalibacterium iburiense; 3, Alkalibacterium indicireducens; 4, Amphibacillus indicireducens; 5, Amphibacillus iburiense; 6, Oceanobacillus indicireducens; 7, Fermentibacillus polygoni; 8, Polygonibacillus indicireducens; 9, Paralkalibacillus indicireducens; 10, Bacillus fermenti; 11, Bacillus cohnii. Data for the strains were obtained from Hirota et al. (2013a; 2013b; 2013c; 2016a; 2016b; 2017; 2018), Nakajima et al. (2005); Spanka and Fritze (1993), Yumoto et al. (2004, 2008). +, positive; –, negative; ND, not determined *Y, yes; N, no. [¶] Per, peritrichous fhagellation. [§] T, terminal; STC, subterminal to central; C, central; ST, subterminal. [‡]These pH values are based on time, while other descriptions are based on the initial pH of the medium.*

was added to *sukumo* to make a paste (1st day), and the 1st, 2nd, and 3rd volume expansions were performed on the 2nd, 5th, and 8th days. For each expansion, one-third of the total volume of wood ash extract was added to the fermentation system (**Figure 2C**). The addition of wood ash extract may induce a dramatic change in the microbiota, concomitant with the change in the environment. In fact, distinct changes in the PCR-DGGE banding pattern were observed from the 1st to 2nd; 2nd to 3rd; 5th to 6th; and 8th to 9th days (66.9, 39.1, 32.1, and 24.1%, respectively). The change in the banding pattern of the microbiota between the 1st and 2nd days (66.9%) was higher than that in the other periods within the first 9 days after preparation of the fermentation mixture. During the initiation of fermentation (1st to 2nd day), the ORP and pH changed dramatically, from −440 to −640 mV and from 11.3 to 10.2, respectively (**Figure 2A**). This substantial change in ORP may be attributed to the consumption of oxygen by aerobic microorganisms and the extracellular reducing activity of the excised microorganisms. The large pH change may be attributed to the byproducts of anaerobic metabolism. The corresponding PCR-DGGE bands that were enhanced were assigned to *Bacillus* sp. (similarity to *Bacillus firmus*: 95%) and *Amphibacillus* spp. Bands corresponding to *Halomonas* sp. and *Bacillus* sp. (similarity to *Bacillus cellulosilyticus*: 98%) were also observed. Therefore, *Bacillus* sp. (similarity to *B. firmus*: 95%) and *Amphibacillus* sp. (similarity to *Amphibacillus xylanus*: 99.2%) may play an important role in the dramatic change observed in the early phase of fermentation. Between the 3rd and 4th days from the initiation of fermentation, characteristics of indigo reduction were observed (**Figure 2B**). During this period, a relatively large change in the microbiota occurred (dissimilarity value, 28.2%). Bands attributed to *Amphibacillus* sp. (similarity to *A. xylanus*: 99.2), *Bacillus* sp. (similarity to *B. cellulosilyticus*: 96.4%), and *Corynebacterium* sp. [similarity to *Corynebacterium* sp. BBP21 (DQ337522): 99.2%] increased in intensity. The bacteria to which these bands were attributed may play significant roles in the transition to indigo reduction.

Since a change in the intensity of indigo dyeing was observed (**Figure 2B**), analysis of the microbiota using a 16S rRNA gene clone library was performed (Aino et al., 2011). On the 3rd day, the major constituents at the genus level were *Halomonas* (54%) and *Tissierella* (14%), whereas the genera *Tissierella* (35%), *Amphibacillus* (19%), and *Paenibacillus* (11%) were observed on the 4th day. The proportion of *Halomonas* dropped to 8% by the 4th day. It can be concluded that the large decrease in the proportion of *Halomonas* (54% → 8%) and the increase in the proportion of the indigo-reducing genus *Amphibacillus* (not detected → 19%) led to a dramatic change in the dyeing intensity. Prior to this study, it was thought that *Alkalibacterium* spp. were the main microbes responsible for indigo reduction. We conclude that there are functional redundancies in indigo reduction within the microbiota.

The same approach was applied to 10-month-old fermentation products to understand how the microbiota behaves under long-term fermentation. The fermentation fluid was obtained from the craft center. Although fermentation had been maintained for a long period, the microbiota was much simpler than expected. The major members identified belonged to the genera *Amphibacillus* (35%), *Alkalibacterium* (18%), *Tissierella* (18%), and *Alcaligenes* (13%), which indicates that the major members were indigo-reducing genera and that the diversity of the microbiota was relatively low. The observed microbiota is an example of the long-term-maintained fermentation fluid, and this information could contribute to understand microbial communities of the long-term fermentation.

INDIGO-REDUCING BACTERIA BELONGING TO THE GENERA *AMPHIBACILLUS* AND *OCEANOBACILLUS*

During a trial aimed at the isolation of indigo-reducing bacteria concomitant with the above analysis of the microbiota from fermentation fluid that we prepared in our laboratory and aged (10-month-old) fermentation fluid obtained from the craft center in Date City, Hokkaido, Japan, using a medium containing 0.2% indigo carmine, indigo-reducing *Oceanobacillus indicireducens* (strain A21^T; **Table 1**) and *Amphibacillus* spp. were isolated (Aino et al., 2011). Strain A21^T was isolated from the fermentation liquor on the 4th day after the initiation of fermentation (the day when indigo reduction was initiated). 16S rRNA gene sequence analysis and the phylogenetic tree based on the sequence indicated that strain A21^T belonged to the genus *Oceanobacillus* (**Figure 4**). According to the polyphasic taxonomic approach, the bacterium was identified as a new species of *Oceanobacillus*, with the proposed name *O. indicireducens* (Hirota et al., 2013b). Surprisingly, this bacterium exhibits aerobic metabolism even though it lacks isoprenoid quinones. This characteristic has been observed in only strain A21 among the members of *Oceanobacillus*. One of the reasons for this peculiar characteristic is probably that the strain was isolated from an anaerobic alkaline environment from which no other *Oceanobacillus* spp. have been isolated.

Two indigo-reducing obligately alkaliphilic strains, namely, C40^T and N214, were isolated from a 10-month-old sample obtained from the craft center in Date City in Hokkaido, Japan (Aino et al., 2011). Strain C40^T exhibited stronger indigo-reducing activity than a strain of *Alkali. indicireducens* and other strains belonging to the genus *Alkalibacterium* within 6 days from the beginning of incubation. 16S rRNA gene sequence analysis and the phylogenetic tree based on the sequence indicated that strains C40^T and N214 belonged to the genus *Amphibacillus* (strain C40^T in **Figure 4**). Based on the polyphasic approach, the two strains were considered to belong to a new species, for which the name *Amphibacillus indicireducens* sp. nov. was proposed (Hirota et al., 2013a; **Table 1**). Strain N314^T was isolated from the same sample. However, this strain exhibited a different phylogenetic position from that of *Amphi. indicireducens* and other reported *Amphibacillus* spp. (**Figure 4**). Therefore, the

name *Amphibacillus iburiensis* sp. nov. was proposed for this strain (Hirota et al., 2013c; **Table 1**). The species exhibited similar characteristics to *Amphi. indicireducens*. This strain also grew on media with an adjusted pH of 8–12. However, the strain was able to change the pH of the medium by producing acid, and growth was initiated at pH 8.9–9.1. Although these growth characteristics may be observed in other indigo-reducing bacteria, we detected these characteristics by monitoring the transition of the medium with strain N314^T. In addition to *Alkalibacterium* spp., *Amphibacillus* spp. also appeared to play important roles in the reduction of indigo in many cases. Species of these genera are able to hydrolyze xylan and cellulose (**Table 1**). This characteristic may explain why wheat bran has long been used for the maintenance of indigo fermentation fluid.

FERMENTIBACILLUS POLYGONI, AN INDIGO-REDUCING BACTERIUM BELONGING TO A NOVEL GENUS AND SPECIES

Although Takahara and Tanabe (1960) isolated an indigo-reducing bacterium belonging to the genus *Bacillus*, as described above, we were unable to detect such a bacterium in our trials. The *Bacillus* sp. isolated by Takahara and Tanabe required a peptide for growth. The peptide was derived from a component of the fermentation liquor. Therefore, during the trial conducted to isolate indigo-reducing bacteria from fermentation fluid prepared in our laboratory, we attempted to isolate indigo-reducing *Bacillus* species using a medium that contained indigo fermentation liquor. An aliquot of the sample was inoculated onto indigo fermentation liquor agar (IFLA) medium, which consisted of only indigo fermentation liquor, 1% Na_2CO_3, and 1.5% agar. The agar plate was incubated at 27°C for 1 week, and 29 colonies were isolated. Two strains, namely, IEB3^T and IEB4, were selected on the basis of the high similarities of their 16S rRNA gene sequences with those of *Bacillus* species and low similarities with those of other valid reported species. The phylogenetic tree constructed from the sequences of these strains and those of related taxa showed that strains IEB3^T and IEB4 occupied a distinct position from the members of the genus *Bacillus* (strain IEB3^T in **Figure 4**). In addition to their distinct phylogenetic position, these strains were distinct from neighboring species or genera in terms of flagellum and spore morphologies. Therefore, we considered these strains to represent a novel species within a novel genus, and the name *Fermentibacillus polygoni* gen. nov., sp. nov. was proposed for this species (Hirota et al., 2016a; **Table 1**). Although the isolates were obtained from IFLA medium, this species did not require indigo fermentation liquid for growth. This isolate was the first example of a novel species within a novel genus isolated from indigo fermentation. New methods for the isolation of constituent bacteria from indigo fermentation systems will increase the ease of isolating undiscovered microorganisms. Media that contain low nutrient concentrations will be useful for the isolation of undiscovered microorganisms associated with indigo fermentation (Janssen and Yates, 2002).

CHANGES IN THE MICROBIOTA IN AGED INDIGO FERMENTATION

Indigo reduction occurs via fermentation performed by naturally occurring microorganisms. This process continues under open-air conditions, and there are many chances for contamination. Indigo fermentation occurs under anaerobic and high-pH conditions. Although such conditions are far from the conditions under which ordinary microorganisms thrive, there are many microorganisms that produce acids in the fermentation fluid. It is presumed that there are microenvironments that have lower pH values than that of the bulk phase in the debris at the bottom of the fermentation fluid. Localized low-pH niches could develop if the liquid is not mixed sufficiently by daily stirring. Thus, although indigo fermentation fluid is a harsh environment for aerobic neutralophiles, there is opportunity for neutralophiles to propagate in this environment. Ordinary indigo fermentation maintains an indigo-reducing state for 6 months on average, and often for longer than 6 months. Hence, there must be mechanisms by which the bacteria involved in fermentation maintain the indigo-reducing state. Identification of the maintenance mechanism underlying long-term indigo fermentation could lead to the development of a novel, long-term, unsterilized bioprocess in the future. To determine the microbiological basis of the maintenance of indigo fermentation, we examined the microbiota in fermentation fluids maintained for more than 6 months (Okamoto et al., 2017). We examined the microbiota in one early-phase batch and two aged batches of indigo fermentation fluid. The first batch (D1: aged 6 and 10 months) mainly consisted of the genera *Alkalibacterium*, *Amphibacillus*, and *Tissierellaceae* (**Figure 5**). The second batch (D2: aged 9, 11, and 14 months) mainly consisted of *Tissierellaceae*, *Proteinivoraceae*, and the genera *Anaerobacillus*, *Amphibacillus*, *Alkalibacterium*, and *Polygonibacillus* (Bacillaceae) (indigo-reducing bacteria, described below) (**Figure 5**). It can be assumed that *Anaerobacillus* spp. contain indigo-reducing bacteria based on their phylogenetic position adjacent to indigo-reducing bacteria and the Fe^{3+}-reducing characteristic, as described above. Therefore, the two types of aged fermentation fluids evaluated in this study were probably primarily composed of indigo-reducing bacteria. The first batch mainly consisted of aerotolerant anaerobes, whereas a majority of the bacteria in the second batch was obligately anaerobic. Thus, there are several possible microbial communities that can perform indigo fermentation for long periods. Although these fermentation fluids remained in the indigo-reducing state for a long period, the microbiota changed dramatically in each batch. These successive changes in the microbiota involved in indigo reduction sustained the indigo-reducing state for this extended period.

We also analyzed the microbiota in the early fermentation period and used principal coordinate analysis (PCoA) to compare two batches maintained for a long period (Okamoto et al., 2017;

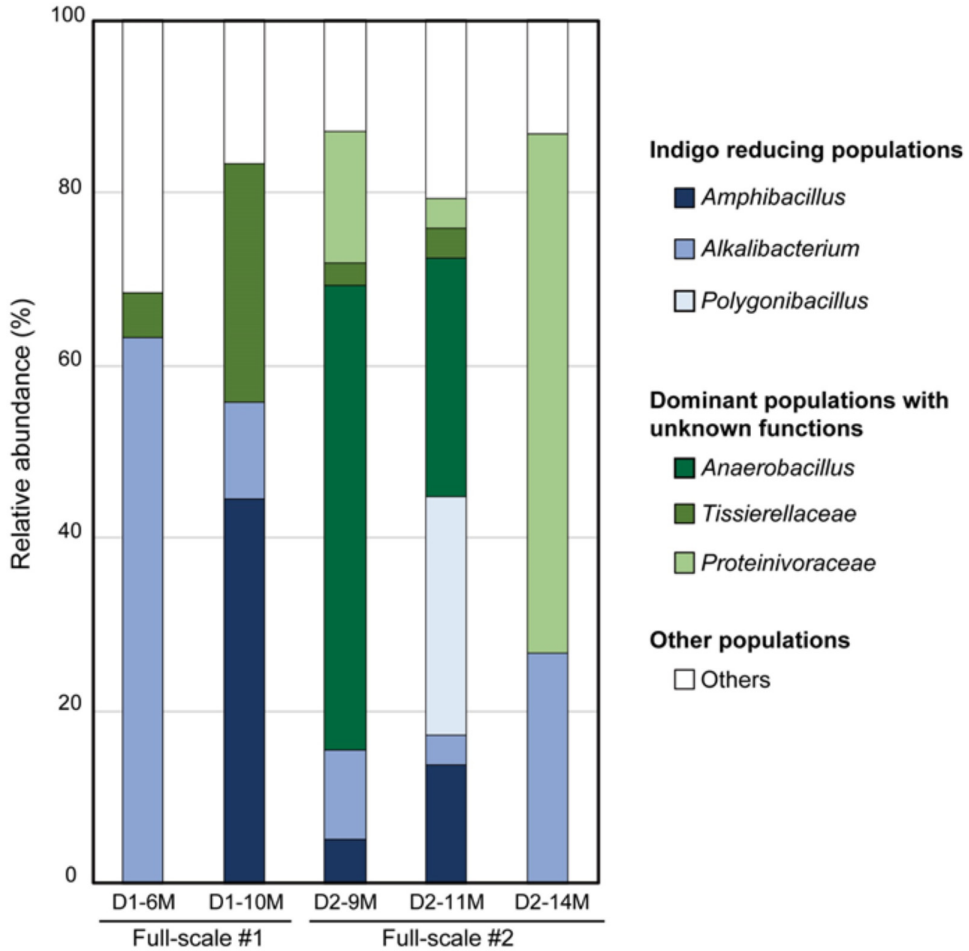

FIGURE 5 | Changes in the bacterial community of the indigo fermentation fluid in aged phases (D1-6M, D1-10M, D2-9M, D2-11M, and D2-14M). The relative abundance of each taxon is shown. D1-6M, 1st-batch sample, aged 6 months, obtained from Date City (42°42′ N, 140°42′g E); D1-10M, 1st-batch sample, aged 10 months, obtained from Date City; D2-9M, 2nd-batch sample aged 9 months, obtained from Date City; D2-11M, 2nd-batch sample, aged 11 months, obtained from Date City; D2-14M, 2nd-batch sample, aged 14 months, obtained from Date City. This figure was cited from a figure in Okamoto et al. (2017) with some modifications. This citation was permitted by Springer-Nature.

Figure 6). Although the transition was slower in the aged fermentation fluid (batches D1 and D2) than in the fluid from the early fermentation period (L batch), substitution of the dominant indigo-reducing bacteria reflected the substantial changes that occur over 3 or 4 months in fermentation baths maintained for longer than 6 months (batches D1 and D2). Although the rates at which the changes occurred were dependent on fermentation conditions, the microbiota changed over the entire fermentation period under all the conditions. These changes may reflect the sustainability of the microbiota over a long period. It is expected that although the microbiota during the preliminary period of fermentation exhibited high flexibility, changes readily occurred in various directions, followed by the formation of a relatively stable state, due to relatively small changes in the 2 months between D2-9M and D2-14M (**Figure 6**). The stable state is characterized mainly by the genus *Anaerobacillus* and may contribute to the duration of fermentation. Over long maintenance periods, the resiliency of the microbiota and the proportion of indigo-reducing bacteria are expected to decrease, although no examples of such a state were detected in these analyses of the microbiota. In the case of indigo fermentation, in spite of the risk of bacterial contamination, substrates such as wheat bran are occasionally added, depending on the dyeing intensity. Therefore, the energy supply for indigo reduction remains high for a long period. In conclusion, the duration of sustained fermentation may be determined by the proportion of indigo-reducing bacteria and the stability of the microbiota, as observed in aged fermentation fluids.

Changes in the microbial diversity of the three different batches were estimated (**Figure 7**). Although distinct changes in the microbiota were observed over a short period in batch L, the corresponding bacterial diversity exhibited little variation. In addition, although distinct changes in the microbiota were observed over a long period in batch D1, there was little corresponding change observed in the diversity of the microbiota. This low diversity may explain why this batch was maintained

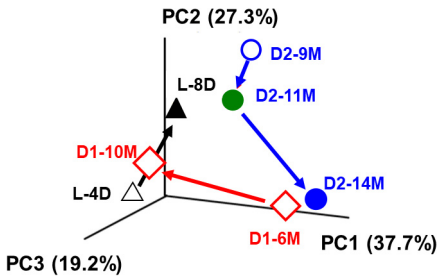

FIGURE 6 | PCoA plot for the bacterial community of the indigo fermentation fluid. Analyzed samples are the initial (L-4D and L-8D) and aged fermentation phases (D1-6M, D1-10M, D2-9M, D2-11M, and D2-14M). L-4D, 4th-day sample, prepared in the laboratory; L-8D, 8th-day sample, prepared in the laboratory; D1-6M, 1st-batch sample, obtained from Date City (42°42′ N, 140°42′ E), aged 6 months; D1-10M, 1st-batch sample, obtained from Date City, aged 10 months; D2-9M, 2nd-batch sample, obtained from Date City, aged 9 months; D2-11M, 2nd-batch sample, obtained from Date City, aged 11 months; D2-14M: 2nd-batch sample, obtained from Date City, aged 14 months. This figure was cited from a figure in Okamoto et al. (2017). This reproduction was permitted by Springer-Nature.

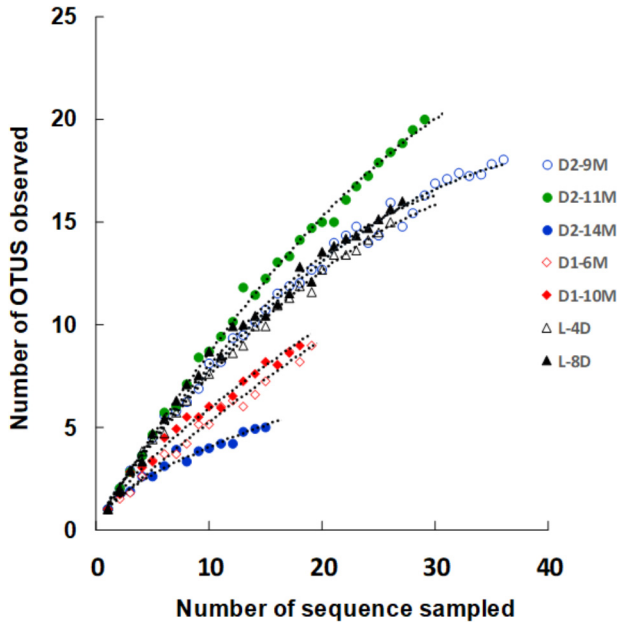

FIGURE 7 | Rarefaction curve of OTUs defined by 3% sequence variation in samples. The indigo fermentation fluids in the initial (L-4D and L8D) and aged phases (D1-6M, D1-10M, D2-9M, D2-11M, and D2-14M) were analyzed. The curve depicts the diversity of each sample. Sample names are the same as those in **Figure 6**. OTUs, operational taxonomic units. This figure was reproduced from a figure in Okamoto et al. (2017). This reproduction was permitted by Springer-Nature.

for a longer than average duration. On the other hand, a distinct change in the diversity of the microbiota was observed in batch D2. An especially dramatic change was observed between 11 and 14 months of fermentation. One reason for the differences in the changes in diversity observed in the different batches may be the differences in the preparation and maintenance procedures. In fact, subtle differences in preparation procedures are thought to induce substantial differences in the microbiota and its diversity.

NOVEL PROCEDURE FOR THE ISOLATION OF INDIGO-REDUCING BACTERIA

As described above, various indigo-reducing bacteria exist in the indigo fermentation liquor, and these bacteria often cannot be detected via culture-independent approaches. In addition, all the indigo-reducing bacterial species in various fermentation fluids and the different fermentation periods of these bacteria have yet to be identified. Until these bacteria are isolated and their indigo-reducing abilities are examined, it will not be possible to identify these species as indigo-reducing bacteria. Therefore, efficient procedures for the isolation of indigo-reducing bacteria are important not only for the accumulation of knowledge regarding indigo-reducing bacteria in fermentation fluid but also for interpreting the results of culture-independent approaches (especially the proportions of indigo-reducing genera or species). However, isolation of indigo-reducing bacteria is not always easy because conventional media are often unsuitable for slow-growing bacteria, which exist at low proportions. Hydrolysates of polysaccharides present during indigo fermentation and unknown substances in the fermentation material (i.e., *sukumo*) are appropriate candidates for promoting isolation of unknown indigo-reducing bacteria. In addition, the use of low nutrient levels to prevent the growth of rapidly growing bacteria will aid the isolation of slow-growing indigo-reducing bacteria. Wheat bran hydrolyzed by cellulase and *sukumo* hydrolyzed by cellulase have been used as novel media components for the isolation of new indigo-reducing bacteria. Media composed of each individual hydrolysate and mixtures thereof are prepared, and the sample-inoculated media is incubated under anaerobic conditions (Nishita et al., 2017). Indigo carmine has also been employed as an indicator of indigo reduction. Indigo fermentation fluid obtained from the indigo-dyeing craft center in Date City, Hokkaido, Japan, was inoculated onto prepared media, including conventional media. Media containing *sukumo* hydrolysate facilitated the isolation of novel *B. pseudofirmus*-related strains (later described as *P. indicireducens* gen. nov., sp. nov.), whereas media containing wheat bran hydrolysate facilitated the colonization of *Amphibacillus* spp. (including novel species, with lower than 98% sequence similarity of 16S rRNA sequences). Seven species (including two novel species) and six species (including three new species) of indigo-reducing bacteria were isolated using wheat bran hydrolysate-containing medium and medium containing both wheat bran and *sukumo* hydrolysate, respectively. These isolated species were more numerous than those in the conventional media. The media that were prepared for the first time in this study may also be useful for facilitating the isolation of bacteria other than indigo-reducing strains from indigo fermentation fluid samples. With this trial, we identified a previously isolated bacterium, *B. cohnii*, as an indigo-reducing bacterium (**Table 1**). This species

is a facultative anaerobe and was isolated from all the tested media. Furthermore, new species of bacteria might exist in indigo fermentation mixtures prepared using different materials (e.g., different types of *sukumo*) or different preparation procedures. With the media used in this study, the isolation of even more species can be facilitated than via the procedures that use conventional media.

ADDITIONAL INDIGO-REDUCING BACTERIA ISOLATED USING NOVEL MEDIA

During the evaluation of the transitions of the microbiota and the trials aimed at isolation from new media, several novel strains were isolated and identified as novel taxa, including two new species belonging to new genera. These species likely appear late in the stable phase of indigo fermentation, approximately 5 months after the initiation of fermentation. Therefore, it is thought that some of these bacteria can be isolated from an indigo fermentation mixture older than 5 months using only specific media. On the other hand, some species of indigo-reducing bacteria can be isolated from indigo fermentation mixtures older than 5 months using ordinary media.

Strains In-9^T and D2-7 were isolated from 11-month-old fermentation fluid obtained from the craft center in Date City, Hokkaido, Japan (Okamoto et al., 2017). The obtained samples were inoculated onto indigo-carmine-containing conventional medium. The phylogenetic tree constructed from the sequences of these strains and those of related taxa suggested that strains In-9^T and D2-7 occupied distinct positions among the members of the genus *Bacillus* (strain In-9^T in **Figure 4**). In addition to their distinct positions in the phylogenetic tree, these strains could be discriminated from neighboring species or genera based on spore morphology and molecular species of menaquinone. Therefore, these strains represent a novel species within a novel genus, for which the name *Polygonibacillus indicireducens* gen. nov., sp. nov. was proposed (Hirota et al., 2016b; **Table 1**). This species was frequently detected in 11-month-old samples from the evaluated batch. Therefore, this species can be detected during only a limited period and only in certain batches. However, there is a possibility that this species contributes to indigo reduction as a minor constituent of the microbiota in various fermentation batches and various fermentation periods.

An aliquot of the sample was inoculated onto media containing *sukumo* hydrolysate and incubated under anaerobic conditions as described above. Thus, strains Bps-1^T, Bps-2, and Bps-3 were isolated during a stable fermentation period from indigo fermentation fluid obtained from the indigo-dyeing craft center in Date City, Hokkaido, Japan. The phylogenetic tree constructed from the sequences of these strains and those of related taxa suggested that strains Bps-1^T, Bps-2, and Bps-3 occupied distinct positions, based on 16S rRNA gene sequences, among the members of the genus *Bacillus* (strain Bps-1^T in **Figure 4**). In addition to their distinct position in the phylogenetic tree, these strains can be discriminated from neighboring species or genera based on their flagella and spore morphologies. Therefore, these strains represent a novel species within a novel genus, for which the name *P. indicireducens* gen. nov., sp. nov. was proposed (Hirota et al., 2017; **Table 1**). Although they were isolated from media containing *sukumo* hydrolysate, these strains do not require *sukumo* hydrolysate for growth. It is possible that components of *sukumo* hydrolysate support colony formation of these strains from the sample contained numerous bacteria.

During the above-described trials aimed at the isolation of indigo-reducing bacteria using various media, 13 strains were isolated (strain Bf-1^T in **Figure 4**). These strains were isolated from all the media used in the study (Nishita et al., 2017). Therefore, conventional media are applicable for the isolation of such strains. Among the 13 isolated strains, three strains, namely, Bf-1^T, Bf-2, and Bf-4, were selected for taxonomic evaluation. Based on the polyphasic study, including phenotypic, chemotaxonomic, and genetic characterizations, these isolates represented a novel species, for which the name *Bacillus fermenti* sp. nov. was proposed (Hirota et al., 2018; **Table 1**). Furthermore, the isolates (obligate alkaliphiles) were clearly differentiated from other neighbors (neutralophilic or alkali-tolerant bacteria) in the maximum-likelihood phylogenetic tree derived from 16S rRNA gene sequences (**Figure 4**). The divergent lineage of the phylogenetic groups may reflect the selective pressures placed upon the organisms by the environmental conditions that these organisms have encountered, resulting in the evolution of an obligate alkaliphile that cannot grow at neutral pH. These findings suggest that these isolates evolved in a niche with a continuous high-alkaline environment, which would eliminate neutralophilic or alkali-tolerant bacteria.

CONCLUSION AND PERSPECTIVES

Rapid initiation of indigo reduction is an important concern in indigo fermentation using *sukumo*. If the desired transitional change in the microbiota occurs, the redox potential decreases rapidly on the 2nd day from the initiation of fermentation. On the 4th day, the abundances of obligately aerobic bacteria dramatically decrease, and aerotolerant and obligately anaerobic bacteria dominate the system, resulting in initiation of the staining of the soaked textile. If appropriate bacteria exist in the *sukumo*, the abundance of these desirable microorganisms increase under anaerobic alkaline conditions with appropriate materials and preparation and maintenance procedures. The transition of the microbiota is faster during the early stage of fermentation than during the stationary stage. This rate may be associated with the adaptability and stability of the microbiota at the early and stationary stages, respectively.

At the beginning of this study, we did not assume that many kinds of indigo-reducing bacteria existed in indigo fermentation fluid. In addition, we assumed that the microbiota profiles did not differ much among the various stages of indigo fermentation. By analysis of the transition of the microbiota, we found that indigo reduction can be performed by different microbial communities. In fact, it was observed that many species of bacteria could reduce indigo. Therefore, microbial communities with various profiles

may exhibit indigo-reducing activity. Substitution of indigo-reducing bacteria may be an important factor for maintaining the indigo-reducing ability for an extended period.

Electron mediators such as quinone, which originate from plants or are produced by microorganisms, may exist in indigo fermentation fluid, especially in woad vat fermentation. However, there may be bacteria that can transfer electrons to extracellular substances without using electron mediators. There are reported cases of such bacteria (Logan, 2009), and these cases fall under three categories. For the first type of bacteria, the final electron acceptors are metal compounds instead of oxygen, and this process is called metal respiration. Electrons that are used for the production of ATP are discarded to extracellular metals, which act as electron sinks. The second type are bacteria that produce their own extracellular electron shuttles. Because the amounts of electron shuttle produced by most of these cases were not high enough for easy detection, there are few examples of such bacteria. There are examples of bacteria that produce flavin and extracellular cytochrome (Marsili et al., 2008; Smith et al., 2014). The third type is bacteria that produce electrically conductive pilus-like "nanowires" that extend outward from the electron-donating bacterial cells. This phenomenon has been reported in the case of *Shewanella oneidensis* (Gorby et al., 2006). It is considered that the mechanism of indigo reduction by indigo-reducing bacteria involves electrons, as byproducts of metabolism, being discarded by any of the methods described above under alkaline anaerobic condition.

There have not been many analyses of the microbiota present in natural fermentation systems. Traditional fermented foods include many examples of natural fermentation. However, fermentation in most of these cases occurs in acidic and salty environments, and it is difficult to manage the microbiota appropriately in nonselective conditions (i.e., conventional neutral conditions). There are few available examples of fermentation in alkaline environments. In indigo fermentation, high pH values and anaerobic conditions exert selective pressures on the microorganisms. This fermentation lasts for 6 months under conditions in which there are many chances for contamination. In addition, the result of indigo fermentation is distinct, and the properties of these fermentation systems can be easily and rapidly tested. The identified microbiota is not very complicated compared with those identified in conventional, natural, neutral environments, such as soil. Therefore, we conclude that indigo fermentation systems are suitable models for unsterilized and long-term natural fermentation. Elucidation of the mechanisms by which the microbiota exhibits resilience and persistence and of the interactions between constituent microorganisms in the microbiota will help improve not only the management of indigo fermentation but also maintenance methods for other anaerobic alkaline environments, such as Fe^{3+} reaction systems (Hobbie et al., 2012; Fuller et al., 2014) for producing electricity or halophilic alkaline natural fermentation systems for foods (Ouoba et al., 2010; Roth et al., 2011; Lucena-Padrós and Ruiz-Baba, 2016).

AUTHOR CONTRIBUTIONS

HM and IY designed the research. KA, KH, TO, and ZT performed the research. IY analyzed the data and wrote the paper.

FUNDING

This work was supported by the Japan Society for the Promotion of Science with a Grant-in-Aid for Science Research (grant numbers 23570128 and 16K07684).

ACKNOWLEDGMENTS

We thank Ms. N. Ushijima (Graduate School of Dentistry, Hokkaido University) for electron microscopy of the negative stain of isolates.

REFERENCES

Aino, K., Narihiro, T., Minamida, K., Kamagata, Y., Yoshimune, K., and Yumoto, I. (2011). Bacterial community characterization and dynamics of indigo fermentation. *FEMS Microbiol. Ecol.* 74, 174–183. doi: 10.1111/j.1574-6941.2010.00946.x

Aird, D., Ross, M. G., Chen, W. S., Danielsson, M., Fennell, T., Russ, C., et al. (2011). Analyzing and minimizing PCR amplification bias in Illumina sequencing libraries. *Genome Biol.* 12:R18. doi: 10.1186/gb-2011-12-2-r18

Balfour-Paul, J. (2000). *Indigo*. London: British Museum Press, 272.

Bechtold, T., Burtscher, E., Amann, A., and Bobleter, O. (1993). Alkali-stable iron complexes as mediators for the electrochemical reduction of dispersed organic dyestuff. *J. Chem. Soc. Faraday Trans.* 89, 2451–2456. doi: 10.1039/ft9938902451

Blum, J. S., Bindi, A. B., Buzzelli, J., Stolz, J. F., and Oremland, R. S. (1998). *Bacillus arsenicoselenatis*, sp. nov., and *Bacillus selenitireducens*, sp. nov.: two haloalkaliphiles from Mono Lake, California that respire oxyanions of selenium and arsenic. *Arch. Microbiol.* 171, 19–30. doi: 10.1007/s002030050673

Božič, M., and Kokol, V. (2008). Ecological alternatives to the reduction and oxidation processes in dyeing with vat and sulphur dyes. *Dyes Pigm.* 76, 299–309. doi: 10.1016/j.dyepig.2006.05.041

Cardon, D. (2007). *Natural Dyes Sources, Tradition, Technology and Science*. London: Archetype Publication, 778.

Chatterjee, S., Mondal, A. K., Begum, N. A., Roychoudhury, S., and Das, J. (1998). Ordered cloned DNA map of the genome of *Vibrio cholerae* 569B and localization of genetic markers. *J. Bacteriol.* 180, 901–908.

Clark, R. J. H., Cooksey, C. J., Daniel, M. A. M., and Withnall, R. (1993). Indigo, woad, and Tyrian Purple: important vat dyes from antiquity to the present. *Endeavour* 17, 191–199. doi: 10.1016/0160-9327(93)90062-8

Clark, W. M. (1960). *Oxidation–Reduction Potentials of Organic Systems*. Baltimore, MD: Williams and Wilkins, 588.

Compton, R. G., Perkin, S. J., Gamblin, D. P., Davis, J., Marken, F., Padden, A. N., et al. (2000). *Clostridium isatidis* colonized carbon electrodes: voltammetric evidence for direct solid state redox processes. *New J. Chem.* 24, 179–181. doi: 10.1039/a909172f

Fuller, S. J., McMillan, D. G. G., Renz, M. B., Schmidt, M., Burke, I. T., and Stewart, D. I. (2014). Extracellular electron transport-mediated Fe3+ reduction by a community of alkaliphilic bacteria that use flavins as electron shuttle. *Appl. Environ. Microbiol.* 80, 128–137. doi: 10.1128/AEM.02282-13

Gilbert, K. G., and Cooke, D. T. (2001). Dyes from plants: past usage, present understanding and potential. *Plant Growth Regul.* 34, 57–69. doi: 10.1023/A:1013374618870

Gorby, Y. A., Yanina, S., McLean, J. S., Rosso, K. M., Moyles, D., Dohnalkova, A., et al. (2006). Electrically conductive bacterial nanowires produced by *Shewanella oneidensis* strain MR-1 and other microorganisms. *Proc. Natl. Acad. Sci. U.S.A.* 103, 11358–11363. doi: 10.1073/pnas.0604517103

Gorlenko, V., Tsapin, A., Namsaraev, Z., Teal, T., Tourova, T., Engler, D., et al. (2004). *Anaerobranca californiensis* sp. nov., an anaerobic alkalithermophilic ferementative bacterium isolated from a hot spring on Mono Lake. *Int. J. Syst. Evol. Microbiol.* 54, 739–743. doi: 10.1099/ijs.0.02909-0

Guindon, S., and Gascuel, O. (2003). A simple, fast, and accurate algorithm to estimate large phylogenies by maximum likelihood. *Syst. Biol.* 52, 696–704. doi: 10.1080/10635150390235520

Hirota, K., Aino, K., Nodasaka, Y., Morita, N., and Yumoto, I. (2013a). *Amphibacillus indicireducens* sp. nov., an alkaliphile that reduces an indigo dye. *Int. J. Syst. Evol. Microbiol.* 63, 464–469. doi: 10.1099/ijs.0.037622-0

Hirota, K., Aino, K., Nodasaka, Y., and Yumoto, I. (2013b). *Oceanobacillus indicireducens* sp. nov., a facultatively alkaliphile that reduces an indigo dye. *Int. J. Syst. Evol. Microbiol.* 63, 1437–1442. doi: 10.1099/ijs.0.034579-0

Hirota, K., Aino, K., and Yumoto, I. (2013c). *Amphibacillus iburiensis* sp. nov., an alkaliphile that reduces an indigo dye. *Int. J. Syst. Evol. Microbiol.* 63, 4303–4308. doi: 10.1099/ijs.0.048009-0

Hirota, K., Aino, K., and Yumoto, I. (2016a). *Fermentibacillus polygoni* gen. nov., sp. nov., an alkaliphile that reduces indigo dye. *Int. J. Syst. Evol. Microbiol.* 66, 2247–2253. doi: 10.1099/ijsem.0.001015

Hirota, K., Nishita, M., Matsuyama, H., and Yumoto, I. (2017). *Paralkalibacillus indicireducens* gen. nov., sp. nov., an indigo-reducing obligate alkaliphile isolated from indigo fermentation liquor for dyeing. *Int. J. Syst. Evol. Microbiol.* 67, 4050–4056. doi: 10.1099/ijsem.0.002248

Hirota, K., Nishita, M., Tu, Z., Matsuyama, Y., and Yumoto, I. (2018). *Bacillus fermenti* sp. nov., an indigo-reducing obligate alkaliphile isolated from indigo fermentation liquor for dyeing. *Int. J. Syst. Evol. Microbiol.* 68, 1123–1129. doi: 10.1099/ijsem.0.002636

Hirota, K., Okamoto, T., Matsuyama, H., and Yumoto, I. (2016b). *Polygonibacillus indicireducens* gen. nov., sp. nov., an indigo-reducing and obligate alkaliphile isolated from indigo fermentation liquor for dyeing. *Int. J. Syst. Evol. Microbiol.* 66, 4650–4656. doi: 10.1099/ijsem.0.001405

Hobbie, S. N., Li, X., Basen, M., Stingl, U., and Brune, A. (2012). Humic substance-mediated Fe (III) reduction by a fermenting *Bacillus* strain from the alkaline gut of humus-feeding scarab beetle larva. *Syst. Appl. Microbiol.* 35, 226–232. doi: 10.1016/j.syapm.2012.03.003

Hurry, J. G. (1930). *The Woad Plant and its Dye*. London: Academic Press, 356.

Janssen, P. H., and Yates, P. S. (2002). Improved culturability of soil bacteria and isolation in pure cultures representative of the phylum-level diversity of soil bacteria. *Appl. Environ. Microbiol.* 68, 2392–2396.

Kimura, M. (1980). A simple method for estimating evolutionary rates of base substitutions through comparative studies of nucleotide sequences. *J. Mol. Evol.* 16, 111–120. doi: 10.1007/BF01731581

Klindworth, A., Pruesse, E., Schweer, T., Peplies, J., Quast, C., Horn, M., et al. (2012). Evaluation of general 16S ribosomal RNA gene PCR primers for classical and next-generation sequencing-based diversity studies. *Nucleic Acids Res.* 41:e1. doi: 10.1093/nar/gks808

Kumar, S., Stecher, G., and Tamura, K. (2016). MEGA7: molecular evolutionary genetics analysis version 7.0 for bigger datasets. *Mol. Biol. Evol.* 33, 1870–1874. doi: 10.1093/molbev/msw054

Lee, C. K., Herbold, C. W., Polson, S. W., Wommack, K. E., Williamson, S. J., MaDonald, I. R., et al. (2012). Groundtruthing next-gen sequencing for microbial ecology-biases and errors in community structure estimates from PCR amplicon pyrosequencing. *PLoS One* 7:e44224. doi: 10.1371/journal.pone.0044224

Logan, B. E. (2009). Exoelectrogenic bacteria that power microbial fuel cells. *Nat. Rev. Microbiol.* 7, 375–381. doi: 10.1038/nrmicro2113

Lucena-Padrós, H., and Ruiz-Baba, J. L. (2016). Diversity and enumeration of halophilic and alkaliphilic bacteria in Spanish-style green table-olive fermentation. *Food Microbiol.* 53, 53–62. doi: 10.1016/j.fm.2015.09.006

Luo, C., Tsementzi, D., Kyrpides, N., Read, T., and Konstantinidis, K. T. (2012). Direct comparison of Illumina vs. Roche 454 sequencing technologies on the same microbial community DNA sample. *PLoS One* 7:e30087. doi: 10.1371/journal.pone.0030087

Ma, C., Zhuang, L., Zhou, S. G., Yang, G. Q., Yuan, Y., and Xu, R. X. (2012). Alkaline extracellular reduction: isolation and characterization of an alkaliphilic and halotolerant bacterium, *Bacillus pseudofirmus* MC02. *J. Appl. Microbiol.* 112, 883–891. doi: 10.1111/j.1365-2672.2012.05276.x

Marsili, E., Baron, D. B., Shikhare, I. D., Coursolle, D., Gralnick, J. A., and Bond, D. R. (2008). Shewanella secretes flavins that mediate extracellular electron transfer. *Proc. Natl. Acad. Sci. U.S.A.* 105, 3968–3973. doi: 10.1073/pnas.0710525105

Milanović, V., Oshimuni, A., Taccari, M., Garofalo, C., Butta, A., Clementi, F., et al. (2017). Insight into the bacterial diversity of fermentation woad dye vats as revealed by PCR-DGGE and pyrosequencing. *J. Ind. Microbiol. Biotechnol.* 44, 997–1004. doi: 10.1007/s10295-017-1921-4

Minami, Y., Takao, H., Kanafuji, T., Miura, K., Kondo, M., Harashima, I., et al. (1997). beta-Glucosidase in the indigo plant: intracellular localization and tissue specific expression in leaves. *Plant Cell Physiol.* 38, 1069–1074. doi: 10.1093/oxfordjournals.pcp.a029273

Nakajima, K., Hirota, K., Nodasaka, Y., and Yumoto, I. (2005). *Alkalibacterium iburiense* sp. nov., an obligate alkaliphile that reduces an indigo dye. *Int. J. Syst. Evol. Microbiol.* 55, 1525–1530. doi: 10.1099/ijs.0.63487-0

Nicholson, S. K., and John, P. (2005). The mechanism of bacterial indigo reduction. *Appl. Microbiol. Biotechnol.* 68, 117–123. doi: 10.1007/s00253-004-1839-4

Nii, O., Honda, K., and Oshima, T. (2006). Indigo reductase and method for producing the same. Japanese Patent No JP2006087422A. Chiyoda: Japanese Patent Office.

Nishita, M., Hirota, K., Matsuyama, H., and Yumoto, I. (2017). Development of media to accelerate the isolation of indigo-reducing bacteria, which are difficult to isolate using conventional media. *World J. Microbiol. Biotechnol.* 33:133. doi: 10.1007/s11274-017-2300-z

O'Donnell, J. L., Kelly, R. P., Lowell, N. C., and Port, J. A. (2016). Indexed PCR primers induce template-specific bias in large-scale DNA sequencing studies. *PLoS One* 11:e0148698. doi: 10.1371/journal.pone.0148698

Okamoto, T., Aino, K., Narihiro, T., Matsuyama, H., and Yumoto, I. (2017). Analysis of microbiota involved in the aged natural fermentation of indigo. *World J. Microbiol. Biotechnol.* 33:70. doi: 10.1007/s11274-017-2238-1

Ooi, T., Shibata, T., Sato, R., Ohno, H., Kinoshita, S., Thuoc, T. L., et al. (2007). An azoreductase, aerobic NADH-dependent flavoprotein discovered from *Bacillus* sp.: functional expression and enzymatic characterization. *Appl. Microbiol. Biotechnol.* 75, 377–386. doi: 10.1007/s00253-006-0836-1

Osimani, A., Aquilanti, L., Baldini, G., Silvestri, G., Butta, A., and Clementi, F. (2012). Implementation of a biotechnological process for vat dyeing with word. *J. Ind. Microbiol. Biotechnol.* 39, 1309–1319. doi: 10.1007/s10295-012-1139-4

Ouoba, L. I. I., Nyanga-Koumou, C. A. G., Parkouda, C., Sawadogo, H., Kobawila, S. C., Keleke, S., et al. (2010). Genotypic diversity of lactic acid bacteria isolated from African traditional alkaline-fermented foods. *J. Appl. Microbiol.* 108, 2019–2029. doi: 10.1111/j.1365-2672.2009.04603.x

Padden, A. N., Dillon, V. M., Edmonds, J., Collins, M. D., Alvarez, N., and John, P. (1998a). An indigo-reducing moderate thermophile from a woad vat, *Clostridium isatidis* sp. non. *Int. J. Syst. Bacteriol.* 49, 1025–1031.

Padden, A. N., Dillon, V. M., John, P., Edmonds, J., Collins, M. D., and Alvarez, N. (1998b). Clostridium used in medieval dyeing. *Nature* 396:225. doi: 10.1038/24290

Padden, A. N., John, P., Collins, M. D., Hutson, R., and Hall, A. R. (2000). Indigo-reducing *Clostridium isatidis* isolated from a variety of sources, including a tenth century Viking woad vat. *J. Archaeol. Sci.* 27, 953–956. doi: 10.1006/jasc.1999.0524

Park, S., Ryu, J.-Y., Seo, J., and Hur, H.-G. (2012). Isolation and characterization of alkaliphilic and thermotolerant bacteria that reduce insoluble indigo to soluble leuco-indigo from indigo dye vat. *J. Korean Soc. Appl. Biol. Chem.* 55, 83–88. doi: 10.1007/s13765-012-0014-3

Pinto, A. J., and Raskin, L. (2012). PCR biases distort bacterial and archaeal community structure in pyrosequencing datasets. *PLoS One* 7:e43093. doi: 10.1371/journal.pone.0043093

Pricelius, S., Held, C., Murkovic, M., Bozic, M., Kokol, V., Cavaco-Paulo, A., et al. (2007). Enzymatic reduction of azo and indigoid compounds. *Appl. Microbiol. Biotechnol.* 77, 321–327. doi: 10.1007/s00253-007-1165-8

Roth, E., Schwenniger, S. M., Eugster-Meier, E., and Lacroix, C. (2011). Facultative anaerobic halophilic and alkaliphilic bacteria isolated from a natural smear

ecosystem inhibit Listeria growth in early ripening stages. *Int. J. Food Microbiol.* 147, 26–32. doi: 10.1016/j.ijfoodmicro.2011.02.032

Smith, J. A., Tremblay, P. L., Shrestha, P. M., Snoeyenbos-West, O. L., Franks, A. E., Nevin, K. P., et al. (2014). Going wireless: Fe(III) oxide reduction without pili by *Geobacter sulfurreducens* strain JS-1. *Appl. Environ. Microbiol.* 80, 4331–4340. doi: 10.1128/AEM.01122-14

Song, J., Imanaka, H., Imamura, K., Kajitani, K., and Nakanishi, K. (2010). Development of a highly efficient indigo dyeing method using indicant with an immobilized β-glucosidase from *Aspergillus niger*. *J. Biosci. Bioeng.* 110, 281–287. doi: 10.1016/j.jbiosc.2010.03.010

Spanka, R., and Fritze, D. (1993). *Bacillus cohnii* sp. nov., a new obligately alkaliphilic oval-spore-forming Bacillus species with ornithine and aspartic acid instead of diaminopimeric acid in the cell wall. *Int. J. Syst. Bacteriol.* 43, 150–156. doi: 10.1099/00207713-43-1-150

Splitstoser, J. C., Dillehay, T. D., Wouters, J., and Claro, A. (2016). Early pre-Hispanic use of indigo blue in Peru. *Sci. Adv.* 2:e1501623. doi: 10.1126/sciadv.1501623

Suzuki, H., Abe, T., Doi, K., and Ohshima, T. (2018). Azoreductase from alkaliphilc *Bacillus* sp. AO1 catalyzes indigo reduction. *Appl. Microbiol. Biotechnol.* doi: 10.1007/s00253-018-9284-y [Epub ahead of print].

Takahara, Y., and Tanabe, O. (1960). Studies on the reduction of indigo in industrial fermentation vat (VII). *J. Ferment. Technol.* 38, 329–331.

Thompson, J. D., Higgins, D. G., and Gibson, T. J. (1994). CLUSTAL W: improving the sensitivity of progressive multiple sequence alignment through sequence weighting, position-specific gap penalties and weight matrix choice. *Nucleic Acid Res.* 22, 4673–4680. doi: 10.1093/nar/22.22.4673

Vickerstaff, T. (1954). *The Physical Chemistry of Dyeing*. London: Oliver, and Boyd, 416.

Wu, J. Y., Jiang, X. T., Jiang, Y. X., Lu, S. Y., Zou, F., and Zhou, H. W. (2012). Effects of polymerase, template dilution and cycle number on PCR based 16S rRNA diversity analysis using the deep sequencing method. *BMC Micobiol.* 10:255. doi: 10.1186/1471-2180-10-255

Yumoto, I., Hirota, K., and Nakajima, K. (2014). "The genus *Akalibacterium*," in *Lactic Acid Bacteria. Biodiversity and Taxonomy. West Sussex*, eds W. H. Holzapfel and B. J. B. Wood (Hoboken, NJ: Wiley-Blackwell), 147–158. doi: 10.1002/9781118655252.ch13

Yumoto, I., Hirota, K., Nodasaka, Y., Tokiwa, Y., and Nakajima, K. (2008). *Alkalibacterium indicireducens* sp. nov., an obligate alkaliphile that reduces an indigo dye. *Int. J. Syst. Evol. Microbial.* 58, 901–905. doi: 10.1099/ijs.0.64995-0

Yumoto, I., Hirota, K., Nodasaka, Y., Yokota, Y., Hoshino, T., and Nakajima, K. (2004). *Alkalibacterium psychrotolerans* sp. nov., a psychrotolerant obligate alkaliphile that reduces an indigo dye. *Int. J. Syst. Evol. Microbiol.* 54, 2379–2383. doi: 10.1099/ijs.0.63130-0

Conflict of Interest Statement: The authors declare that the research was conducted in the absence of any commercial or financial relationships that could be construed as a potential conflict of interest.

frontiers in Microbiology

REVIEW
published: 02 October 2018
doi: 10.3389/fmicb.2018.02331

Formation of Proton Motive Force Under Low-Aeration Alkaline Conditions in Alkaliphilic Bacteria

*Toshihide Matsuno[1], Toshitaka Goto[2,3], Shinichi Ogami[2,3], Hajime Morimoto[1,4], Koji Yamazaki[5], Norio Inoue[6], Hidetoshi Matsuyama[4], Kazuaki Yoshimune[7] and Isao Yumoto[2,3]**

[1] Department of Chemistry and Biology, National Institute of Technology, Fukui College, Sabae, Japan, [2] Bioproduction Research Institute, National Institute of Advanced Industrial Science and Technology (AIST), Sapporo, Japan, [3] Graduate School of Agriculture, Hokkaido University, Sapporo, Japan, [4] Department of Bioscience and Technology, School of Biological Sciences and Engineering, Tokai University, Sapporo, Japan, [5] Division of Marine Life Science, Faculty of Fisheries Sciences, Hokkaido University, Hakodate, Japan, [6] Hakodate Junior College, Hakodate, Japan, [7] College of Industrial Technology, Nihon University, Narashino, Japan

In Mitchell's chemiosmotic theory, a proton (H^+) motive force across the membrane (Δp), generated by the respiratory chain, drives F_1F_O-ATPase for ATP production in various organisms. The bulk-base chemiosmotic theory cannot account for ATP production in alkaliphilic bacteria. However, alkaliphiles thrive in environments with a H^+ concentrations that are one-thousandth (ca. pH 10) the concentration required by neutralophiles. This situation is similar to the production of electricity by hydroelectric turbines under conditions of very limited water. Alkaliphiles manage their metabolism via various strategies involving the cell wall structure, solute transport systems and molecular mechanisms on the outer surface membrane. Our experimental results indicate that efficient ATP production in alkaliphilic *Bacillus* spp. is attributable to a high membrane electrical potential ($\Delta\Psi$) generated for an attractive force for H^+ on the outer surface membrane. In addition, the enhanced F_1F_O-ATPase driving force per H^+ is derived from the high $\Delta\Psi$. However, it is difficult to explain the reasons for high $\Delta\Psi$ formation based on the respiratory rate. The Donnan effect (which is observed when charged particles that are unable to pass through a semipermeable membrane create an uneven electrical charge) likely contributes to the formation of the high $\Delta\Psi$ because the intracellular negative ion capacities of alkaliphiles are much higher than those of neutralophiles. There are several variations in the adaptation to alkaline environments by bacteria. However, it could be difficult to utilize high $\Delta\Psi$ in the low aeration condition due to the low activity of respiration. To explain the efficient ATP production occurring in H^+-less and air-limited environments in alkaliphilic bacteria, we propose a cytochrome *c*-associated "H^+ capacitor mechanism" as an alkaline adaptation strategy. As an outer surface protein, cytochrome *c*-550 from *Bacillus clarkii* possesses an extra Asn-rich segment between the region anchored to the membrane and the main body of the cytochrome *c*. This structure may contribute to the formation of the proton-binding network to transfer H^+ at the outer surface membrane in obligate alkaliphiles. The H^+ capacitor mechanism is further enhanced under low-aeration conditions in both alkaliphilic *Bacillus* spp. and the Gram-negative alkaliphile *Pseudomonas alcaliphila*.

Keywords: alkaliphilic, bioenergetic mechanism, cytochrome *c*, membrane electrical potential, Donnan effect, proton condenser, *Bacillus*, *Pseudomonas*

OPEN ACCESS

Edited by:
Masahiro Ito,
Toyo University, Japan

Reviewed by:
Jun Liu,
Tianjin Institute of Industrial Biotechnology (CAS), China
Saori Kosono,
The University of Tokyo, Japan

****Correspondence:***
Isao Yumoto
i.yumoto@aist.go.jp

Specialty section:
This article was submitted to Extreme Microbiology, a section of the journal Frontiers in Microbiology

Received: *29 May 2018*
Accepted: *11 September 2018*
Published: *02 October 2018*

Citation:
Matsuno T, Goto T, Ogami S, Morimoto H, Yamazaki K, Inoue N, Matsuyama H, Yoshimune K and Yumoto I (2018) Formation of Proton Motive Force Under Low-Aeration Alkaline Conditions in Alkaliphilic Bacteria. Front. Microbiol. 9:2331. doi: 10.3389/fmicb.2018.02331

INTRODUCTION

Bacteria that thrive under extreme environmental conditions, such as low or high temperatures and high or low pH, are called extremophiles. Each extremophile possesses certain strategies for adaptation under different conditions. These complex strategies consist of environmental adaptation mechanisms, such as alterations in specific characteristics of enzymes and membranes. Although there is a common fundamental basis for extremophile metabolism, these organisms differ slightly in the characteristics of certain components necessary for environmental adaptation (e.g., modification of cell surface structures and protein characteristics and production of molecular chaperones).

Alkaliphiles are defined as microorganisms that exhibit better growth at pH $\geq$ 9 than at pH $<$ 9. Since Vedder (1934) isolated the obligate alkaliphile *Bacillus alcalophilus*, many alkaliphilic *Bacillus* strains have been isolated from common environments such as garden soil and horse manure in the search for enzymatic resources, as alkaliphilic *Bacillus* strains produce heat-stable enzymes (Horikoshi and Akiba, 1982; Horikoshi and Grant, 1998; Horikoshi, 2006, 2011). Although various strains have been isolated, until Nielsen et al. (1995) proposed nine new *Bacillus* spp., it was not known whether alkaliphilic bacteria comprise multiple species due to the lack of a molecular identification method concomitant with a gene sequence database. Since the discovery made by Nielsen et al. (1995) many additional alkaliphilic bacteria have been isolated and identified as new species. Related reports indicate that diverse alkaliphiles are distributed in a variety of environments, which may indicate the presence of numerous small alkaline niches [e.g., the termite gut (Thongaram et al., 2003)] and/or large high-pH environments (e.g., alkaline lakes). Alkaline environments have been present throughout Earth's history. Zavarzin (1993) hypothesized that modern soda lakes may represent a refuge for relict terrestrial communities from ancient continents of the Early Proterozoic Eon. In contrast, a leading hypothesis suggests that the origin of life can be track back to ocean-floor-based alkaline hydrothermal vents (Lane and Martin, 2012). Natural H^+ gradients across the membranes of iron monosulfide bubbles could lead to the formation of protocells (Russell and Hall, 1997).

The phylogenetic diversity and wide distribution of alkaliphiles on Earth indicates that the evolution of alkaliphiles is not a specific phenomenon but a common event in natural environments. Therefore, many variations in alkaline adaptation mechanisms should be present in alkaliphiles. The range of reported alkaline adaptation mechanisms has not been explained to date. However, diverse adaptation mechanisms involving secondary cell wall variations were reported by Aono and Horikoshi (1983), Aono et al. (1993,1995,1999). The formation of a negatively charged secondary cell wall results in the pH at the outer surface membrane being lower than the extracellular pH (i.e., medium pH) (Tsujii, 2002). The diversity of environmental adaptation mechanisms underlying the survival of numerous alkaliphiles of different taxa provides various possible explanations for the existence of life in alkaline environments. Alkaliphilic *Bacillus* spp. have an acidic secondary cell wall. *B. halodurans* C-125 produces an acidic secondary cell walls consisting of teichurono-peptide and teichuronic acid. In contrast, *B. pseudofirmus* OF4 cells produces the cell surface protein SlpA and polyglutamic acid (Gilmore et al., 2000). These structures attract H^+ and repel OH^-, and the structural functions of those components protects the intracellular metabolic pathways from severe extracellular environments. Although the acidic secondary cell wall is indispensable for alkaline adaptation in alkaliphilic *Bacillus* spp., the variations in the secondary cell wall structure, which are shared among alkaliphilic *Bacillus* spp., have not been elucidated to date.

Alkaline environments are not always favorable for alkaliphilic bacteria. Alkaliphilic *Bacillus* spp. have been reported to produce acid to reduce the pH when the ambient pH is too high for metabolism (Horikoshi, 2006). This acid production can often be observed even in media lacking sugars. In contrast, these bacteria create an alkaline environment when the ambient pH is too low for metabolism. These phenomena indicate that several alkaliphiles have the ability to increase the favorability of the ambient environment. *Amphibacillus iburiensis* is able to grow in broth medium adjusted to pH 11 prior to inoculation (Hirota et al., 2013). However, this bacterium exhibits distinct growth initiation at pH 9 after lowering the pH of the medium via acid production, as observed by monitoring the change in pH during incubation.

Alkaliphiles adapt to the environment by employing various combinations of mechanisms to adjust to alkaline conditions. Alkaliphilic *Bacillus* strains have been reported to adjust the intracellular pH to an appropriate level via the Na^+/H^+ antiporter, Na^+ channels or stator force generator that drives Na^+-dependent motility (Kitada et al., 1982; Ito et al., 2004a,b; Padan et al., 2005), which contribute to replace the H^+-potential base transport system with the Na^+-potential base transport system. Thus, the Na^+/H^+ antiporter and other Na^+ or K^+-related transport systems reduce the utilization of H^+ by transport systems, which is very important for alkaliphiles that thrive at one-thousandth the concentration of H^+ found under neutral conditions. In addition, the rotational torque of the flagella of alkaliphilic *Bacillus* strains is produced by the influx of Na^+ derived from the Na^+-base potential across the membrane (Ito et al., 2004a).

It is reasonable to consider that the entire solute transport system functions via the Na^+ potential across the membrane. However, the ATP synthase-based energy production system is derived from the H^+-base potential across the membrane (Dimroth and Cook, 2004), which may indicate localization of the H^+-base potential across the membrane in the vicinity of the respiratory chain in the horizontal direction. In addition, if H^+ is not attracted to the interface in the vicinity of the outer surface membrane, the H^+ concentration will be quite low. The H^+-base potential may also be present in the vicinity of the outer surface membrane in the perpendicular direction.

Alkaliphilic *Bacillus* spp. have been reported to exhibit higher membrane electrical potentials ($\Delta\Psi$) than neutralophilic *Bacillus* strains (Yumoto, 2003; Goto et al., 2005). However, the calculation of bulk-base parameters [$\Delta\Psi$ and transmembrane pH gradient (ΔpH)] for the Δp driving F_1F_o-ATPase does not account for ATP production because the high deficiency in ΔpH is not compensated by $\Delta\Psi$. We demonstrated the importance of

a large $\Delta\Psi$ in alkaliphiles by showing the contribution of $\Delta\Psi$ to the retention of H^+ in the vicinity of the outer surface of the membrane in the vertical direction and the contribution of efficient ATP production under conditions involving H^+ scarcity (Yoshimune et al., 2010). Furthermore, $\Delta\Psi$ ensures efficient ATP production to enhance the F_1F_o-ATPase driving force per H^+. In addition, structural and physicochemical mechanisms to retain H^+ at the outer surface of the membrane are indispensable. However, it could be difficult to utilize high $\Delta\Psi$ in the low aeration condition due to the low activity of respiratory system. In this context, we highlight "a high-potential H^+ capacitor mechanism" based on the existence of membrane-bound or periplasmic cytochrome *c* in alkaliphiles.

BACKGROUND ON THE GENERAL BIOENERGETICS AND GROWTH OF ALKALIPHILIC *Bacillus* spp.

According to Peter Mitchell's chemiosmotic theory (Mitchell, 1961), the Δp across the membrane that drives F_1F_o-ATPase to produce ATP consists of ΔpH (intracellular pH minus extracellular pH) and the difference in electrical potential across the membrane, i.e., $\Delta\Psi$ (intracellulary electronegative and extracellularly electropositive across the membrane). The Δp can be calculated by the following formula.

$$\Delta p = \Delta\Psi - Z\Delta pHZ = 2.3RT/F = ca.59\,mV(at25^{\circ}C) \quad (1)$$

R = gas constant (8.315 J mol^{-1}); T = absolute temperature (298 K = 25°C); F = Faraday constant (96.485 kj [v·mol]$^{-1}$).

The H^+ gradient is also utilized for other energy-requiring processes such as transmembrane solute transport and signaling. In general, the parameters Δp, $\Delta\Psi$, and ΔpH apply to the bulk-base. Although it is difficult to estimate the values of $\Delta\Psi$ and ΔpH based on the vicinity of the membrane surface, localization of these parameters in the vicinity of the membrane surface in both the horizontal and vertical directions should be considered, especially in the case of the outer surface membrane of alkaliphilic *Bacillus* spp. (Gennis, 2016; Sjöholm et al., 2017). These characteristics are common to biological energy production mechanisms. Alkaliphilic bacteria must possess distinctive characteristics at the outer surfaces of the membrane to effectively utilize existing stores of H^+ at the outer surface membranes.

Although bulk-base calculations cannot account for ATP production by alkaliphilic *Bacillus* spp. Due to the great hindrance conferred by negative ΔpH values, the growth of these bacteria is vigorous under alkaline conditions (Guffanti and Hicks, 1991). The growth features of facultative alkaliphilic *B. pseudofirmus* OF4 were estimated at a steady state under various pH-controlled culture conditions. Strain OF4 exhibits specific growth rates of 0.77 and 1.10 h^{-1} in media maintained at pH values of 7.5 and 10.6, respectively. We estimated the growth characteristics of the obligate alkaliphilic *B. clarkii* K24-1U in batch culture. Strain K24-1U exhibited more rapid growth (μ_{max} = 0.33 h^{-1}) than the neutralophilic *B. subtilis* IAM 1026 (μ_{max} = 0.26 h^{-1}) (Hijikata, 2004). These superior growth characteristics are attributable to vigorous ATP production. Thus, in alkaliphilic *Bacillus* spp., these growth characteristics are not accounted for by bulk-based bioenergetic parameters.

BACKGROUND ON PROTON BEHAVIOR AT THE OUTER SURFACE OF THE MEMBRANE

The zone formed in the vicinity of the outer surface of the membrane formed due to the presence of phosphate and carbonyl headgroups stabilizes excess hydrated H^+ relative to the bulk solution. However, the pH of the bulk phase at the outer side membrane in alkaliphiles is expected to be at least 2 units higher than that in neutralophiles. In addition, the rate of H^+ exchange between the deep interface zone in the vicinity of the outer surface membrane and the bulk phase in alkaliphiles may be greater than that in neutralophiles due to the large difference in pH between the deep interface zone and the bulk phase at the outer membrane (Mulkidjanian et al., 2006; Gennis, 2016). Therefore, it survival under proton-less conditions without specific alkaline adaptation mechanisms is difficult. Although many neutralophilic *Bacillus* spp. can grow at pH 9, most cannot grow well at pH 10, unlike alkaliphilic *Bacillus* spp.

The H^+ transfer mechanism on the outer surface of the membrane is dependent on the distance between the H^+-vent (e.g., a respiratory complex such as cytochrome *c* oxidase) and H^+-sink (e.g., F_1F_o-ATPase). Sjöholm et al. (2017) investigated the distance effect between the terminal oxidase, cytochrome bo_3 and F_1F_o-ATPase by reconstituting these proteins in a vesicle and measuring ATP synthesis activity. An even shorter distance between the H^+-vent and H^+-sink than that observed in neutralophiles was expected to be favorable in alkaliphiles. A high cytochrome content has been reported in alkaliphilic *Bacillus* spp. (Lewis et al., 1980; Guffanti et al., 1986; Yumoto et al., 1997; Goto et al., 2005). This feature will relate to H^+ behavior at the outer surface membrane.

PROTON BEHAVIOR AT THE OUTER SURFACE MEMBRANE IN ALKALIPHILES

It is considered that the H^+ concentration at the outer surface membrane in alkaliphiles is lower than that in neutralophiles due to the low background H^+ concentration in alkaliphiles. In addition, the rate constant of H^+ exchange between the deep interface zone of the outer surface membrane and the adjacent bulk zone may be higher in alkaliphiles than in neutralophiles due to the larger pH gap between the deep interface zone of the outer surface membrane and the adjacent bulk zone in alkaliphiles than that in neutralophiles. In addition to the membrane-surface-based ΔpH (ΔpH values) (Xiong et al., 2010), membrane-surface-based $\Delta\Psi$ values may also exist (Lyu and Lazár, 2017). In addition, proteins present on the outer surface membrane may play a role in the retention of H^+ in this region. A comparative experiment to detect H^+ in the bulk

phase during respiration in the obligate alkaliphilic *B. clarkii* K24-1U and the neutralophilic *B. subtilis* IAM 1026 was performed by monitoring the change in pH (Yoshimune et al., 2010). Whole-cell suspensions of both *Bacillus* stains consumed oxygen immediately after the introduction of oxygen, and a lag period was observed for H^+ extrusion by the respiratory chain into the bulk phase. The lag period for alkaliphilic *B. clarkii* K24-1U was significantly longer at pH 10 than at other pH values and significantly longer than those for *B. subtilis* at various pH values. This observation may indicate that H^+ was transferred into the bulk phase after all the H^+ retention sites were occupied by H^+ translocated via respiratory complexes. The introduction of monensin, which exchanges extracellular H^+ for intracellular Na^+, similar to a Na^+/H^+ antiporter, resulted in a prolonged lag period for H^+ extrusion to the bulk, indicating that the H^+ present at H^+ retention sites on the outer surface membrane translocated to the intracellular side via countertransport with the Na^+ present in the intracellular space. In contrast, when a $\Delta\Psi$-disrupting agent such as valinomycin or ETH-157 was introduced, the lag phase disappeared. These experiments reveal the meaning of $\Delta\Psi$ values in alkaliphilic *Bacillus* spp. are larger than those in neutralophilic *Bacillus* spp.

EFFICIENCY OF H^+ TRANSLOCATION FROM THE OUTER SURFACE MEMBRANE TO F_1F_o-ATPase

The growth of alkaliphilic *Bacillus* spp. is much faster than that of neutralophilic *Bacillus* spp. as described above, which may be attributable to the higher ATP production rate in alkaliphilic *Bacillus* spp. than that in neutralophilic *Bacillus* spp. The ATP production rate was estimated using the obligate alkaliphile *B. clarkii* DSM 8720^T and neutralophilic *B. subtilis* IAM 1026 (Hirabayashi et al., 2012). *B. clarkii* DSM 8720^T produced 7.2 nmol ATP·mg $protein^{-1}\cdot min^{-1}$ (endogenous substrate) at pH 10, which was comparable to the amount produced by *B. pseudofirmus* OF4 (6.6 ± 3.9 nmol ATP·mg $protein^{-1}\cdot min^{-1}$ [starved cells re-energized with malate]) at pH 10.5 (Guffanti and Krulwich, 1992). In contrast, *B. subtilis* IAM 1026 produced 0.96 nmol ATP·mg $protein^{-1}\cdot min^{-1}$ at pH 7. Thus, the ATP production rate in alkaliphilic *Bacillus* spp. was much higher (6.9−7.5 times) than that in neutralophilic *B. subtilis*.

If rapid ATP production by alkaliphilic *Bacillus* spp. was attributable to rapid H^+ translocation across the membrane by respiratory complexes, then these bacteria would exhibit a rapid O_2 consumption and/or high efficiency of H^+ translocation across the membrane per molecule of O_2 consumed. However, the oxygen consumption rate of *B. clarkii* DSM 8720^T cells was 0.19 μmol $O_2\cdot min^{-1}\cdot$mg cell $protein^{-1}$ at pH 10. Although these data were obtained with an endogenous substrate, the results were comparable to those obtained using malate as the substrate in other alkaliphilic *Bacillus* spp. (Lewis et al., 1980; Guffanti et al., 1986; Aono et al., 1996). The oxygen consumption rate of *B. subtilis* IAM 1026 was 0.50 μmol $O_2\cdot min^{-1}\cdot$mg cell $protein^{-1}$ at pH 7. Thus, the oxygen consumption rate of whole *B. subtilis* IAM 1026 cells at pH 7 was 2.6 times higher than that of *B. clarkii* DSM 8720^T at pH 10. Unlike the theoretical H^+/O ratio calculated for *Bacillus* spp. (complex III, 4 plus complex IV, 2 = 6) (Sone et al., 1999), the H^+/O ratio in *B. clarkii* DSM 8720^T was 3.6 at pH 10. In contrast, the H^+/O ratio in *B. subtilis* IAM 1026 was 5.3. The H^+/O ratio in *B. subtilis* IAM 1026 was 1.5 times higher than that in *B. clarkii* DSM 8720^T (Goto et al., 2016). Considering both the O_2 consumption rate and the H^+/O ratio in both strains, the H^+ translocation rate in *B. subtilis* IAM 1026 (pH 7) was 3.9 times higher than that in *B. clarkii* DSM 8720^T (pH 10). This finding indicated that the higher ATP production rate in neutralophilic *B. subtilis* IAM 1026 than that in alkaliphilic *B. clarkii* DSM 8720^T cannot be accounted for by the rate of H^+ translocation across the membrane via the respiratory chain. The large differences in ATP production rates between *B. clarkii* DSM 8720^T and *B. subtilis* IAM 1026 are attributable to differences in the F_1F_o-ATPase driving force per H^+, which may arise from differences in $\Delta\Psi$. It is difficult to translocate H^+ from the intracellular to the extracellular side of the membrane because $\Delta\Psi$ hinders translocation in that direction by electrical attraction. However, once translocated to the outer surface of the membrane, H^+ has high potential to drive F_1F_o-ATPase. It has been reported that the $\Delta\Psi$ in alkaliphilic *Bacillus* spp. is larger than that in neutralophilic *Bacillus* spp. (Hoffmann and Dimroth, 1991; Krulwich, 1995; Yumoto, 2002; Goto et al., 2005; Hirabayashi et al., 2012). The same phenomenon has been observed in the alkaliphilic *B. clarkii* DSM 8720^T and neutralophilic *B. subtilis* IAM 1026. The $\Delta\Psi$ values of *B. clarkii* DSM 8720^T and *B. subtilis* IAM 1026 were −192 mV at pH 10 and −122 mV at pH 7, respectively (Goto et al., 2016).

OCCURRENCE OF $\Delta\Psi$

As described above, $\Delta\Psi$ is very important for attracting H^+, which translocates via the respiratory chain to the outer surface membrane. Generally, the $\Delta\Psi$ across the membrane is generated by translocation of positively charged H^+ from the intracellular to the extracellular region across the membrane. However, the larger $\Delta\Psi$ in alkaliphilic *Bacillus* spp. than that in neutralophilic *Bacillus* spp. cannot be accounted for by the rate of H^+ translocation. The large $\Delta\Psi$ values of alkaliphilic *Bacillus* spp. may be attributed to the production of high Donnan potentials (Donnan, 1924). The Donnan effect is observed in the presence of membrane-impermeable charged molecules on only one side of the membrane. If a membrane-impermeable negatively charged molecules are present only on the intracellular side of the membrane, these molecules contribute to the formation of the $\Delta\Psi$. To estimate the contribution of the Donnan effect to the large $\Delta\Psi$ in alkaliphilic *Bacillus* spp., intracellular negative ion capacity was estimated in the obligate alkaliphilic *B. clarkii* DSM 8720^T and facultative alkaliphilic *B. cohnii* YN-2000 and compared to that of the neutralophilic *B. subtilis* IAM 1026. To estimate the intracellular negative ion capacity, a cell extract containing inside-out membrane vesicles was prepared and titrated using the positively charged substance clupein sulfate.

Negative ion capacity is the amount of negative surface charge of substances in a solution (substances in the intracellular fraction of bacterial cells in this study) estimated by the colloid titration method. This method is one procedure by which the net charge density of surfaces, polyelectrolytes levels, and charge demand of colloidal materials in a solution may be estimated. The measured parameter is the capacity of the mixture to adsorb a polyelectrolyte with the opposite net charge. The intracellular negative ion capacity in alkaliphilic *Bacillus* spp. increased with increasing pH in the range of pH 6−8, whereas the intracellular negative ion capacity of neutralophilic *B. subtilis* IAM 1026 changed very little within this pH range. To understand the corresponding negative ion capacity when alkaliphilic *Bacillus* spp. were grown under alkaline conditions, the intracellular pH of the alkaliphilic strains was estimated at an extracellular pH of 10 (Goto et al., 2016). The intercellular pH of the alkaliphilic *Bacillus* spp. *B. clarkii* DSM 8720^{T} and *B. cohnii* YN-2000 was 8.1, which is comparable to values reported previously using other alkaliphilic *Bacillus* spp. (Guffanti et al., 1986; Guffanti and Hicks, 1991). At this intracellular pH, the negative ion capacities of *B. clarkii* DSM 8720^{T} and *B. cohnii* YN-2000 were 2.9 and 3.3 ($\times 10^{6}$ eq·mg protein^{-1}), respectively. The intracellular pH of neutralophilic *B. subtilis* IAM 1026 was 6.7 when the extracellular pH was 7. At this intracellular pH, the negative ion capacity of *B. subtilis* IAM 1026 was 0.7 ($\times 10^{6}$ eqmg protein^{-1}). This finding indicates that alkaliphilic *Bacillus* spp. possess a much higher intracellular negative ion capacity than neutralophilic *B. subtilis*. This high intracellular negative ion capacity contributes to the intrinsic $\Delta\Psi$. There may be questions regarding the existence of such a high intracellular negative ion capacity. One explanation is that the intracellularly expressed acidic proteins in alkaliphilic *Bacillus* spp. are negatively charged at slightly higher intercellular pH values (ca. pH 8) than those in neutralophiles (pH 6−7). Whole-genome analyses have been performed previously in alkaliphilic *Bacillus* spp. as well as neutralophilic *Bacillus* spp., and Janto et al. (2011) estimated the average p*I* values of proteins localized in intracellular and extracellular spaces, the cell wall and the membrane. Despite a tendency toward a high frequency of acidic proteins in the cell wall and extracellular proteins in alkaliphiles, the obligate alkaliphile *B. selenitireducens* ML10 possesses much higher levels of low p*I* proteins than neutralophiles. The combination of the acidic nature of the intracellular side chains of acidic membrane proteins and intercellular acidic proteins is predicted to contribute to the high negative ion capacity in alkaliphilic *Bacillus* spp.

CYTOCHROMES *c* FROM VARIOUS *Bacillus* spp. AND RELATED TAXA

The primary role of cytochrome *c* is to transfer electrons between complex III (cytochrome bc_1 complex) and complex IV (cytochrome *c* oxidase) proteins. A typical class I cytochrome *c* possesses one low-spin heme *c* in the N-terminal region bound to the protein by two thioether bonds with cysteine residues (Ambler, 1991). The proximal side and distal side of the iron ligands have a histidine residue and a methionine residue, respectively. The molecular weight of cytochrome *c* is approximately 8,000−14,000, and cytochrome *c* is a soluble protein in mitochondria and Gram-negative bacteria (Pettigrew and Moore, 1987; Moore and Pettigrew, 1990; Yamanaka, 1992; Brayer and Murphy, 1996).

Although numerous studies have assessed soluble cytochromes *c* from various sources, including mitochondria and Gram-negative bacteria, there have been limited examples of cytochrome *c* from Gram-positive bacteria. Despite having some outer surface membrane space, Gram-positive bacteria do not have outer membranes similar to those of Gram-negative bacteria. Therefore, Gram-positive bacteria do not possess a periplasmic space equivalent to that in Gram-negative bacteria. Consequently, all the cytochrome *c* in Gram-positive bacteria is membrane-bound. For example, *B. subtilis* possesses two types of membrane-bound cytochromes: *c*-550 and *c*-551. Cytochrome *c*-550 has a molecular mass of 13 kDa, with a membrane-anchored domain consisting of a single α-helical transmembrane segment of a hydrophobic polypeptide containing 30 amino acids (von Wachenfeldt and Hederstedt, 1990). The midpoint redox potential of cytochrome *c*-550 is +178 mV (von Wachenfeldt and Hederstedt, 1993). The other cytochrome *c*, namely, *c*-551, has a molecular mass of 10 kDa and binds to the membrane via a diacyl-glyceryl-cysteine moiety (Bengtsson et al., 1999). The midpoint redox potential of cytochrome *c*-551 is >100 mV. The functions of these two membrane-binding cytochromes *c* have not been characterized. However, it is expected that these proteins are involved in transport of electrons between complexes III and IV.

It has been reported that alkaliphilic *Bacillus* spp. contain higher amounts of membrane-bound cytochrome *c* than neutralophilic *B. subtilis* (Yumoto et al., 1997; Hijikata, 2004). In addition, the amount of membrane-bound cytochrome *c* is low in mutant strains that lack the ability to grow in alkaline media (Lewis et al., 1980). These findings suggest that membrane-bound cytochrome *c* in alkaliphiles may contribute to adaptation in alkaline environments. Cytochrome *c*-552 from *B. pseudofirmus* RAB was first purified and characterized from alkaliphilic *Bacillus* spp., exhibiting a molecular mass of 16.5 kDa and midpoint redox potential of +66 mV at pH 7, which decreases as the surrounding pH is increased (Davidson et al., 1988). This cytochrome *c* is normally membrane bound but was purified as a soluble protein. Cytochrome *c* proteins are predicted to play a role in electron transport between complexes III and IV.

The primary and 3D structures of cytochrome *c* were first studied in alkaliphilic *Bacillus*-related taxa using cytochrome *c*-553 purified from *Sporosarcina pasteurii* (formerly *B. pasteurii*) (Benini et al., 2000). Cytochrome *c*-553 has a low molecular mass of 9.6 kDa and a low midpoint redox potential (+47 mV) (Benini et al., 1998). The crystal structure of the protein exhibits a highly asymmetric charge distribution. Most of the charges are located on the side opposite to that exposed to the heme edge. The localization of charges is related to H^{+} transfer on the outer surface membrane. Analyses of the physicochemical parameters reveal that the heme solvent accessibility is correlated with entropy. This finding suggests a

direct link between the major determinant of the electrochemical potential (entropy) and a structural parameter (heme solvent exposure). The low midpoint redox potential of cytochrome *c*-553 could be explained by the decrease in reduction entropy via extrusion of water molecules from the protein hydration shell, affecting a large number of water molecules in the case of increased solvent accessibility, which occurs upon heme reduction.

The abundance of alkaliphilic *Bacillus* spp.-specific membrane-bound cytochrome *c* (Yumoto et al., 1991) has also been studied using the facultative alkaliphile *B. cohnii* YN-2000 (Yumoto et al., 2000). The abundance of membrane-bound cytochrome *c* is higher during growth at pH 10 than during growth at pH 7. In addition, cytochrome abundance is further increased under low-aeration conditions. Solubilized *B. cohnii* YN-2000 membranes prepared from cells grown at pH 10 using the detergent Triton X-100 contain larger amounts of cytochrome *c*-553 than solubilized membranes prepared with cells grown at pH 7. The native molecular mass of cytochrome *c*-553, which was solubilized by Triton X-100 in a buffer, was determined to be 127 kDa by gel filtration. The molecular mass of Triton X-100, which was used to solubilize cytochrome *c*-553 in solution is 90 kDa. Therefore, if cytochrome *c*-553 is contained in micelles of Triton X-100, the actual native molecular mass should be 37 kDa. The stoichiometry of cytochrome c-553 and Triton X-100 is considered to be 1:1. In contrast, the molecular mass of cytochrome *c*-553 was determined to be 10,500 Da by sodium dodecyl sulfate-polyacrylamide gel electrophoresis (SDS-PAGE). The results described above suggest that cytochrome *c*-553 forms a tetramer in its native form in solution or in the original membrane. Cytochrome *c*-553 from *B. cohnii* YN-2000 also exhibits a low midpoint redox potential of +87 mV at the pH values ranging from 6 to 8.

A novel type of cytochrome *c* oxidase, cytochrome aco_3, was purified and characterized from *B. cohnii* YN-2000 (Qureshi et al., 1990; Yumoto et al., 1993; Denda et al., 2001). Cytochrome *c*-533 can react with cytochrome aco_3, and the reaction is greatly enhanced in the presence of the positively charged substance poly-L-lysine, which may accelerate binding to two negatively charged molecules: cytochrome *c*-553 and cytochrome aco_3. Although cytochrome aco_3 was present in equal amounts in cells grown at pH 10 and pH 7, the cytochrome *c*-553 content was higher in cells grown at pH 10 than in those grown at pH 7. The midpoint redox potential of the attached cytochrome *c* was +95 mV at pH 7 (Orii et al., 1991). In contrast, cytochrome *a* exhibited two forms with midpoint redox potentials of +250 mV and +323 mV at pH 7 (Orii et al., 1991). A stopped-flow study on cytochrome aco_3 showed that the cytochrome *a* component exhibited the highest affinity for electrons and only a minimal contribution to O_2 reduction among the involved redox components. Therefore, membrane-bound cytochrome *c*-553 may directly react not only with cytochrome *c* in cytochrome aco_3 but also with the cytochrome *a* moiety in cytochrome aco_3. During electron flow from cytochrome *c*-553 or cytochrome *c* to cytochrome *a* in cytochrome aco_3, there is a large midpoint redox potential difference between each component. This significant difference is necessary for electron flow between each cytochrome *c* and cytochrome *a* in cytochrome aco_3 to overcome the large $\Delta\Psi$ (Yumoto et al., 1993). Therefore, the large difference in redox potential between the outer surface redox components and intramembrane redox components sustains electron transfer in the respiratory system in alkaliphilic *Bacillus* spp. In summary, this large difference in midpoint redox potential may be necessary for the generation of produce the large energy potential required for the translocation of intracellular H^+ to overcome the hindrance conferred by the high $\Delta\Psi$ and to retain H^+ on the intracellular side of the membrane.

MEMBRANE-BOUND CYTOCHROME *c*-550 FROM THE OBLIGATE ALKALIPHILE *Bacillus clarkii* K24-1U

A previous study suggested that cytochrome *c* has an important role in the adaptation to alkaline environments based on its abundance (Lewis et al., 1980; Guffanti et al., 1986; Yumoto et al., 1991, 1997). In addition, cytochrome *c* is likely located at the outer surface membrane and associated with H^+ transfer in the vicinity of the membrane. Therefore, we attempted to elucidate the precise structure of membrane-bound cytochrome *c* in alkaliphilic *Bacillus* spp. An experiment was performed to isolate intact protein from the obligate alkaliphile *B. clarkii* K24-1U. *Bacillus* spp. generally exhibit strong protease activity, making it difficult to isolate intact cytochrome *c* from their cells. This strong protease activity often causes isolated cytochrome *c* to exhibit an anchor-less, soluble protein. First, an attempt was made to isolate obligate alkaliphilic *Bacillus* spp. that exhibit low protease activity. Screening was performed using soil samples from approximately 10 sites in the Hokkaido region of Japan. One strain, K24-1U, isolated from Yuubari in Hokkaido Japan (43°04′ N, 141°58′ E), was found to be an obligate alkaliphile that exhibited very weak protease activity. The cytochrome *c*-550 gene sequence was determined and cloned, and the protein was purified and characterized (Ogami et al., 2009). Purified cytochrome *c*-550 was attached to a diacylglycerol-cysteine moiety. According to the analyzed gene sequence of cytochrome *c*-550, a signal peptide was present at the 5′ end of the gene. During the processing of mature cytochrome *c*-550, expressed cytochrome *c*-550 was translocated to the extracellular side of the membrane by the signal peptide. After the signal peptide was dissociated, the terminal cystatin was modified by attaching diacylglycerol and acetyl moieties. Cytochrome *c*-550 binds to fatty acids with carbon lengths of C_{15}, C_{16}, and C_{17} via glycerol-Cys_{18}. Although the length of the internal carbon chain is always C_{15}, the external chain length varies from C_{15}−C_{17}. The diacylglycerol moiety exhibits flexibility in its fatty acid molecular species. Therefore, if the expressed amount of cytochrome *c*-550 is dependent on the culture conditions, the fatty acid composition of the membrane may be minimally influenced.

The amino acid sequence of cytochrome *c*-550 was deduced from the gene sequence and aligned with the amino acid

sequences of cytochromes *c* from obligate and facultative alkaliphilic and neutralophilic *Bacillus* spp. and related taxa (Ogami et al., 2009). The results indicated that cytochrome *c*-550 contains only two basic amino acids, including histidine, in the heme *c* axial ligand. This scarcity of basic amino acids is more pronounced in obligate alkaliphilic *Bacillus* spp. than in facultative alkaliphiles and neutralophiles. Cytochrome *c*-550 contains the distinct amino acid sequence $Gly_{22}-Asn_{34}$, which is absent in facultative alkaliphilic and neutralophilic *Bacillus* spp. Thus, this sequence exists specifically for adaptation to alkaline environments. The amino acid sequence $Gly_{22}-Asn_{34}$ contains the H^+-transferable amino acids Asp and Glu at ratios of 3/13 and 1/13, respectively. The most prominent constituent of the $Gly_{22}-Asn_{34}$ sequence is Asn. Asn is present at a ratio of 7/17 in the $Asn_{21}-Asn_{37}$ region and may play an important role in the H^+ transfer network in the vicinity of the outer surface membrane.

Although Asn is theoretically H^+-transferable, there have been a few examples of the contribution of H^+ transfer processes due to weak hydrogen binding of the involved residues. Doukov et al. (2007) reported a very interesting hypothetical model of a hydrogen-bond network involving the H^+-transferable characteristics of Asn in the methyltetrahydrofolate (MTHF) corrinoid-iron-sulfur protein methyltransferase. The enzyme catalyzes the transfer of the methyl group of MTHF to cob(I)amide. This transfer reaction requires electrophilic activation of the methyl group of MTHF, which includes proton transfer to the N5 group of the pterin ring of MTHF. However, the resolved crystal structure of the methyltransferase revealed no obvious H^+ donor within hydrogen-bonding distance of the N5 position of MTHF. Combining kinetic and structural evidence, it was predicted that the extended hydrogen-bond network contributes to H^+ transfer to the N5 group of the pterin ring of MTHF. This extended hydrogen-bonding network contains an Asn, a conserved Asp and a water molecule. The evidence from this study suggests that even amino acid residues that exhibit weak hydrogen bonding, such as Asn can contribute to a cumulative hydrogen-bond network such that the overall effect on this transitional state is greater than expected based on the individual components alone. If this knowledge is applied to the $Asn_{21}-Asn_{37}$ region in cytochrome *c*-550 in *B. clarkii* K24-1U, then the region contributes to a cumulative hydrogen-bond network.

Based on the structures of other reported membrane-bound cytochromes *c* (David et al., 2000), it can be assumed that the region from Asn_{21} to Asn_{37} is located outside the α-helical domain from the N-terminus to the surrounding heme *c*. Thus, the region is located in the vicinity of the outer surface membrane. In addition, we attempted to elucidate the structure of cytochrome *c*-550 in *B. clarkii* K24-1U at the original membrane. Cytochrome *c*-550 with a membrane-anchoring diacylglycerol-cysteine moiety exhibits a tetrameric structure in the presence of the detergent Triton X-100. In addition, a mutant protein containing an N-terminal Cys_{18} to Met mutation in the mature protein also exists as a tetramer in the absence of Triton X-100. This finding indicates that cytochrome *c*-550 may exist as a tetramer on the outer surface membrane. This structure may be important not only for the regulation of the redox reaction involving four redox centers, as in the case of cytochrome c_3 in *Desulfovibrio gigas* (Messias et al., 2006) but also for the formation of the hydrogen-bond network.

H^+-COUPLING FUNCTION OF CYTOCHROME *c*

The above-described H^+/O ratio in *B. clarkii* DSM 8720^T (H^+/O ratio = 3.6) cannot be explained by the conventional understanding of the function of respiratory chain because the theoretical H^+/O ratio in *Bacillus* spp. should be 6 (complex III, 4 *plus* complex IV, 2 = 6) (Sone et al., 1999). The H^+/O ratio in *B. clarkii* DSM 8720^T, which is lower than the theoretical value, may be attributable to the high amount of energy required to translocate H^+ across the membrane under a larger $\Delta\Psi$ value than those of neutralophiles. Due to the low translocation of H^+ to the outer surface of the membrane, mechanisms for retaining H^+ and/or regulating H^+ behavior on the outer surface membrane are necessary. It is expected that the membrane-bound cytochrome *c* concomitant with physicochemical factors assumes these functions on the outer surface of the membrane.

Electron transfer-coupled H^+ transfer was studied by Murgida and Hildebrandt (2001) via deuterium substitution. Horse heart cytochrome *c* was bound as a self-assembled monolayer (SAM) on a Ag electrode produced using different chain lengths (C_2-C_{16}) of ω-carboxyl alkanethiols. Cytochrome *c* redox reactions were performed by changing the electrical potential of the Ag electrode and monitoring changes in the Raman spectra. When the distance between cytochrome *c* and the electrode was short (C_2; distance between cytochrome *c* and the electrode: 6.3 Å), the electron transfer rate between cytochrome *c* and the Ag electrode was slower in D_2O (33 s^{-1}) than that in H_2O (132 s^{-1}). However, there was no difference in the electron transfer rate (0.073−0.074 s^{-1}) between cytochrome *c* and the Ag electrode when the distance between cytochrome *c* and the electrode was large (C_{16}; distance between cytochrome *c* and the electrode: 24 Å), regardless of whether the aqueous solvent was D_2O or H_2O. These results indicate that the D^+ exchange rate with amino acids in cytochrome *c* was not the rate-limiting step when the electron transfer rate between cytochrome *c* and the Ag electrode was low. H^+-exchange-coupled electron transfer between cytochrome *c* and the Ag electrode may be the rate-limiting step if the rate of electron transfer between cytochrome *c* and the Ag electrode is high. The above-described rate-limiting H^+/D^+ transfer-coupled electron transfer was observed during self-assembly but not in solution. Therefore, differentiated H^+/D^+ transfer-coupled electron transfer can be observed only in the accumulated nanolayers of cytochromes affected by changes in the electric field (Coulomb's force) of the Ag electrode when an electron is taken in and out concomitant with electron transfer (associated H^+/D^+ transfer). The fluctuating electric field may be equivariant to the local electric field strength at biological interfaces (Murgida and Hildebrandt, 2004). This finding suggests that the H^+ transfer rate between cytochrome

c and the H^+ transfer network on the outer surface membrane is affected not only by electron transfer to cytochrome *c* but also by the local electric field strength on the outer surface membrane. Electron transfer and local electric field strength on the outer surface membrane may fluctuate depending on the electron transfer events in the respiratory chain.

The sulfate-reducing bacterium *D. gigas*, which reduces sulfuric acid to hydrogen sulfide, possesses large quantities of cytochrome c_3, with four heme molecules in one protein (Coutinho and Xavier, 1994). The redox potential of cytochrome *c* changes depending on the pH, affecting the electric field and reducing the sequence of these hemes. Cytochrome c_3 has been reported to facilitate the transfer of H^+ to the electron transfer complex or F_1F_o-ATPase by cooperative H^+/e^- linkage (redox-Bohr effect) (Louro et al., 1997; Messias et al., 2006). The midpoint redox potentials of heme I, heme II, heme III, and heme IV of cytochrome c_3 are −306, −327, −308, and −297 mV, respectively, in solution but −332, −384, −381, and −457 mV, respectively, on the SAM on the electrode. The differences in midpoint redox potentials between the solution and the SAM follow the sequence heme IV (160 mV) > heme III (73 mV) > heme II (57 mV) > heme I (16 mV), which is consistent with the sequence for the distance between hemes and the electrode (shorter distances with larger differences in redox potentials) (Rivas et al., 2005). This finding indicates that the midpoint redox potential is affected by structural changes in the protein concomitant with changes in the electric field (Coulomb's force). Thus, the redox potential of heme *c* is affected by localized structural changes in the vicinity of heme *c*. Changes in the intensity of the redox potential may be accounted for by the reduced distances between the hemes, and the electrode may be affected by the enhanced electric field.

To summarize the above-described phenomena regarding the behavior of redox reactions concomitant with H^+ exchange in the aqueous phase in cytochrome *c* (or heme *c*), H^+ transfer via the H^+ exchange network is affected not only by the redox change in heme *c* but also by the change in the intensity of the electric field on the SAM of cytochrome *c*. In addition, the same cumulative configuration of the structure of the assembled cytochrome *c* was indispensable for these events.

A H^+-CONDENSER PRODUCED BY CYTOCHROME *c*-550

In this section, we consider respiratory regulatory mechanisms based on the obtained experimental data for *B. clarkii* DSM 8720^T and *B. clarkii* K24-1U because both strains belong to the same species. As described above, the cytochromes *c* from alkaliphilic *Bacillus* spp. exhibited lower redox potentials (+47−+95 mV) than those from neutralophilic bacteria (+170−+230 mV) (Hicks and Krulwich, 1995; Yumoto, 2002; Goto et al., 2005) due to electron transport across the membrane between the redox center located in the outer membrane to the intramembrane side and/or transport of the heavier H^+ from the intracellular to the extracellular side in the presence of a large $\Delta\Psi$. Although the midpoint redox potential of cytochrome *c*-550 in *B. clarkii* K24-1U was +83 mV, based on redox titration, the potential was even lower when determined by cyclic voltammetric measurements (Ogami et al., 2009), probably because the redox potential was affected by the electric field of the electrode during cyclic voltammetric measurement. In the abovementioned example of cytochrome *c* in the SAM, the midpoint redox potential and H^+ transfer behavior of cytochrome *c*-550 were also affected by $\Delta\Psi$. For example, the $\Delta\Psi$ of *B. clarkii* DSM 8720^T was lower under low-aeration conditions than under high-aeration conditions (Goto et al., 2016). Thus, electron transport via the respiratory chain concomitant with H^+ transport across the membrane is relatively easy under low-aeration conditions, whereas the Δp per H^+ is lower under low-aeration conditions than under high-aeration conditions. Under high-aeration conditions, the cytochrome *c* content of *B. clarkii* K24-1U (0.23 nmolmg $protein^{-1}$) in the membrane is lower than that (1.38 nmolmg $protein^{-1}$) under low-aeration conditions (**Figure 1**). This finding suggested that the membrane-bound cytochrome *c* in *B. clarkii* plays an important role under low-aeration conditions at a pH of approximately 10. Growth characteristics were studied under both conditions for alkaliphilic *B. clarkii* K24-1U (**Table 1**). The μ_{max} and $OD_{650,max}$ of *B. clarkii* under low-aeration conditions were 0.26 h^{-1} and 0.96 (18 h), respectively, whereas the μ_{max} and $OD_{650,max}$ under high-aeration conditions were 0.21 h^{-1} and 1.27 (12 h), respectively. These results indicated that although the growth rate and intensity of *B. clarkii* were greatly influenced by aeration conditions, the bacterium retained a high growth rate under low-aeration conditions. In addition, despite a culture duration of 21 h, the growth intensity remained high. This finding is quite remarkable considering the low H^+ concentration at the outer surface membrane and the low number of terminal electron acceptors (low O_2 concentration) in the conducting respiratory system. Therefore, it can be assumed that an increased level of membrane-bound cytochrome *c* affects H^+ transfer at the outer surface of the membrane as follows: H^+ condensation at the outer surface membrane via both (i) the electrical force (in reduced form) (ii) the hydrogen-bond network produced by the chemical characteristics of the protein (via Asn-rich structures). Thus, we hypothesize that the H^+-condensation mechanism produced by cytochrome *c* in certain alkaliphilic *Bacillus* spp. plays very significant role under condition of limited aeration (**Figure 2**).

SOLUBLE FORM CYTOCHROME *c* IN THE GRAM-NEGATIVE ALKALIPHILE *Pseudomonas alcaliphila* AL15-21^T

Gram-negative alkaliphiles have been studied far less investigated than Gram-positive alkaliphiles, probably because most of the sources for alkaliphile isolation have been terrestrial samples, such as soil. The facultative alkaliphile *P. alcaliphila* AL15-21^T was isolated from seawater obtained from the coast of Rumoi, Hokkaido, Japan (43°56′N 141°38′E) (Yumoto et al., 2001), and the cytochromes *c* of this bacterium was studied because Gram-negative bacteria possess soluble cytochromes *c* (Matsuno et al.,

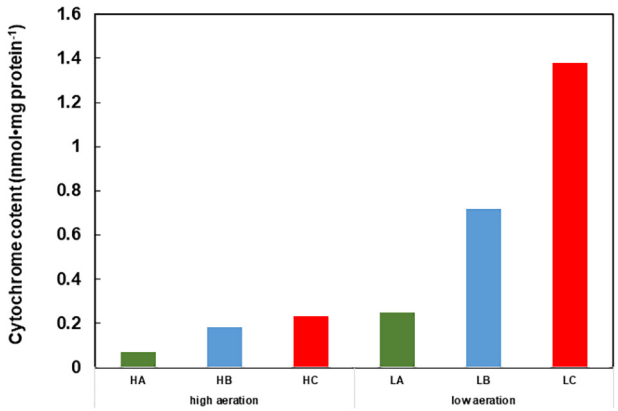

FIGURE 1 | Cytochrome content of cell extracts of Gram-positive obligately alkaliphilic *Bacillus clarkii* K24-1U (grown at pH 10) under low-aeration and high-aeration conditions. HA, HB, and HC are the cytochrome *a*, *b,* and *c* levels, respectively, under high-aeration conditions. LA, LB, and LC are the cytochrome *a*, *b,* and *c* levels, respectively, under low-aeration conditions. This difference in cytochrome *c* content may indicate that cytochrome *c* has an important function under low-aeration conditions at pH 10. Low-aeration conditions were produced by using 15 L of a medium in a 20-L stainless-steel fermenter (Takasugi Seisakusho, Tokyo, Japan) with an agitation speed of 106 rpm and an air flow rate of 20 Lmin^{-1}, while high-aeration conditions were produced by using 15 L of a medium in a 30-L stainless-steel fermenter (Marubishi, Tokyo, Japan) with an agitation speed of 250 rpm and an air flow rate of 20 Lmin^{-1}. This figure was made according to the data of Hijikata (2004).

TABLE 1 | Growth characteristics of the obligately alkaliphilic *Bacillus clarkii* K24-1U.

	Growth condition	
	Low-aeration	**High-aeration**
μ_{max}(h^{-1})	0.26	0.21
OD_{max}	0.96	1.27
Time to OD_{max} (h)	21	14
Is the growth saturated at OD_{max}?	No	Yes

Obligately alkaliphilic B. clarkii K24-1U grew at pH 10. The low aeration condition was produced by using 15 L of a medium in a 20-L stainless-steel fermenter (Takasugi Seisakusho, Tokyo, Japan) at an agitation speed of 106 rpm with an air flow rate of 20 Lmin^{-1}, while the high-aeration condition was produced by using 15 L of a medium in a 30-L stainless-steel fermenter (Marubishi, Tokyo, Japan) at an agitation speed of 250 rpm with an air flow rate of 20 Lmin^{-1}. This table was prepared according to the data of Hijikata (2004).

2007, 2009; Matsuno and Yumoto, 2015). This property is due to the presence of periplasmic space in Gram-negative bacteria on the outer side of the membrane. *Pseudomonas* spp. belonging to the same node as *P. alcaliphila* (such as *P. mendocina* and *P. toyotomiensis*) in a phylogenetic tree based on the 16S rRNA gene sequence are able to grow at pH 10 (Hirota et al., 2011). This relationship between alkaline adaptation and phylogenetic position based on 16S rRNA gene sequences is similar to that observed for alkaliphilic *Bacillus* spp.

The soluble cytochrome *c* content in cells grown at pH 7−10 under low- or high-aeration conditions was estimated (Matsuno et al., 2007). The highest amount of cytochrome *c* was observed in cells grown at pH 10 under low-aeration conditions. The cytochrome *c* content in cells grown at pH 10 under low-aeration conditions (0.47 ± 0.05 nmolmg protein^{-1}) was 3.6 times higher than that in cells grown at pH 7 under high-aeration conditions, which was the lowest cytochrome *c* content among the tested samples (0.13 ± 0.05 nmolmg protein^{-1}) (Matsuno et al., 2009). The increased cytochrome *c* content at high pH under low-aeration conditions was similar to that observed for facultative alkaliphilic *Bacillus* spp. such as *B. clarkia* K24-1U (**Figure 1**; Hijikata, 2004).

The soluble fraction of *P. alcaliphila* AL15-21^T contains three types of cytochrome *c*: cytochrome *c*-552, cytochrome *c*-554, and cytochrome *c*-551. Cytochrome *c*-522 is the major soluble cytochrome *c* component, constituting 64% of the total cytochrome *c* content in *P. alcaliphila* AL15-21^T (Matsuno and Yumoto, 2015). One particular characteristic of cytochrome *c*-552 is that the resting state of this protein is similar to its fully reduced state (Matsuno et al., 2009). Thus, cytochrome *c*-552 possesses electron-retention characteristics. The molecular mass of this protein is 7.5 kDa, as determined by SDS-PAGE, which is somewhat smaller than the reported masses of cytochrome *c* proteins isolated from neutralophilic *P. aeruginosa* (9−15 kDa). A phylogenetic analysis performed using the amino acid sequence of cytochrome *c*-552 classified it as a small cytochrome c_5 belonging to group 4 of class I cytochrome *c* proteins (Matsuno et al., 2007; Matsuno and Yumoto, 2015). Class I cytochromes *c* consist of six groups, and group four contains monoheme cytochromes *c* form Gram-negative bacteria such as *Pseudomonas* spp. and *Shewanella* spp. (Sone and Toh, 1994; Bertini et al., 2006; Matsuno and Yumoto, 2015). The midpoint redox potential of cytochrome *c*-552 determined by redox titration (+228 mV) was almost the same as that determined by cyclic voltammetry (+224 mV) (Matsuno et al., 2009). Cytochrome *c*-552 reacts with the terminal oxidase in the respiratory system (Matsuno et al., 2009).

The pH dependence of the cytochrome *c*-552 reduction rate was determined by estimating the reduction rate under anaerobic conditions (Matsuno et al., 2009). Cytochrome *c*-552 was fully reduced after 40 h at pH 8.5 but was fully reduced after 4 h at pH 10 in the presence of the electron mediator TMPD (*N*,*N*,*N*′,*N*′-tetramethyl-*p*-phenylenediamine). The reduction rate exhibited first-order reaction constants of 0.07 and 0.56 h^{-1} at pH 8.5 and pH 10, respectively. The oxidation rates of cytochrome *c*-552 and horse heart cytochrome *c* were estimated at pH 6−10 under ambient conditions. Cytochrome *c*-552 was oxidized very slowly at pH 8−10, with the slowest rate observed at pH 8, but was oxidized rapidly from pH 6−7. The oxidation rates of horse heart cytochrome *c* were consistently high at pH 6−10. The results demonstrated that cytochrome *c*-552 possessed distinctive electron retention characteristics. If electron-transfer-coupled H^+ transfer (redox-Bohr effect) is possible, then cytochrome *c*-552 retains H^+ in the periplasmic space.

To understand the physiological function of *P. alcaliphila* AL15-21^T cytochrome *c*-552, an antibiotic-marker-less cytochrome *c*-552-deficient mutant was constructed to exclude the effects of antibiotics (Matsuno et al., 2011). The growth features of the wild-type *P. alcaliphila* AL15-21^T and cytochrome

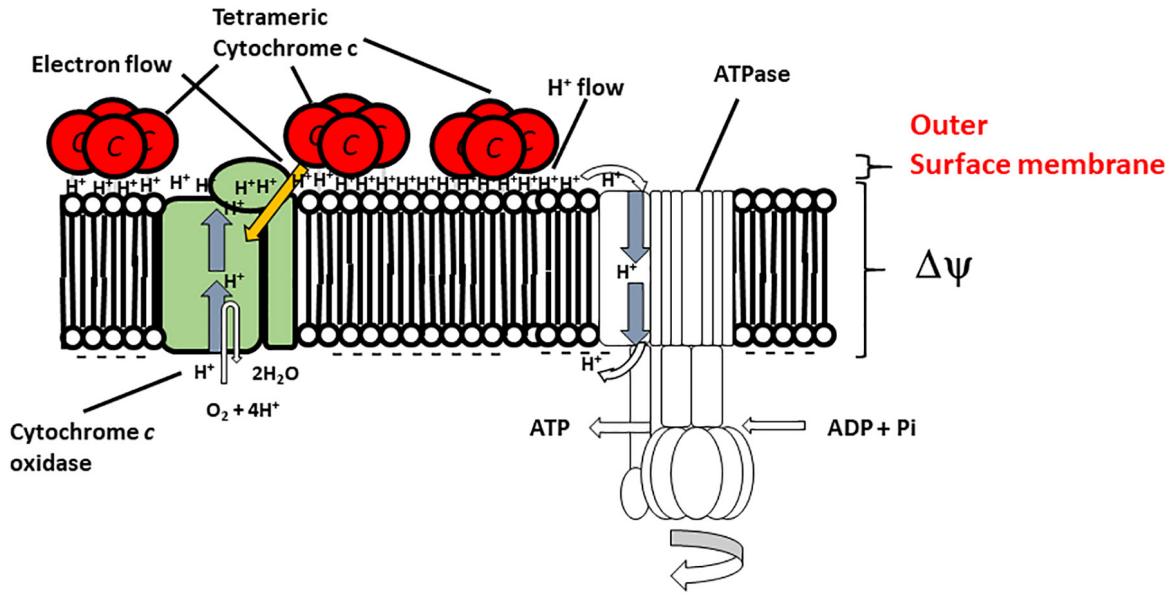

FIGURE 2 | Hypothetical model of the function of membrane-bound cytochrome *c*-550 in the respiratory system of *B. clarkii* K24-1U. Cytochrome *c*-550 contains the specific structure Gly_{22}–Asn_{34} (Asn-rich) at the N-terminal region of its sequence, which may facilitate H^+ transfer at the interface of the outer surface membrane. The tetrameric structure is predicted to be important for enhancement of the H-bound network. The production of cytochrome *c*-550 was enhanced under low-aeration conditions. This enhanced cytochrome *c*-550 on the outer surface of the membrane led to the accumulation of electrons, H^+ and the H^+-condenser construct. This structure facilitates the growth of the microorganism, especially under high-pH and low-aeration conditions. This figure was produced as an original hypothetical model for this review.

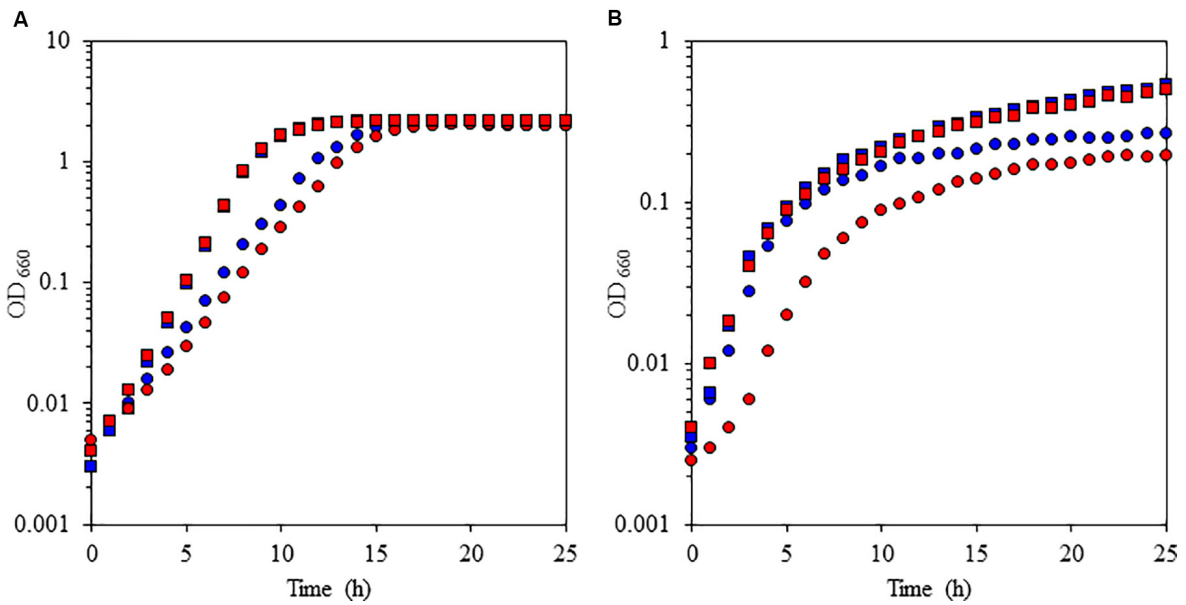

FIGURE 3 | Growth characteristics of the facultative alkaliphile *Pseudomonas alcaliphila* AL15-1^T (wild type: blue symbols) and the cytochrome *c*-522 deletion mutant derived from the wild-type strain (mutant: red symbols) under high-aeration **(A)** and low-aeration **(B)** conditions at pH 10 (squares) and pH 7 (circles). The reproducibility of the results was confirmed by performing three independent experiments. This figure was reproduced from Matsuno and Yumoto (2015).

c-552 deletion mutant strains were compared at pH 10 and 7 under low- and high-aeration conditions by estimating the maximum specific growth rate (μ_{max} [h^{-1}]) and maximum cell turbidity ($OD_{660,max}$) (**Figure 3** and **Table 2**). The most significant differences in the growth parameters were observed at pH 10 under low-aeration conditions between the wild-type (μ_{max} [h^{-1}] = 0.85, $OD_{660,max}$ = 0.27) and the cytochrome *c*-522 deletion mutant (μ_{max} [h^{-1}] = 0.69, $OD_{660,max}$ = 0.20). The

TABLE 2 | Growth characteristics of wild-type and cytochrome *c*-552 deletion mutant strains of *P. alcaliphila* AL15-21^T.

	Growth condition							
	Low-aeration				High-aeration			
Strain	pH 10.0		pH 7.0		pH 10.0		pH 7.0	
	$m_{max}(h^{-1})$	OD_{max}	$m_{max}(h^{-1})$	OD_{max}	$m_{max}(h^{-1})$	OD_{max}	$m_{max}(h^{-1})$	OD_{max}
Wild-type	0.85	0.27	0.97	0.53	0.56	2.06	0.89	2.18
Δ*c*-552	0.69	0.20	0.92	0.50	0.49	2.06	0.72	2.17

Wild-type: P. alcaliphila AL15-21^T. Δc-552: an unmarked cytochrome c-552 deletion mutant. The mutant strain was derived from P. alcaliphila AL15-21^T. μ_{max}, maximum specific growth rate. OD_{max}, maximum cell turbidity. μ_{max} and OD_{max} were estimated from growth at 660 nm with a model TN-2612 Biophotometer. These date were reproduced from Matsuno and Yumoto (2015).

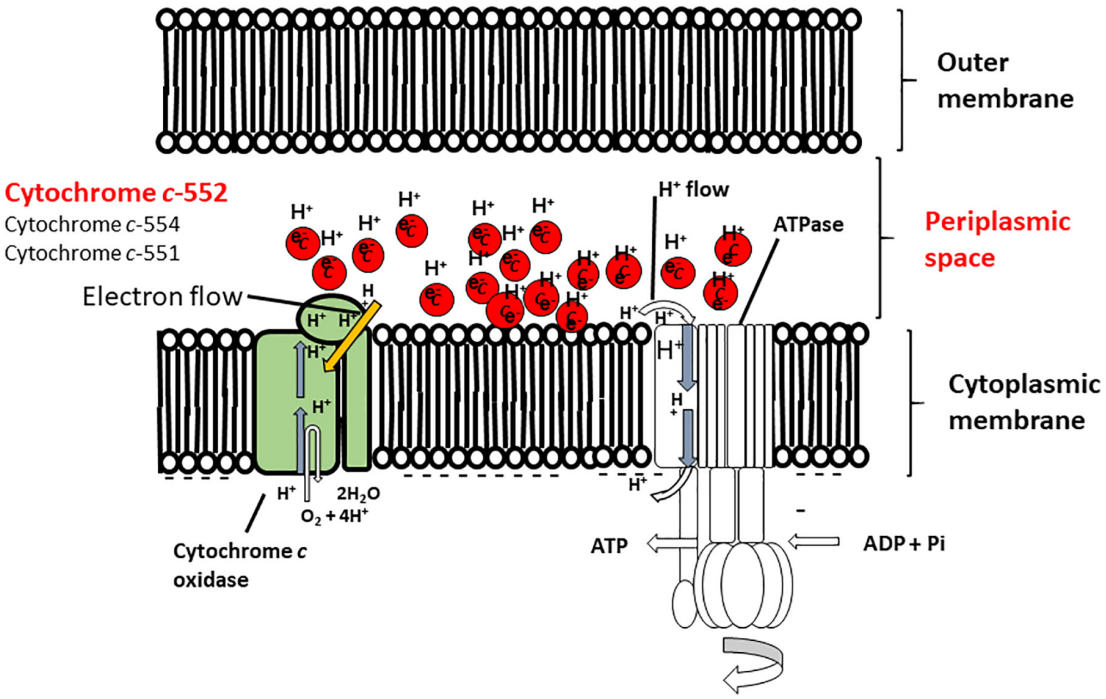

FIGURE 4 | Hypothetical model of the function of cytochrome *c*-552 in the respiratory system of the Gram-negative facultative alkaliphilic *P. alcaliphila* AL15-1^T. This bacterium possesses cytochrome *c*-552 (monoheme), cytochrome *c*-554 (monoheme), and cytochrome 551 (diheme), all of which tend to retain the reduced state. Cytochrome *c*-552 is a major soluble cytochrome *c* constituent in the periplasmic space. The features of cytochrome *c*-552 cause in high electron retention and attract H^+, and the development of electron- and H^+ -retention conditions occurs in the periplasmic space of microorganisms concomitant with an abundance of this cytochrome *c* under low-aeration conditions at pH 10. Thus, Gram-negative *P. alcaliphila* AL15-1^T expresses an electron and H^+ condenser in the periplasmic space. This figure was reproduced based on a hypothetical model presented in Matsuno and Yumoto (2015).

μ_{max} (h^{-1}) of the deletion mutant was 1.5 times higher, whereas the $OD_{660,max}$ was 26% lower than that of the wild-type strain (**Table 2**).

The oxygen consumption rates of cell suspensions of the wild-type strain and the cytochrome *c*-522 deletion mutant of *P. alcaliphila* AL15-21^T were assessed under different conditions (i.e., pH 7 or pH 10; high or low aeration) (Matsuno et al., 2011). The oxygen consumption rates in the cytochrome *c*-522 deletion mutant cells under low- and high-aeration conditions increased by 12 and 17%, respectively, compared to those in the wild type. This finding indicates that cytochrome *c*-552 hinders the direct electron transfer in the respiratory chain. A possible role of this protein might be the formation of an electron bypass to construct an electron reservoir in the periplasmic space. This hypothesis is consistent with the finding that cytochrome *c*-552 has strong electron retention ability at a high pH values (**Figure 4**).

CONCLUSION AND PERSPECTIVES

Bacteria utilize several strategies to adapt to high pH, avoid OH^- and manage scarce H^+ resources via secondary cell wall components, the Na^+-based transportation system and flagellar

rotation. However, for the respiratory system, the management of energy production under one-thousandth of the ambient concentrations of H^+ is difficult. In the case of alkaliphilic *Bacillus* spp., a large $\Delta\Psi$ is indispensable for adaptation at high pH. This high value not only compensates for the deficient ΔpH but also attracts H^+ moieties that are translocated by the respiratory chain and affect the redox potential of the cytochrome *c* bound to the outer surface membrane. However, although we have not determined the $\Delta\Psi$ of alkaliphilic *Pseudomonas* spp., $\Delta\Psi$ is not believed to greatly influence the cytochrome *c* in the periplasmic space. This difference may be attributable to differences in the proteins present in the periplasmic space in Gram-negative *Pseudomonas* spp. Thus, the effect of $\Delta\Psi$ is assumed to encompass the outer surface membrane, although this parameter hardly affects the entire periplasmic space. The main region involved in alkaline adaptation in alkaliphilic *Bacillus* spp. is the outer surface membrane, comprising the $\Delta\Psi$ (physical parameter) and proteins (associated with the acidic nature and retention and transportation of H^+ and electrons) located at the outer surface membrane. In contrast, the main region involved in adaptation in alkaliphilic *Pseudomonas* spp. is the periplasmic space and the corresponding localized proteins (associated with the acidic nature and retention and transportation of H^+ and electrons).

Cytochrome *c* is a well-known electron carrier in the respiratory chain. However, as described above, despite several reports regarding the H^+-transferring characteristics of cytochrome *c*, it is difficult to conclude that these characteristics are well understood. Studies of cytochrome *c* in alkaliphilic bacteria have shown that not only the H^+-transferring characteristics but also the H^+-retention features of cytochrome *c* are important for energy production, especially under low-aeration conditions. We propose that cytochrome *c* participates in the "H^+ capacitor mechanism" as an energy production strategy under low-aeration and alkaline conditions. Surprisingly, although the cell surface structure is completely different between Gram-positive and Gram-negative bacteria, the H^+ and electron retention characteristics of cytochrome *c* are important. However, there are several differences (the charge in redox potential depends on $\Delta\Psi$, the value of the redox potential and electron retention ability) among cytochrome *c* proteins. These changes may be attributable to strategic differences in the reaction site, which is an interfacial surface (outer surface membrane) or space (periplasmic space). As described above, cytochrome *c* has multiple functions (electron carrier or reservoir, H^+ carrier or reservoir and acidic nature). However, pronounced expression of cytochrome *c* is not considered indispensable for adaptation under alkaline conditions because some alkaliphilic *Bacillus* spp. do not express large amounts of cytochrome *c*. According to the experimental results described above, alkaliphiles that express large amounts of cytochrome *c* likely exhibit superior growth features at a high pH at low-oxygen concentrations.

AUTHOR CONTRIBUTIONS

KoY, NI, HiM, KaY, and IY designed the research. TM, TG, SO, and HaM performed the research. KaY and IY analyzed the data and wrote the paper.

FUNDING

This work was supported by an internal grant from the National Institute of Advanced Industrial Science and Technology (AIST) (to IY).

ACKNOWLEDGMENTS

We wish to thank Dr. Tamotsu Tsukahara, Mr. Nozomu Morishita, Mr. Shoichi Hijikata, and Mr. Toshikazu Hirabayashi for providing technical assistance.

REFERENCES

Ambler, R. P. (1991). Sequence variability in bacterial cytochrome c. *Biochim. Biophys. Acta* 1058, 42–47. doi: 10.1016/S0005-2728(05)80266-X

Aono, R., and Horikoshi, K. (1983). Chemical composition of cell walls of alkalophilic strains of alkalophilic strains of *Bacillus*. *J. Gen. Microbiol.* 129, 1083–1087.

Aono, R., Ito, M., and Horikoshi, K. (1993). Occurrence of teichurono peptide in cell walls of group 2 alkaliphilic *Bacillus* sp. *J. Gen. Microbiol.* 139, 2738–2744. doi: 10.1099/00221287-139-11-2739

Aono, R., Ito, M., Joblin, K. N., and Horikoshi, K. (1995). A high cell wall negative charge is necessary for the growth of alkaliphile *Bacillus lentus* C-125 at elevated pH. *Microbiology* 141, 2955–2964. doi: 10.1099/13500872-141-11-2955

Aono, R., Ito, M., and Machida, T. (1999). Contribution of the cell wall component teichuronopeptide to pH homeostasis and alkaliphily in the alkaliphilic *Bacillus lentus* C-125. *J. Bacteriol.* 181, 6600–6606.

Aono, R., Kaneko, H., and Horikoshi, K. (1996). Alkaline growth pH-dependent increase of respiratory and NADH-oxidation activities of the facultatively alkaliphilic strain *Bacillus lentus* C-125. *Biosci. Biotech. Biochem.* 60, 1243–1247. doi: 10.1271/bbb.60.1243

Bengtsson, J., Rivolta, C., Hederstedt, L., and Karamata, D. (1999). *Bacillus subtilis* contains two small c-type cytochromes with homologous heme domains but different type of membrane anchors. *J. Biol. Chem.* 274, 26179–26184. doi: 10.1074/jbc.274.37.26179

Benini, S., Borsari, M., Ciurli, S., Dikiy, A., and Lamborghini, M. (1998). Modulation of *Bacillus pasteurii* cytochrome c553 reduction potential by structural and solution-parameters. *J. Biol. Inorg. Chem.* 3, 371–382. doi: 10.1007/s007750050247

Benini, S., González, A., Rypniewski, W. R., Wilson, K. S., Van Beeumen, J. J., and Ciurli, S. (2000). Crystal structure of oxidized *Bacillus pasteurii* cytochrome c553 at 0.97-Å resolution. *Biochemistry* 39, 13115–13126. doi: 10.1021/bi000402j

Bertini, I., Cavallaro, G., and Rosato, A. (2006). Cytochrome *c*: occurrence and functions. *Chem. Rev.* 106, 90–115. doi: 10.1021/cr050241v

Brayer, G. D., and Murphy, M. P. (1996). "Structural studies of eukaryotic cytochromes c," in *Cytochrome c. A Multidisciplinary Approach*, eds R. A. Scott and A. G. Mauk (Sausalio, CA: University Science Books), 103–166.

Coutinho, I. B., and Xavier, A. V. (1994). Inorganic microbial sulfur metabolism. *Methods Enzymol.* 234, 119–140. doi: 10.1016/0076-6879(94)43011-X

David, P. S., Dutt, P. S., Wathen, B., Jia, Z., and Hill, B. C. (2000). Characterization of structural model of membrane bound cytochrome c-550 from *Bacillus subtilis*. *Arch. Biochem. Biophys.* 377, 22–30. doi: 10.1006/abbi.2000.1732

Davidson, M. W., Gray, K. A., Knaff, D. B., and Krulwich, T. A. (1988). Purification and characterization of two soluble cytochromes from the alkalophile *Bacillus firmus* RAB. *Biochim. Biophys. Acta* 933, 470–477. doi: 10.1016/0005-2728(88)90082-5

Denda, K., Oshima, A., and Fukumori, Y. (2001). Structural analyses of the deduced amino acid sequences of a novel type heme-copper terminal oxidase, cytochrome aco3, from alkalophilic *Bacillus* YN-2000. *Can. J. Microbiol.* 47, 1075–1081. doi: 10.1139/w01-114

Dimroth, P., and Cook, G. M. (2004). Bacterial Na^+- or H^+-coupled ATP synthases operating at low electrochemical potential. *Adv. Microb. Physiol.* 49, 175–218. doi: 10.1016/S0065-2911(04)49004-3

Donnan, F. G. (1924). The theory of membrane equilibria. *Chem. Rev.* 1, 73–90. doi: 10.1021/cr60001a003

Doukov, T. I., Hemmi, H., Drenman, C. L., and Ragsdale, S. W. (2007). Structural and kinetic evidence for extended hydrogen-bonding network in catalysis of methyl group transfer. Role of active site asparagine residue in activation of methyl transfer by methyltransferase. *J. Biol. Chem.* 282, 6609–6618. doi: 10.1074/jbc.M609828200

Gennis, R. B. (2016). Proton dynamics at the membrane surface. *Biophys. J.* 110, 1909–1911. doi: 10.1074/jbc.M609828200

Gilmore, R., Messner, P., Guffanti, A. A., Kent, R., Scheberl, A., Kendrick, N., et al. (2000). Two-dimensional gel electrophoresis of pH-dependent protein expression in facultatively alkaliphilic *Bacillus pseudofirmus* OF4 lead to characterization of an S-layer protein with a role in alkaliphily. *J. Bacteriol.* 182, 5969–5981. doi: 10.1016/j.bpj.2016.04.001

Goto, T., Hirabayashi, T., Morimoto, H., Yamazaki, K., Inoue, N., Matsuyama, H., et al. (2016). Contribution of intracellular negative ion capacity to Donnan effect across the membrane in alkaliphilic *Bacillus* spp. *J. Bioeng. Biomembr.* 48, 87–96. doi: 10.1007/s10863-015-9641-9

Goto, T., Matsuno, T., Hishinuma-Narisawa, M., Yamazaki, K., Matsuyama, H., Inoue, N., et al. (2005). Cytochrome c and bioenergetic hypothetical model for alkaliphilic *Bacillus* spp. *J. Biosci. Bioeng.* 100, 365–379. doi: 10.1007/s10863-015-9641-9

Guffanti, A. A., Finkelthal, O., Hicks, D. B., Falk, L., Sidhu, A., Garro, A., et al. (1986). Isolation and characterization of new facultatively alkalophilic strains of *Bacillus* species. *J. Bacteriol.* 167, 766–773. doi: 10.1263/jbb.100.365

Guffanti, A. A., and Krulwich, T. A. (1992). Features of apparent nonchemiosmotic energization of oxidative phosphorylation by alkaliphilic *Bacillus firmus* OF4. *J. Biol. Chem.* 267, 9580–9588. doi: 10.1128/jb.167.3.766-773.1986

Guffanti, A. A., and Hicks, D. B. (1991). Molar growth yields and bioenergetic parameters of extremely alkaliphilic *Bacillus* species in batch cultures, and growth in a chemostat at pH 10.5. *J. Gen. Microbiol.* 137, 2375–2379. doi: 10.1099/00221287-137-10-2375

Hicks, D. B., and Krulwich, T. A. (1995). The respiratory chain of alkaliphilic bacteria. *Biochim. Biophys. Acta* 1229, 303–314. doi: 10.1016/0005-2728(95)00024-D

Hijikata, S. (2004). *Purification and Characterization of Cytochrome c-550 from Obligate Alkaliphilc Bacillus Clarkii K24-1U*. Master's thesis, Hokkaido University, Sapporo.

Hirabayashi, T., Goto, T., Morimoto, H., Yoshimune, K., Matsuyama, H., and Yumoto, I. (2012). Relationship between rates of respiratory proton extrusion and ATP synthesis in obligately alkaliphilic *Bacillus clarkii* DSM 8720T. *J. Bioeng. Biomembr.* 44, 265–272. doi: 10.1007/s10863-012-9430-7

Hirota, K., Aino, K., and Yumoto, I. (2013). *Amphibacillus iburiensis* sp. nov., an alkaliphile that reduces an indigo dye. *Int. J. Syst. Evol. Microbiol.* 63, 4303–4308. doi: 10.1099/ijs.0.048009-0

Hirota, K., Yamahira, K., Nakajima, K., Nodasaka, Y., Okuyama, H., and Yumoto,, I. (2011). *Pseudomonas toyotomiensis* sp. nov., a psychrotolerant facultative alkaliphile that utilizes hydrocarbons. *Int. J. Syst. Evol. Microbiol.* 61, 1842–1848. doi: 10.1099/ijs.0.024612-0

Hoffmann, A., and Dimroth, P. (1991). The electrochemical proton potential of *Bacillus alcalophilus*. *Eur. J. Biochem.* 201, 467–473. doi: 10.1111/j.1432-1033.1991.tb16304.x

Horikoshi, K. (2006). *Alkaliphiles*. New York, NY: Kodansha.

Horikoshi, K. (2011). "Enzymes isolated from alkaliphiles," in *Extremophiles Handbook*, eds K. Horikoshi, G. Antranikian, A. T. Bull, F. T. Robb, and K. O. Stetter (Tokyo: Springer), 163–181. doi: 10.1007/978-4-431-53898-1_9

Horikoshi, K., and Akiba, T. (1982). *Alkaliphilic Microorganisms. A New Microbial World*. Berlin: Springer-Verlag.

Horikoshi, K., and Grant, W. D. (1998). *Extremophiles, Microbial Life in Extreme Environments*. Hoboken, NJ: John Wiley Sons, 322.

Ito, M., Hicks, D. B., Henkin, T. M., Guffanti, A. A., Powers, B. D., Zvi, L., et al. (2004a). MotPS is the stator-force generator for motility of alkaliphilic *Bacillus*, and its homologue is a second functional Mot in *Bacillus subtilis*. *Mol. Microbiol.* 53, 1035–1049.

Ito, M., Xu, H. X., Guffanti, A. A., Wei, Y., Zvi, L., Clapham, D. E., et al. (2004b). The voltage-gated Na^+ NavBP has a role in motility, chemotaxis, and pH homeostasis of an alkaliphilic *Bacillus*. *Proc. Natl. Acad. Sci. U.S.A.* 101, 10566–10571.

Janto, B., Ahmed, A., Ito, M., Liu, J., Hicks, D. B., Pagni, S., et al. (2011). Genome of alkaliphilic *Bacillus pseudomonas* OF4 reveals adaptation that support the ability to grown in external pH range from 7.5 to 11.4. *Environ. Microbiol.* 13, 3289–3309. doi: 10.1111/j.1462-2920.2011.02591.x

Kitada, M., Guffanti, A. A., and Krulwich, T. A. (1982). Bioenergetic properties and viability of alkalophilic *Bacillus firmus* RAB as a function of pH and Na^+ contents of the incubation medium. *J. Bacteriol.* 152, 1096–1104.

Krulwich, T. A. (1995). Alkaliphiles: 'basic' molecular problems of pH tolerance and bioenergetics. *Mol. Microbiol.* 15, 403–410. doi: 10.1111/j.1365-2958.1995.tb02253.x

Lane, N., and Martin, W. F. (2012). The origin of membrane bioenergetics. *Cell* 151, 1406–1416. doi: 10.1016/j.cell.2012.11.050

Lewis, R. J., Belkina, S., and Krulwich, T. A. (1980). Alkalophiles have much higher cytochrome contents than conventional bacteria and than their own non-alkaliphilic mutant derivatives. *Biochem. Biophys. Res. Commun.* 95, 857–863. doi: 10.1016/0006-291X(80)90866-9

Louro, R. O., Catario, T., LaGall, J., and Xavier, A. V. (1997). Redox-Bohr effect in electron/proton energy transduction: cytochrome c3 coupled to hydrogenase works as a 'proton thruster' in *Desulfivibrio vulgais*. *J. Biol. Inorg. Chem.* 2, 488–491. doi: 10.1007/s007750050160

Lyu, H., and Lazár, D. (2017). Modeling the light-induced electric potential difference ($\Delta\Psi$), the pH difference (ΔpH) and the proton motive force across the thylakoid membrane in C3 leaves. *J. Theor. Biol.* 413, 11–23. doi: 10.1016/j.jtbi.2016.10.017

Matsuno, T., Mie, Y., Yoshimune, K., and Yumoto, I. (2009). Physiological role and redox properties of a small cytochrome c_5, cytochrome *c*-552, from alkaliphile, *Pseudomonas alcaliphila* AL15-21^T. *J. Biosci. Bioeng.* 108, 465–470. doi: 10.1016/j.jbiosc.2009.06.008

Matsuno, T., Morishita, N., Yamazaki, K., Inoue, N., Sato, Y., Ichise, N., et al. (2007). Cytochrome *c*-552 from gram-negative alkaliphilic *Pseudomonas alcaliphila* AL15-21^T alters the redox properties at high pH. *J. Biosci. Bioeng.* 103, 247–254. doi: 10.1263/jbb.103.247

Matsuno, T., Yoshimune, K., and Yumoto, I. (2011). Physiological function of soluble cytochrome *c*-552 from alkaliphilic *Pseudomonas alcaliphila* AL15-21^T. *J. Bioeng. Biomembr.* 43, 473–481. doi: 10.1007/s10863-011-9376-1

Matsuno, T., and Yumoto, I. (2015). Bioenergetics and the role of soluble cytochromes *c* for alkaline adaptation in Gram-negative alkaliphilic *Pseudomonas*. *Bio. Med. Res. Int.* 14:847945. doi: 10.1155/2015/847945

Messias, A. C., Aguiar, A. P., Brennan, L., Salgueiro, C. A., Saraiva, L. M., Xavier, A. V., et al. (2006). Solution structures of tetrahaem ferricytochrome c_3 from *Desulfovibrio vulgaris* (Hildenborough) and its K45Q mutant: the molecular basis of cooperativity. *Biochim. Biophys. Acta* 1757, 143–153. doi: 10.1016/j.bbabio.2006.01.007

Mitchell, P. (1961). Coupling of phosphorylation to electron and hydrogen transfer by a chemi-osmotic type of mechanism. *Nature* 191, 144–148. doi: 10.1038/191144a0

Moore, G. R., and Pettigrew, G. W. (1990). *Cytochrome c: Evolutionary, Structural and Physicochemical Aspects*. Belin: Springer-Verlag. doi: 10.1007/978-3-642-74536-2

Mulkidjanian, A. Y., Heberle, J., and Cherepanov, D. V. (2006). Protons @ interfaces: implications for biological energy conversion. *Biochim. Biophys. Acta* 1757, 913–930. doi: 10.1016/j.bbabio.2006.02.015

Murgida, D. H., and Hildebrandt, P. (2001). Proton-coupled electron transfer of cytochrome *c*. *J. Am. Chem. Soc.* 123, 4062–4068. doi: 10.1021/ja004165j

Murgida, D. H., and Hildebrandt, P. (2004). Electron-transfer processes of cytochrome *c* at interfaces. New insights by surface-enhanced resonance Raman spectroscopy. *Acc. Chem. Res.* 47, 854–861. doi: 10.1021/ar0400443

Nielsen, P., Fritze, D., and Priest, F. G. (1995). Phenetic diversity of alkaliphilic *Bacillus* strains: proposal for nine new species. *Microbiology* 141, 1745–1761. doi: 10.1099/13500872-141-7-1745

Ogami, S., Higikata, S., Tsukahara, T., Mie, Y., Matsuno, T., Morita, N., et al. (2009). A novel membrane-anchored cytochrome *c*-550 of alkaliphilic *Bacillus clarkii* K24-1U: expression, molecular features and properties of redox potential. *Extremophiles* 13, 491–504. doi: 10.1007/s00792-009-0234-6

Orii, Y., Yumoto, I., Fukumori, Y., and Yamanaka, T. (1991). Stopped-flow and rapid-scan studies of the redox behavior of cytochrome aco from faculataive alkalophilc *Bacillus*. *J. Biol. Chem.* 266, 14310–14316.

Padan, E., Bibi, E., Ito, M., and Krulwich, T. A. (2005). Alkaline pH homeostasis in bacteria: new insight. *Biochim. Biophys. Acta* 1717, 67–88. doi: 10.1016/j.bbamem.2005.09.010

Pettigrew, G. W., and Moore, G. R. (1987). *Cytochrome c: Biological Aspects*. Berlin: Springer-Verlag. doi: 10.1007/978-3-642-72698-9

Qureshi, M. H., Yumoto, I., Fujiwara, T., Fukumori, Y., and Yamanaka, T. (1990). A novel aco-type cytochrome-c oxidase from a facultative alkalophilic *Bacillus*: purification, and some molecular and enzymatic features. *J. Biochem.* 107, 480–485. doi: 10.1093/oxfordjournals.jbchem.a123071

Rivas, L., Soares, C. M., Baptista, A. M., Simaan, J., Di Palo, R. E., Murgida, D. H., et al. (2005). Electric-field-induced redox potential shifts of tetraheme cytochrome c3 immobilized on self-assembled monolayers: surface-enhanced resonance Raman spectroscopy and simulation studies. *Biophys. J.* 88, 4188–4199. doi: 10.1529/biophysj.104.057232

Russell, M. J., and Hall, A. J. (1997). The emergence of life from iron monosulphide bubbles at a submarine hydrothermal redox and pH front. *J. Geol. Soc. London* 154, 377–402. doi: 10.1144/gsjgs.154.3.0377

Sjöholm, J., Bergstrand, J., Nilsson, T., Šachl, R., Christoph, C. V., von Ballmoos, C., et al. (2017). The lateral distance between a proton pump and ATP synthase determines the ATP-synthesis rate. *Sci. Rep.* 7:2926. doi: 10.1038/s41598-017-02836-4

Sone, N., and Toh, H. (1994). Membrane-bound *Bacillus* cytochromes *c* and their phylogenetic position among bacterial class I cytochromes *c*. *FEMS Microbiol. Lett.* 122, 203–210. doi: 10.1111/j.1574-6968.1994.tb07168.x

Sone, N., Tsukita, S., and Sakamoto, J. (1999). Direct correlation between proton translocation and growth yield: an analysis of the respiratory chain of *Bacillus stearothermophilus*. *J. Biosci. Bioeng.* 87, 495–499. doi: 10.1016/S1389-1723(99)80099-1

Thongaram, T., Kosono, S., Ohkuma, M., Hongoh, Y., Kitada, M., Yoshinaka, T., et al. (2003). Gut of higher termites as a niche for alkaliphiles as shown by culture-based and culture-Independent studies. *Microbes. Environ.* 18, 152–159. doi: 10.1264/jsme2.18.152

Tsujii, K. (2002). Donnan equilibria in microbial cell walls: a pH-homeostatic mechanism in alkaliphiles. *Coll. Surf. B Biointerfaces* 24, 247–251. doi: 10.1016/S0927-7765(01)00244-2

Vedder, A. (1934). *Bacillus alcalophilus* n. sp benevens enkele ervaringen met sterk alcalische voedingsbodems. *Antonie Leeuwenhoek* 1, 141–147. doi: 10.1007/BF02543931

von Wachenfeldt, C., and Hederstedt, L. (1990). *Bacillus subtilis* 13-kilodalton cytochrome *c*-550 encoded by cccA consists of a membrane-anchor and a heme domain. *J. Biol. Chem.* 265, 13939–13948.

von Wachenfeldt, C., and Hederstedt, L. (1993). Physico-chemical characterisation of membrane-bound and water-soluble forms of *Bacillus subtilis* cytochrome *c*-550. *Eur. J. Biochem.* 212, 499–509. doi: 10.1111/j.1432-1033.1993.tb17687.x

Xiong, J.-W., Zhu, L., Jiao, X., and Liu, S.-S. (2010). Evidence for ΔpH surface component (ΔpHs) of proton motive force in ATP synthesis of mitochondria. *Biochim. Biophys. Acta* 1800, 213–222. doi: 10.1016/j.bbagen.2009.07.032

Yamanaka, T. (1992). *The Biochemistry of Bacterial Cytochromes*. Tokyo: Japan Scientific Society Press, 91–168.

Yoshimune, K., Morimoto, H., Hirano, Y., Sakamoto, J., Matsumoto, H., and Yumoto, I. (2010). The obligate alkaliphile *Bacillus clarkii* K24-1U retains extruded protons at the beginning of respiration. *J. Bioeng. Biomembr.* 42, 111–116. doi: 10.1007/s10863-010-9278-7

Yumoto, I. (2002). Bioenergetics of alkaliphilic *Bacillus* spp. *J. Biosci. Bioeng.* 93, 343–353. doi: 10.1016/S1389-1723(02)80066-4

Yumoto, I. (2003). Electron transport system in alkaliphilic *Bacillus* spp. *Recent Res. Dev. Bacteriol.* 1, 131–149.

Yumoto, I., Fukumori, Y., and Yamanaka, T. (1991). Purification and characterization of two membrane-bound *c*-type cytochromes from a facultative alkalophilic *Bacillus*. *J. Biochem.* 110, 267–273. doi: 10.1093/oxfordjournals.jbchem.a123569

Yumoto, I., Nakajima, K., and Ikeda, K. (1997). Comparative study on cytochrome content of alkaliphilic Bacillus strains. *J. Ferment. Bioeng.* 83, 466–469. doi: 10.1016/S0922-338X(97)83002-4

Yumoto, I., Takahashi, S., Kitagawa, T., Fukumori, Y., and Yamanaka, T. (1993). The molecular features and catalytic activity of Cu_A-containing aco_3-type cytochrome *c* oxidase from a facultative alkalophilic *Bacillus*. *J. Biochem.* 114, 88–95. doi: 10.1093/oxfordjournals.jbchem.a124145

Yumoto, I., Yamazaki, K., Hishinuma, M., Nodasaka, Y., Inoue, N., and Kawasaki, K. (2000). Identification of facultatively alkaliphilic *Bacillus* sp. strain YN-2000 and its fatty acid composition and cell-surface aspects depending on culture pH. *Extremophiles* 4, 285–290. doi: 10.1007/s007920070015

Yumoto, I., Yamazaki, K., Hishinuma, M., Nodasaka, Y., Suemori, A., Nakajima, K., et al. (2001). *Pseudomonas alcaliphila* sp. nov., a novel facultatively psychrophilic alkaliphile isolated from seawater. *Int. J. Syst. Evol. Microbiol.* 51, 349–355. doi: 10.1099/00207713-51-2-349

Zavarzin, G. A. (1993). Epicontinental soda lakes are probable relict biotopes of terrestrial biota formation. *Microbiology* 62, 473–479.

Conflict of Interest Statement: The authors declare that the research was conducted in the absence of any commercial or financial relationships that could be construed as a potential conflict of interest.

frontiers in Microbiology

ORIGINAL RESEARCH
published: 16 October 2018
doi: 10.3389/fmicb.2018.02458

A Novel Alkaliphilic *Streptomyces* Inhibits ESKAPE Pathogens

*Luciana Terra[1], Paul J. Dyson[1], Matthew D. Hitchings[1], Liam Thomas[1], Alyaa Abdelhameed[1], Ibrahim M. Banat[2], Salvatore A. Gazze[1], Dušica Vujaklija[3], Paul D. Facey[1], Lewis W. Francis[1] and Gerry A. Quinn[3]**

[1] Institute of Life Sciences, Swansea University Medical School, Swansea, United Kingdom, [2] School of Biomedical Sciences, Ulster University, Coleraine, United Kingdom, [3] Laboratory for Molecular Genetics, Ruđer Bošković Institute, Zagreb, Croatia

In an effort to stem the rising tide of multi-resistant bacteria, researchers have turned to niche environments in the hope of discovering new varieties of antibiotics. We investigated an ethnopharmacological (cure) from an alkaline/radon soil in the area of Boho, in the Fermanagh Scarplands (N. Ireland) for the presence of *Streptomyces*, a well-known producer of antibiotics. From this soil we isolated a novel (closest relative 57% of genome relatedness) *Streptomyces* sp. capable of growth at high alkaline pH (10.5) and tolerant of gamma radiation to 4 kGy. Genomic sequencing identified many alkaline tolerance (antiporter/multi-resistance) genes compared to *S. coelicolor* M145 (at 3:1), hence we designated the strain *Streptomyces* sp. myrophorea, isolate McG1, from the Greek, myro (fragrance) and phorea (porter/carrier). *In vitro* tests demonstrated the ability of the *Streptomyces* sp. myrophorea, isolate McG1 to inhibit the growth of many strains of ESKAPE pathogens; most notably carbapenem-resistant *Acinetobacter baumannii* (a critical pathogen on the WHO priority list of antibiotic-resistant bacteria), vancomycin-resistant *Enterococcus faecium*, and methicillin-resistant *Staphylococcus aureus* (both listed as high priority pathogens). Further *in silico* prediction of antimicrobial potential of *Streptomyces* sp. myrophorea, isolate McG1 by anti-SMASH and RAST software identified many secondary metabolite and toxicity resistance gene clusters (45 and 27, respectively) as well as many antibiotic resistance genes potentially related to antibiotic production. Follow-up *in vitro* tests show that the *Streptomyces* sp. myrophorea, isolate McG1 was resistant to 28 out of 36 clinical antibiotics. Although not a comprehensive analysis, we think that some of the Boho soils' reputed curative properties may be linked to the ability of *Streptomyces* sp. myrophorea, isolate McG1 to inhibit ESKAPE pathogens. More importantly, further analysis may elucidate other key components that could alleviate the tide of multi-resistant nosocomial infections.

Keywords: alkaliphile, antimicrobial, *Streptomyces*, ESKAPE pathogens, multi-resistant, ethnopharmacology

OPEN ACCESS

Edited by:
Masahiro Ito,
Toyo University, Japan

Reviewed by:
Saori Kosono,
The University of Tokyo, Japan
Isao Yumoto,
National Institute of Advanced Industrial Science and Technology (AIST), Japan

****Correspondence:***
Gerry A. Quinn
gquinn@irb.hr

Specialty section:
This article was submitted to Extreme Microbiology, a section of the journal Frontiers in Microbiology

Received: *17 May 2018*
Accepted: *25 September 2018*
Published: *16 October 2018*

Citation:
Terra L, Dyson PJ, Hitchings MD, Thomas L, Abdelhameed A, Banat IM, Gazze SA, Vujaklija D, Facey PD, Francis LW and Quinn GA (2018) A Novel Alkaliphilic Streptomyces Inhibits ESKAPE Pathogens. Front. Microbiol. 9:2458. doi: 10.3389/fmicb.2018.02458

INTRODUCTION

The global increase in multi-resistant ESKAPE pathogens (*Enterococcus faecium*, *Staphylococcus aureus*, *Klebsiella pneumoniae*, *Acinetobacter baumannii*, *Pseudomonas aeruginosa*, and *Enterobacter* species) has created an urgent need to develop replacement therapies. ESKAPE pathogens are responsible for the top 6 health care-associated infections (HAIs) and many have

been identified as priority antibiotic-resistant bacteria (Jelic et al., 2016; Santajit and Indrawattana, 2016; Founou et al., 2017; Tacconelli et al., 2018). Infections with multi-resistant pathogens are extremely hard to treat and may spread throughout a hospital or community environment (Jelic et al., 2016; Santajit and Indrawattana, 2016). It was thought that developing new antibiotics from combinatorial chemistry would be able to eliminate these resistant bacteria. However, years of trials have not produced anything like the number of new drugs necessary to stem the tide of multi-resistant bacteria (Lewis, 2013). In addition, the production of new antibiotics tapered off in the early 1980s due to unfavorable market conditions which has led to a crisis in the supply line of new antibiotics (Santajit and Indrawattana, 2016; Founou et al., 2017). Normally, bacterial infections are treated with the simplest, most effective antibiotics, however, multi-resistant pathogens usually require treatment with higher tier antibiotics or antibiotics of last resort (Santajit and Indrawattana, 2016). There are no guarantees of success with these treatments and they can involve expensive and sometimes toxic chemotherapy. If all solutions fail, infections by ESKAPE pathogens can lead to death of the patient and a spread of multi-resistant strains. Antibacterial resistance has now been detected for nearly all new antibiotics, even those of last resort (Jelic et al., 2017; Li and Webster, 2018). As a consequence, the WHO have created an urgent priority list for discovery of new antibiotics (Tacconelli et al., 2018).

Current strategies to alleviate the shortage of new antibiotics have turned to niche environments such as deserts, thermal vents, and alkaline environments in the hope that they might produce exotic varieties of current antibiotics (Sato et al., 1983; Mao et al., 2007; Yucel and Yamac, 2010; Mohammadipanah and Wink, 2015). Alkaline environments in particular have proven to be a rich source of antibiotics, many derived from *Streptomyces* bacteria (Sato et al., 1983; Yucel and Yamac, 2010; Behroozian et al., 2016; Maciejewska et al., 2016). Together with other members of the phylum Actinobacteria, *Actinomycetes*, are responsible for the synthesis of more than half of modern medicines including antimicrobial, anti-cancerous (Noomnual et al., 2016), antiviral (Yokomizo et al., 1998), antifungal (Nguyen and Kim, 2015), and antiparasitic compounds (Procopio et al., 2012). In 1943, it was streptomycin (from *Streptomyces*) that was the great savior against the formally incurable scourge of tuberculosis (Schatz et al., 1944).

Another promising avenue of drug (re)discovery lies in the investigation of traditional medicines or ethnopharmacology. Although ancient medical traditions are well known in Chinese and Native American cultures, less is known about European folk medicines (Foley, 2015; Behroozian et al., 2016; Kung et al., 2018). One of the last vestiges of continuous ethnopharmacological culture can be found on the most westerly fringes of Europe, in rural locations on the island of Ireland (Foley, 2015). One such cure originates from a region of the West Fermanagh Scarplands known locally as Boho (pronounced Bo) in Northern Ireland. This cure is derived from an alkaline soil deposited in the late Pleistocene period (circa 9,126,000–11,700 years ago) on a bedrock of Carboniferous Dartry limestone (circa 335 million years ago) imparting an alkaline/high radon character to the soil (Brunton and Mason, 1979). Traditionally, this cure had been used to treat a variety of conditions from toothache to infections by placing a small portion of the soil wrapped in cloth next to the infection or underneath the users' pillow for 9 days. The soil was then returned to the area of sampling. The exact specificity and origins of the cure are obscured by lack of documentation, however, some relatively recent written records remain, associating it with the grave of James McGirr, a cleric and healer who died in 1815 (Gallachair, 1975). Previous to this time the area had significance as an amphitheater for the Druids and a symbolic place for Neolithic peoples as evidenced by the nearby Reyfad stones (Halpin and Newman, 2009).

The purpose of this paper is to report the isolation of a novel alkaliphilic strain of *Streptomyces* from soil with antimicrobial activity against multiresistant ESKAPE pathogens which may have potential clinical applications.

MATERIALS AND METHODS

Sampling

The Boho soil sample was collected from an alkaline escarpment region (Latitude-54.364637°N Longitude-7.820939°W) at the Sacred Heart Church, in the townland of Toneel North, Boho, Fermanagh, United Kingdom (Donnelly et al., 2003) on the 28 July 2015. The test soil, which was pre-aliquoted into small cloth bags on site, was sampled with a sterile spatula. Instructions as to the traditional uses and practices with the soil are displayed on the door of an adjacent building. Approximately 25 g of this soil sample was collected in a sterile conical sample tube (50 ml) and dispatched to the laboratory for analysis. For laboratory analysis, 1 g of the Boho soil sample was diluted in 1 ml sterile water, vortexed, and cultured on International Streptomyces Project (ISP) 2 agar (1/5th strength), and Starch agar (1/5th strength) for the initial *Streptomyces* isolation.

Microorganism Strains

Escherichia coli (ATCC, K12-MG1655) was provided by Dr. D. Zahradka, Ruđer Bošković Institute (RBI), Zagreb, Croatia.
Bacillus subtilis (strain 168) was provided by Dr. D. Vujaklija (RBI, Croatia).
ESKAPE pathogens listed below and other ATCC strains listed were provided by Dr. M. Jelić (Jelic et al., 2016, 2017).
Enterococcus faecium – strains: a, b, c (VRE), d, e, and f.
Staphylococcus aureus – strains: a, b (MRSA), c, d, and e (MRSA).
Klebsiella pneumoniae – strains: a, b, c, and d.
Acinetobacter baumannii – strains: a, b, c, d, and e.
Pseudomonas aeruginosa – strains: a, b, c, and ATCC 27853.
Enterobacter cloacae – strain: a.

The ESKAPE pathogens were clinical isolates collected through regular hospital activities. Species identification was performed using standard biochemical methods (tests) and the VITEK 2 system (bioMérieux, France) (Jelic et al., 2016, 2017).

Isolates were assigned unique isolate IDs and subsequently anonymized with designations a, b, c, etc. (meaning the strains cannot be linked to patients in any identifiable manner) in accordance with European regulations. Stocks of original *Streptomyces* were frozen at −80°C in 18% glycerol after their initial isolation.

Microbiological Media

Microbiological media used in these experiments: ISP 2 media (1/5th strength: meaning 20% of standard ingredients except agar which was 2%) and Starch media (1/5th strength) for initial *Streptomyces* isolation. Soy Flour Mannitol (SFM) for *Streptomyces* sub culture and growth. Alkaline SFM for selection of alkaline tolerant *Streptomyces* (soy flour 10 g, mannitol 10 g, agar 20 g, $CaCO_3$ 1 g, humic acid 0.002 g, pH adjusted to 8.3 before sterilization). Blood agar was used for the isolation and cultivation of clinical isolates and Mueller-Hinton agar used for antimicrobial tests unless organisms specifically required enriched blood media.

For the determination of *Streptomyces* alkaline tolerance, we used ISP-2 media supplemented with *Streptomyces* minor elements solution [consisting of 0.1% (wt/vol) (each) of $ZnSO_4{\cdot}7H_2O$, $FeSO_4{\cdot}7H_2O$, $MnCl_2{\cdot}4H_2O$, and $CaCl_2$ anhydrous], 1% (wt/vol) glucose, and 0.02% (vol/vol) NaH_2PO_4–K_2HPO_4 buffer (0.1 M, pH 6.8). It was necessary to increase the concentration of agar to 4% after pH 13.2, and 6% after 13.4, due to the inability of lower agar concentrations to solidify. The pH of the agar was adjusted after sterilization (when the agar had cooled but was still liquid, i.e., 42–45°C) by the addition of appropriate volumes of filter sterilized sodium carbonate buffer (0.2 M Na_2CO_3 + 0.2 M NaH_2CO_3; pH 9.2 → 10.7) and potassium chloride/sodium hydroxide buffer (0.2 M KCl + 0.2 M NaOH; pH 11.6 → 13.0). The pH of the agar was checked immediately after the agar had set.

On the occasions when the robust growth of frozen stocks of *Streptomyces* isolates seemed to decline (as was observed from 2-year-old stocks, even when stored in glycerol at −80°C), stocks were revived by cultivation of the *Streptomyces* sp. myrophorea, isolate McG1 on ISP 2 agar (1/5th) supplemented with *Streptomyces* minor elements solution. In some cases, a mineral solution was made from alkaline soil by dissolving 1 g soil in 1 g water, vortexed (1-min), centrifuged (15,616 × *g*, 10 min) to clear the supernatant and then added at a concentration of 0.5% (vol/vol) to pre-solidified agar. In both cases supplements were filter sterilized (syringe filter, 0.2 μm) prior to their addition to the agar to prevent precipitation of ferric compounds. Cores of this agar were used as negative controls in antimicrobial inhibition assays involving Mueller-Hinton agar. All reagents were supplied by Oxoid (Basingstoke, Hampshire, United Kingdom) except agar which was supplied by Melford (Melford, Suffolk, United Kingdom).

Atomic Force Microscopy

Atomic Force Microscopy (Bruker BioScope Catalyst; Bruker Instruments, Santa Barbara, CA, United States) was used to visualize *Streptomyces* hyphae growing on glass cover slips. The measurements were conducted in air, using TESPA cantilevers (Bruker Instruments, Santa Barbara, CA, United States) in Tapping Mode, with a nominal spring constant of 40 N/m and a nominal resonant frequency of 300 kHz. Off-line processing involved first-order plane fitting and flattening using the software Nan scope Analysis 1.50 (Bruker Instruments, Santa Barbara, CA, United States).

pH Measurement

Soil pH was measured by dissolving 1 g of soil in 5 ml distilled water, shaking for 5 min and then waiting 1 h for the soil to settle (measuring in triplicate using a pH-meter; Mettler-Toledo Seven Compact, Leicester, United Kingdom). A similar procedure was used with pH paper, where 1 g of soil was dissolved in 2 ml distilled water, vortexed for 15 min, and applied in small aliquots to pH indicator strips (EMD Millipore ColorpHast, Burlington, MA, United States). The pH strips were accurate to 0.5 pH units.

To test the alkaline tolerance of bacteria, a pH gradient was established from pH 9.0 to 13.0 in ISP-2 by adding sterilized buffer as described above. The pH of agar surface was continuously monitored using flat pH sticks (Macherey-Nagel GmbH & Co. KG, Düren, Germany) as described (Jones et al., 2017). The pH strip accuracy was routinely tested against standard pH calibration solutions.

Gamma-Irradiation of *Streptomyces* sp. Myrophorea, Isolate McG1 Spores

Streptomyces sp. myrophorea, isolate McG1 spore concentrations were estimated by cultivation of dilutions of the spore stock. A 1 ml spore suspension (estimated to be 1×10^5 spores/ml) received gamma radiation doses of 0.25, 0.5, 1.0, 2.0, 4.0, 10.0, 15.0, and 20.0 kiloGray (kGy) from a cobalt source (^{60}Co, 8.2645 Gy/s). Spore suspensions were contained in 2 ml plastic microfuge tubes surrounded by a layer of ice inside a polystyrene ice container. After irradiation, aliquots of the spore suspensions were spread (100 μl) on SFM agar and cultivated for 2–3 weeks. The growth of one colony (colony-forming units = CFU) was interpreted to be the survival of one spore.

Antimicrobial Tests

Agar Overlay

A standard agar overlay combined with an antibiotic assay was used to test the inhibitory potential of *Streptomyces* sp. myrophorea, isolate McG1 against ESKAPE pathogens (Nkanga and Hagedorn, 1978; Lehrer et al., 1991). Briefly, wells were made in a base layer (15 ml) of Mueller-Hinton agar. Control wells contained standard amounts of dissolved antibiotics were allowed to absorb into the agar over a period of 2 h. Once the wells were dry, an agar core of *Streptomyces* sp. myrophorea, isolate McG1 (cultivated for 9 days 20°C) was placed in an empty well in addition to a negative control of the original media without *Streptomyces* sp. myrophorea, isolate McG1. This base layer was then overlaid with 15 ml Mueller-Hinton agar (cooled to 43°C) that incorporating the test organisms (ESKAPE pathogens with a minimum 5×10^5 CFU/ml). Bacterial inhibition was indicated

by a clear zone in the confluent growth of the test organism after overnight incubation.

Kirby–Bauer

Antibiotic sensitivity tests (antibiograms) for the *Streptomyces* sp. myrophorea, isolate McG1 and for ESKAPE pathogens followed the Kirby–Bauer protocol (Bauer et al., 1966). The resistance profiles (antibiograms) of clinical isolates (ESKAPE pathogens) were determined using standard concentrations of antibiotic impregnated discs (Oxoid) as proposed by the European Committee on Antimicrobial Susceptibility Tests (EUCAST) (**Supplementary Table S1**). Breakpoint tables for interpretation of MICs and zone diameters can be found in Version 8.0, 2018[1].

Genotypic Characterization of *Streptomyces* sp. Myrophorea, Isolate McG1

Genome Sequencing

Cultures of *Streptomyces* sp. myrophorea, isolate McG1 were grown on 1/10th strength LB agar for DNA extraction using a Qiagen DNA mini kit (Qiagen, MD, United States) with the inclusion of a lysis step using lysozyme. Genomic DNA was prepared for sequencing using Qiagen FX and sequenced on an Illumina MiSeq platform using a 600 cycle V3 reagent kit.

Assembly and Annotation of Genome

Paired-end reads were subjected to quality filtering using the Trimmomatic tool (4 bp sliding window of Q20) (Bolger et al., 2014) prior to *de novo* genome assembly using SPAdes under default parameters (Bankevich et al., 2012). The genome assembly was assessed using QUAST (Gurevich et al., 2013) and annotated using Prokka (Seemann, 2014) and Rapid Annotation using Subsystem Technology (RAST)[2] (Aziz et al., 2008).

Phylogenetic Analysis

In silico DNA–DNA hybridization was performed using the Genome–Genome Distance Calculator (GGDC) v 2.1 (Auch et al., 2010) using all *Streptomyces* genomes (868 sequences) as references. All genomes were downloaded from GenBank[3].

Phylogenetic placement of *Streptomyces* sp. myrophorea, isolate McG1 was performed using PhyloPhlAn (Segata et al., 2013). Protein sequences from annotated *Streptomyces* genomes were retrieved autonomously from the GenBank FTP site using the term "*Streptomyces*" as a query. Ortholog identification and alignment was performed in Phylophlan. A maximum-likelihood phylogeny was reconstructed from the concatenated alignments in FastTree MP (JTT + CAT) implemented in the Cipres Science Gateway Server (Miller et al., 2010). The robustness of the phylogeny was assessed using 1000 bootstrap pseudoreplicates.

Secondary Metabolite Analysis

Gene clusters known to be involved in secondary metabolite biosynthesis, self-immunity, or resistance were identified using Antibiotics and Secondary Metabolite Analysis Shell (antiSMASH) version 4.0.0 (Medema et al., 2011). The GenBank sequence file (from Prokka annotation) was submitted to the web interface selecting all extra features of annotation.

[1]http://www.eucast.org

[2]http://rast.nmpdr.org

[3]https://www.ncbi.nlm.nih.gov/genome/genomes/13511

RESULTS

Isolation of *Streptomyces* From Soil

Aliquots (20 μl) of diluted soil samples were cultivated on several agars to select for *Streptomyces* including ISP2 (1/5th) and alkaline SFM (**Figure 1**). The original soil was returned to the sampling site as per local tradition.

Preliminary screening of the Boho soil sample resulted in the isolation of eight (visually different) *Streptomyces*-like colony types as determined by colony morphology and growth characteristics. The *Streptomyces* isolate which had the most consistent inhibitory activity toward Gram-positive and Gram-negative bacteria (initially labeled as *Streptomyces* sp. myrophorea, isolate McG1) was selected for further characterization and testing (**Figure 1**).

Streptomyces Characterization

Visually *Streptomyces* sp. myrophorea, isolate McG1 had (powdery) light to dark green colonies on SFM agar with green to very light green/white spores (**Figures 1B,C**). After a period of approximately 3–5 days, colonies emitted a distinctly "germaline" odor. *Streptomyces* sp. myrophorea, isolate McG1 appeared to be a non-motile, spore forming bacteria with very slender vegetative and aerial hyphae. Atomic force microscopy revealed that the bacterial hyphae were approximately 0.5–1.0 μm width, with spores in a linear

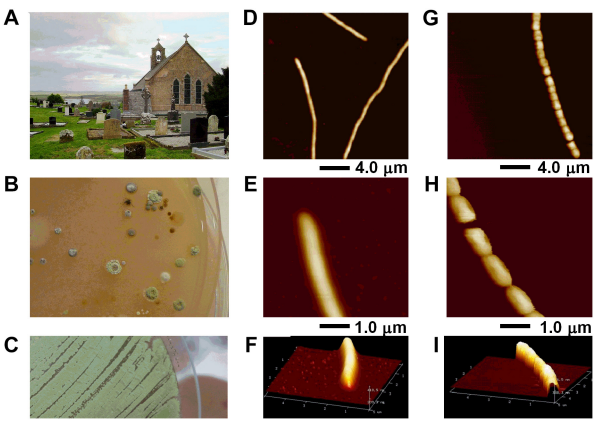

FIGURE 1 | *Streptomyces* sp. myrophorea isolation from **(A)** Boho soil sample site, **(B)** selective enrichment agar, and **(C)** pure culture. **(D–I)** AFM data of *Streptomyces* sp. myrophorea, isolate McG1 grown on glass coverslips and imaged in air by Tapping Mode. Both vegetative **(D–F)** and sporulating **(G–I)** stages are shown. Hyphae overviews are shown in **D** and **G**, while higher resolution scans in **E** and **F** for vegetative hyphae, and in **H** and **I** for sporulating hyphae.

conformation (17–20 spores) having a width of approximately 0.5–1.0 μm (**Figures 1D–I**).

Alkaline Tolerance of *Streptomyces* sp. Myrophorea, Isolate McG1

The Boho soil sample had an average pH of 7.8 (mean ± standard deviation 0.35, by pH meter). Parallel measurements using pH strips indicated a wider range of pH from pH 7.8 to pH 8.5 (six readings at two different time points).

To measure the pH tolerance of *Streptomyces* sp. myrophorea, isolate McG1, a pH gradient was prepared as described. The pH levels of the agar surface were measured after it had set and every subsequent day after this using flat pH sticks (see the section "Materials and Methods"). The results revealed pronounced *Streptomyces* sp. myrophorea, isolate McG1 growth around pH 9.0 to pH 10 after 3–4 days. Growth was slower when bacteria were inoculated on agar that was prepared at pH 11.5 and took 5 days to be visible, however, during this time the pH of the agar also dropped to pH 10.5 (**Figure 2A**). In addition, we observed that *Streptomyces* sp. myrophorea, isolate McG1 inoculated at pH 12.2 or 13.0 could survive several days without prominent growth. As above, we noted that bacterial biomass became visible once the pH of the agar decreased to pH 10.5. In contrast *S. coelicolor* M145 was unable to grow in high alkaline conditions (pH 9 and above) implying that our new strain of *Streptomyces* was more alkaliphilic.

In contrast to the alkaline conditions, *Streptomyces* sp. myrophorea, isolate McG1 did not grow well under acidic conditions, the lowest pH for growth being pH 6.5.

Based on changes in pH during sterilization of media and between buffered and unbuffered media, we realize that it is very important to measure the pH of the agar surface throughout the bacterial growth cycle.

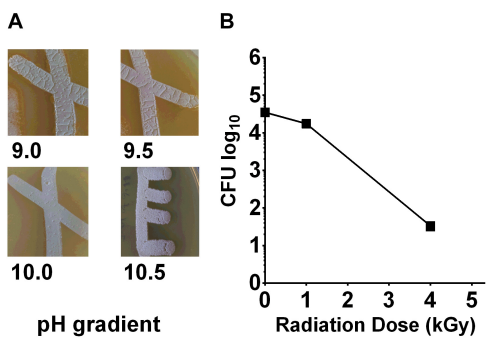

FIGURE 2 | *Streptomyces* sp. myrophorea, isolate McG1 development on pH and irradiation gradients. **(A)** *Streptomyces* sp. myrophorea, isolate McG1 cultivated on ISP-2 agar under increasing pH. Images indicate final measurements, pH 9.0 (originally pH 9.5), pH 9.5 (originally pH 10.0), pH 10.0 (originally pH 10.7), and pH 10.5 (originally pH 11.6). Images are representative of three independent experiments. **(B)** Effect of γ-irradiation (^{60}Co) on spore survival of *Streptomyces* sp. myrophorea, isolate McG1. All tests performed in triplicate. The variation in spore survival is indicated using standard error of the mean.

Radio-Tolerance of *Streptomyces* sp. Myrophorea, Isolate McG1

The alkaline environment of the Boho area is not the only characteristic which makes this region a niche habitat. The (limestone/shale) bedrock also releases radon gas which can be found at levels as high as 710 bq/m^3 (domestic dwelling annual totals) in Boho and adjacent areas (Daraktchieva et al., 2015).

To test the effects of radiation on the survival of *Streptomyces* sp. myrophorea, isolate McG1, we subjected spore solutions to increasing levels of gamma radiation, i.e., spores were removed from a chamber after an exposure to absorbed doses of 0.25 → 20 kGy. After irradiation, aliquots (100 μl) of spores were spread evenly on diluted ISP2 agar in triplicate. The agar plates were then incubated at 4–10°C for 3 weeks before enumeration. Our measurements indicated that spores of *Streptomyces* sp. myrophorea, isolate McG1 were able to tolerate doses of 4 kGy of gamma irradiation and still remain viable (**Figure 2B**). In comparison, another *Streptomyces*, *Streptomyces radiopugnans* resists radiation expose of up to 15 kGy, whereas vegetative cells such as *Deinococcus radiodurans* tolerates an exposure of 12 kGy, *E. coli* 600 Gy, and human cells 4 Gy (Mao et al., 2007; Daly, 2012).

Antimicrobial Tests

To test antimicrobial potential of *Streptomyces* sp. myrophorea, isolate McG1, agar cores from the *Streptomyces* were embedded in Mueller-Hinton test agar and overlaid with a suspension of ESKAPE pathogens. The pathogens were isolated from different hospitals in Croatia based on clinical antimicrobial susceptibility data. Controls consisted of ampicillin (Amp-20 μg), chloramphenicol (Cam-20 μg), ciprofloxacin (Cip-5 μg), gentamicin (Gen-30 μg), kanamycin (Kan-10 μg), streptogramin (10 μg), and ampicillin + sulbactam (Amp + Sulf-10 μg + 10 μg). An agar core from the original ISP2 supplemented agar was used as a negative control.

ESKAPE pathogens were considered susceptible (S) to antibiotics if the zone of inhibition was greater than 12 mm diameter; resistant (R), if zone was less than 8 mm radius and of intermediate status (I) if the zone was between 8 and 12 mm or there were a few colonies appearing in between the beginning of the zone and the edge of the antibiotic disc. A single mark indicates uniformity of result in a triplicate. Tests with variable results are indicated by the result of each replicate, i.e., S/R/S indicates the result of 1st/2nd/3rd test (**Table 1**).

ESKAPE pathogens are known to resist many clinical antibiotics including aminoglycosides, beta-lactams, carbapenems and glycopeptides (Founou et al., 2017). Our data on the incubation of ESKAPE pathogens reveal that *Streptomyces* sp. myrophorea, isolate McG1 was broadly inhibitory to both Gram-positive and Gram-negative bacteria. Specifically *Streptomyces* sp. myrophorea, isolate McG1 inhibited carbapenem-resistant *A. baumannii* [listed as a critical pathogen in the WHO priority pathogens list), vancomycin-resistant *E. faecium*, and methicillin-resistant *S. aureus* (which are both listed as high priority on the WHO pathogen list)] and *K. pneumoniae* (**Figure 3** and **Table 1**). Some strains of *E. faecium*

TABLE 1 | Inhibitory effects of *Streptomyces* sp. myrophorea, isolate McG1 against ESKAPE pathogens.

Bacteria	*Streptomyces* sp. myrophorea, isolate McG1	Antibiotic sensitivity	
E. faecium			
Strain (a)	S	Amp R,	Cam S
Strain (b)	S	Amp S,	Cam R
Strain (c) (VRE)**	S	Amp R,	Cam R
Strain (d)±	R	Amp S,	Cam S
Strain (e)±	R	Amp S,	Cam S
Strain (f)±	R	Amp R,	Cam S
S. aureus			
Strain (a)	S	Amp S/S/R,	Cam S
Strain (b) MRSA**	S	Amp R,	Cam S
Strain (c)	S	Amp S,	Cam S
Strain (d)	S	Kan S,	Cam S/S/R
Strain (e) MRSA **	S	Amp R,	Cam S
K. pneumoniae			
Strain (a)	S	Amp S,	Cam S
Strain (b)	S	Amp S,	Cam S
Strain (c)	S	Amp R,	Cam R
Strain (d)	S	Amp R,	Cam S/R/S
A. baumannii			
Strain (a)*	S		Cam R
Strain (b)	R	Amp + Sul S,	Cam R
Strain (c)	I	Amp + Sul R,	Cam R
Strain (d)*	S		Cam R
Strain (e)*	S	Amp R,	Cam R
P. aeruginosa			
Strain (a)	I/S/I	Streptogramin R,	Cip S
Strain (b)	S	Kan S,	Cam R
Strain (c)	R/S/R	Streptogramin R,	Cip S
Strain 27853 ATCC	R	Gen S,	Cip S
E. cloacae			
Strain (a)	S	Amp R,	Cam R
E. coli K12	S	Amp S,	Cam S
B. subtilis 168	S	Amp S,	Kan S

The inhibitory effects of Streptomyces sp. myrophorea, isolate McG1 were compared to those of ampicillin (Amp-10 μg), chloramphenicol (Cam-20 μg), ciprofloxacin (Cip-5 μg), gentamicin (Gen-30 μg), kanamycin (Kan-10 μg), streptogramin: ampicillin + sulbactam (Amp + Sulf-10 μg + 10 μg)) and a negative control (an agar core from the original ISP2 supplemented agar) using the agar overlay method. ESKAPE pathogens were considered susceptible (S) to antibiotics if the zone of inhibition was greater than 12 mm diameter; resistant (R), if zone was less than 8 mm radius and of intermediate status (I) if the zone was between 8 and 12 mm or there were a few colonies appearing in between the beginning of the zone and the edge of the antibiotic disc. A single mark indicates uniformity of result in a triplicate. Tests with variable results are indicated by a sign for each replicate, i.e., S/R/S indicates the result of 1st/2nd/3rd test. Could only be cultivated on blood agar (±), WHO critical-priority bacteria (*), and WHO high priority bacteria (**).

that could not be cultivated on Mueller-Hinton agar (they only grew on blood agar) as well as some strains of multi-resistant *P. aeruginosa* were resistant to *Streptomyces* sp. myrophorea, isolate McG1 (**Table 1**).

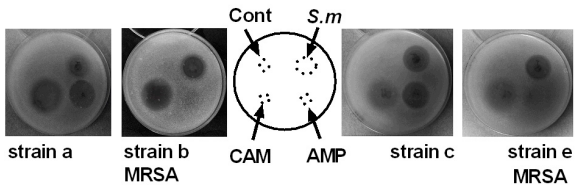

FIGURE 3 | Inhibition of clinical strains of *S. aureus* by agar cores of *Streptomyces* sp. myrophorea, isolate McG1. *S. aureus* (SA) strains: SA strain **a**, SA strain **b** (MRSA, ciprofloxacin resistant), SA strain **c** and SA strain **e** (MRSA, ciprofloxacin sensitive) were cultivated on Mueller-Hinton agar together with agar cores of *Streptomyces* sp. myrophorea, isolate McG1 (S.m). Other test wells contained chloramphenicol (CAM-20 μg), ampicillin (AMP-20 μg), and a negative control of the original ISP-2 agar with mineral supplement (cont). Images are representative of three independent experiments.

Genome Sequencing of *Streptomyces* sp. Myrophorea, Isolate McG1

Whole-genome sequencing of *Streptomyces* sp. myrophorea, isolate McG1 was performed using the Illumina MiSeq system. The total assembled size of the *Streptomyces* sp. myrophorea, isolate McG1 genome was almost 9 MB pairs with a GC content of 71.6%. Parameters predicted by Prokka and QUAST (Gurevich et al., 2013; **Table 2**).

Deposition of Genome Sequence

The genome sequence was deposited in NCBI under the name of "*Streptomyces* sp. myrophorea, isolate McG1" (TaxID 2099643) or "*Streptomyces* sp. McG1," Biosample accession number SAMN08518548, BioProject accession number PRJNA433829, Submission ID: SUB3653175, and Locus tag prefix: C4625. The project information is accessible on publication from http://www.ncbi.nlm.nih.gov/bioproject/433829.

Streptomyces sp. myrophorea, isolate McG1 was deposited with the National Collection of Type Cultures (NCTC 14177), United Kingdom and the Deutsche Sammlung von Mikroorganismen und Zellkulturen (DSMZ) GmbH, Germany.

TABLE 2 | *Streptomyces* sp. myrophorea, isolate McG1 genome characterization and assembly (Prokka).

Genome characterization	Filtered
Total length (bp)	8,950,068
Number of contigs	110
GC content (%)	71.64
Predicted no. of genes	7643
Number of tRNAs	78
Number of rRNAs	8
N50 score	409,278
Number of Ns per 100 kbp	0

The "Number of Ns per 100 kbp" is the average number of uncalled bases (Ns) per 100,000 assembly bases, the N50 is defined as the minimum contig length needed to cover 50% of the genome.

DNA–DNA Hybridization

The top 12 matches against *Streptomyces* genomes and the intergenomic distances for *in silico* DNA–DNA hybridization (DDH) were calculated using GGDC (**Table 3**). The calculation of GGDC Formula 2 is independent of genome length (calculated by dividing found identities by high-scoring pairs and not by whole-sequence length). An absence of any DDH values over the recognized threshold of 70% revealed that our isolate was an uncharacterized species of *Streptomyces*.

Alkaline and Radio Tolerance Genes

The ability of bacteria such as *Streptomyces* sp. myrophorea, isolate McG1 to tolerate high levels of alkalinity is often attributed to alkaline shock genes, proton antiporters (like *nhaA*), and multidrug resistance factors (like *mdt*/*mdfA*) (Krulwich et al., 2011; Holdsworth and Law, 2013). We identified the presence of these genes in the annotated genomes of *Streptomyces* sp. myrophorea, isolate McG1 and *S. coelicolor* M145 listing 25 of these genes in *Streptomyces* sp. myrophorea, isolate McG1 and 9 genes in the genome of *S. coelicolor* M145 (**Table 4**). Only *Streptomyces* sp. myrophorea, isolate McG1 possessed alkaline shock genes, aspartate/ammonium antiporters, and multidrug transporters of the type *mdtH* (**Table 4**). Hence, the *Streptomyces* sp. was referred to as strain myrophorea, isolate McG1, from the Greek myro (fragrance; the isolate emits a strong fragrant odor) and phorea (porter/carrier; in recognition of the number of predicted antiporter genes).

A similar identification of the number of DNA repair genes for *Streptomyces* sp. myrophorea, isolate McG1, and *S. coelicolor* M145 revealed little difference (**Supplementary Table S2**).

Phylogeny

To infer the evolutionary history of *Streptomyces* sp. myrophorea, isolate McG1 a maximum-likelihood phylogeny was performed using a concatenation of 400 protein sequences (**Figure 4**).

Identification of Secondary Metabolites

Potential antibiotic synthesis clusters from *Streptomyces* sp. myrophorea, isolate McG1 were predicted using anti-SMASH (Adamek et al., 2017). This revealed that *Streptomyces* sp. myrophorea, isolate McG1 possessed a total of 45 secondary metabolite biosynthesis gene clusters including multiple clusters with genes encoding the following secondary metabolite families: non-ribosomal peptide synthetase (NRPS) – 5 clusters; type I polyketide synthase (TI PKS) – 10 clusters; type III polyketide synthase (TIII PKS) – 2 clusters; terpenes – 5 clusters, lantipeptides – 3 clusters, and other biosynthesis genes clusters (BGCs) (**Table 5**).

Streptomyces sp. Myrophorea, Isolate McG1 Resistance to Antibiotics

Antibiotic producing bacteria such as *Streptomyces* often require resistance genes to ameliorate the potentially toxic nature of their secondary metabolites. Such resistance elements can also be associated with antimicrobial biosynthesis gene clusters and can be used to predict potential antimicrobial synthesis (Nodwell, 2007). To better characterize these resistance elements, we cultivated *Streptomyces* sp. myrophorea, isolate McG1 in the presence of 36 different antibiotics (in triplicate). *Streptomyces* sp. myrophorea, isolate McG1 was resistant to 20 out of the 36 antibiotics tested after 2 days growth (**Table 6** and **Figure 5A**). Resistance to a further eight antibiotics was visually apparent after a further 4 days, most notably in vancomycin, produced by *Amycolatopsis orientalis*; imipenim, a β-lactam stablized version of thienamycin, produced by *Streptomyces cattleya* and erythromycin, a macrolide antibiotic produced by *Saccharopolyspora erythraea* (**Figure 5B**).

In silico Prediction of Antibiotic-Resistance Genes (ARGs) in *Streptomyces* sp. Myrophorea, Isolate McG1

Antibiotic resistance gene clusters for *Streptomyces* sp. myrophorea, isolate McG1 were predicted *in silico* using anti-SMASH. Many copies of multiple antibiotic resistance elements were also predicted through RAST including β-lactamases (classes A and C), metal-dependant hydrolase of β-lactams (metallo β-lactamase L1), β-lactamase (cephalosporinase), and other penicillin binding proteins (**Supplementary Table S3**). In addition many metal resistance elements were identified

TABLE 3 | The closest 12 matches to *Streptomyces* sp. myrophorea, isolate McG1 in NCBI (by GGDC) (Formula 2 statistics).

Isolate	Accession number	DDH	Prob. DDH ≥ 70%	Distance
Streptomyces anulatus strain ATCC 11523^T	PRJNA257397	55.1	35.24	0.061
Streptomyces europaeiscabiei strain NCPPB 4064	PRJNA255689	55.0	35.11	0.061
Streptomyces sp. EN16	PRJNA338712	54.9	34.79	0.061
Streptomyces sp. Root63	SAMN04155842	54.7	33.99	0.062
Streptomyces sp. Root1295	SAMN04155717	54.5	33.31	0.062
Streptomyces sp. W007	PRJNA74679	53.5	29.81	0.064
Streptomyces griseus subsp. griseus strain NRRL B-2682^T	SAMN05558834	52.9	27.86	0.065
Streptomyces sp. OspMP-M43	SAMN04883176	52.6	27.01	0.066
Streptomyces griseus strain NRRL B-2165^T	SAMN05558833	52.6	26.98	0.066
Streptomyces sp. MNU77	SAMN03200165	51.8	24.39	0.068
Streptomyces griseus subsp. griseus strain NRRL WC-3480	SAMN02645398	51.8	24.40	0.068

TABLE 4 | List of alkaline tolerance genes identified in *Streptomyces* sp. myrophorea, isolate McG1 and *S. coelicolor* M145.

***Streptomyces* sp. myrophorea, isolate McG1**		***S. coelicolor* M145**	
Gene		**Gene**	
504	Alkaline shock protein 23	HPPA_STRCO	K^+ insensitive pyrophosphate
6561	Alkaline shock protein 23	Q9S2Y0_STRCO	Putative Na^+/H^+ antiporter
1049	Ammonium/H^+ antiporter subunit *amhM*	Q9F3L8_STRCO	Putative Na^+/H^+ antiporter
2800	Aspartate/alanine antiporter	Q9KYW0_STRCO	Putative Na^+/H^+ antiporter
2801	Aspartate/alanine antiporter	Q9XAJ9_STRCO	Putative Na^+/H^+ antiporter
6218	Aspartate/alanine antiporter	NHAA1_STRCO	Na^+/H^+ antiporter *nhaA*
3284	Enhanced intracellular survival protein	NHAA2_STRCO	Na^+/H^+ antiporter *nhaA2*
159	K^+/H^+ antiporter *nhaP*	NHAA3_STRCO	Na^+/H^+ antiporter *nhaA3*
3788	K^+/H^+ antiporter *nhaP2*	Q93JF3_STRCO	Putative integral membrane ion exchanger
1050	K^+/H^+ antiporter *yhaU*		
2193	K^+/H^+ antiporter *yhaU*		
1325	K^+ insensitive pyrophosphate-energized proton pump		
923	Multidrug resistance protein *mdtH*		
3240	Multidrug resistance protein *mdtH*		
3252	Multidrug resistance protein *mdtH*		
6781	Multidrug resistance protein *mdtH*		
1282	Na^+/H^+ antiporter *nhaA*		
4210	Na^+/H^+ antiporter subunit A		
4211	Na^+/H^+ antiporter subunit C		
4212	Na^+/H^+ antiporter subunit D		
4215	Na^+/H^+ antiporter subunit G		
660	$Na^+/(H^+$ or $K^+)$ antiporter *gerN*		
3425	$Na^+/(H^+$ or $K^+)$ antiporter *gerN*		
7210	Putative Na^+/H^+ exchanger		
1727	Sodium, potassium, lithium, and rubidium/H^+ antiporter		

(through RAST) to mercury, copper, cobalt, zinc/cadmium, and arsenic which have been linked to increased antibacterial resistance (Chenia and Jacobs, 2017) (**Supplementary Table S3**). It is also possible that resistance may also be mediated through other mechanisms such as general multi-resistance clusters.

DISCUSSION

We have isolated a novel species of *Streptomyces* from an alkaline/radon environment that inhibits the growth of many multiresistant ESKAPE pathogens. There have been several reports in recent years of the presence of *Streptomyces* and other organisms in alkaline environments that can tolerate high pH levels (Tiago et al., 2004; Yucel and Yamac, 2010; Janto et al., 2011; Maciejewska et al., 2016). Our original hypothesis presumed that the Boho soil sample most likely contained *Streptomyces* which may produce antibiotics given the alkaline nature of the environment (Kontro et al., 2005). However, we were surprised to find that our isolate, *Streptomyces* sp. myrophorea, isolate McG1 inhibited the growth of many of the multiresistant ESKAPE pathogens. Some of these bacteria have been listed in a recent WHO document on priority pathogens urgently requiring the development of new antibiotics, such as carbapenem-resistant *A. baumannii* (at the top of this list) classified as a critical priority pathogen and vancomycin-resistant *Enterobacter faecium* and methicillin-resistant *S. aureus* classified as high priority pathogens (Tacconelli et al., 2018).

We have not ascertained the active component(s) responsible for inhibition of ESKAPE pathogens by *Streptomyces* sp. myrophorea, isolate McG1 as yet but this forms part of our ongoing research. Many *Streptomyces* species have the capacity to produce multiple antibiotics whose composition and identity can vary from species to species (Watve et al., 2001; Procopio et al., 2012). Given that our isolate encodes many antimicrobial gene clusters, it is entirely possible that some of these are responsible for the inhibition of ESKAPE pathogens. Given that our species is also novel and has the capacity to inhibit many multi-resistant pathogens also raises the possibility that some of its inhibitory components could be novel.

Another unexpected finding of the research was that although the pH of the Boho soil sample was around pH 8; our species of *Streptomyces* was able to grow at pH 10.5. This suggested not only tolerance of high alkaline conditions but the capacity to grow and divide in an extreme environments. More detailed tests will have to be made to ascertain the specifics of these optimal growth conditions.

The mechanism by which organisms such as *Streptomyces* can ameliorate high alkaline conditions is thought to be a product of a group of pH homeostasis genes, some of which

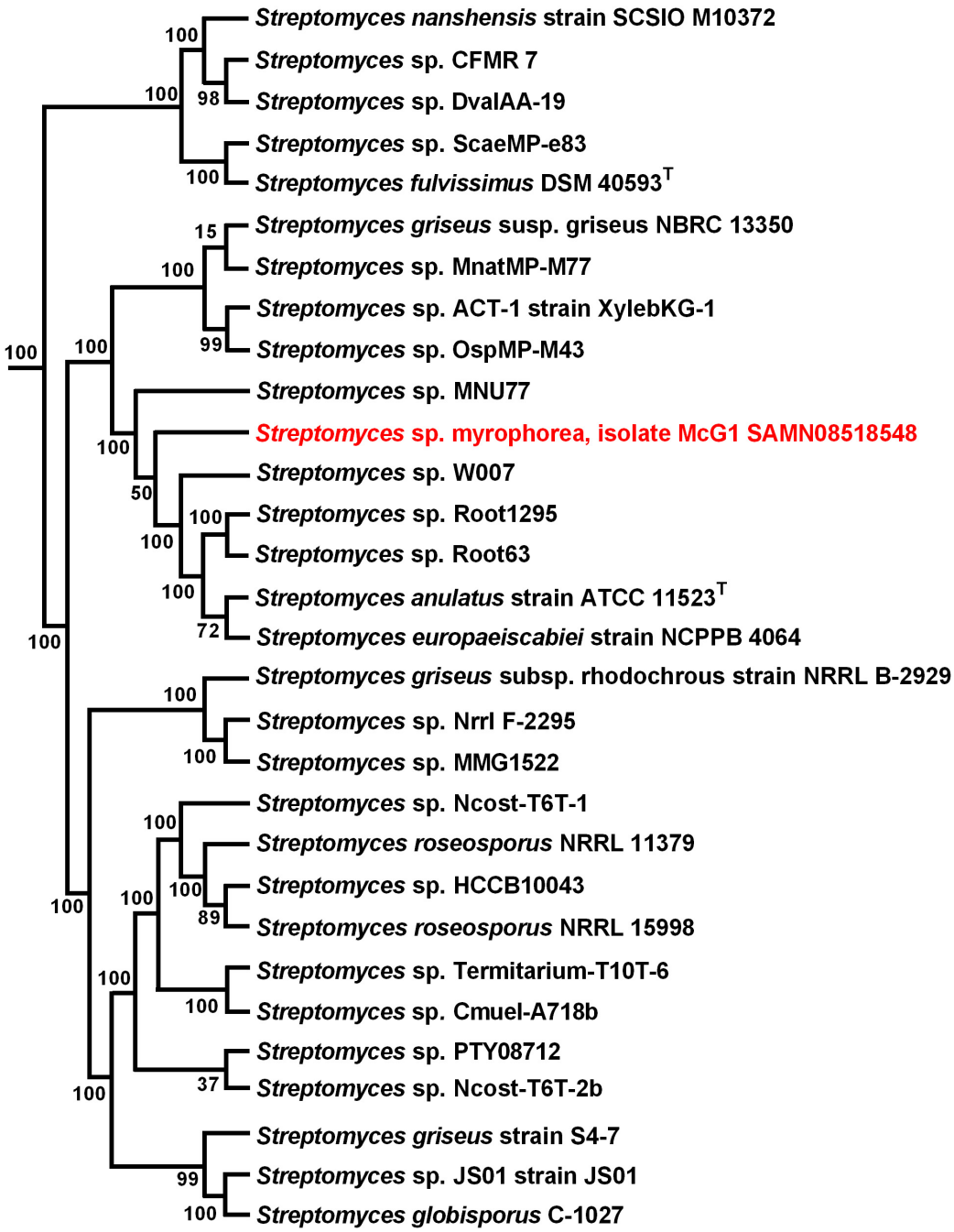

FIGURE 4 | Maximum-likelihood phylogenetic tree of *Streptomyces* sp. myrophorea, isolate McG1. Tree shows the phylogenetic relationships between the closest GGDC matches; constructed with PhyloPhlAn. The phylogenetic tree was drawn in Fasttree from a concatenated alignment of 400 protein sequences in PhyloPhlAn. Numbers at nodes represent bootstrap values.

have been identified in other species as alkaline shock genes, multidrug resistance factors (*mdt*/*mdfA*) and proton antiporters (*nhaA*) (Krulwich et al., 2011; Holdsworth and Law, 2013). Alkaline tolerance is also linked to the production of antibiotics through the presence of multidrug resistance factors which are often associated with antimicrobial biosynthesis gene clusters (Nodwell, 2007).

In support of our results, genome sequencing of *Streptomyces* sp. myrophorea, isolate McG1 revealed that it contained more annotated alkaline tolerance genes than *S. coelicolor* M145 (at 25/9). Furthermore alkaline shock genes, ammonium and aspartate antiporters and multidrug resistance antiporters of the type *mdt*H were only identified in the *Streptomyces* sp. myrophorea, isolate McG1 genome and not in *S. coelicolor* M145

TABLE 5 | The distribution of biosynthesis gene clusters in the *Streptomyces* sp. myrophorea, isolate McG1.

Gene type	From	To	Biosynthetic gene cluster (BGC)
Aminoglycoside	211467	235061	Streptomycin BGC (19%)
Bacteriocin	60075	71379	–
Bacteriocin	58414	69211	Tetronasin BGC (3%)
Butyrolactone	86467	97372	Coelimycin BGC (8%)
Ectoine	67460	77858	Ectoine BGC (100%)
Ladderane-Arylpolyene-NRPS	171438	299095	Skyllamycin BGC (46%)
Lantipeptide	97251	120571	–
Lantipeptide	49038	71665	AmfS BGC (100%)
Melanin	98889	109311	Melanin BGC (100%)
Melanin	466637	477122	Melanin BGC (100%)
NRPS	121282	183145	Arixanthomycin BGC (5%)
NRPS	45983	133910	Coelichelin_BGC (90%)
NRPS	139743	190212	Griseoviridin_/_viridogrisein_BGC (5%)
NRPS	105944	148690	A54145_BGC (3%)
NRPS	1	38617	Friulimicin BGC (12%)
Other KS	103777	144736	Salinilactam BGC (8%)
Siderophore	55548	70283	–
Siderophore	8280	20058	Desferrioxamine B BGC (100%)
TI PKS	244352	272539	Kirromycin BGC (5%)
TI PKS	27526	57767	Nystatin-like pseudonocardia polyene BGC (26%)
TI PKS	1	9188	–
TI PKS	1	7809	Piericidin A1 BGC (50%)
TI PKS	1	42606	Kendomycin BGC (25%)
TI PKS	1	5761	Cremimycin BGC (17%)
TI PKS	1	7661	Nanchangmycin BGC (30%)
TI PKS	1	5579	–
TI PKS	1	22496	Piericidin A1 BGC (50%)
TI PKS	595702	666824	Lidamycin BGC (41%)
TI PKS-Linaridin	1	37834	Cypemycin BGC (77%)
TI PKS-NRPS	212061	264613	Daptomycin BGC (7%)
TI PKS-NRPS	8668	63347	Enduracidin BGC (8%)
TI PKS-NRPS	483977	533453	SGR_PTMs BGC (100%)
TI PKS-other KS	86013	144228	Borrelidin BGC (18%)
TIII PKS	201579	242697	Herboxidiene BGC (6%)
TIII PKS	509840	550892	Alkylresorcinol_ BGC (100%)
Terpene	51484	72797	2-Methylisoborneol BGC (100%)
Terpene	33012	55225	–
Terpene	309196	335766	Hopene BGC (69%)
Terpene	314534	335541	–
Terpene-NRPS	362776	437437	Isorenieratene BGC (100%)
Terpene-TI-PKS	1	44677	BE-7585A BGC (23%)
Thiopeptide	5614	38302	–
Trans-AT-PKS-other KS	40047	120375	Daptomycin BGC (6%)
Trans AT-PKS-TI PKS-Other KS, NRPS	356818	421396	–

Biosynthesis gene clusters (%, indicates the proportion of genes showing similarity). TI PKS, Type I polyketide synthase; TIII PKS, Type III polyketide synthase; transAT-PKS, trans-amino transferase polyketide synthase; NRPS, non-ribosomal synthesized peptide; other KS, other ketide synthases.

genome. Indeed, it was this abundance of porters and the fragrant smell of the *Streptomyces* that prompted us to refer to the strain as myrophorea, isolate McG1, myro (Greek for fragrance) and phorea (Greek for porter).

The sequencing of the *Streptomyces* sp. myrophorea, isolate McG1 genome also enabled the prediction of potential antibiotics through anti-Smash and RAST (Aziz et al., 2008; Medema et al., 2011). However, given the cryptic nature of many *Streptomyces* spp. metabolites, it cannot be assumed these antibiotics are produced until their products are identified. We were also able to predict many antibiotic resistance clusters through RAST which are often associated with antimicrobial biosynthesis gene

TABLE 6 | Antibiogram of *Streptomyces* sp. myrophorea, isolate McG1.

Antibiotic	Amt (μg)	2 days	6 days
Amikacin	30	S	S
Ampicillin	20	R	R
Ampicillin + sulbactam	20	R	R
Augmentin	30	S	R
Apromycin	20	S	R
Carbenicillin	20	R	R
Cefepime	30	R	R
Ceftazidime	10	R	R
Ceftibuten	30	R	R
Cefoxitin	30	R	R
Ceftriaxone	30	R	R
Cefuroxime	30	R	R
Cefurin	5	R	R
Ciprofloxacin	5	I	R
Clavuranic acid	10	R	R
Ertapenem	10	R	R
Erythromycin	15	I	I
Gentamicin	10	S	S
Imipenem	10	S	R
Kanamycin	20	S	R
Linezolid	10	S	I
Meropenem	10	I	R
Mupiricin	200	R	R
Netilmicin	10	S	S
Nitrofurantoin	100	R	R
Novobiocin	5	S	R
Piperacillin + tazobactam	36	R	R
Quinpristin + dalropristin	5	R	R
Rifampicin	5	S	R
Streptomycin	20	R	R
Tigecycline	15	S	R
Tetracycline	20	R	R
Trimethoprim + sulfamethoxazole	25	R	R
Vancomycin	5	S	R

Streptomyces sp. myrophorea, isolate McG1 was cultivated with clinical antibiotics. An inhibitory zone greater than 12 mm diameter was considered sensitive (S) to these antibiotics, a zone between 12 and 8 mm or a few colonies scattered in the inhibition zone was considered intermediate (I) and a zone of 8 mm diameter or less was considered resistant (R).

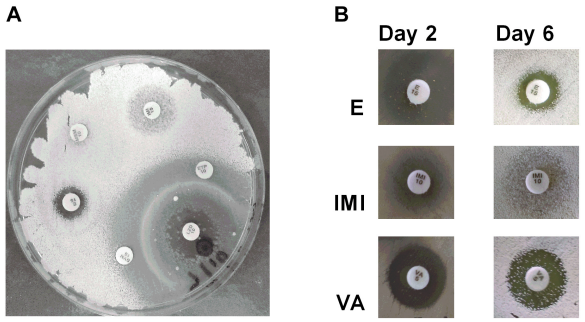

FIGURE 5 | Antibiogram of *Streptomyces* sp. myrophorea, isolate McG1. **(A)** *Streptomyces* sp. myrophorea, isolate McG1 cultivated on ISP-2 agar (6 days) in the presence of an array of clinical antibiotics starting at the top the image and moving clockwise: imipenem (IMI 10), ertapenem (ETP 10), linezolid (LZD 10), quinpristin + dalropristin (SYN 15), erythromycin (E 15) and meropenem (MEM 10). **(B)** Delayed development of antibiotic resistance in *Streptomyces* sp. myrophorea, isolate McG1 only became apparent for some antibiotics after 6 days incubation in the case of erythromycin (E-15 μg), imipenem (IMI-10 μg), and vancomycin (VA-5 μg). The full antibiogram list is available in **Table 6**.

clusters (Nodwell, 2007). Antimicrobial resistance predictions were followed by *in vitro* experiments on 36 clinical antibiotics. This data showed that *Streptomyces* sp. myrophorea, isolate McG1 was resistant to 28 out of 36 antibiotics. Specifically it was resistant to nearly all the β-lactams, with the exception of augmentin to which resistance developed after 6 days. The same pattern of delayed resistance was seen for glycopeptides, fluoroquinones (such as ciprofloxacin), and tetracyclines (such as tigecycline).

It is interesting that the ancient healers of Boho made a connection between alkaline soils (containing *Streptomyces* sp.) and (skin) infections. It has only recently been discovered that the pH of the specific infection sites can rise from normal skin pH about pH 5.5 to 8.5 and that bacterial biofilms, which can colonize wounds, can also reach similar pH levels (Schneider et al., 2007; Hostacka et al., 2010; Percival et al., 2014). Perhaps the indigenous people, who were undoubtedly in close proximity to the soil, noted (after many years) its curative properties under specific conditions. However, it is difficult to know the exact genesis of this cure because the previous occupants of the Boho site, the Druids, left no surviving records of healing and their Neolithic counterparts left only undeciphered carvings on some nearby stones. Anthropologically, the Boho folk tradition is similar to that of Kisameet Bay clay in Canada, another indigenous soil cure which was found to have inhibitory activity against a range of ESKAPE pathogens (Behroozian et al., 2016).

CONCLUSION

We have isolated and genome sequenced a novel alkaline and radio-tolerant species of *Streptomyces* from an ethnopharmacological soil cure; *Streptomyces* sp. myrophorea, isolate McG1. This *Streptomyces* sp. inhibits many multi-resistant ESKAPE pathogens including carbapenem-resistant *A. baumannii* (a critical priority species from the WHO priority list of antibiotic-resistant bacteria), vancomycin-resistant *E. faecium*, and methicillin-resistant *S. aureus* (listed as high priority by the WHO). Although not a complete elucidation of the antibacterial components of the Boho soil; we think that inhibition of such pathogens by *Streptomyces* sp. myrophorea, isolate McG1 may explain some of its reputed curative properties. It is hoped to further characterize some of these inhibitory components from *Streptomyces* sp. myrophorea, isolate McG1 and investigate the properties of other species contained in alkaline soil. We hope this will advance progress in stemming the tide of multi-resistant bacteria.

DATA AVAILABILITY

All datasets (GENERATED/ANALYZED) for this study are included in the manuscript and the **Supplementary Files**.

AUTHOR CONTRIBUTIONS

The idea for the isolation of extreme *Streptomyces* was an offshoot from the work of PD and LuT. Microbiology, strain growth, and testing were by GQ, LuT, DV, and IB. Genomic isolation and sequencing by AA and MH. Bioinformatics by PF, MH, PD, LiT, and AA. Imaging by SG and LF. Manuscript ideas and editing of relevant sections by all authors.

FUNDING

This study was supported in part by the Centre of Excellence for Bioprospecting, Ruđer Bošković Institute, Croatia, and from the kind donations of our collaborators at Swansea University and the University of Ulster.

ACKNOWLEDGMENTS

We would like to acknowledge the help of reviewers of this manuscript. We would also like to thank Dr. Marko Jelić, Zagreb University Hospital for Infectious Diseases for the provision of the ESKAPE pathogens; Igor Sajko of the Radiation Chemistry and Dosimetry Lab at the RBI for his help in γ-irradiation; Dr. Petar Mitrikeski, Zelimira Filić, and Ela Šarić for help with pH measurements and imaging; Fermanagh local historian, F. McHugh, Parish of Botha, church curator Rev. J. McPhillips for background information and permissions; Mary McGurn, Pat McGurn, Mary Egan, and Bridget Quinn for knowledge of locations and customs; Vale Romani for illustrations and Vasilios Theocharidis for consultations on Greek etymology.

SUPPLEMENTARY MATERIAL

The Supplementary Material for this article can be found online at: https://www.frontiersin.org/articles/10.3389/fmicb.2018.02458/full#supplementary-material

REFERENCES

Adamek, M., Spohn, M., Stegmann, E., and Ziemert, N. (2017). Mining bacterial genomes for secondary metabolite gene Clusters. *Methods Mol. Biol.* 1520, 23–47.

Auch, A. F., von Jan, M., Klenk, H.-P., and Göker, M. (2010). Digital DNA-DNA hybridization for microbial species delineation by means of genome-to-genome sequence comparison. *Stand. Genomic Sci.* 2, 117–134. doi: 10.4056/sigs.531120

Aziz, R. K., Bartels, D., Best, A. A., DeJongh, M., Disz, T., Edwards, R. A., et al. (2008). The RAST server: rapid annotations using subsystems technology. *BMC Genomics* 9:75. doi: 10.1186/1471-2164-9-75

Bankevich, A., Nurk, S., Antipov, D., Gurevich, A. A., Dvorkin, M., Kulikov, A. S., et al. (2012). SPAdes: a new genome assembly algorithm and its applications to single-cell sequencing. *J. Comput. Biol.* 19, 455–477. doi: 10.1089/cmb.2012.0021

Bauer, A. W., Kirby, W. M., Sherris, J. C., and Turck, M. (1966). Antibiotic susceptibility testing by a standardized single disk method. *Am. J. Clin. Pathol.* 45, 493–496. doi: 10.1093/ajcp/45.4_ts.493

Behroozian, S., Svensson, S. L., and Davies, J. (2016). Kisameet clay exhibits potent antibacterial activity against the eskape pathogens. *mBio* 7, e1842–e1815. doi: 10.1128/mBio.01842-15

Bolger, A. M., Lohse, M., and Usadel, B. (2014). Trimmomatic: a flexible trimmer for illumina sequence data. *Bioinformatics* 30, 2114–2120. doi: 10.1093/bioinformatics/btu170

Brunton, C. H. C., and Mason, T. R. (1979). Palaeoenvironments and correlation of the carboniferous rocks in West Fermanagh. Northern Ireland. *Bull. Br. Mus. Nat. Hist. Geol.* 32, 91–108.

Chenia, H. Y., and Jacobs, A. (2017). Antimicrobial resistance, heavy metal resistance and integron content in bacteria isolated from a South African tilapia aquaculture system. *Dis. Aquat. Organ.* 126, 199–209. doi: 10.3354/dao03173

Daly, M. J. (2012). Death by protein damage in irradiated cells. *DNA Repair.* 11, 12–21. doi: 10.1016/j.dnarep.2011.10.024

Daraktchieva, Z., Appleton, J. D., Rees, D. M., Adlam, K. A. M., Myers, A. H., Hodgson, S. A., et al. (2015). *Radon in Northern Ireland: Indicative Atlas.* Available at: https://www.gov.uk/government/publications/radon-indicative-atlas-for-northern-ireland

Donnelly, C., MacDonald, P., Murphy, E., and Beer, N. (2003). Excavations at boho high cross, toneel north, county fermanagh. *Ulst. J. Archaeol.* 62, 121–142.

Foley, R. (2015). Indigenous narratives of health: (Re)placing folk-medicine within irish health histories. *J. Med. Humanit.* 36, 5–18. doi: 10.1007/s10912-014-9322-4

Founou, R. C., Founou, L. L., and Essack, S. Y. (2017). Clinical and economic impact of antibiotic resistance in developing countries: a systematic review and meta-analysis. *PLoS One* 12:e0189621. doi: 10.1371/journal.pone.0189621

Gallachair, P. Ó. (1975). Clogherici: a dictionary of the catholic clergy of the diocese of clogher (1535-1835) (continued). *Clogher Rec.* 8, 271–280. doi: 10.2307/27695713

Gurevich, A., Saveliev, V., Vyahhi, N., and Tesler, G. (2013). QUAST: quality assessment tool for genome assemblies. *Bioinformatics* 29, 1072–1075. doi: 10.1093/bioinformatics/btt086

Halpin, A., and Newman, C. (2009). *Ireland: An Oxford Archaeological Guide to Sites from Earliest Times to AD 1600*. Oxford: Oxford Univ. Press.

Holdsworth, S. R., and Law, C. J. (2013). Multidrug resistance protein MdtM adds to the repertoire of antiporters involved in alkaline pH homeostasis in *Escherichia coli*. *BMC Microbiol.* 13:113. doi: 10.1186/1471-2180-13-113

Hostacka, A., Ciznar, I., and Stefkovicova, M. (2010). Temperature and pH affect the production of bacterial biofilm. *Folia Microbiol.* 55, 75–78. doi: 10.1007/s12223-010-0012-y

Janto, B., Ahmed, A., Ito, M., Liu, J., Hicks, D. B., Pagni, S., et al. (2011). The genome of alkaliphilic *Bacillus pseudofirmus* OF4 reveals adaptations that support the ability to grow in an external ph range from 7.5 to 11.4. *Environ. Microbiol.* 13, 3289–3309. doi: 10.1111/j.1462-2920.2011.02591.x

Jelic, M., Butic, I., Plecko, V., Cipris, I., Jajic, I., Bejuk, D., et al. (2016). KPC-Producing *Klebsiella pneumoniae* isolates in croatia: a nationwide survey. *Microb. Drug Resist.* 22, 662–667. doi: 10.1089/mdr.2015.0150

Jelic, M., Skrlin, J., Bejuk, D., Koscak, I., Butic, I., Guzvinec, M., et al. (2017). Characterization of isolates associated with emergence of OXA-48-producing *Klebsiella pneumoniae* in croatia. *Microb. Drug Resist.* 24, 973–979. doi: 10.1089/mdr.2017.0168

Jones, S. E., Ho, L., Rees, C. A., Hill, J. E., Nodwell, J. R., and Elliot, M. A. (2017). Streptomyces exploration is triggered by fungal interactions and volatile signals. *eLife* 6:e21738. doi: 10.7554/eLife.21738

Kontro, M., Lignell, U., Hirvonen, M.-R., and Nevalainen, A. (2005). pH effects on 10 *Streptomyces* spp. growth and sporulation depend on nutrients. *Lett. Appl. Microbiol.* 41, 32–38. doi: 10.1111/j.1472-765X.2005.01727.x

Krulwich, T. A., Sachs, G., and Padan, E. (2011). Molecular aspects of bacterial pH sensing and homeostasis. *Nat. Rev. Microbiol.* 9, 330–343. doi: 10.1038/nrmicro2549

Kung, S. H., Lund, S., Murarka, A., McPhee, D., and Paddon, C. J. (2018). Approaches and recent developments for the commercial production of semi-synthetic artemisinin. *Front. Plant Sci.* 9:87. doi: 10.3389/fpls.2018.00087

Lehrer, R. I., Rosenman, M., Harwig, S. S., Jackson, R., and Eisenhauer, P. (1991). Ultrasensitive assays for endogenous antimicrobial polypeptides. *J. Immunol. Methods* 137, 167–173. doi: 10.1016/0022-1759(91)90021-7

Lewis, K. (2013). Platforms for antibiotic discovery. *Nat. Rev. Drug Discov.* 12, 371–387. doi: 10.1038/nrd3975

Li, B., and Webster, T. J. (2018). Bacteria antibiotic resistance: new challenges and opportunities for implant-associated orthopaedic infections. *J. Orthop. Res.* 36, 22–32. doi: 10.1002/jor.23656

Maciejewska, M., Adam, D., Martinet, L., Naome, A., Calusinska, M., Delfosse, P., et al. (2016). A phenotypic and genotypic analysis of the antimicrobial potential of cultivable *Streptomyces* isolated from cave moonmilk deposits. *Front. Microbiol.* 7:1455. doi: 10.3389/fmicb.2016.01455

Mao, J., Tang, Q., Zhang, Z., Wang, W., Wei, D., Huang, Y., et al. (2007). *Streptomyces radiopugnans* sp. nov., a radiation-resistant actinomycete isolated from radiation-polluted soil in China. *Int. J. Syst. Evol. Microbiol.* 57, 2578–2582. doi: 10.1099/ijs.0.65027-0

Medema, M. H., Blin, K., Cimermancic, P., de Jager, V., Zakrzewski, P., Fischbach, M. A., et al. (2011). antiSMASH: rapid identification, annotation and analysis of secondary metabolite biosynthesis gene clusters in bacterial and fungal genome sequences. *Nucleic Acids Res.* 39, W339–W346. doi: 10.1093/nar/gkr466

Miller, M. A., Pfeiffer, W., and Schwartz, T. (2010). "Creating the CIPRES science gateway for inference of large phylogenetic trees," in *2010 Gateway Computing Environments Workshop (GCE)*, New Orleans, LA, 1–8. doi: 10.1109/GCE.2010.5676129

Mohammadipanah, F., and Wink, J. (2015). Actinobacteria from arid and desert habitats: diversity and biological activity. *Front. Microbiol.* 6:1541. doi: 10.3389/fmicb.2015.01541

Nguyen, T. M., and Kim, J. (2015). Antifungal and antibacterial activities of *Streptomyces polymachus* sp. nov. Isolated from soil. *Int. J. Syst. Evol. Microbiol.* 65, 2385–2390. doi: 10.1099/ijs.0.000268

Nkanga, E. J., and Hagedorn, C. (1978). Detection of antibiotic-producing streptomyces inhabiting forest soils. *Antimicrob. Agents Chemother.* 14, 51–59. doi: 10.1128/AAC.14.1.51

Nodwell, J. R. (2007). Novel links between antibiotic resistance and antibiotic production. *J. Bacteriol.* 189, 3683–3685. doi: 10.1128/JB.00356-07

Noomnual, S., Thasana, N., Sungkeeree, P., Mongkolsuk, S., and Loprasert, S. (2016). Streptanoate, a new anticancer butanoate from *Streptomyces* sp. DC3. *J. Antibiot.* 69, 124–127. doi: 10.1038/ja.2015.95

Percival, S. L., McCarty, S., Hunt, J. A., and Woods, E. J. (2014). The effects of pH on wound healing, biofilms, and antimicrobial efficacy. *Wound Repair Regen.* 22, 174–186. doi: 10.1111/wrr.12125

Procopio, R. E., Silva, I. R., Martins, M. K., Azevedo, J. L., and Araújo, J. M. (2012). Antibiotics produced by *Streptomyces*. *Braz. J. Infect. Dis.* 16, 466–471. doi: 10.1016/j.bjid.2012.08.014

Santajit, S., and Indrawattana, N. (2016). Mechanisms of antimicrobial resistance in ESKAPE pathogens. *Biomed Res. Int.* 2016:2475067. doi: 10.1155/2016/2475067

Sato, M., Beppu, T., and Arima, K. (1983). Studies on antibiotics produced at high alkaline pH. *Agric. Biol. Chem.* 47, 2019–2027. doi: 10.1080/00021369.1983.10865910

Schatz, A., Bugie, E., and Waksman, S. (1944). Streptomycin: a substance exhibiting antibiotic activity against gram-positive and gram-negative bacteria. *Proc. Soc. Exp. Biol. Med.* 55, 66–69. doi: 10.3181/00379727-55-14461

Schneider, L. A., Korber, A., Grabbe, S., and Dissemond, J. (2007). Influence of pH on wound-healing: a new perspective for wound-therapy? *Arch. Dermatol. Res.* 298, 413–420. doi: 10.1007/s00403-006-0713-x

Seemann, T. (2014). Prokka: rapid prokaryotic genome annotation. *Bioinformatics* 30, 2068–2069. doi: 10.1093/bioinformatics/btu153

Segata, N., Bornigen, D., Morgan, X. C., and Huttenhower, C. (2013). PhyloPhlAn is a new method for improved phylogenetic and taxonomic placement of microbes. *Nat. Commun.* 4:2304. doi: 10.1038/ncomms3304

Tacconelli, E., Carrara, E., Savoldi, A., Harbarth, S., Mendelson, M., Monnet, D. L., et al. (2018). Discovery, research, and development of new antibiotics: the WHO priority list of antibiotic-resistant bacteria and tuberculosis. *Lancet Infect. Dis.* 18, 318–327. doi: 10.1016/S1473-3099(17)30753-3

Tiago, I., Chung, A. P., and Veríssimo, A. (2004). Bacterial diversity in a nonsaline alkaline environment: heterotrophic aerobic populations. *Appl. Environ. Microbiol.* 70, 7378–7387. doi: 10.1128/AEM.70.12.7378-7387.2004

Watve, M. G., Tickoo, R., Jog, M. M., and Bhole, B. D. (2001). How many antibiotics are produced by the genus *Streptomyces*? *Arch. Microbiol.* 176, 386–390. doi: 10.1007/s002030100345

Yokomizo, K., Miyamoto, Y., Nagao, K., Kumagae, E., Habib, E. S., Suzuki, K., et al. (1998). Fattiviracin A1, a novel antiviral agent produced by *Streptomyces microflavus* strain No. 2445. II. Biological properties. *J. Antibiot.* 51, 1035–1039. doi: 10.7164/antibiotics.51.1035

Yucel, S., and Yamac, M. (2010). Selection of *Streptomyces* isolates from turkish karstic caves against antibiotic resistant microorganisms. *Pak. J. Pharm. Sci.* 23, 1–6.

Conflict of Interest Statement: The authors declare that the research was conducted in the absence of any commercial or financial relationships that could be construed as a potential conflict of interest.

frontiers in Microbiology

ORIGINAL RESEARCH
published: 18 December 2018
doi: 10.3389/fmicb.2018.03141

Genomic and *in-situ* Transcriptomic Characterization of the Candidate Phylum NPL-UPL2 From Highly Alkaline Highly Reducing Serpentinized Groundwater

Shino Suzuki[1,2,3]*, *Kenneth H. Nealson*[3] and *Shun'ichi Ishii*[2,4]

[1] *Kochi Institute for Core Sample Research, Japan Agency for Marine-Earth Science and Technology, Nankoku, Japan,* [2] *Department of Microbial and Environmental Genomics, J. Craig Venter Institute, La Jolla, CA, United States,* [3] *Department of Earth Sciences, University of Southern California, Los Angeles, CA, United States,* [4] *R&D Center for Submarine Resources, JAMSTEC, Nankoku, Japan*

OPEN ACCESS

Edited by:
Masahiro Ito,
Toyo University, Japan

Reviewed by:
William J. Brazelton,
University of Utah, United States
Jeremy Dodsworth,
California State University,
San Bernardino, United States
Gaël Erauso,
Aix-Marseille Université, France

***Correspondence:**
Shino Suzuki
sisuzuki@jamstec.go.jp

Specialty section:
This article was submitted to Extreme Microbiology, a section of the journal Frontiers in Microbiology

Received: *29 August 2018*
Accepted: *04 December 2018*
Published: *18 December 2018*

Citation:
Suzuki S, Nealson KH and Ishii S (2018) Genomic and in-situ Transcriptomic Characterization of the Candidate Phylum NPL-UPL2 From Highly Alkaline Highly Reducing Serpentinized Groundwater. Front. Microbiol. 9:3141. doi: 10.3389/fmicb.2018.03141

Serpentinization is a process whereby water interacts with reduced mantle rock called peridotite to produce a new suite of minerals (e.g., serpentine), a highly alkaline fluid, and hydrogen. In previous reports, we identified abundance of microbes of the candidate phylum NPL-UPA2 in a serpentinization site called The Cedars. Here, we report the first metagenome assembled genome (MAG) of the candidate phylum as well as the *in-situ* gene expression. The MAG of the phylum NPL-UPA2, named Unc8, is only about 1 Mbp and its biosynthetic properties suggest it should be capable of independent growth. In keeping with the highly reducing niche of Unc8, its genome encodes none of the known oxidative stress response genes including superoxide dismutases. With regard to energy metabolism, the MAG of Unc8 encodes all enzymes for Wood-Ljungdahl acetogenesis pathway, a ferredoxin:NAD^+ oxidoreductase (Rnf) and electron carriers for flavin-based electron bifurcation (Etf, Hdr). Furthermore, the transcriptome of Unc8 in the waters of The Cedars showed enhanced levels of gene expression in the key enzymes of the Wood-Ljungdahl pathway [e.g., Carbon monoxide dehydrogenase /Acetyl-CoA synthase complex (CODH/ACS), Rnf, Acetyl-CoA synthetase (Acd)], which indicated that the Unc8 is an acetogen. However, the MAG of Unc8 encoded no well-known hydrogenase genes, suggesting that the energy metabolism of Unc8 might be focused on CO as the carbon and energy sources for the acetate formation. Given that CO could be supplied via abiotic reaction associated with deep subsurface serpentinization, while available CO_2 would be at extremely low concentrations in this high pH environment, CO-associated metabolism could provide advantageous approach. The CODH/ACS in Unc8 is a Bacteria/Archaea hybrid type of six-subunit complex and the electron carriers, Etf and Hdr, showed the highest similarity to those in Archaea, suggesting that archaeal methanogenic energy metabolism was incorporated into the bacterial acetogenesis in NPL-UPA2. Given that serpentinization systems are viewed as potential habitats for early

life, and that acetogenesis via the Wood-Ljungdahl pathway is proposed as an energy metabolism of Last Universal Common Ancestor, a phylogenetically distinct acetogen from an early earth analog site may provide important insights in primordial lithotrophs and their habitat.

Keywords: serpentinization, metagenome, acetogen, last universal common ancestor, alkaliphile ecology, subsurface microbial community, metatranscriptome, carbon monoxide dehydrogenase

INTRODUCTION

It is an honor to take part in this issue reminding us of the many accomplishments of Professor Koki Horikoshi in the world of alkaliphiles (Horikoshi, 1971, 1996, 1999; Kudo, 2016). We discuss here properties of a member of an undescribed phylum of bacteria that we propose naming after Professor Horikoshi. The metagenome assembled genome (MAG) of the bacteria was recovered from The Cedars, an ancient and widespread environment called a serpentinization site (Schulte et al., 2006; Sleep et al., 2011; Sleep, 2018), where highly alkaline (pH $\geq$ 11.5) anoxic strongly reducing water (E_h = −900 to −500 mV) is produced by geological processes (Morrill et al., 2013; Schrenk et al., 2013; Suzuki et al., 2017). The properties we discuss here are inferred from analysis of the gene content of the MAG of Unc8, as well as examination of the *in situ* transcribed genes of Unc8.

Having environmentally relevant microbes in culture is beneficial for microbiology; genomic, transcriptomic and proteomic analyses, when coupled to physiological data can reveal how microorganisms interact with their environment and other microorganisms, thus defining the ecophysiology of the microorganisms and their interactions (Strous et al., 2006; Ettwig et al., 2010; Suzuki et al., 2014; Laso-Perez et al., 2016; McGlynn, 2017; Kato et al., 2018). However, cultivation of environmentally relevant microbes is not always possible, and one is left with the challenge of piecing together the metabolic roles of the microbes using molecular approaches. Improvement of sequencing technologies and the development of bioinformatic techniques have enabled the recovery of high-quality genomes from environmental metagenomes, making it possible to address potential microbial function(s) and roles in the natural ecosystem (Wrighton et al., 2012; Hug et al., 2013; Ishii et al., 2013; Suzuki et al., 2017; Ishii et al., 2018; Probst et al., 2018; Woodcroft et al., 2018).

Recent studies based on MAGs have revealed unprecedented insights into microbial diversity, including the identification of "Candidate Phyla Radiation" (CPR), with entire phyla having significantly reduced genomes that lack many of the genes responsible for biosynthesis and energy metabolism (Brown et al., 2015; Anantharaman et al., 2016; Suzuki et al., 2017; Castelle and Banfield, 2018), and the identification of distributed methane-producing potential in not only the *Euryarchaeota* but in the *Bathyarchaeota* and the *Verstraetearchaeota* (Evans et al., 2015; Vanwonterghem et al., 2016). All those facts have demonstrated that a wealth of evidence of unrecognized microbial diversity may lie buried in the genomes of these uncultivated microorganisms.

We report here the study of the MAG of one of these candidate phyla, NPL-UPA2, in the domain Bacteria. While the initial MAG named Unc8 was retrieved from the metagenome of highly alkaline springs at The Cedars serpentinization site in our previous studies (Morrill et al., 2013; Suzuki et al., 2013, 2017), detail of the metabolic capabilities has not been analyzed. In this study, in order to illustrate the potential metabolic and physiological features of the undescribed phylum NPL-UPA2, we have refined the MAG of Unc8 with additional sequencing and bioinformatics efforts and analyzed the gene expression profile in The Cedars springs. Analyses of the MAG of Unc8 and the transcriptome of natural communities in The Cedars springs suggested that acetogenesis via the Wood-Ljungdahl pathway is the key energy metabolism of this organism. Although serpentinization systems are viewed as potential habitats for early life and the acetogenesis via the Wood-Ljungdahl pathway is proposed as an energy metabolism of primordial lithotrophs, genomic and physiological features of acetogens inhabiting serpentinization sites remain undescribed; thus, the understanding may contribute to idenify the life strategies of primordial acetogens and their habitats.

MATERIALS AND METHODS

Sample Collection

Microbial samples were collected from two different hyperalkaline springs in The Cedars active serpentinization site, BS5sc (elevation 282 m, N: 38°37.282', W: 123°7.987') that is a source water of BS5 spring (Suzuki et al., 2013) and Grotto Pool Spring 1 (GPS1) (elevation 273 m, N: 38°37.268' W: 123°8.014'), by using 0.22 μm in-line filters (Millipore) as described previously (Suzuki et al., 2017). For GPS1 spring, approximately 1000 L of spring water was collected in 2011 and 2012 (Suzuki et al., 2017), while approximately 200 L of spring water was collected for BS5sc in 2014. The filtered cells were immediately frozen with dry ice at each sampling site and kept at dry ice temperature during the transportation. The samples were stored in -80°C in our lab until the DNA and RNA are extracted.

DNA and RNA Sequencing

Both DNA and RNA were coextracted using a MObio PowerBiofilm RNA Isolation Kit (MO BIO, San Diego, CA, United States) as described previously (Suzuki et al., 2017). The extracted total nucleic acids were eluted in nuclease free water and separated into DNA and RNA using AllPrep DNA/RNA Mini Kit (Qiagen, Germantown, MD, United States). A DNA library of the GPS1 sample was prepared and sequenced as described previously (Suzuki et al., 2017). A DNA library of the BS5sc sample for NGS was prepared from 1 ng DNA using

the Nextera XT library preparation Kit (Illumina, San Diego, CA, United States) according to the manufacturer's protocol. Total RNAs from both GPS1 and BS5sc samples were treated with Turbo DNA free kit (Thermo Fisher Scientific, Waltham, MA, United States) for the complete removal of contaminating DNA. DNase-treated total RNA samples were directly applied for library construction by using ScriptSeq v2 (Illumina, San Diego, CA, United States) without rRNA removal step to avoid unnecessarily bias.

The DNAs were separately sequenced using Illumina HiSeq2000 platform (Illumina, San Diego, CA, United States) as the 101 bp PE for GPS1 samples and as the 151 bp PE for BS5sc samples by Illumina's standard protocol. The DNA sequences of GPS1 sample have already been deposited in the NCBI Short Read Archive (SRA) under accession numbers DRX086601 and DRX086602, while newly sequenced metagenomic reads from the BS5sc sample was deposited in the SRA under accession number SRX5014375. RNAs from GPS1 and BS5sc samples were sequenced using Illumina HiSeq2000 platform (Illumina, San Diego, CA, United States) as the 101 bp PE for GPS1 sample and as the 151 bp PE for BS5sc sample by Illumina's standard protocol. Read stats of DNA and RNA sequences are shown in **Supplementary Table S1**.

Metagenomic reads from biofilm of hydrothermal field in Prony Bay (SRA; SRS734862 and SRS734863) were used for *de novo* assembly of CLC Genomic Workbench v8.6 (CLCbio, Boston, MA, United States) with default parameters.

Genome Refinement of Unc8

A MAG of NPL-UPA2 bacterium Unc8, recovered from the GPS1-2012 metagenome (Suzuki et al., 2017), was used as a template for the further genome refinement in this study. The contaminated scaffolds in the MAG were removed by using differential coverage plots between GPS1 metagenomes and the new BS5sc metagenome (Albertsen et al., 2013; Ishii et al., 2013). The cross-read mapping analyses were run using Map Reads to Reference algorism in CLC Genomics Workbench (version 8.5) with the settings as 0.7 of minimum length and 0.95 of minimum similarity fractions. The scaffolds of MAG Unc8 were then cleaved to contigs at the gap regions. The potential connections of contigs were analyzed by Collect Paired Read Statistics tool in CLC Genome Finishing Module (CLCbio, Boston, MA, United States). The analysis allowed to remove wrong contigs included in the MAG Unc8 (Albertsen et al., 2013). Based on the potential connections, the contigs were manually connected by using Align Contigs tool after the extension of contig edge by using Extend Contig tool in CLC Genome Finishing Module. After the manual curation, in order to polish contigs, metagenomic reads of GPS1 2011 and 2012 were mapped to the contigs with the settings as 0.7 of minimum length and 0.95 of minimum similarity fractions, and the consensus sequences were extracted. The refined MAG Unc8 was deposited in NCBI under Biosample SAMN06718453.

To obtain the minimum information about a MAG (miMAG) proposed by Genomic Standards Consortium (Bowers et al., 2017), genome completeness and contamination were analyzed by using CheckM software (Parks et al., 2015) on KBase (Arkin et al., 2018). The numbers of tRNA and rRNA were counted by using NCBI prokaryotic genome annotation pipeline (Tatusova et al., 2016). The genome quality classification was assigned from miMAG criteria (Bowers et al., 2017).

A BLAST Ring image generator (BRIG) (Alikhan et al., 2011) was employed for visualizing a genome as a circular image and for comparison between the MAG Unc8 from The Cedars spring and the metagenomic contigs of ST09 from Prony Bay hydrothermal field (Mei et al., 2016). The total DNA and RNA reads of BS5sc spring were separately mapped to the Unc8 contigs by using CLC Genomics Workbench with the settings as 0.5 of minimum length and 0.95 of minimum similarity fractions. From the SAM files of the read mapping, coverage graph was generated in the BRIG software, and the coverage graph of the RNA reads were normalized by the coverage graph of the DNA reads.

Functional Annotation

Metagenome assembled genome of Unc8 was processed in NCBI prokaryotic genome annotation pipeline for open reading frame (ORF) calling and functional annotation (Tatusova et al., 2016). For the KEGG orthologous (KO) group assignment for each ORF, we used the KEGG Automatic Annotation Server (KAAS) with the SBH (single-directional best hit) method set to 37 as the threshold assignment score (Moriya et al., 2007). ORFs were assigned to the Clusters of Orthologous Groups of proteins (COGs) by the best BLAST hit to the reference data (Galperin et al., 2015) using an *e*-value cutoff of $1e^{-6}$. Localization of the proteins was analyzed by prediction of transmembrane helices in TMHMM server version 2.0 (Krogh et al., 2001), and PSORTb version 3.0.2 (Yu et al., 2010). Taxonomic assignment of each ORF was analyzed by using GhostKOALA (Kanehisa et al., 2016). Microbial cell activity-, biogenesis, and metabolisms-associated marker genes were selected from the KEGG module or KEGG pathway databases and analyzed as described previously (Ishii et al., 2015; Suzuki et al., 2017; Ishii et al., 2018). Protein abbreviations used in this study are summarized in **Supplementary Table S2**.

Read Mapping of Raw Reads to ORFs

RPKM (Reads Per Kilobase per Million mapped reads) values (Mortazavi et al., 2008) for both DNA and mRNA samples were separately generated by the RNA-Seq Analysis pipeline in CLC Genomics Workbench (version 8.6), and used for analyzing ORF frequency (DNA-RPKM) and gene expression levels (mRNA-RPKM). The Unc8 ORFs were used as references, and read mapping was conducted using 0.5 as the minimum length and 0.95 as the minimum similarity fractions. The calculated median of the DNA-RPKM for each sample was used to normalize the related mRNA-RPKM values for each sample.

Phylogenetic Tree Analyses

Amino acid sequences of CdhA, CdhB, CdhC, CdhE/AcsC, CedD/AcsD, AcsE in the Unc8 MAG were blasted against nr database. Twenty closest amino acid sequences were retrieved from the database for applying the tree construction. MUSCLE (Edgar, 2004) and Maximum Likelihood with RaxML

(Stamatakis et al., 2008) were used for the sequence alignment and tree construction, respectively.

RESULTS AND DISCUSSION

Genome Quality of the MAG of the Cedars NPL-UPA2

In our previous study, the MAG of Unc8 was recovered from the two different metagenomic assemblies delivered from the two different years' samples (2011 and 2012) of GPS1 at The Cedars (Suzuki et al., 2017). The MAG of Unc8 was constituted with 166 scaffolds and 291 contigs. In this study, the MAG was further refined with the assembled data of the other spring (BS5sc), and the genome size now became 996,215 bp consisting of only 24 contigs (**Table 1** and **Supplementary Figure S1**). Genome completeness was 87.6% estimated by the Check M with the Bacterial marker linkage (Parks et al., 2015). MAG criteria for the high-quality genome are (1) over 90% of the completeness, (2) a less than 5% contamination, (3) multiple fragments where gaps span repetitive regions, (4) the presence of the 23S, 16S and 5S rRNA genes and (5) at least 18 tRNAs. The MAG of Unc8 meets the criteria except for that of over 90% completeness (87.6%). Thus, the MAG of Unc8 is a middle-quality draft genome (**Table 1**). However, it is likely that the NPL-UPA2 has a genome lacking a number of the single copy marker genes listed in the bacterial marker linkage from the genome as is often seen in the genomes of other candidate divisions (Suzuki et al., 2017), and if this is the case, the quality should be very close to that of a high-quality draft genome, and the MAG of Unc8 may well be appropriate for further genomic and transcriptomic investigation.

TABLE 1 | MAG criteria and genome stats for Unc8.

General genome metadata currently not in MIGS	
Analysis project type	Metagenome-assembled genome (MAG)
Taxa id	16S rRNA gene (KC574886)
Assembly software	CLC Genomics Workbench 8.6
Annotation	NCBI Prokaryotic Genome Annotation Pipeline (PGAP)
Genome quality	
Assembly quality	Nearly High-Quality Draft
Completeness score	87.60%
Contamination score	2.43%
Completeness software	checkm
Number of contigs	24
16S recovered	Yes
16S recovery software	rnammer
Number of standard tRNAs extracted	20
tRNA extraction software	trnascan-se
Completeness approach	Marker gene based
MAG metadata	
Bin parameters	Coverage + broken pair mates
Binning software	Differential Coverage plots (by hand)
	CLC Genome Finishing Module
Reassembly post binning	Yes
MAG coverage software	CLC Genomics Workbench 8.6
Genome stats	
Genome size	996,215 bp
Number of contigs	24
N50	77,401 bp
Frequency in GPS1 (2011)	×34.6 (0.9%)
Frequency in GPS1 (2012)	×31.1 (0.8%)
Frequency in BS5sc (2014)	×48.1 (0.8%)
BioProject	PRJNA351917
BioSample	SAMN06718453
CDS (coding)	985
Complete rRNAs	1, 1, 1 (5S, 16S, 23S)
tRNAs	43
ncRNAs	2
Pseudo Genes (total)	18
Potential membrane associated proteins	181

Phylogeny and the Environmental Distribution of NPL-UPA2

Members of the candidate phylum NPL-UPA2 have been detected in a variety of different environments, including the oceanic subsurface sediment (Hoshino et al., 2011), deep-sea anoxic brines (Guan et al., 2015), crustal fluids (Huber et al., 2006) and subterranean serpentinization sites (Brazelton et al., 2006; Postec et al., 2015) (**Figure 1**). The 16S rRNA genes recovered from the three serpentinization sites, Lost City (Brazelton et al., 2006), Prony Bay (Postec et al., 2015) and The Cedars (Suzuki et al., 2013) group together as a clade in the phylogenetic tree. In general, members of this phylum were detected as rare members of the respective communities. Relatively abundant populations of NPL-UPA2 have been reported only at the shallow marine serpentinizing Prony Hydrothermal Field (13.8%) (Postec et al., 2015) and the deep groundwater of the continental serpentinizing site The Cedars (4%) (Suzuki et al., 2013).

Geochemical studies of The Cedars springs revealed that the site has two different serpentinized water sources, a deep source that interacts with peridotite body as well as km-deep marine sediments, and a shallow source that interacts only with the overlying peridotite (Morrill et al., 2013; Suzuki et al., 2013). Considering that the Unc8 is associated with The Cedars deep groundwater which is influenced by the subducted oceanic plate below the peridotite body, and that other members of this phylum are also associated with marine subsurface environments (Brazelton et al., 2006; Huber et al., 2006; Hoshino et al., 2011; Guan et al., 2015; Postec et al., 2015), it may well be that such marine, subsurface, anoxic, highly reducing environments define the habitat of the phylum NPL-UPA2.

Habitat of Unc8 and Its Closest Relative in the Phylum NPL-UPA2

The MAG of Unc8 within the phylum NPL-UPA2 was recovered from the metagenomic sequences of The Cedars serpentinized spring and further refined in this study. Serpentinization is

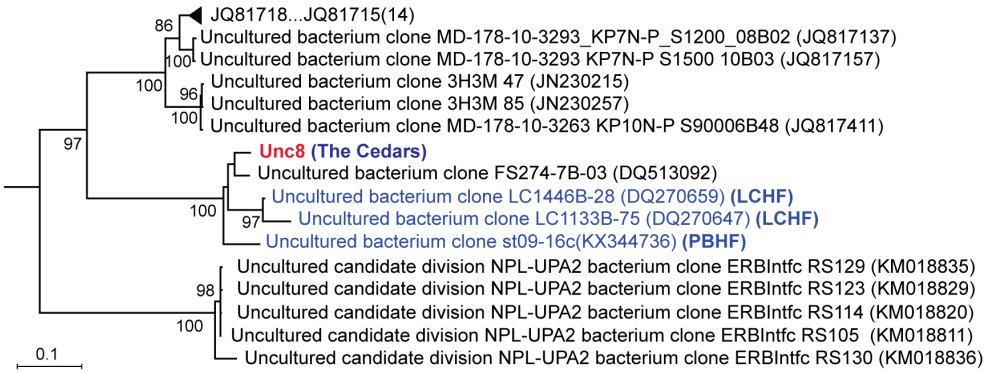

FIGURE 1 | Phylogenetic relationships among NPL-UPA2 16S rRNA genes. Tree topologies are supported by bootstrap values for 100 replicates. Red font denotes the Unc8 from The Cedars and blue font denotes phylotypes recovered from the serpentinization sites; Lost City hydrothermal field (LCHF) and Prony Bay hydrothermal field (PBHF). Accession numbers of OTU included in the triangle region are JQ816227, GU553753, JQ817159, JN676031, JX000976, JQ817187, JQ817075, JQ816462, JQ817138, JQ816442, JN230011, EU385719, JQ816456 and JQ818038. Ca. *Desulforudis audaxviator* was root of the tree.

a process whereby water interacts with ultramafic minerals (e.g., peridotite) delivered from the Earth's mantle to produce a new suite of rock (e.g., serpentinite) (Schrenk et al., 2013). The reaction results in the oxidation of ferrous iron from olivine and pyroxene minerals in the peridotite with molecular hydrogen being produced during the oxidation process. The hydrogen and carbon dioxide present in the system are thought to react under the highly reducing and alkaline conditions through Fischer-Tropsch Type (FTT) synthesis, leading to the formation of methane and hydrocarbons and the concomitant production of carbon monoxide, formate, formaldehyde and methanol (McCollom and Seewald, 2001; McCollom and Seewald, 2007; Schrenk et al., 2013). Since the reduced compounds in the fluid can support microbial energy metabolisms, an energy-rich fluid containing organic carbon could be a favorable habitat for life. However, studies of deep fluids in serpentinized setting have shown that these ecosystems host extremely low-abundance microbial communities (Brazelton et al., 2012; Suzuki et al., 2013; Tiago and Verissimo, 2013), which is attributed to: (1) the highly alkaline condition of the fluid; (2) the extremely low concentrations of oxidants (electron acceptors); and, (3) the low levels of nutrients (available carbon and phosphate).

The Cedars is an active terrestrial serpentinization site located in northern California (Morrill et al., 2013). While there are about a hundred of springs in The Cedars area with a variety of differences in geochemistry, spring waters discharged from The Cedars generally have extremely high pH (11–12), very low E_h (-900—550 mV) values and are rich in Ca^{2+} (∼1 mM), hydrogen and methane gas, and contain low levels of dissolved organic carbon, total inorganic carbon, ammonium, phosphate and electron acceptors (oxygen, nitrate, sulfate) (Morrill et al., 2013; Suzuki et al., 2013).

Comparison of the contigs assembled from the Prony Bay metagenome (Mei et al., 2016) revealed high similarity to the MAG of Unc8, suggesting that Unc8-like microbe(s) are present in the Prony Bay Hydrothermal Field and may share similar evolutionary histories with Unc8 (**Figure 2**). The Prony Bay Hydrothermal Field is also an active site of serpentinization but at the seafloor in a shallower lagoonal environment (Monnin et al., 2014). Fluids discharged from the Prony Bay are the high-pH fluids (pH = ∼10.5) rich in H_2 and CH_4. While the outlet of the fluid is located in the seafloor, the high-pH fluid is of meteoric origin.

Biosynthesis, Stress Response, Motility, Transporters and Thermophily of the Unc8

While the MAG size of Unc8 is small, only about 1 Mbp, it encodes complete biosynthetic pathways for amino acids, nucleic acids, lipids, lipopolysaccharide and peptidoglycan, suggesting that Unc8 is capable of living independently (**Supplementary Data S2B**). Diverse inorganic ion transporters are also encoded (**Supplementary Data S1**), including the ABC type phosphate (PstABCS), iron (FepBDC), tungstate (TupABC) and cobalt/nickel (CbiOQML) transporters, Ca^{2+}/Na^{+} antiporter (YrbG), potassium uptake system (TrkAH), magnesium transporter (MgtE) and multisubunit Na^{+}/H^{+} antiporter complex (MrpEFGBBBCD, MrpDD) (**Figure 3**). Protein abbreviations are summarized in **Supplementary Table S2**. Since the Mrp complex is involved with the maintenance and homeostasis of the cytosolic pH (Ito et al., 2017), one expects it to be important for life in the highly alkaline environment. High level of expression was seen in the genes for the YrbG (Besserer et al., 2012) and PstS (Liu et al., 1998) in both springs, implying that Unc8 is managing against the extremely alkaline and low phosphate condition occurring at the setting (**Figure 4**). Other than the inorganic ion transporting system, the MAG of Unc8 encodes only three other transport systems (basic amino acid/polyamine antiporter, biopolymer transport protein, glycoside/pentoside/hexuronide:cation symporter) This paucity of transporters is curious, but may suggest that the Unc8 is incapable of importing organic/inorganic carbon from the environment via transporters. Except for genes coding for type VI pili, no motility-related genes (flagellum chemotaxis) were encoded (**Supplementary Data S1**).

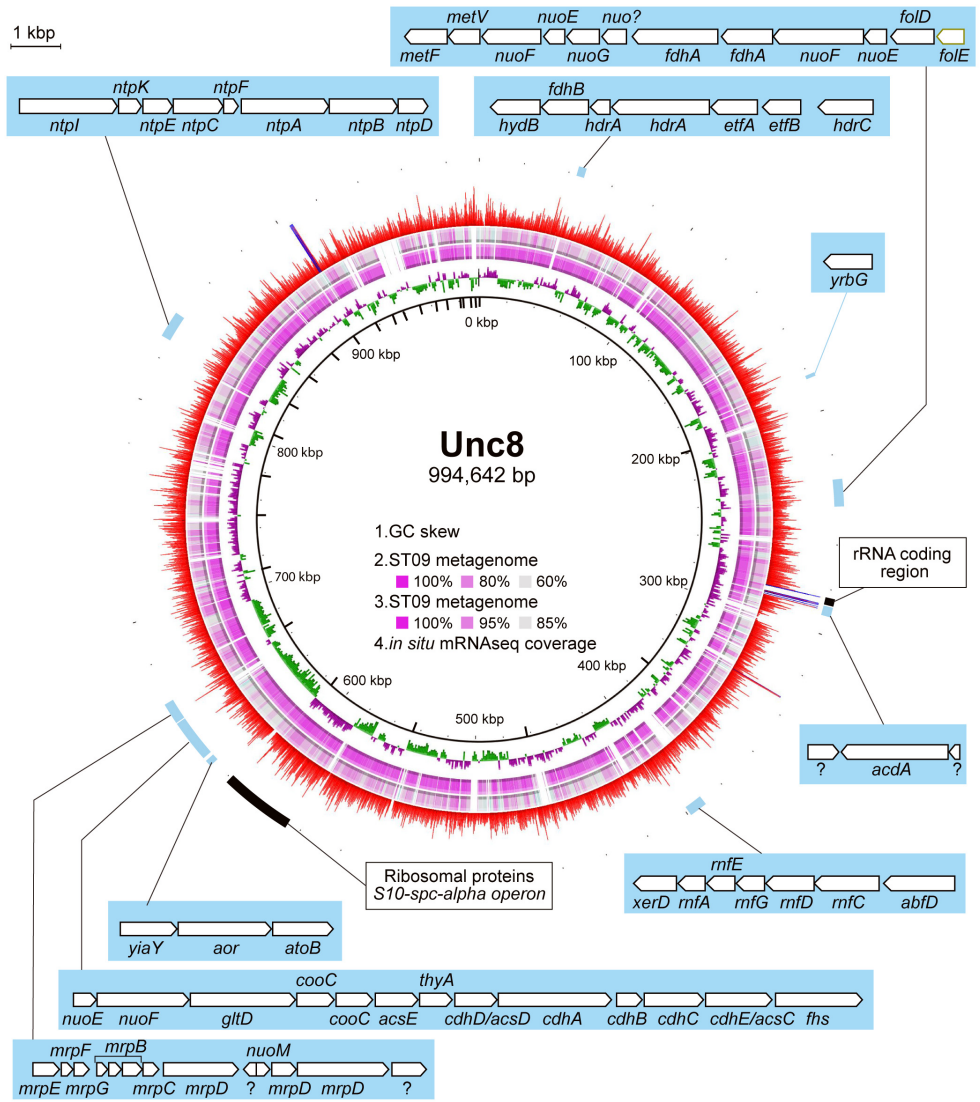

FIGURE 2 | MAG of Unc8 with key genes highlighted. The inner scales designate the coordinates (in kbp). The first (inner-most) circle shows the GC-skew. The second and third circles show the blastn analysis against the Prony Bay metagenome with different similarity cutoff. The lower and upper identity threshold in the blastn analysis is shown in the circle. The fourth circle shows the gene expression level (RNA reads normalized by the DNA reads) in BS5sc. The locations of some genes of interest are indicated.

Notably, oxidative stress response genes (catalase and superoxide dismutase) are absent on the genome of Unc8 (oxidative stress section in **Supplementary Data S2A**). Since many anaerobic bacteria and archaea are known to have superoxide dismutases to provide protection from radical oxygen species (ROS), and even the Last Universal Common Ancestor (LUCA) is also estimated to encode the enzymes (Slesak et al., 2012; Weiss et al., 2016), the lack of these suggests that Unc8 and perhaps the NPL-UPA2 relatives are relegated to very reduced environments on the Earth; whether this has any impact on our view of LUCA remains an interesting question.

Given that serpentinization is an exothermic process, and that the geothermal gradient leads to the subsurface warming with depth, the habitat of Unc8 in the deep ground water is almost certainly at higher temperature than that encountered in surface environments. Zeldovich et al. (2007) reported that fraction of a set of amino acids, namely isoleucine, valine, tryptophan, arginine, glutamic acid, and leucine, in whole coded proteins is highly correlated with the optimum temperature for growth of every organism. The enumerated quantitative relationship between the optimum growth temperature (T_{opt}) and fraction F of IVYWREL amino acids reads estimated that the optimum growth temperature of the Unc8 was 67.36°C. Meanwhile, G+C contents of the 16S rRNA gene is also reported the strong correlation to the optimum growth temperatures of prokaryote (Kimura et al., 2006). Estimation of optimum growth temperature of the Unc8 based on the G+C content of 16S rRNA gene was 43.09°C. Both results suggest that habitat of Unc8

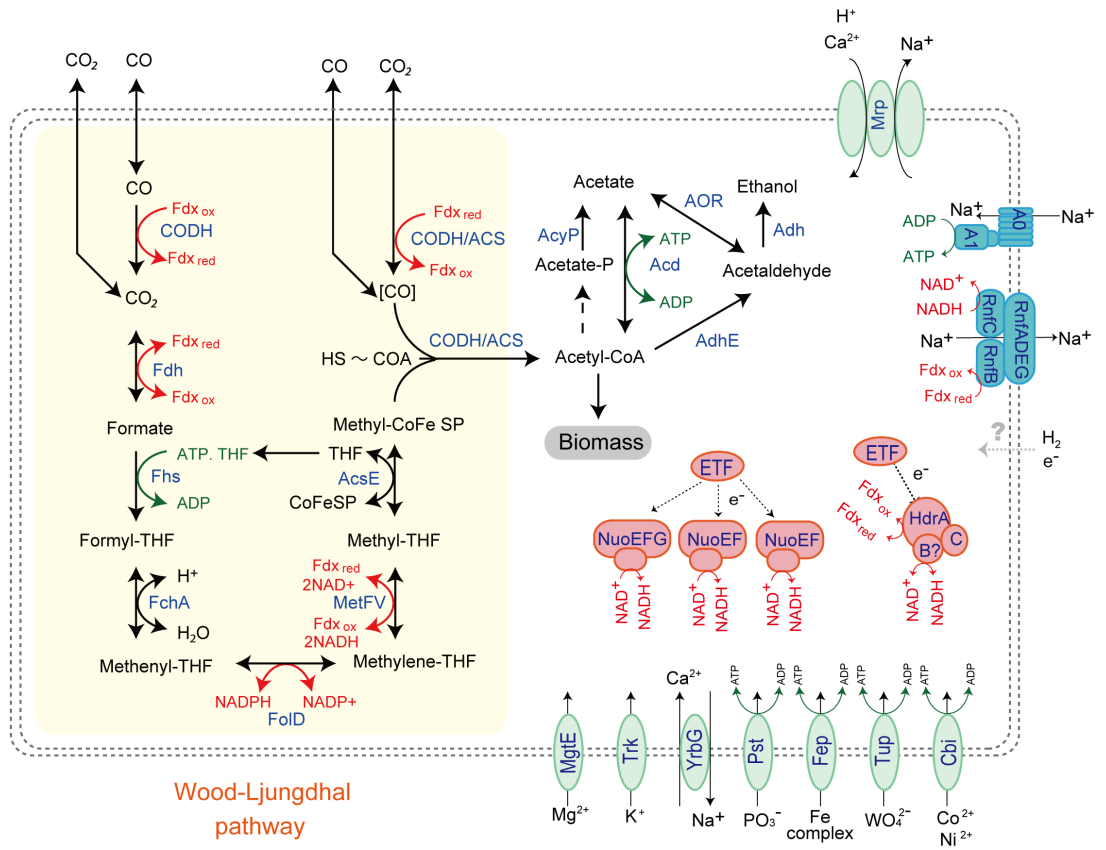

FIGURE 3 | Predicted energy metabolism for Unc8. Proteins and complexes are colored based on the functional categories. Abbreviations: CODH-Carbon monoxide dehydrogenase, Fdh-Formate dehydrogenase, Fhs-Formyl-THF synthase, Fch-Formyl-THF cyclohydrolase, FolD-Methylene-THF dehydrogenase, MetFV-Methylene-THF reductase, AcsE-Methyltransferase, CODH/ACS-Carbon monoxide dehydrogenase/Acetyl-CoA synthase complex, AcyP-Acylphosphatase, Acd-ADP forming Acetyl-CoA synthetase, Adh-Alcohol dehydrogenase, Nuo-NADH-quinone oxidoreductase, ETF-Electron transfer flavoprotein, HdrABC-Heterodisulfide reductase, Mrp-Multiple resistance and pH antiporter, A_1A_O-ATPase,-an Archaeal type ATPase, Rnf-proton/sodium-translocating ferredoxin-NAD:oxidoreductase complex, MgtE-Magnesium transporter, Trk-Potassium uptake system, YrbG-Ca^{2+}/Na^{+} antiporter, Pst-ABC-type Phosphate transporter, Fep-Iron transporter, Tup-Tungstate transporter, Cbi-Cobalt/Nickel transporter.

should be high: perhaps it is a thermophile. This also remains an interesting question: one whose answer may depend on obtaining an Unc8 cultivar.

Energy Metabolism of the Unc8

The MAG of Unc8 encodes limited metabolic potentials (**Figure 3** and **Supplementary Data S2C**). It does not encode genes for the TCA cycle, terminal electron acceptor reductases (cytochrome oxidase, sulfate reductase and nitrate reductase) or a standard electron transport chain including cytochromes and all membrane-bound Complex I subunits, indicating that Unc8 does not possess a typical respiratory metabolism. Furthermore, while a nearly complete set of glycolysis pathway genes is present, neither glucose transporters nor the genes responsible for forming glucose-6-phospate from glucose are seen. Since the origin of the deep water at The Cedars is far removed from the photosynthetic world, fermentative metabolism of sugars is not expected. In keeping with this, the genes responsible for the glycolysis pathway exhibited very low expression levels in the transcriptomic analyses (**Supplementary Data S1**). Amino acid fermentation is also unlikely to occur in the Unc8 because the MAG of Unc8 encodes no ABC-type amino acid transport systems to uptake amino acids from the outside of the cell (**Supplementary Data S2C**). As mentioned above, the MAG of Unc8 encodes almost no transporters to uptake organic compounds from outside of the cell, thus, substrates for the energy metabolisms of Unc8 must be permeable molecules, probably dissolved gasses or perhaps low molecule compounds that are transportable without specific transporters.

Genomic and transcriptomic data suggest that the major metabolism of the Unc8 is acetogenesis presumably involved in the Wood-Ljungdahl pathway which is the only pathway that couples the fixation of inorganic carbon to energy conservation (Schuchmann and Muller, 2014) (**Figure 3** and **Supplementary Datas S1, S2C**). The MAG of Unc8 encodes key enzymes for the Wood-Ljungdahl pathway including Carbon monoxide dehydrogenase/Acetyl-CoA synthase complex (CODH/ACS), Formate dehydrogenase (Fdh), Formyl-THF synthase (Fhs), Formyl-THF cyclohydrolase (Fch), Methylene-THF dehydrogenase (FolD), Methylene-THF reductase (MetVF),

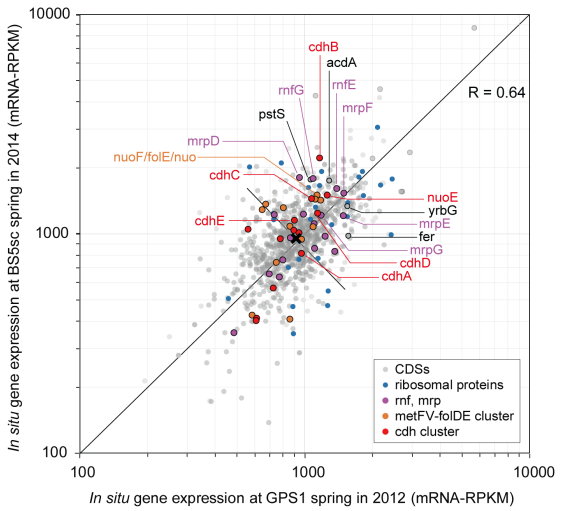

FIGURE 4 | Scatter plots of *in situ* gene expression of Unc8 in The Cedars springs. Scatter plots of all CDS in Unc8 responses as measured by mRNA frequency (mRNA-RPKM) between GPS1 and BS5sc. Key genes for acetogenesis are shown as unique colors, all other groups are shown in gray.

Methyltransferase (AcsE). The ATP synthase of Unc8 is an Archaeal type ATPase (A-ATPase), and the homology search of NtpC, a c-subunit of A_1A_O-ATPase, indicated a sodium-dependent A-ATPase (**Figure 5**). The MAG of Unc8 harbors genes for the proton/sodium-translocating ferredoxin-NAD:oxidoreductase complex (Rnf) (Biegel et al., 2011; Buckel and Thauer, 2013, 2018), which is presumably a key complex for the sodium translocation from the cytosol to the cell exterior to power the sodium-dependent A-ATPase for the ATP production (Mulkidjanian et al., 2008; Chowdhury et al., 2016). YrbG (Ca^{2+}/Na^{+} antiporter) (Besserer et al., 2012), MrpEFGBBBCD and MrpDD (Na^{+}, Ca^{2+}, K^{+}/H^{+} antiporter) (Ito et al., 2017) also may contribute to the export of sodium for ATP production. Three sets of *nuo* gene cluster (two sets of *nuoEF* and one set of *nuoEGF*), which encode a NADH dehydrogenase module, are also present on the genome and those may serve to regenerate NADH. Sets of the *nuoEF* and *nuoEGF* are located close to the *fdhAB* (Formate dehydrogenase) and *folD* (Methenyl-THF cyclohydrolase) on the genome and one set of the *nuoEF* is close to the gene cluster coding the CODH/ACS complex (**Figures 2**, **3**). Such close localizations of related genes on the genome may indicate that those are controlled under the same regulatory system. The MAG of Unc8 also contains the genes coding for the cytoplasmic electron transfer proteins through a flavin-based electron bifurcation mechanism, including two sets of the EtfAB (Electron transfer flavoprotein) and one set of HdrABC-like complex (Heterodisulfide reductase) (Buckel and Thauer, 2013, 2018). While genes for the HdrA and HdrC were identified, one for HdrB was not present. Since the heterodisulfide of coenzyme M and coenzyme B (CoM-S-S-CoB), a substrate of HdrB in typical methanogenic archaea, is not present in bacterial acetogens, the feature is reasonable. Based on the gene locations, HdrB in Unc8 was replaced with HydB (Sulfhydrogenase beta subunit) which is also a reductase with 4Fe-4S cluster, but the substrate is $NADH/NAD^{+}$. One set of the *etfAB* genes and the *hydB-hdrAC* genes are located in tandem on the MAG (**Figure 2**), implying that the Hdr-like complex works together with Etf instead of Mvh, a hydrogenase coupled with Hdr complex in methanogens (Buckel and Thauer, 2018). Further investigations are required.

The end products of Unc8 could be either acetate or ethanol as evidenced by the presence of Acd and alcohol dehydrogenase (AdhE, Adh) on the genome (**Figure 3** and **Supplementary Data S2C**). Higher expression was seen in the gene for Acetyl-CoA synthetase that is capable of converting Acetyl-coA to

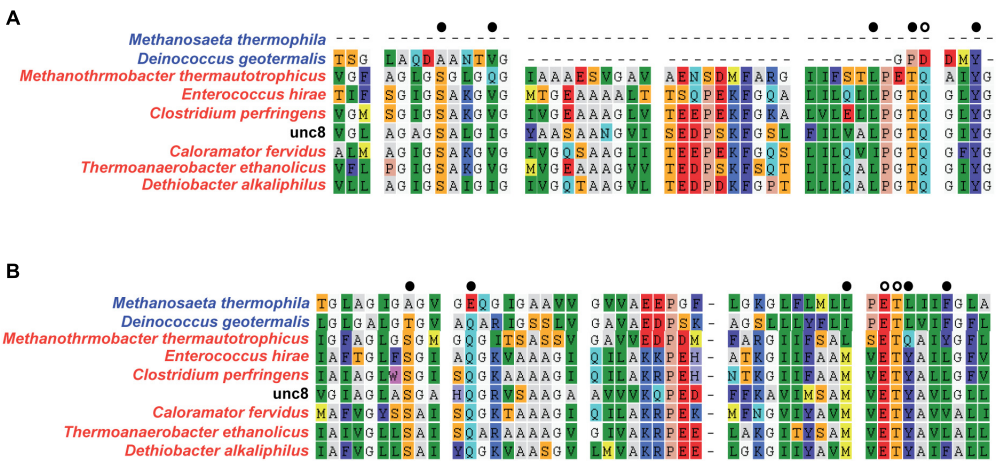

FIGURE 5 | Alignment of NtpC amino acid sequences from Unc8 to determine the interactive cations (i.e., sodium or proton) (Mulkidjanian et al., 2008). N-end **(A)** and C-end **(B)** of NtpC that include active sites are shown. Colors in the species names indicate the genomes encoding proton (blue) or sodium (red) coupled A-ATPases. Active site residues are shown with black/white dots at the top of each alignment and white dots indicate specific residues that are conserved in sodium-ligands and are partly absent in proton binding subunit (Mulkidjanian et al., 2008).

acetate with the formation of ATP (Musfeldt and Schonheit, 2002) (**Figure 4**), implying that the acetogenesis is the major mode for the energy conservation in the Unc8.

Taken together, these data suggested that Unc8 employs acetogenesis for energy conservation. The gene expression profile is consisting with this idea, showing the importance of the Ferredoxin, CODH/ACS, ADP forming Acetyl-CoA synthetase and Rnf complex as indicated by the higher expression of genes (**Figure 4**). However, the absence of any of well-known hydrogenases genes on the genome is puzzling (see Section "Hydrogenase" in **Supplementary Data S2C**): Hydrogenases catalyze the oxidation of hydrogen and allow bacteria to use hydrogen as an energy source for their growth. All the cultivated acetogens with the Wood-Ljungdahl pathway are able to gain energy through hydrogen-oxidizing CO_2-reducing acetate formation and the reaction is generally described as $4\ H_2 + 2\ CO_2 \rightarrow CH_3COOH + 2\ H_2O$ ($\Delta G^0 = -95$ kJ/mol). In addition, all of the cultivated acetogens known so far encode genes for hydrogenases on their genomes (Schuchmann and Muller, 2012) and hydrogen is the most abundant reduced substrate in the serpentinized fluid from The Cedars (Morrill et al., 2013). One possibility for unusual absence of hydrogenase genes is that Unc8 has uncharacterized hydrogenases coded by the hypothetical or function-unknown genes. Alternatively, it is possible that the Unc8 does not employ hydrogen-oxidizing CO_2-reduction but rather exploits carbon monoxide for acetate formation and energy conservation (Bertsch and Muller, 2015) as described $4\ CO + 2\ H_2O \rightarrow CH_3COOH + 2\ CO_2$ ($\Delta G^0 = -165.5$ kJ/mol). If carbon monoxide is available, utilization of CO would have a significant advantage in this environment due to the CO_2, a key substrate for acetogenesis, which will be present at extremely low concentrations because of the high innate alkalinity and the high concentration of calcium and as the potential energetical advantage (Diender et al., 2015). While organisms that can grow with only CO are rare, a few are known *Thermoanaerobacter kivui* (Weghoff and Muller, 2016) and *Methanosarcina acetivorans* C2A (Rother and Metcalf, 2004) in which CO consumption is coupled to acetate formation. Considering that CO is likely being produced as the intermediate of FTT synthesis from CO_2 to CH_4 under extremely reducing condition (Schrenk et al., 2013), it is reasonable to suggest that Unc8 employs CO for energy conservation rather than using molecular hydrogen as an electron source for CO_2 reduction in the deep subsurface. Yet, another possibility is that Unc8 is tightly associated with the reduced minerals or the reduced settings existing in The Cedars (the deep groundwater E_h is between -900 and -700 mV) and the oxidized ferredoxin or NAD^+ in the cell are reduced by electrons accumulated outside of the cells via chemical, enzymatic or metal-proteinous reactions.

Phylogenetic Analysis of Carbon Monoxide Dehydrogenase/Acetyl-CoA Synthase

Bifunctional CODH/ACS is generally a five-subunit enzyme complex and a key to carbon fixation in the Wood-Ljungdahl pathway (**Figure 6**). Four of the five subunits are homologous between Bacteria and Archaea. In Archaea, they are called CdhA (α-subunit), CdhC (β-subunit), CdhD (δ subunit), and CdhE (γ subunit), while in Bacteria, their respective homologs are called AcsA (β), AcsB (α), AcsD (δ), and AcsC (γ) (Adam et al., 2018). In addition, there exists a subunit exclusive to Archaea called CdhB (ε-subunit), and one exclusive to Bacteria (AcsE) (**Figures 2**, **6**). CdhABC in the Archaea and AcsAB in the Bacteria are responsible for the oxidoreductase module of the CODH/ACS and CdhDE in Archaea and AcsCDE in Bacteria

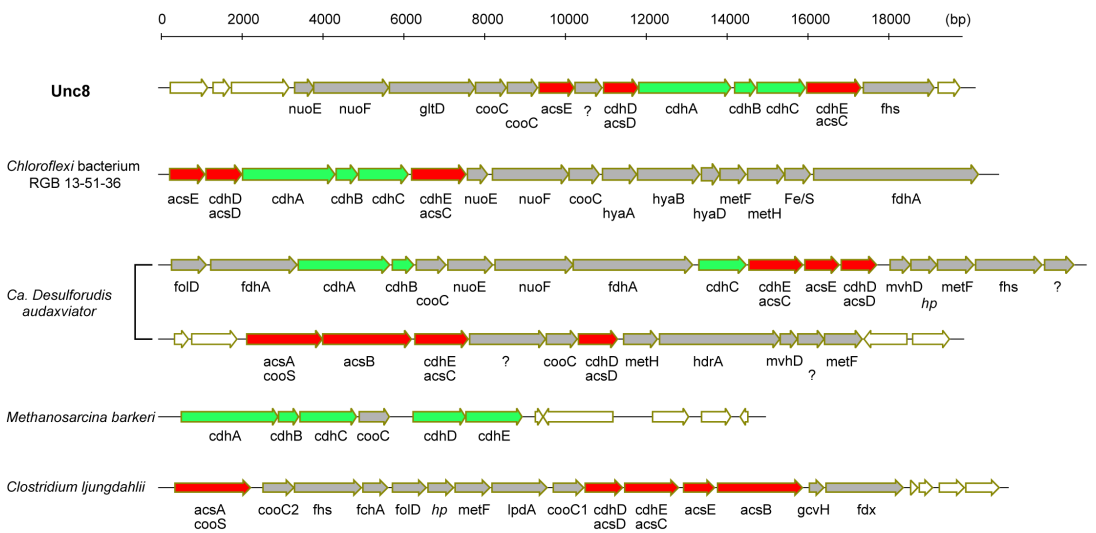

FIGURE 6 | Comparison of gene clusters for CODH and ACS. Green colored genes are archaeal in origin and red colored genes are bacterial in origin. In general, CODH/ACS is a five-subunits enzyme but Unc8, *Chloroflexi* bacterium RGB 13-51-36 and *Ca. Desulforudis audaxviator* encode a bacterial and archaeal hybrid type of six-subunits enzyme. *Ca. Desulforudis audaxviator* have two different clusters of gene sets for CODH/ACS on the MAG. Respective homologs of *cdhA, cdhC, cdhD*, and *cdhE* in Archaea are *acsA, acsB, acsD and acsC* in Bacteria (Adam et al., 2018). *cdhB* is exclusive to Archaea and *acsE* is exclusive to Bacteria.

are for the methyltransferase module. CODH/ACS complex in the Unc8 was, however, a hybrid of bacterial and archaeal type, and the CdhABC (oxidoreductase module) is the Archaeal type and AcsCDE (methyltransferase module) is the Bacterial type (**Figure 6** and **Supplementary Figure S2**). Bacteria/Archaea hybrids of six-subunit CODH/ACS are unusual but they have been seen in the MAG of *Candidatus Desulforudis audaxviator* recovered from alkaline groundwater in the deep subsurface gold mine (Chivian et al., 2008) and the MAG of *Chloroflexi* bacterium RGB_13_51_36 recovered from a sediment core drilled from a well at the Rifle Integrated Field Research Challenge (Hug et al., 2013) (**Figure 6** and **Supplementary Data S3**). Although Unc8, *Ca. D. audaxviator* and *Chloroflexi* bacterium RGB_13_51 are affiliated with different phyla (NPL-UPA2, *Firmicutes* or *Chloroflexi*, respectively), our phylogenetic analysis of the individual proteins suggests that Archaeal CdhABC complex was delivered at a single horizontal transfer from the *Euryarchaeota* to the *Bacteria* and that subsequent transfers occurred among bacterial lineages as discussed by Adam et al. (2018) (**Figure 6**). Phylogenetic trees of CdhA, CdhB and CdhC showed that those enzymes coded by Unc8 are closest to the archaeal cluster among those coded by the other bacterial members, implying that the *cdhABC* gene cluster on Unc8 genome were perhaps delivered from Archaea at the early stage of the horizontal gene transfer

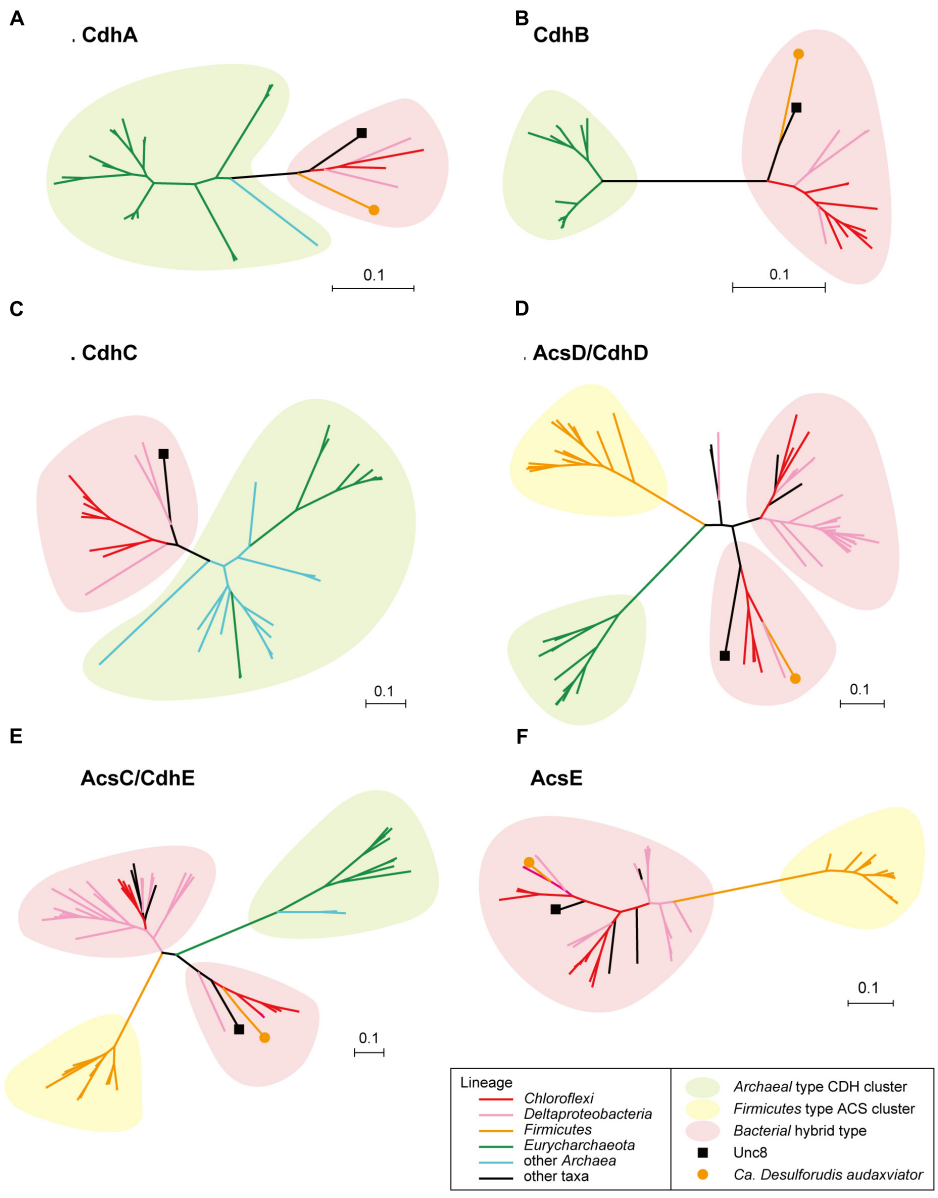

FIGURE 7 | Protein phylogeny of CODH/ACS complex. Phylogenetic trees were constructed for CdhA **(A)**, CdhB **(B)**, CdhC **(C)**, AcsD/CdhD **(D)**, AcsC/CdhE **(E)** and AcsE **(F)**. Detailed trees are shown in **Supplementary Figure S2**.

(**Figure 7** and **Supplementary Figure S2**). Further genomic studies targeted to other subsurface environments may identify the distribution and evolution of this type of enzyme complex in diverse bacterial phyla (**Figure 7** and **Supplementary Figure S2**). Unfortunately, since there are no cultivated organisms having the hybrids of six-subunit CODH/ACS, the advantages of such enzymes are unclear. The advantages may be related to the life strategies living in the environment depleted carbon dioxide and/or of the carbon monoxide mode of acetogenesis. Further enzymatic biochemistry of the hybrid CODH/ACS may provide us with important insights into the energy metabolism of the subsurface microbes and communities.

Archaeal Methanogenic Components in Unc8

The MAG of Unc8 indicates that the pathway to acetogenesis involves a mixture of archaeal and bacterial components (**Figure 6** and **Supplementary Figure S2**): while the Wood-Ljungdahl pathway and Rnf are known in association with bacterial acetogenesis (Ragsdale and Pierce, 2008; Schuchmann and Muller, 2014; Buckel and Thauer, 2018), the ATP synthase in Unc8 is an archaeal type (A_1A_O), the CODH/ACS is a bacterial/archaeal hybrid type of enzyme (Buckel and Thauer, 2018) and an Hdr complex is usually employed by the methanogenic archaea as an electron carrier. The origin of the electron transfer flavoprotein (EtfAB) is unsure; one of the two sets of *etf*AB genes is located close together with *hydB-hdr*AC genes on the Unc8 genome (**Figure 2**) and the *etf*AB genes show the highest similarity to those in the *Candidatus* Bathyarchaeota archaeon BA2 (Evans et al., 2015). Similar features were seen in the *Chloroflexi* bacterium RGB_13_51, namely, the *Chloroflexi* bacterium RGB_13_51 partly utilizes archaeal methanogenic system such as A-ATPase, hybrid CODH/ACS and Hdr although the RGB_13_51 is capable of using hydrogenases, one of which (Mvh) is also the Archaeal type of hydrogenase (Hug et al., 2013) (**Supplementary Data S3**). One interpretation of this is that archaeal methanogenic energy metabolism was incorporated into a bacterial acetogen and then transferred horizontally among bacterial lineages of lithotrophic acetogens.

Implications

Given that this is the first genomic and transcriptomic description of candidate phylum NPL-UPA2, to honor Professor Horikoshi, we propose the provisional taxonomic assignment to "*Candidatus* Horikoshi bacteria" phylum. nov.. The "*Ca.* Horikoshi bacteria" bacterium Unc8 from highly alkaline highly reducing groundwater at The Cedars is presumably an acetogen via Wood-Ljungdahl pathway. Several of the key enzymes are archaeal in origin. While lack of hydrogenases is puzzling, acetogenesis from carbon monoxide could be a favorable energy metabolism in this setting. Alternatively, during the evolution under highly alkaline and highly reducing condition, Unc8 might obtain some unknown metabolic systems for utilizing reducing power outside of the cell without using well-known hydrogenases and cytochromes. Namely, redox potentials needed to reduce ferredoxin and NADH are E_h = -430 and -320 mV, respectively (Schuchmann and Muller, 2014). E_h of The Cedars deep ground water is between –900 and –700 mV at pH 12, which at pH 8 (assumed intracellular pH) would be equivalent to –640 and –440 mV, respectively. If Unc8 can reduce ferredoxin and NADH by using the reducing power outside of the cell in some ways, synthesis of ATP could easily occur by subsequent acetogenesis. Further investigations may shed light on this fascinating question.

As a final point, serpentinizing systems are viewed as both analogs for planetary bodies and potential early Earth environments (Schulte et al., 2006; Martin and Russell, 2007; Sleep et al., 2011; Sleep, 2018), where highly reducing mineralogy was likely widespread in an undifferentiated crust. The life strategies of LUCA proposed by Weiss et al. (2016) include many properties of Unc8, e.g., (1) the MAG of Unc8 harbors only CODH/ACS associated carbon fixation and energy metabolism, (2) has sodium-dependent ATPase and Mrp complex and (3) is a potential thermophile. However, the Unc8 MAG doesn't harbor nitrogenase, hydrogenase, or superoxide dismutase. Since many studies have proposed that acetogenesis via the Wood-Ljungdahl pathway would have been a potential energy metabolism for primordial lithotrophic autotrophs (Martin and Russell, 2007; Fuchs, 2011; Lane and Martin, 2012; Martin et al., 2014), the acetogen from an analog site of early Earth may provide important insights about ancient lithotrophs and their habitats.

AUTHOR CONTRIBUTIONS

SS and SI designed the research and performed the analyses. SS, SI, and KN wrote the paper.

FUNDING

This work was funded by the NSF-EAR Grant No. 1424646 and JSPS KAKENHI Grant Number 18H02501. SS was partially funded by JSPS KAKENHI Grant Numbers 16K14647 and 26106004 and Astrobiology Center Program of National Institutes of Natural Sciences (NINS) Grant Number AB301015.

ACKNOWLEDGMENTS

We greatly appreciate Prof. J. Gijs Kuenen and Dr. Fumio Inagaki for constructive discussions. We much appreciate Mr. Roger Raiche and Mr. David McCrory having permitted us to use their private land for our research. We appreciate Ms. Bette Campbell for encouraging our sampling activities. We appreciate Dr. Kozue Matsuzaki from JAMSTEC and Ms. Takara Matsuzaki from Marine Works Japan for the technical assistance.

SUPPLEMENTARY MATERIAL

The Supplementary Material for this article can be found online at: https://www.frontiersin.org/articles/10.3389/fmicb.2018.03141/full#supplementary-material

REFERENCES

Adam, P. S., Borrel, G., and Gribaldo, S. (2018). Evolutionary history of carbon monoxide dehydrogenase/acetyl-CoA synthase, one of the oldest enzymatic complexes. *Proc. Natl. Acad. Sci. U.S.A.* 115, E1166–E1173. doi: 10.1073/pnas.1716667115

Albertsen, M., Hugenholtz, P., Skarshewski, A., Nielsen, K. L., Tyson, G. W., and Nielsen, P. H. (2013). Genome sequences of rare, uncultured bacteria obtained by differential coverage binning of multiple metagenomes. *Nat. Biotechnol.* 31, 533–538. doi: 10.1038/nbt.2579

Alikhan, N. F., Petty, N. K., Ben Zakour, N. L., and Beatson, S. A. (2011). BLAST ring image generator (BRIG): simple prokaryote genome comparisons. *BMC Genomics* 12:402. doi: 10.1186/1471-2164-12-402

Anantharaman, K., Brown, C. T., Hug, L. A., Sharon, I., Castelle, C. J., Probst, A. J., et al. (2016). Thousands of microbial genomes shed light on interconnected biogeochemical processes in an aquifer system. *Nat. Commun.* 7:13219. doi: 10.1038/ncomms13219

Arkin, A. P., Cottingham, R. W., Henry, C. S., Harris, N. L., Stevens, R. L., Maslov, S., et al. (2018). KBase: the United States Department of Energy systems biology knowledgebase. *Nat. Biotechnol.* 36, 566–569. doi: 10.1038/nbt.4163

Bertsch, J., and Muller, V. (2015). CO metabolism in the acetogen *Acetobacterium woodii*. *Appl. Environ. Microbiol.* 81, 5949–5956. doi: 10.1128/AEM.01772-15

Besserer, G. M., Nicoll, D. A., Abramson, J., and Philipson, K. D. (2012). Characterization and purification of a Na(/Ca2(exchanger from an archaebacterium. *J. Biol. Chem.* 287, 8652–8659. doi: 10.1074/jbc.M111.331280

Biegel, E., Schmidt, S., Gonzalez, J. M., and Muller, V. (2011). Biochemistry, evolution and physiological function of the Rnf complex, a novel ion-motive electron transport complex in prokaryotes. *Cell Mol. Life. Sci.* 68, 613–634. doi: 10.1007/s00018-010-0555-8

Bowers, R. M., Kyrpides, N. C., Stepanauskas, R., Harmon-Smith, M., Doud, D., Reddy, T. B. K., et al. (2017). Minimum information about a single amplified genome (MISAG) and a metagenome-assembled genome (MIMAG) of bacteria and archaea. *Nat. Biotechnol.* 35, 725–731. doi: 10.1038/nbt.3893

Brazelton, W. J., Nelson, B., and Schrenk, M. O. (2012). Metagenomic evidence for h(2) oxidation and h(2) production by serpentinite-hosted subsurface microbial communities. *Front. Microbiol.* 2:268. doi: 10.3389/fmicb.2011.00268

Brazelton, W. J., Schrenk, M. O., Kelley, D. S., and Baross, J. A. (2006). Methane- and sulfur-metabolizing microbial communities dominate the Lost City hydrothermal field ecosystem. *Appl. Environ. Microbiol.* 72, 6257–6270. doi: 10.1128/AEM.00574-06

Brown, C. T., Hug, L. A., Thomas, B. C., Sharon, I., Castelle, C. J., Singh, A., et al. (2015). Unusual biology across a group comprising more than 15% of domain Bacteria. *Nature* 523, 208–211. doi: 10.1038/nature14486

Buckel, W., and Thauer, R. K. (2013). Energy conservation via electron bifurcating ferredoxin reduction and proton/Na^+ translocating ferredoxin oxidation. *Biochim. Biophys. Acta* 1827, 94–113. doi: 10.1016/j.bbabio.2012.07.002

Buckel, W., and Thauer, R. K. (2018). Flavin-based electron bifurcation, ferredoxin, flavodoxin, and anaerobic respiration with protons (Ech) or NAD^+ (Rnf) as electron acceptors: a historical review. *Front. Microbiol.* 9:401. doi: 10.3389/fmicb.2018.00401

Castelle, C. J., and Banfield, J. F. (2018). Major new microbial groups expand diversity and alter our understanding of the tree of life. *Cell* 172, 1181–1197. doi: 10.1016/j.cell.2018.02.016

Chivian, D., Brodie, E. L., Alm, E. J., Culley, D. E., Dehal, P. S., DeSantis, T. Z., et al. (2008). Environmental genomics reveals a single-species ecosystem deep within earth. *Science* 322, 275–278. doi: 10.1126/science.1155495

Chowdhury, N. P., Klomann, K., Seubert, A., and Buckel, W. (2016). Reduction of flavodoxin by electron bifurcation and sodium ion-dependent reoxidation by NAD^+ catalyzed by ferredoxin-NAD^+ reductase (Rnf). *J. Biol. Chem.* 291, 11993–12002. doi: 10.1074/jbc.M116.726299

Diender, M., Stams, A. J., and Sousa, D. Z. (2015). Pathways and bioenergetics of anaerobic carbon monoxide fermentation. *Front. Microbiol.* 6:1275. doi: 10.3389/fmicb.2015.01275

Edgar, R. C. (2004). MUSCLE: multiple sequence alignment with high accuracy and high throughput. *Nucleic Acids Res.* 32, 1792–1797. doi: 10.1093/nar/gkh340

Ettwig, K. F., Butler, M. K., Le Paslier, D., Pelletier, E., Mangenot, S., Kuypers, M. M., et al. (2010). Nitrite-driven anaerobic methane oxidation by oxygenic bacteria. *Nature* 464, 543–548. doi: 10.1038/nature08883

Evans, P. N., Parks, D. H., Chadwick, G. L., Robbins, S. J., Orphan, V. J., Golding, S. D., et al. (2015). Methane metabolism in the archaeal phylum *Bathyarchaeota* revealed by genome-centric metagenomics. *Science* 350, 434–438. doi: 10.1126/science.aac7745

Fuchs, G. (2011). Alternative pathways of carbon dioxide fixation: insights into the early evolution of life? *Annu. Rev. Microbiol.* 65, 631–658. doi: 10.1146/annurev-micro-090110-102801

Galperin, M. Y., Makarova, K. S., Wolf, Y. I., and Koonin, E. V. (2015). Expanded microbial genome coverage and improved protein family annotation in the COG database. *Nucleic Acids Res.* 43, D261–D269. doi: 10.1093/nar/gku1223

Guan, Y., Hikmawan, T., Antunes, A., Ngugi, D., and Stingl, U. (2015). Diversity of methanogens and sulfate-reducing bacteria in the interfaces of five deep-sea anoxic brines of the Red Sea. *Res. Microbiol.* 166, 688–699. doi: 10.1016/j.resmic.2015.07.002

Horikoshi, K. (1971). Production of alkaline enzymes by alkalophilic microorganisms part II. alkaline amylase produced by *Bacillus* No, A-40-2. *Agric. Biol. Chem.* 35, 1783–1791. doi: 10.1271/bbb1961.35.1783

Horikoshi, K. (1996). Alkaliphiles — from an industrial point of view. *FEMS Microbiol. Rev.* 18, 259–270. doi: 10.1111/j.1574-6976.1996.tb00242.x

Horikoshi, K. (1999). Alkaliphiles: some applications of their products for biotechnology. *Microbiol. Mol. Biol. Rev.* 63, 735–750.

Hoshino, T., Morono, Y., Terada, T., Imachi, H., Ferdelman, T. G., and Inagaki, F. (2011). Comparative study of subseafloor microbial community structures in deeply buried coral fossils and sediment matrices from the challenger mound in the porcupine seabight. *Front. Microbiol.* 2:231. doi: 10.3389/fmicb.2011.00231

Huber, J. A., Johnson, H. P., Butterfield, D. A., and Baross, J. A. (2006). Microbial life in ridge flank crustal fluids. *Environ. Microbiol.* 8, 88–99. doi: 10.1111/j.1462-2920.2005.00872.x

Hug, L. A., Castelle, C. J., Wrighton, K. C., Thomas, B. C., Sharon, I., Frischkorn, K. R., et al. (2013). Community genomic analyses constrain the distribution of metabolic traits across the *Chloroflexi phylum* and indicate roles in sediment carbon cycling. *Microbiome* 1:22. doi: 10.1186/2049-2618-1-22

Ishii, S., Suzuki, S., Norden-Krichmar, T. M., Tenney, A., Chain, P. S. G., Scholz, M. B., et al. (2013). A novel metatranscriptomic approach to identify gene expression dynamics during extracellular electron transfer. *Nat. Commun.* 4:1601. doi: 10.1038/ncomms2615

Ishii, S., Suzuki, S., Tenney, A., Nealson, K. H., and Bretschger, O. (2018). Comparative metatranscriptomics reveals extracellular electron transfer pathways conferring microbial adaptivity to surface redox potential changes. *ISME J.* 12, 2844–2863. doi: 10.1038/s41396-018-0238-2

Ishii, S., Suzuki, S., Tenney, A., Norden-Krichmar, T. M., Nealson, K. H., and Bretschger, O. (2015). Microbial metabolic networks in a complex electrogenic biofilm recovered from a stimulus-induced metatranscriptomics approach. *Sci. Rep.* 5:14840. doi: 10.1038/srep14840

Ito, M., Morino, M., and Krulwich, T. A. (2017). Mrp antiporters have important roles in diverse bacteria and archaea. *Front. Microbiol.* 8:2325. doi: 10.3389/fmicb.2017.02325

Kanehisa, M., Sato, Y., and Morishima, K. (2016). BlastKOALA and GhostKOALA: KEGG tools for functional characterization of genome and metagenome sequences. *J. Mol. Biol.* 428, 726–731. doi: 10.1016/j.jmb.2015.11.006

Kato, S., Sakai, S., Hirai, M., Tasumi, E., Nishizawa, M., Suzuki, K., et al. (2018). Long-term cultivation and metagenomics reveal ecophysiology of previously uncultivated thermophiles involved in biogeochemical nitrogen cycle. *Microbes Environ.* 33, 107–110. doi: 10.1264/jsme2.ME17165

Kimura, H., Sugihara, M., Kato, K., and Hanada, S. (2006). Selective phylogenetic analysis targeted at 16S rRNA genes of thermophiles and hyperthermophiles in deep-subsurface geothermal environments. *Appl. Environ. Microbiol.* 72, 21–27. doi: 10.1128/AEM.72.1.21-27.2006

Krogh, A., Larsson, B., von Heijne, G., and Sonnhammer, E. L. (2001). Predicting transmembrane protein topology with a hidden Markov model: application to complete genomes. *J. Mol. Biol.* 305, 567–580. doi: 10.1006/jmbi.2000.4315

Kudo, T. (2016). In memoriam: Koki Horikoshi (1932–2016). *Extremophiles* 20, 383–384. doi: 10.1007/s00792-016-0842-x

Lane, N., and Martin, W. F. (2012). The origin of membrane bioenergetics. *Cell* 151, 1406–1416. doi: 10.1016/j.cell.2012.11.050

Laso-Perez, R., Wegener, G., Knittel, K., Widdel, F., Harding, K. J., Krukenberg, V., et al. (2016). *Thermophilic archaea* activate butane via alkyl-coenzyme M formation. *Nature* 539, 396–401. doi: 10.1038/nature20152

Liu, W., Qi, Y., and Hulett, F. M. (1998). Sites internal to the coding regions of phoA and pstS bind PhoP and are required for full promoter activity. *Mol. Microbiol.* 28, 119–130. doi: 10.1046/j.1365-2958.1998.00779.x

Martin, W., and Russell, M. J. (2007). On the origin of biochemistry at an alkaline hydrothermal vent. *Philos. Trans. R. Soc. Lond. B* 362, 1887–1925. doi: 10.1098/rstb.2006.1881

Martin, W. F., Sousa, F. L., and Lane, N. (2014). EVOLUTION energy at life's origin. *Science* 344, 1092–1093. doi: 10.1126/science.1251653

McCollom, T. M., and Seewald, J. S. (2001). A reassessment of the potential for reduction of dissolved CO2 to hydrocarbons during serpentinization of olivine. *Geochim. Cosmochim. Acta* 65, 3769–3778. doi: 10.1016/S0016-7037(01)00655-X

McCollom, T. M., and Seewald, J. S. (2007). Abiotic synthesis of organic compounds in deep-sea hydrothermal environments. *Chem. Rev.* 107, 382–401. doi: 10.1021/cr0503660

McGlynn, S. E. (2017). Energy metabolism during anaerobic methane oxidation in ANME archaea. *Microbes Environ.* 32, 5–13. doi: 10.1264/jsme2.ME16166

Mei, N., Postec, A., Monnin, C., Pelletier, B., Payri, C. E., Menez, B., et al. (2016). Metagenomic and PCR-based diversity surveys of [FeFe]-hydrogenases combined with isolation of alkaliphilic hydrogen-producing bacteria from the serpentinite-hosted prony hydrothermal field, new caledonia. *Front. Microbiol.* 7:1301. doi: 10.3389/fmicb.2016.01301

Monnin, C., Chavagnac, V., Boulart, C., Menez, B., Gerard, M., Gerard, E., et al. (2014). Fluid chemistry of the low temperature hyperalkaline hydrothermal system of Prony Bay (New Caledonia). *Biogeosciences* 11, 5687–5706. doi: 10.5194/bg-11-5687-2014

Moriya, Y., Itoh, M., Okuda, S., Yoshizawa, A. C., and Kanehisa, M. (2007). KAAS: an automatic genome annotation and pathway reconstruction server. *Nucleic Acids Res.* 35, W182–W185. doi: 10.1093/nar/gkm321

Morrill, P. L., Kuenen, J. G., Johnson, O. J., Suzuki, S., Rietze, A., Sessions, A. L., et al. (2013). Geochemistry and geobiology of a present-day serpentinization site in California: the cedars. *Geochim. Cosmochim. Acta* 109, 222–240. doi: 10.1016/j.gca.2013.01.043

Mortazavi, A., Williams, B. A., Mccue, K., Schaeffer, L., and Wold, B. (2008). Mapping and quantifying mammalian transcriptomes by RNA-Seq. *Nat. Method* 5, 621–628. doi: 10.1038/nmeth.1226

Mulkidjanian, A. Y., Galperin, M. Y., Makarova, K. S., Wolf, Y. I., and Koonin, E. V. (2008). Evolutionary primacy of sodium bioenergetics. *Biol. Direct.* 3:13. doi: 10.1186/1745-6150-3-13

Musfeldt, M., and Schonheit, P. (2002). Novel type of ADP-forming acetyl coenzyme A synthetase in hyperthermophilic archaea: heterologous expression and characterization of isoenzymes from the sulfate reducer *Archaeoglobus fulgidus* and the methanogen *Methanococcus jannaschii*. *J. Bacteriol.* 184, 636–644. doi: 10.1128/JB.184.3.636-644.2002

Parks, D. H., Imelfort, M., Skennerton, C. T., Hugenholtz, P., and Tyson, G. W. (2015). CheckM: assessing the quality of microbial genomes recovered from isolates, single cells, and metagenomes. *Genome Res.* 25, 1043–1055. doi: 10.1101/gr.186072.114

Postec, A., Quemeneur, M., Bes, M., Mei, N., Benaissa, F., Payri, C., et al. (2015). Microbial diversity in a submarine carbonate edifice from the serpentinizing hydrothermal system of the Prony Bay (New Caledonia) over a 6-year period. *Front. Microbiol.* 6:857. doi: 10.3389/fmicb.2015.00857

Probst, A. J., Ladd, B., Jarett, J. K., Geller-McGrath, D. E., Sieber, C. M. K., Emerson, J. B., et al. (2018). Differential depth distribution of microbial function and putative symbionts through sediment-hosted aquifers in the deep terrestrial subsurface. *Nat. Microbiol.* 3, 328–336. doi: 10.1038/s41564-017-0098-y

Ragsdale, S. W., and Pierce, E. (2008). Acetogenesis and the Wood–Ljungdahl pathway of CO2 fixation. *Biochim. Biophys. Acta – Proteins Proteom.* 1784, 1873–1898. doi: 10.1016/j.bbapap.2008.08.012

Rother, M., and Metcalf, W. W. (2004). Anaerobic growth of *Methanosarcina acetivorans* C2A on carbon monoxide: an unusual way of life for a methanogenic archaeon. *Proc. Natl. Acad. Sci. U.S.A.* 101, 16929–16934. doi: 10.1073/pnas.0407486101

Schrenk, M. O., Brazelton, W. J., and Lang, S. Q. (2013). Serpentinization, carbon, and deep life. *Carbon Earth* 75, 575–606. doi: 10.1515/9781501508318-020

Schuchmann, K., and Muller, V. (2012). A bacterial electron-bifurcating hydrogenase. *J. Biol. Chem.* 287, 31165–31171. doi: 10.1074/jbc.M112.395038

Schuchmann, K., and Muller, V. (2014). Autotrophy at the thermodynamic limit of life: a model for energy conservation in acetogenic bacteria. *Nat. Rev. Microbiol.* 12, 809–821. doi: 10.1038/nrmicro3365

Schulte, M., Blake, D., Hoehler, T., and McCollom, T. (2006). Serpentinization and its implications for life on the early Earth and Mars. *Astrobiology* 6, 364–376. doi: 10.1089/ast.2006.6.364

Sleep, N. H. (2018). Geological and geochemical constraints on the origin and evolution of life. *Astrobiology* 18, 1199–1219. doi: 10.1089/ast.2017.1778

Sleep, N. H., Bird, D. K., and Pope, E. C. (2011). Serpentinite and the dawn of life. *Philos. Trans. R. Soc. Lond. B* 366, 2857–2869. doi: 10.1098/rstb.2011.0129

Slesak, I., Slesak, H., and Kruk, J. (2012). Oxygen and hydrogen peroxide in the early evolution of life on earth: in silico comparative analysis of biochemical pathways. *Astrobiology* 12, 775–784. doi: 10.1089/ast.2011.0704

Stamatakis, A., Hoover, P., and Rougemont, J. (2008). A rapid bootstrap algorithm for the RAxML Web servers. *Syst. Biol.* 57, 758–771. doi: 10.1080/10635150802429642

Strous, M., Pelletier, E., Mangenot, S., Rattei, T., Lehner, A., Taylor, M. W., et al. (2006). Deciphering the evolution and metabolism of an anammox bacterium from a community genome. *Nature* 440, 790–794. doi: 10.1038/nature04647

Suzuki, S., Ishii, S., Hoshino, T., Rietze, A., Tenney, A., Morrill, P. L., et al. (2017). Unusual metabolic diversity of hyperalkaliphilic microbial communities associated with subterranean serpentinization at The Cedars. *ISME J.* 11, 2584–2598. doi: 10.1038/ismej.2017.111

Suzuki, S., Ishii, S., Wu, A., Cheung, A., Tenney, A., Wanger, G., et al. (2013). Microbial diversity in the cedars, an ultrabasic, ultrareducing, and low salinity serpentinizing ecosystem. *Proc. Natl. Acad. Sci. U.S.A.* 110, 15336–15341. doi: 10.1073/pnas.1302426110

Suzuki, S., Kuenen, J. G., Schipper, K., van der Velde, S., Ishii, S., Wu, A., et al. (2014). Physiological and genomic features of highly alkaliphilic hydrogen-utilizing *Betaproteobacteria* from a continental serpentinizing site. *Nat. Commun.* 5:3900. doi: 10.1038/ncomms4900

Tatusova, T., DiCuccio, M., Badretdin, A., Chetvernin, V., Nawrocki, E. P., Zaslavsky, L., et al. (2016). NCBI prokaryotic genome annotation pipeline. *Nucleic Acids Res.* 44, 6614–6624. doi: 10.1093/nar/gkw569

Tiago, I., and Verissimo, A. (2013). Microbial and functional diversity of a subterrestrial high pH groundwater associated to serpentinization. *Environ. Microbiol.* 15, 1687–1706. doi: 10.1111/1462-2920.12034

Vanwonterghem, I., Evans, P. N., Parks, D. H., Jensen, P. D., Woodcroft, B. J., Hugenholtz, P., et al. (2016). Methylotrophic methanogenesis discovered in the archaeal phylum *Verstraetearchaeota*. *Nat. Microbiol.* 1:16170. doi: 10.1038/nmicrobiol.2016.170

Weghoff, M. C., and Muller, V. (2016). CO Metabolism in the thermophilic acetogen *Thermoanaerobacter kivui*. *Appl. Environ. Microbiol.* 82, 2312–2319. doi: 10.1128/AEM.00122-16

Weiss, M. C., Sousa, F. L., Mrnjavac, N., Neukirchen, S., Roettger, M., Nelson-Sathi, S., et al. (2016). The physiology and habitat of the last universal common ancestor. *Nat. Microbiol.* 1:16116. doi: 10.1038/nmicrobiol.2016.116

Woodcroft, B. J., Singleton, C. M., Boyd, J. A., Evans, P. N., Emerson, J. B., Zayed, A. A. F., et al. (2018). Genome-centric view of carbon processing in thawing permafrost. *Nature* 560, 49–54. doi: 10.1038/s41586-018-0338-1

Wrighton, K. C., Thomas, B. C., Sharon, I., Miller, C. S., Castelle, C. J., VerBerkmoes, N. C., et al. (2012). Fermentation, hydrogen, and sulfur metabolism in multiple uncultivated bacterial phyla. *Science* 337, 1661–1665. doi: 10.1126/science.1224041

Yu, N. Y., Wagner, J. R., Laird, M. R., Melli, G., Rey, S., Lo, R., et al. (2010). PSORTb 3.0: improved protein subcellular localization prediction with refined localization subcategories and predictive capabilities for all prokaryotes. *Bioinformatics* 26, 1608–1615. doi: 10.1093/bioinformatics/btq249

Zeldovich, K. B., Berezovsky, I. N., and Shakhnovich, E. I. (2007). Protein and DNA sequence determinants of thermophilic adaptation. *PLoS Comput. Biol.* 3:e5. doi: 10.1371/journal.pcbi.0030005

Conflict of Interest Statement: The authors declare that the research was conducted in the absence of any commercial or financial relationships that could be construed as a potential conflict of interest.

Advantages of publishing in Frontiers

OPEN ACCESS
Articles are free to read for greatest visibility and readership

FAST PUBLICATION
Around 90 days from submission to decision

HIGH QUALITY PEER-REVIEW
Rigorous, collaborative, and constructive peer-review

TRANSPARENT PEER-REVIEW
Editors and reviewers acknowledged by name on published articles

Frontiers
Avenue du Tribunal-Fédéral 34
1005 Lausanne | Switzerland

Visit us: www.frontiersin.org
Contact us: info@frontiersin.org | +41 21 510 17 00

REPRODUCIBILITY OF RESEARCH
Support open data and methods to enhance research reproducibility

DIGITAL PUBLISHING
Articles designed for optimal readership across devices

FOLLOW US
@frontiersin

IMPACT METRICS
Advanced article metrics track visibility across digital media

EXTENSIVE PROMOTION
Marketing and promotion of impactful research

LOOP RESEARCH NETWORK
Our network increases your article's readership